Investigating the Au and Pd uptake and detoxification mechanisms in Arabidopsis

Jessica Alice Dobson

PhD

University of York

Biology

August 2022

Abstract

Metals are a finite resource, yet over the years, many of the rarer and more valuable metals have been mined, then during or following use, dispersed, and diluted back into the environment. The necessary shift from a linear to a circular economy necessitates the recovery of materials for reuse. Phytoremediation and phytomining are two processes which could work hand in hand as potentially cost-effective and environmentally friendly approaches for metal recovery and remediation of contaminated soils. A significant hurdle in phytomining precious metals is the low uptake rates by plants. Towards this, we need to understand the biology behind metal uptake, focusing in this study on precious metals gold (Au) and palladium (Pd). *Arabidopsis thaliana* (Arabidopsis) is a model plant organism for genetic research and has been used in this study to investigate Au and Pd uptake and detoxification. This study is based on key building blocks of research relating to metal uptake and detoxification in plants. Prior to this work, the copper uptake transporter 2 (COPT2) had been identified as a potential Au uptake transporter in Arabidopsis. It had also been reported that Au and Pd are deposited *in planta* as nanoparticles (NPs). A AuNP-forming peptide (GP) had been previously expressed *in planta* in our laboratory prior to this work, which resulted in a shift in the heterogeneous morphology of NPs formed in plants towards smaller (10 nm), more catalytically active, and commercially valuable NPs.

In chapter three, these discoveries were utilised with the aim of generating plant lines with increased Au uptake and tolerance, and enhanced NP formation. The interaction between Au and COPT2 was investigated using *Saccharomyces cerevisiae* (yeast)*,* Arabidopsis *copt2* mutants, and Arabidopsis overexpression (*35S-COPT2*) lines. The NP-forming ability and resultant detoxification of Au ions was investigated in *GP* expressing plant lines. Promising results from these experiments encouraged the generation of double transgenic lines expressing an elevated level of *COPT2* alongside the GP to investigate Au uptake and tolerance. The increased expression of *COPT2*, combined with the presence of the GP, resulted in increased Au uptake into shoot tissue. In addition to Au, my studies revealed that COPT2 also transports Pd.

The approach utilised in chapter three was applied in chapter four to investigate the interaction of COPT2 and GP with Pd, to attempt to generate plant lines that could accumulate increased levels of Pd with enriched 10 nm NPs. There was a significant interaction between COPT2, GP and Pd, but this was less strong than the interaction with Au. Despite promising studies in yeast and Arabidopsis, the double transgenic lines did not contain increased levels of Pd, suggesting that other transporters may play a more prominent role in Pd uptake, and/or that the GPs are less effective with Pd.

The response of the Arabidopsis transcriptome to Pd is explored in chapter 5, and the profile of genes involved in uptake and detoxification appears similar to Cd exposure. The transcriptomic response is complex, involving changes in the expression of transcription factors, transporters, phytochelatins, aquaporins, oxidases, peroxidases, chaperones, and genes relating to cellular processes. The most enriched biological processes were dominated by general stress and hypoxia responses in the roots, with a specific metal ion response in the shoot tissue. The genes encoding for the Heavy-Metal ATPase transporter, HMA2, and the aquaporin/arsenite transmembrane transporter NLM1, were significantly downregulated in the shoot tissue response to Pd, as was COPT2. Genes encoding the vacuolar located ABCC3 and ABCC11 proteins, glutathione transporting ATPases, were upregulated in response to Pd exposure, and may be involved in a glutathione or phytochelatin related Pd detoxification response. A plasma membrane located xenobiotic transmembrane transporter (DTX14), shown to be involved in the export of the antibiotic norfloxacin, was also upregulated in response to Pd, and may serve to export Pd from cells. Together these findings demonstrate the effect on Au uptake in plants by increasing the expression of *COPT2* alongside GP, which is within the interest of developing plants for phytomining Au. The work presented in this thesis also provides a deeper understanding of the genes involved in Pd uptake and tolerance, which may be used in future work to engineer plants for effective phytomining.

Table of contents

List of figures

List of tables

Acknowledgements

The biggest of thank yous to everyone who has supported me over the past few years.

To my supervisor Neil Bruce, thank you for all your guidance, advice and very necessary calm when the stress piled on. To Liz Rylott, I cannot thank you with enough brownies or cakes to show you my gratitude for the amount of feedback and support you have given me. I am especially grateful to both you and Neil for your support over the last year, between the pandemic, family health issues and devastating news, I don't know how I would have been able to complete my thesis without your support, understanding and kindness, and I am so grateful.

To my secondary supervisor Frans Maathuis, thank you for sharing your expertise and guidance, especially relating to yeast and metal transporters.

To Andrea Harper, thank you for your support within my Thesis Advisory Panel meetings, and being an ear to listen to the problems I encountered during this time.

To everyone in CNAP, especially members of the Bruce group past and present, who made working in the labs so much fun, and gave their time to my many questions. A special thanks to the legendary Paulina Dani, one of the most knowledgeable, kind and silly people I have had the joy of meeting, thank you for your advice and friendship, and for keeping me sane over Zoom when we both caught Covid.

To the other members of my PhD group who have been by my side throughout this experience, Annie, Grace C, Grace D and Sarah, I feel very lucky to have been part of this with you. Extra big love to Sarah for being a stand out housemate and undefeated programme seller, and to Grace D for being the best write-up buddy and keeping me sane.

Finally, thank you to my family for their tremendous support, love and many, many vegan snacks.

This thesis is dedicated to Professor Simon McQueen-Mason, who was a part of so many of my PhD experiences and a source of boundless enthusiasm and scientific knowledge; and to my friend Greg, who I always had the best time with, taught me how to take over a dance floor, and who I wish I'd had more time with. Thank you for being such a good friend.

Author's declaration

I declare that the work presented in this thesis is my own original research, except where due reference has been given to collaborators and co-workers.

This thesis has not previously been presented for an award at this, or any other, University.

All sources are acknowledged as references.

Abbreviations

ABC	ATP-binding cassette
(A)	Agar
$^1O_2$	Singlet oxygen
A. halleri	*Arabidopsis helleri*
AAS	Atomic absorption spectroscopy
ABA	Abscisic acid
Ag	Silver
Agrobacterium	*Agrobacterium tumefaciens*
ALA	Aminophospholipid ATPases
ALD	Adrenoleukodystrophy protein related
Arabidopsis	*Arabidopsis thaliana*
ARE	Auxin-responsive element
ARF	Auxin response factors
As	Arsenic
At	*Arabidopsis thaliana*
ATP	Adenosine 5′-triphosphate
Au	Gold
Ca	Calcium
CaMV-35S	Cauliflower mosaic virus 35S promoter
Cd	Cadmium
cDNA	Complementary DNA
Cl	Chlorine
Co	Cobalt
Col0	Columbia-0
COPT	Copper uptake transporter
COPT2	Copper uptake transporter 2
Cr	Chromium
CT	Cycle threshold
CTAB	Cetyltrimethylammonium bromide
CTCF	Corrected total cell fluorescence
Cu	Copper
CYP	Cytochrome P450
D. alaskensis	*Desulfovibrio alaskensis*
DCF	Dichlorofluorescein
DE	Differentially expressed
DEG	Differentially expressed gene
DMSO	Dimethyl sulfoxide
DNA	Deoxyribonucleic acid
dNTP	Deoxynucleoside triphosphate
E. coli	*Escherichia coli*
ER	Endoplasmic reticulum
Et	Ethylene
FAS	Flame emission spectroscopy
Fe	Iron
FPKM	Fragments per kilobase million
FRO4	Ferric Reductase Oxidase 4

FRO5	Ferric Reductase Oxidase 5
GABA	Gamma-aminobutyric acid
gal	Galactose
GC	Guanine cytosine
gDNA	Genomic DNA
GF-AAS	Graphite-furnace AAS
glu	Glucose
GO	Gene ontology
GP	Gold-nanoparticle forming peptide
GPD	Glyceraldehyde-3-phosphate dehydrogenase
GS	Glutamine synthetases
GSH	Glutathione
GST	Glutathione transferases
H_2DCF	2',7'-dichlorodihydrofluorescein
H_2DCFDA	2´,7´-dichlorofluorescin diacetate
H_2O_2	Hydrogen peroxides
HA	Hyperaccumulator
HCl	Hydrochloric acid
Hg	Mercury
HMA	Heavy metal associated protein
ICP-MS	ICP mass spectrometry
ICP-OES	Inductively coupled plasma optical emission spectroscopy
IDT	Integrated DNA technologies
Ir	Iridium
JA	Jasmonic acid
JA-Ile	Jasmonyl-isoleucine
JAT	Jasmonic acid transporters
JAZ	Jasmonate zim-domain
K	Potassium
kb	Kilobase
kg	Kilogram
LB	Luria broth
LB	Left border
MATE	Multidrug and toxic compound extrusion
MDR/TAP	Multidrug resistance / Transporter associated with antigen processing
Mg	Magnesium
miRNA	Micro RNA
mRNA	Messenger RNA
MRP	Multidrug resistance-associated protein
MS	Murashige & Skoog
MT	Metallothionein
N	Nitrogen
N. caerulscens	*Noccaea caerulescens*
Na	Sodium

NADH	Nicotinamide adenine dinucleotide (NAD) + hydrogen (H)
NADPH	Reduced nicotinamide adenine dinucleotide phosphate
NAP	Non-intrinsic ABC protein
NASC	Nottingham Arabidopsis stock centre
Ni	Nickel
NIP	Nodulin-26-like intrinsic protein
nm	Nanometre
NP	Nanoparticle
NPK	Nitrogen phosphorus potassium
NRAMP	Natural resistance-associated macrophage protein
NRC	National research council
nt	Nucleotide
O. muralis	*Osbeckia muralis*
O_2^-	Superoxide
OABP	Organic anion binding protein
OH$^{\cdot}$	Hydroxyl radical
ORF	Open reading frame
ori	Origin of replication
P	Phosphorus
Pb	Lead
PBS	Phosphate-buffered saline
PC	Phytochelatin
PCA	Principal component analysis
PCR	Polymerase chain reaction
Pd	Palladium
PdNP	Palladium nanoparticle
PDR	Pleiotropic drug resistance
PGM	Platinum group metal
PIP	Plasma membrane intrinsic protein
polyA	Polyadenylated
ppb	Parts per billion
ppm	Parts per million
Pt	Platinum
qPCR	Quantitative PCR
R. serpentina	*Rauvolfia serpentina*
RB	Right border
RNA-seq	RNA sequencing
ROS	Reactive oxygen species
RPK	Reads per kilobase
RPKM	Reads per kilobase million
rRNA	Ribosomal RNA
RT-PCR	Reverse transcription polymerase chain reaction
SA	Salicylic acid
SBS	Sequencing by synthesis

SC	Synthetic complete
SD-U	Synthetic defined medium without Uracil
SIP	Small basic intrinsic proteins
SpR	Spectinomycin resistance
StR	Streptomycin resistance
T1	Transgenic generation 1
T2	Transgenic generation 2
T3	Transgenic generation 3
TAE	Tris-acetate-EDTA
TAIR	The Arabidopsis Information Resource
TAP	Transporter associated with antigen processing
T-DNA	Transfer DNA
TIP	Tonoplast intrinsic protein
Tm	Primer melting temperature
TMD	Transmembrane domain
Tobacco	*Nicotiana tabacum*
TPKM	Transcripts per kilobase million
tRNA	Transfer RNA
UNAMIT	Usually multiple acids move in and out transporters
UV	Ultraviolet
vir	Virulence
WT	Wild type
XRF	X-ray fluorescence
YPD	Yeast peptone dextrose
ZIP	Zinc-regulated, iron-regulated transporter-like protein
Zn	Zinc

1. Introduction

Recent public actions have put pressure on governments to move towards a greener, more sustainable society, and bio-based approaches are becoming recognised for their potential to help solve environmental issues. Worldwide, metal pollution of waters and soils is a major environmental topic with mining activities playing a significant role. The extraction and purification of metals including Au and Pd are by far the most energy-requiring step in the lifecycle of these elements. Furthermore, these steps generate a huge volume of waste, often stored as toxic tailing sludge (1). Phytoremediation and phytomining are two processes which could work hand in hand as potentially cost-effective and environmentally friendly approaches for metal recovery and remediation of contaminated soils. Phytoremediation is the process of using plants to remove toxic metals and organic compounds from the environment, and can be used to clean-up polluted land; whereas, phytomining is the process of cultivating plants on a metal-rich medium to extract and accumulate an element of interest, which is then purified from the plant for use in commercial applications (2). Plant mediated clean-up of contaminated soil has many advantages: as a greener alternative to current, chemical-based techniques, potential low maintenance and cost, and with the promise of a further economic incentive through the extraction of metals and plant biomass-derived products (3–5). It is therefore crucial to identify or develop plants capable of withstanding the toxicity of the metal concentration present in these environments, and with a high uptake and biomass production capability. Arabidopsis is a model organism for genetic research in plants and is used in this study as a proxy to investigate the genetic basis for Au and Pd uptake and detoxification. As we move towards a circular economy model for the use of valuable, finite resources, plants can close the circle between use, dilution, and dispersal into the environment, and allow recapture in an economically viable form. Developing an efficient real-world application of phytomining faces several obstacles. There would need to be significant investment to identify potential sites, engineer or identify suitable plants, and generate the necessary infrastructure. Noble metals such as Au and Pd are an excellent focus for phytomining due to the high, and increasing value of these metals, which could help to alleviate the costs of the process. Plants involved in phytomining would need to have high uptake and tolerance. Hyperaccumulators (HAs) are plants that have evolved to accumulate a high concentration of metals in their shoot tissue with little adverse effects due to an abnormally high concentration of the metal in their natural environment (6,7). Natural hyperaccumulators would be ideal for phytomining, as these plants have adapted to have high tolerance to the metal present in their environment; however, there are no known hyperaccumulators of Au or Pd. The process of phytomining Au and Pd, including the obstacles and opportunities, are explored in further detail in this introduction.

1.1. Phytomining

Phytomining or phytoremediation could remove or stabilise pollutants from the soil, sediment, water and air, maintain the structure and fertility of the soil (8), and present a low cost and publicly acceptable approach (9). Li et al., (2020), published a systematic review of the phytomining research

area, based on citation data (10). Between 1998 and 2022, there were 271 publications related to phytomining, and the chronological distribution of these papers is shown in Figure 1.1. Research into phytomining has slightly increased over the period shown, though this increase is minor compared to other areas of research. The number of publications relating to biofortification, for example, has increased from < 10 publications per year in 2000, to over 350 publications per year by 2019 (11) .
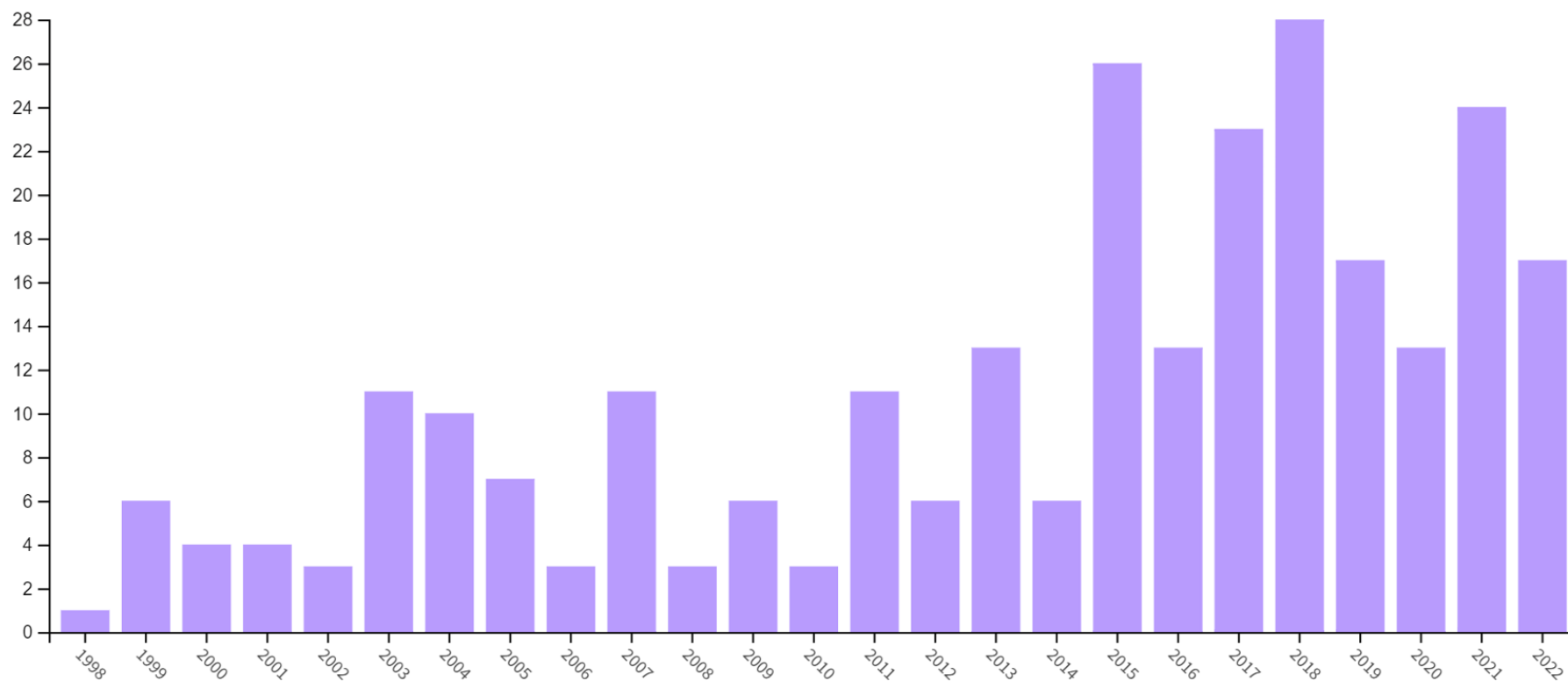
Figure 1.1. Chronological distribution of phytomining research publications (1998 – 2022). Graphic is derived from Clarivate *Web of Science*, Copyright Clarivate 2022. All rights reserved.

There are three main steps in the phytomining process: phytoextraction, enrichment and extraction (12). Phytoextraction refers to the removal of an element of interest from the matrix through plant uptake (13). In the enrichment step, the concentration of the element in the tissue is increased to a level that would result in a cost-effective product, whilst maintaining the health of the plant (12). The extraction process chosen relies upon the downstream applications. The first step is to break down the metal-containing biomass, e.g. by composting, compaction or thermal conversion, followed by isolation of the metal e.g. by acid wash, or smelting (14–16)

1.1.1. Metals of interest

The six platinum group metals (PGM) comprise platinum (Pt), Pd, rhodium, ruthenium, osmium, and iridium; these six metals alongside Au make up the noble metals (17). The noble metals are resistant to corrosion and oxidation under conditions which would otherwise favour these activities, such as high humidity and heat (18). These elements are part of the larger group of transition metals, shown in Figure 1.2, defined by the International Union of Applied Chemistry as an "element whose atom has a partially filled *d* sub-shell, or which can give rise to cations with an incomplete *d* sub-shell' (19).

Figure 1.2. Periodic Table of the Elements. Figure reproduced from the Encyclopaedia Britannica, 2022 (20) The star icons to indicate the Platinum Group Metals (PGMs) / the Noble Metals have been added.

To date, the mechanisms of uptake and detoxification of noble metals in plants have attracted less research attention than metals that are essential to biological processes, or which are more abundant (e.g., Na, Cu, Cd). The noble metals are distributed through the earth's crust at extremely low

concentrations, and the primary ores of Pd and Au are steadily depleting. The concentrations of Pd and Au in the earth's crust are 0.015 mg / kg and 0.004 mg / kg respectively, far lower than Fe at 56,300 mg / kg and Zn at 70 mg / kg (21). However, anthropogenic activities, such as mining, industrial discharge, agricultural activities, and automation have increased the concentration of metals in surface soils significantly. The presence of these polluting metals is a cause for concern as they can enter the food production process, accumulating in plants, livestock and humans to toxic levels (22). Contaminated soils include large swathes of land, which are unfit for use for agriculture or housing (8). Potential phytomining and remediation sites of interest, otherwise unsuitable for extraction using traditional mining methods, are (2,23,24):

- Metalloid contaminated soil

- Mill tailings (the sandy process waste material from mining operations)

- Overburdens (the material that lies above the mineral deposit)

- Low-grade ores (containing a small percentage of the mineral)

- Mineralised soil

1.1.2. Commercial phytomining

Nickel (Ni) is one of the most researched metals in the field of phytomining, with multiple Ni HAs species having been identified since *Odontarrhena bertolonii* was first reported to contain a high concentration (> 100 mg / kg) of Ni in the above ground biomass in 1948 by Minguzzi and Vergnano (25). Studies have since explored the application of phytomining Ni from various sources.

The Geissois genera contains several Ni HAs, which are plant species capable of accumulating elements to inordinately high concentrations (26). In 1979, Jaffre et al. investigated 17 *Geissois* species for uptake of Ni, cobalt, chromium or iron (Fe), and identified six HA species (26). The Ni concentration in these six newly discovered HA species was 1000 µg/g or above – a normal Ni concentration lies between 50 – 100 µg/g. Notably, *Geissois intermedia* had 22, 900 µg/g Ni in its above ground tissues. The Geissois species assessed also showed higher than expected chromium content. Plants rarely exceed 10 µg/g chromium, and *Geissois pruinosa* and *Geissois montana* contained 463 µg/g and 197 µg/g chromium in their above ground dry biomass, respectively.

Biomass production and improved soil health are important components of commercial phytomining, as they prolong the use of sites of interest and can help to maximise the total metal content for harvest. In 2018, Osmani et al. performed a three-year study investigating the effect of various agronomic practices on the Ni uptake of *Odontarrhena chalcidica*, a Ni HA species (27). Plants that were irrigated and treated with fertilisers reached a final biomass yield of 1.1 kg/m^2 and an Ni concentration of 853 mg/m^2. In comparison, the maximum biomass of the untreated plants was 0.5 kg/m^2, and the highest Ni concentration was reported at 313 mg/m^2 (27). A field experiment, performed by Rosenkranz et al., in 2019, investigating the potential of *O. chalcidica* and *Noccaea*

goesingensis on an Austrian serpentine (Ni-rich) site (28). The sites were either untreated, sulfur-applied, or had intercropping with the legume *Lotus corniculatus*. The highest biomass achieved was 55 kg Ni/ha in sulfur-treated sites using *O. chalcidica* (28). A follow-on study sought to improve upon the work performed by Rosenkranz et al. in 2019. Hipfinger et al. investigated the effect of fertilisation on Ni phytomining efficiency using *O. chalcidica* (29)*.* It was observed that the plants, grown on an Austrian serpentine site, produced higher biomass when treated with nitrogen-phosphorus-potassium (NPK) fertiliser or pig manure than the untreated plants. Whilst there was no significant difference in Ni concentration, the soil quality was also substantially improved following fertilisation (29). A one-year field study carried out in a serpentine quarry in Galicia, Spain, tested the Ni uptake of the Mediterranean HA plants *Bornmuellera emarginata* and *Odontarrhena muralis* alongside the native populations of *Noccaea caerulescens* and *Odontarrhena serpyllifolia* (30). The compost amended soil demonstrated a reduced soil pH from 7.8 to 6.6, increased soil cation exchange capacity, nutrient contents, and Ni availability, microbial density, and activity. The biomass produced was significantly higher in the compost amended soils than after NPK fertilisation, and whilst the shoot Ni concentration decreased in plants (except for *O. muralis*) in the compost amended conditions, the increase in biomass production increased the total extract Ni concentration significantly (30).

Noble metals are used in diverse applications, from jewellery to industrial, technological, or medical applications. As shown in Figure 1.3, despite the primary ore supplies becoming exhausted, the supply, demand, and subsequently the price of noble metals is steadily increasing as more applications take advantage of their unique properties. The price of one kg of Au has increased from $46,973 in 2018 to $65,856 in 2021, a little over 40% price increase over three years (31); the cost of Pd has had an even sharper rise, from $ 35,411 in 2018 to $77,103 in 2021, a 118 % price rise over the same period (32). The proportion of metals that are recycled has gradually increased over the past few years, accounting for around 15 – 25 % of the total supply. Current recycling techniques focus mainly on recovery from electronic wastes or spent catalysts (33), but phytomining offers another option for recovery of these finite, important metals (34).
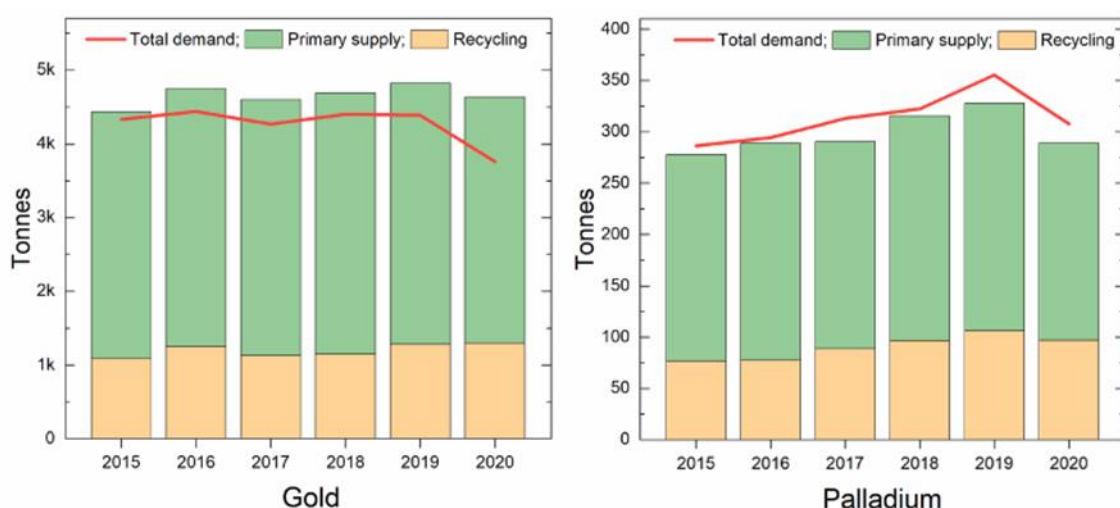
Figure 1.3. Supply and demand of Au and Pd between 2015 – 2020. The decline in supply and demand in 2020 was a result of the Covid-19 pandemic triggering mine closures and disruption in many sectors (17).

Anderson et al., (2005), stated that a yield of 1 kg / ha of Au would make phytomining economically viable (35). This analysis reflected the price of Au in 2005, which was ~$650 / oz. As shown in Figure 1.4, the price of Au in 2022 is $1950 / oz, three times this value, and it has not been lower than $1300 / oz since 2010 (36). The price of Pd in 2022 is comparable at $1800 / oz (37). At the current Au or Pd price, a yield of 0.33 kg / ha Au or 0.36 kg / ha Pd would make phytomining economically workable, according to the analysis performed by Anderson et al., (2005) (35).

Figure 1.4. Historical price of Au (A) and Pd (B) over the past 20 years. The prices shown have been inflation-adjusted, and periods of global recession are shown in grey (36,37)

1.1.3.   Phytoextraction and metal accumulation

There are three classifications of plants dependent on their metal uptake ability; indicators, excluders and HAs (7). Indicators concentrate metals in their tissues at levels that reflect the abundance in the surrounding environment, and therefore can be used for exploring potential sites for phytomining. Excluders utilise an avoidance approach to grow in soils containing high metal concentrations, and do not accumulate elevated levels of metals in their tissues. Hyperaccumulators are plants that can accumulate a high concentration of metals in their shoot tissue with little adverse effects (6,7). There have been over 400 HA species reported, but none for Au or Pd (38).

The phytoextraction capability of several plant species have been assessed on waste mining substrates, and the varied concentration of Au and Pd in these studies reflects the real-life nature of Au or Pd concentration to vary between and within substrates. Gold cyanidation is a hydrometallurgical process which results in the extraction of Au from ore by converting the Au to a water-soluble complex, dicyanoaurate, which can then be taken up by plants (39). The uptake capabilities of *Brassica juncea* and *Zea mays* were investigated on an ore pile substrate containing 0.6 mg / kg Au, following cyanide and thiocyanate treatment (35). *Brassica juncea* had previously been shown to exhibit induced hyperaccumulation of Au following soil amendment with ammonium thiocyanate (40), and in this study demonstrated 39 mg / kg Au in biomass following soil treatment with sodium cyanide (35).

Australian native plant species and exotic agricultural species were tested for their Au uptake ability on oxide ore containing 1.75 mg / kg Au, using cyanide-induced phytoextraction of Au from crushed ore (41). Two concentrations of cyanide were tested (1 g / kg vs. 0.1 g / kg) and the higher concentration of cyanide resulted in a higher shoot Au concentration in *Trifolium repens* (41).

Helianthus annuus (Sunflower) and *Kalanchoe serrata* were tested on mine tailings treated with sodium cyanide, ammonium thiocyanate, ammonium thiosulphate, and thiourea containing 2.35 mg / kg Au (42). Treatment with these lixiviants resulted in an increase in the concentration of Au in the plant biomass, but also severely reduced the health of the plants. The reduction in plant health was suggested to result from toxic concentrations of elements, e.g., Cu, as a result of the soil amendments. The studies referenced above utilised 'induced hyperaccumulation,' which involves pretreating the substrate with a chemical to increase the bioavailability of the metal. However, the chemicals used to treat the ore can remain in the substrate and potentially be hazardous to humans and the environment. Using chemical lixiviants as a bulk technique to extract desired metals from a substrate has the potential to cause environmental and human harm, resulting in the release of contaminating chemicals (including the lixiviant itself and any released chemicals) into the surrounding environment. The National Research Council (NRC) (2003) stated that 'if contaminants in soil and sediment are not bioavailable, then more contaminant mass can be left in place without creating additional risk' (43). Therefore, the development of phytomining technologies that do not rely upon the addition of lixiviants would be beneficial to human and environmental health.

1.1.4. Extraction of metals from biomass following phytomining

Following remediation of soils by the plant-mediated uptake and accumulation of metals, the ultimate step in the phytomining process is to access the metals that are stored in the plant tissues. There are several approaches that have been assessed to access this resource, many involving extraction by ashing and then treatment with chemical leaching agents. These approaches use potentially costly and potentially dangerous solvents, the disposal of which generates further costs and complications due to the associated environmental problems. An interesting approach is to sidestep the chemical extraction process, and utilise the NP-containing plant biomass as a catalyst (15). In work described by Parker et al. (2014), liquid culture-grown Arabidopsis plants were dosed with an aqueous solution of K_2PdCl_4, and biomass carbonized under pyrolysis (decomposition bought about by high temperatures). The resultant carbon-supported PdNP matrix was used in a range of Suzuki-Miyaura reactions, described in detail in chapter 4, and the matrix was successful at catalysing reactions to produce high yields even compared to commercially available catalysts (15); therefore demonstrating that it is possible to produce commercially useful NPs from plant tissue, without needing high volumes of potentially toxic chemicals or an energy intensive process.

1.2. Nanoparticles

Nanoparticles are defined as particles with sizes between 1 to 100 nm, that have properties that are absent from the bulk metal: they have a large surface-to-volume ratio, more energised surface molecules, and an electron confining ability (44,45). These NP-specific features mean they are used in a range of technologies, with the properties of Au shown, as an example, in Figure 1.5 (46,47).
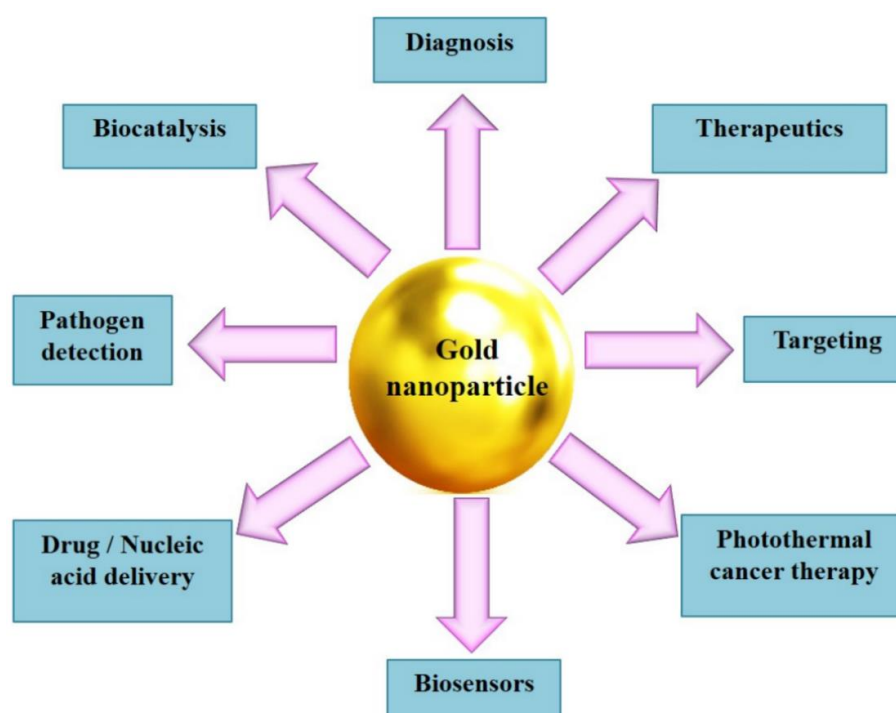
Figure 1.5. Multifunctional applications of AuNPs (47)

The AuNPs have a unique interaction with visible light that allows them to be used in high technology applications such as sensory probes, therapeutic agents, drug delivery in biological and medical applications, electronic conductors, and catalysts. Many diverse industries rely on AuNPs, electronics, catalysis, cancer detection, paints, food-quality checking and cosmetics (48,49). The surface plasmon resonance (SPR) of AuNPs mean that differently sized NPs absorb and scatter light of different intensities. As shown in Figure 1.6, this property means that a red/purple colouration is indicative of AuNP formation. The red or purple colour of solutions containing AuNPs results from the conduction electrons on the NP surface undergoing a collective oscillation when they are excited by light at specific wavelengths.

Figure 1.6. Colour of AuNPs compared to the bulk metal in a stable solution in water. The sizes of the NPs in solution are 20 nm (left), >100 nm (middle) and the 'bulk' metal (right). Image reproduced from Sustainable Nano website (50)

The SPR causes the absorption and scattering intensities of AuNPs to be much higher than identically sized non-plasmonic NPs. The AuNP absorption and scattering properties can be tuned by controlling the particle size, shape, and the local refractive index near the particle surface.

The optical properties of AuNPs change when NPs aggregate and the conduction electrons near each NP surface become delocalized and are shared amongst neighbouring NPs. When this occurs, the SPR shifts to lower energies, causing the absorption and scattering peaks to red shift to longer wavelengths. UV-Visible spectroscopy can be used as a simple and reliable method for monitoring the stability of NP solutions. As the solution becomes more acidic, the carboxy group is protonated and the zeta potential is reduced, resulting in destabilized NPs that aggregate (44).

1.2.1.   Nanoparticle synthesis

Conventionally NPs have been synthesised by various physical and chemical methods, which can negatively impact the environment (51). Plant-mediated NP synthesis may present a greener alternative to current chemical production techniques, avoiding the use of toxic chemicals or an energy-intensive process (15,52). Taylor et al., (53) and others (52,54–56), have reported that Au and Pd are deposited *in planta* as NPs. Both Au and Pd NPs have been synthesised by biogenic approaches utilising plant extracts of various species such as *Glycine max* (soy bean)*, Musa paradisiac* (banana)*,* and *Pinus resinosa* (51); however, there has been less research into Au and Pd NPs *in planta.* In living organisms, NPs are composed of a core and a surrounding layer (corona) formed of ions, and inorganic and organic compounds. Organic compounds surrounding an inorganic NP core are stabilising agents, preventing further growth of the NP and inhibiting aggregation of bare NPs that would otherwise come together and fall out of solution (57,58).

Whilst plants can produce metal NPs, the size and morphology vary depending on their localisation, potentially hindering their use in applications where specific, finely tuned sizes and shapes are required (51). It would therefore be beneficial to manipulate the morphology of these NPs (59,60). As mentioned earlier, following a low-energy pyrolysis treatment, NP-containing Arabidopsis plant biomass could be used as a catalyst with activity comparable to commercially available catalysts, adding value beyond recovering the bulk metal (5,15). In addition, life cycle analysis studies predict that this method of catalyst production could be more environmentally friendly than current, chemical-based techniques (5).

1.2.2.   Manipulating NP formation in plants

In plants, NPs are very frequently found in association with specific peptide sequences (59). Tan et al., (2010), analysed the 20 naturally occurring amino acids individually to determine their potential for reduction or binding of metal ions, the two features that are most important in AuNP formation, as shown in Figure 1.7 (59).
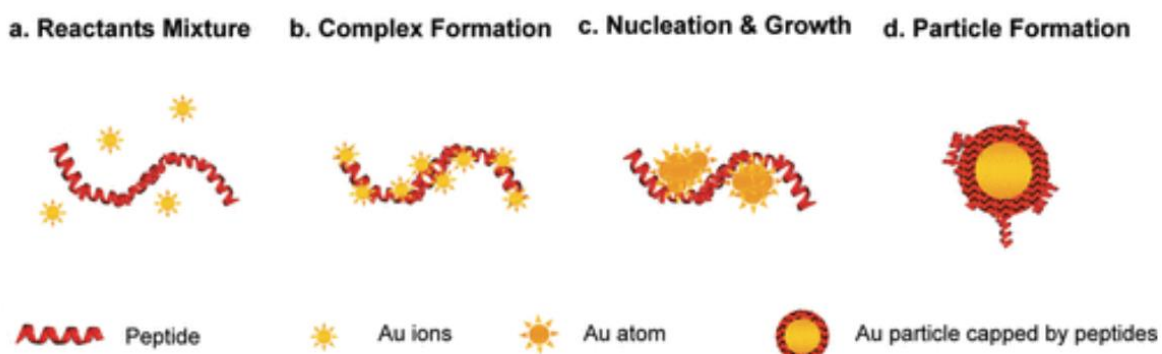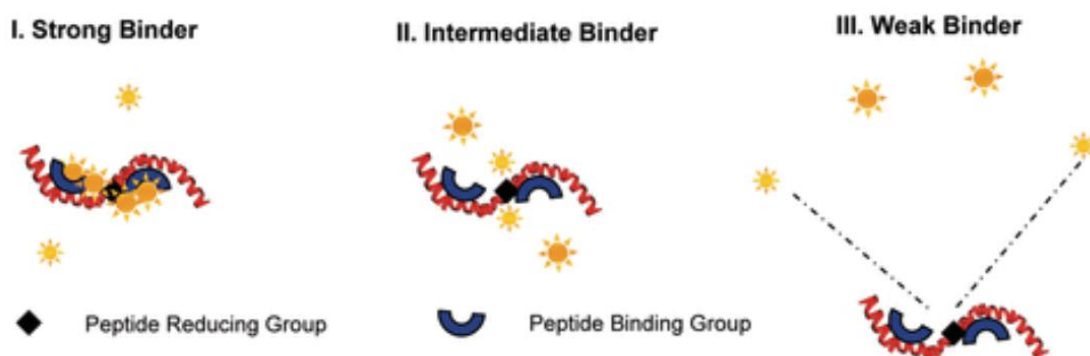
Figure 1.7. Schematic 1: A proposed model for the peptide synthesis of gold nanoparticles (AuNP) in an aqueous solution. (a) The reactant mixture of peptides and chloroaurate ions. (b) The formation of peptide−AuCl$_4^-$ complexes. Strong complexes inhibited the subsequent reduction to Au(0). (c) Reduction facilitated by peptides to form Au atoms for nucleation. (d) Growth of nuclei into crystalline particles by addition of more Au atoms from the solutions or by fusion with other nuclei. Schematic 2: The molecular interactions between peptide and Au ions and peptide and Au atoms which determined the reactivity of the peptide for reduction. The reducing residues of the peptide were sandwiched by the (I) strong, (II) intermediate, and (III) weak Au-binding residues, respectively. Figure reprinted (adapted) with permission from Tan et al (2010). Copyright 2022 American Chemial Society (59).

The amino acid sequence of a peptide can greatly affect the size, morphology, and number of nascent NPs because of the binding capability of residues in proximity to those with a high reduction ability (59). Amino acid sequences identified by phage-display were found to dictate AuNP morphology when used to form a repeating peptide sequence, GASL- and SEKL- (61). These sequences were incorporated into peptides, bordering residues found to have specific binding and reduction capabilities (59). As shown in Figure 1.8, the synthetic peptide GASLWWSEKL (reducing residues underlined) rapidly reduced metal ions to form small (> 10 nm in diameter) NPs. When these sequences were swapped to form the peptide SEKLWWGASL, this led to a slower reduction reaction that resulted in the formation of larger nanospheres and nanotriangles about 40 nm in diameter (59).

Slower reduction kinetics result in larger AuNPs, and faster reduction kinetics result in smaller AuNPs (59).
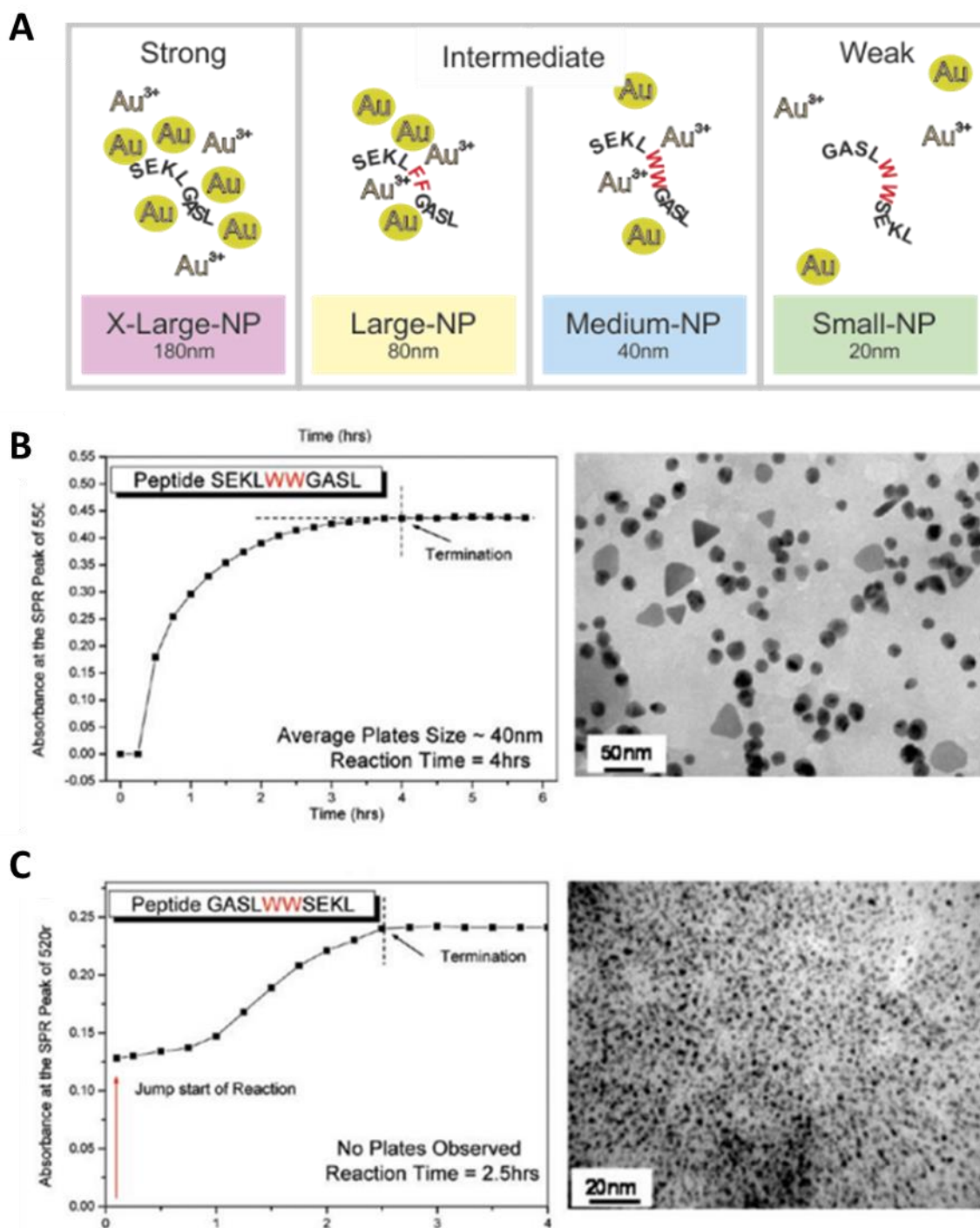
Figure 1.8. The amino acid sequence of short, synthetic peptides shown to influence the formation of NPs *in vitro*. (A) The amino acid sequences tested and the size of NP formed as a result. *In vitro* TEM images (right) and the corresponding reduction kinetics of peptide directed synthesis of AuNPs (left) using short, synthetic peptides. Amino acids in red show the reducing residues. (B) SEKLWWGASL amino acid sequence. (C) GASLWWSEKL amino acid sequence. Panels (B) and (C) were reprinted (adapted) with permission from Tan et al. Copyright 2022 American Chemical Society (59)

Preliminary, unpublished studies by Dr. Liz Rylott have shown that plants expressing these short, synthetic peptides can be used to seed the formation of size controlled AuNPs *in planta*. Manipulating the NP formation in aerial tissues using this method could potentially be used to increase uptake, translocation, NP deposition and improve catalytic ability. The peptides in these lines are under the control of the near-constitutively expressing CaMV35S promoter, and transgenic plant lines were generated by the *pART7* and pART27 binary vector system for *Agrobacterium*-mediated plant transformation by floral dip. As shown in Figure 1.9a, the plant material exposed to Au became a brown/purple colour, indicating the formation of NPs in the tissue. The wild type (WT) plants demonstrated a wide range of AuNP sizes as shown in Figure 1.9b. With the expression of peptides shown to seed the formation of *X-large, Large, Medium* or *Small* NPs, the distribution of NP sizes is altered in these plant lines. The plants expressing the *X-large* peptides had a smaller distribution of NPs below 10 nm in diameter ($p < 0.05$), and a larger distribution of NPs above 30 nm in diameter compared to the WT ($p < 0.01$).
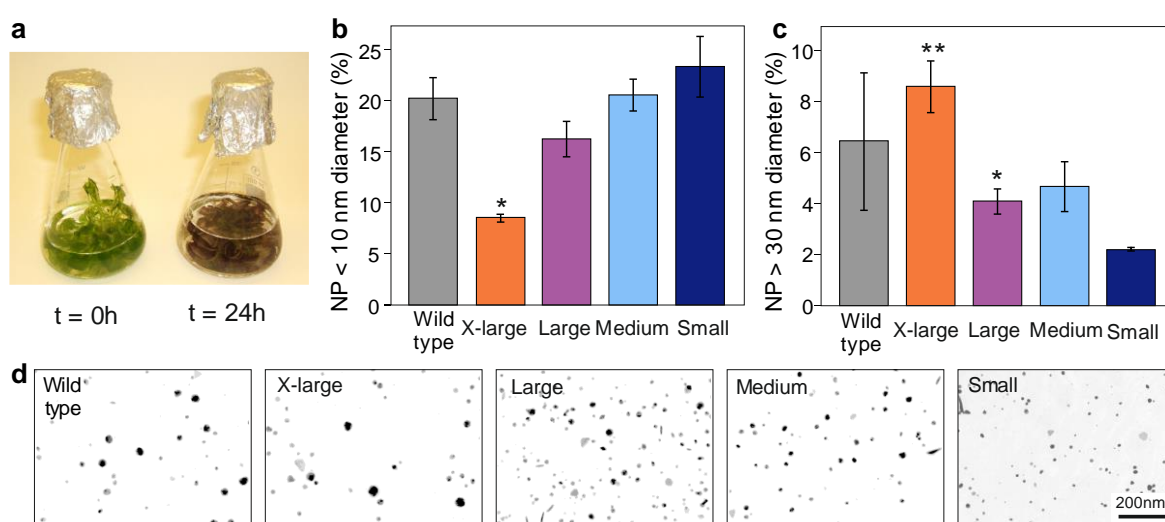
Figure 1.9. Liquid culture grown Arabidopsis exposed to Au. (a) Appearance of three week old, liquid culture grown plants prior to, and 24 hours after, dosing with 0.75 mM potassium (III) tetrachloroaurate. (b) and (c) Percentage distribution of NP diameters in liquid-culture-grown Arabidopsis plants expressing synthetic peptides. Results are mean from three sections from each of three independently-transformed lines ± SD. (d) Representative transmission electron micrographs showing NP present in the plastids. Figure received with gratitude from Dr Liz Rylott, University of York.

This work presents evidence of the use of synthetic biology to help engineer plants to function as factories for generation of size-controlled NPs, using a AuNP-forming peptide (GP).

1.3. Metals in plants

Plants require a vast array of components from their environment to survive, and these components are kept in a careful balance. The need for water, for cell expansion and maintaining structure, amongst its other roles, is balanced by its loss through stomatal pores which must open to allow the acquisition of necessary carbon dioxide from the air. Plants use the high concentration of solutes in their cells to generate osmotic forces which drive the uptake of water from soil. However, with too much water in the soil, there is little space for the oxygen required for respiration to exist in between soil particles, resulting in oxygen starvation. Alongside maintaining a water balance, plants need to acquire organic and inorganic components from the soil which may be in limited quantity. These components reside in the cells of plants for many different purposes, in diverse tissue and cellular localisations. The targeting of these components to tissues or cellular compartments is necessary to permit many different processes to occur at the same time, and requires transport across membranes both within and between organelles (62).

To access these necessary solutes, which include metals, they must be accessible to the plant. The bioavailability of metals in soil can be altered by chemical weathering and biological processes. The 'bioavailability processes' have been defined by the NRC committee (43) as 'the individual physical, chemical and biological processes that determine the exposure of organisms to chemicals present in soils and sediments'. There are four processes involved:

1. Release from the solid phase

2. Transport to the membrane of an organism

3. Movement across a physiological membrane

4. Incorporation into an organism through metabolic processes (43)

The bioavailability of metals has since been described in three theoretical stages, shown in Figure 1.10 (63,64):

- Environmental availability, or bioaccessible content
- Environmental bioavailability
- Toxicological bioavailability
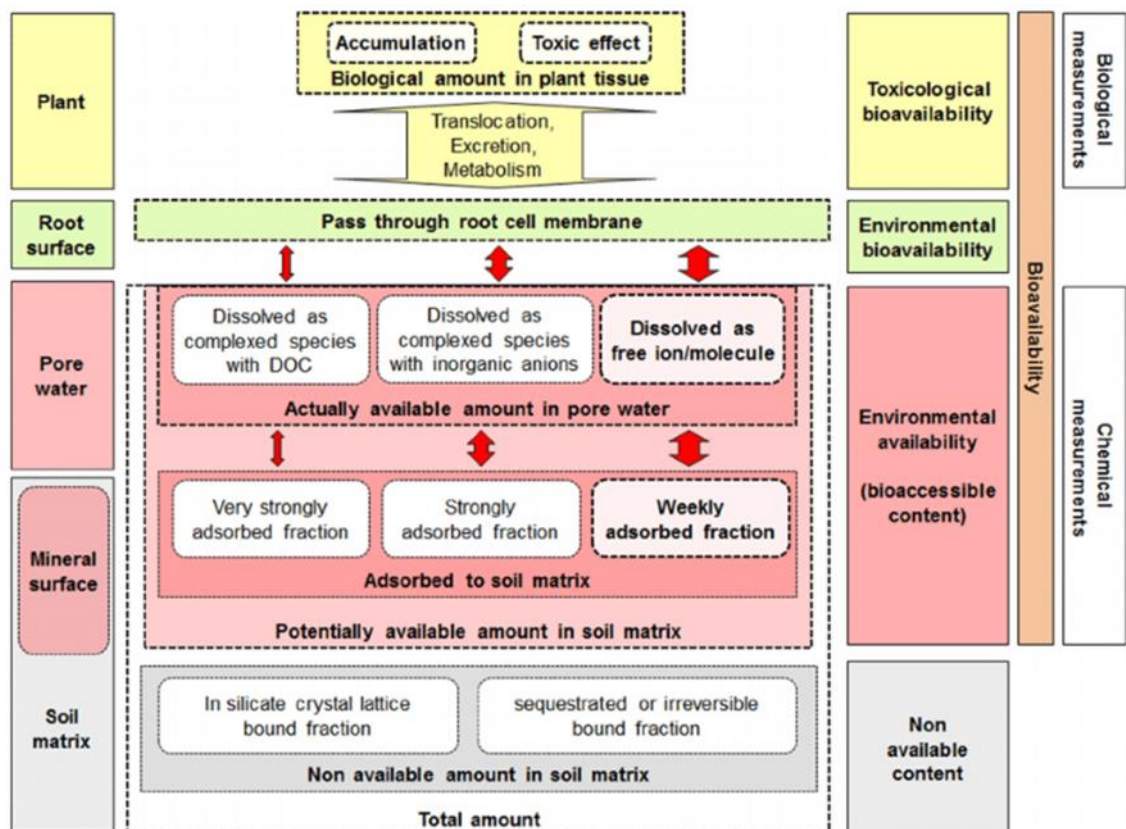
Figure 1.10. The three-step concept of metal bioavailability in soils for plants. Thick arrows indicate the most important factors affecting bioavailability. The 'bioavailability' definitions, 'toxicological bioavailability', 'environmental bioavailability' and 'environmental availability' or 'bioaccessible content', and 'non available content' are used to describe the various states of metals. The 'non-available content' refers to metals that cannot be accessed by plants as they are irreversibly bound to the soil matrix. The 'environmentally available' or 'bioaccessible content' refers to metals that are available to the plant but not in the immediate surrounding environment. The 'environmentally bioavailable' content refers to the metal content within the immediate surrounding substrate of the root system. The 'toxicologically bioavailable' content refers to the content of metals within the plant tissue. Figure reproduced from Kim et al (2007), following modification after Derz et al.2012 ; Harmsen 2007 ; ISO 2008; Lanno et al.2004. Reprinted with permission from Springer Nature: Environmental Geochemistry and Health (65).

The environmentally available or bioaccessible content of metals in the soil depends on the properties of the soil (e.g. composition, pH, water content) and the properties of the metal, and includes the directly available pool of metals in the pore water as well as the potentially available fractions which could be desorbed from the soil matrix (64) (Figure 1.10). The environmentally available content may include dissolved ions and those which have been complexed with dissolved organic matter or with inorganic anions. The environmentally bioavailable content is the portion of

dissolved ions in the pore water which is available to be extracted by the plant through the root system (Figure 1.10). The third concept, toxicological bioavailability, is the biological engagement of metals within plants, including processes such as translocation, metabolism, and detoxification. All these processes are important at various stages of the phytomining process; metals within the soil need to be made available to plant uptake systems without using bulk lixiviants (mainly used for noble metals), which have the potential to cause environmental and human harm, and plants need to be able to obtain a high metal concentration and subsequent detoxification of metal ions above a toxic level, combined with efficient translocation to the shoot tissue for ease of harvest.

Whilst the metallic requirements of different plant species vary wildly, plants require the same 'essential' solutes: nitrogen (N), phosphorus (P), sulfur (S), potassium (K), magnesium (Mg), calcium (Ca), Fe, Manganese, zinc (Zn), copper (Cu), boron, molybdenum, chlorine, and Ni, and potentially sodium and silicon. Neither Au nor Pd are essential metals, but if plants are to be engineered for enhanced uptake of these elements, the underlying cellular metal homeostasis needs to be studied. Due to the essential nature of many metals for the proper functioning of plants, there is a conserved network of interacting proteins which manage their concentration. When both deficient and surplus concentrations of metals produce toxic impacts in plant tissues, the end result is a complex and tightly controlled homeostasis of many metals in plant tissue (66). For example, transporters, chaperones, and P-type ATPases respond to changes in Cu concentration at both high and low concentrations. Specifically, del Pozo et al (2010) found that the expression level of the transporters *COPT2, COPT4, ZIP2*, and the *CCH* chaperone were downregulated in response to excess Cu. The transporter genes *HMA1, PAA1, PAA2* and *RAN1* demonstrated reduced transcript levels following Cu exposure, though *HMA5* was upregulated in roots. Contrastingly, Cu chaperones *ATX1, CCS, COX17-1* and two putative mitochondrial chaperones were up-regulated in response to excess Cu. In response to Cu deficiency, *COPT2, ZIP2, HMA1* and *PAA2* were upregulated in the shoot tissue (66).

1.3.1.   Uptake of metals in plants

Metal bioavailability is a key factor controlling metal uptake by plants. In soils, bioavailability can be influenced by numerous factors: pH, redox potential, soil type, cation exchange capacity, metal concentration, microbial presence, and the mycorrhiza. Metals are absorbed, as cations, through the roots with some translocation to aerial tissues.

Plants use root exudates to increase the accessibility of the bioaccessible fraction of metals adsorbed to the soil matrix or available in pore water in the rhizosphere (67) (Figure 1.10). Uptake occurs by passive (by diffusion or mass flow) and active (metabolic) processes (Figure 1.10). Specialised transporters or H^+-coupled carrier proteins at the root cell plasma membrane mediate influx and efflux of metal ions in root cells and for translocation to the shoots (68). The metal transporters identified in plants are categorised by sequence homology into diverse transporter families, including the COPTs, HMAs, NRAMPs, MATEs, MTPs and ZIP proteins, and shown in Figure 1.11.
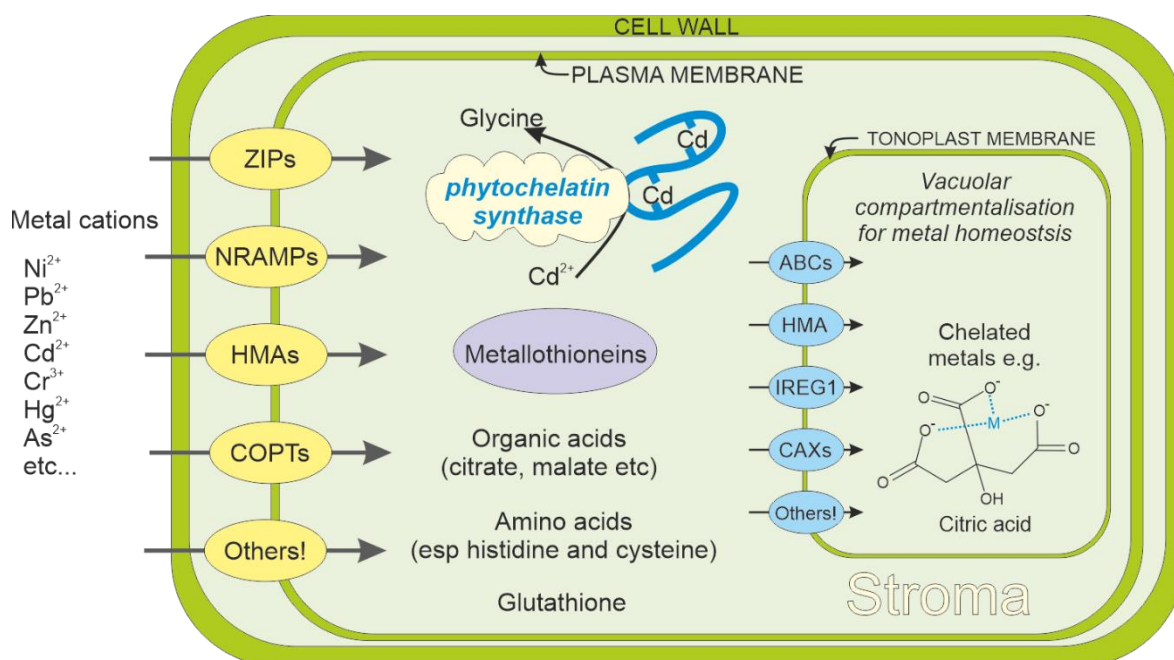
Figure 1.11. A schematic diagram showing some of the mechanisms involved in metal uptake and detoxification in plants. Metal cations can be taken up into the cell by plasma membrane located transporters (e.g. zinc-regulated, iron-regulated transporter-like protein (ZIP), natural resistance-associated macrophage protein (NRAMP), heavy metal ATPases (HMA), copper uptake transporter protein (COPTs)) where they may interact with metallothioneins, organic acids, amino acids, glutathione or phytochelatins. The chelated metals may be transported into the vacuole for compartmentalisation by vacuole located transporters (e.g. ATP-binding cassette transporters (ABCs), HMAs, iron-regulated transporter 1 (IREG1), or cation antiporters (CAX)). Efflux from the cell also plays a key role in detoxification, though the transporters are not shown in this diagram.

1.3.1.1. Cu uptake transporter 2 (*COPT2*)

The Cu transporter family (Ctr in yeast, COPT in Arabidopsis) functions alongside Ferric Reductase Oxidase 4 and 5 (FRO4, FRO5). These cell surface metalloreductases reduce Cu^{2+} to Cu^+ to allow for transport inside the root cell via the COPT proteins (69,70). Vital to many metabolic processes in plants, Cu can act as a cofactor in electron transfer proteins and metalloenzymes to catalyse redox reactions and electron chemistry (71). In soils, Cu is transported inside plant cells by divalent metal ion transporters such as Zn-/Fe-regulated transporter proteins two and four (ZIP2, ZIP4) (72). The membrane located COPT2 proteins are formed of three monomers, each containing three transmembrane domains (TMDs) linked by two loops, with the C-termini and the first loop located in the cytosol (73). As shown in Figure 1.12, the COPT family of proteins have conserved features. The conserved features include three TMDs, with an essential Mx3Mx12Gx3G motif within TMDs two and three, and an amino-terminal region rich in methionine and/or histidine residues (74). The X-ray crystal structure of the *Salmo salar* (salmon) Ctr1 protein has been studied in the Cu^+ free and Cu^+ bound state. It was observed that two layers of methionine triads in TMD2 act as selectivity filers to engage with Cu^+ at the extracellular side of the protein (75).
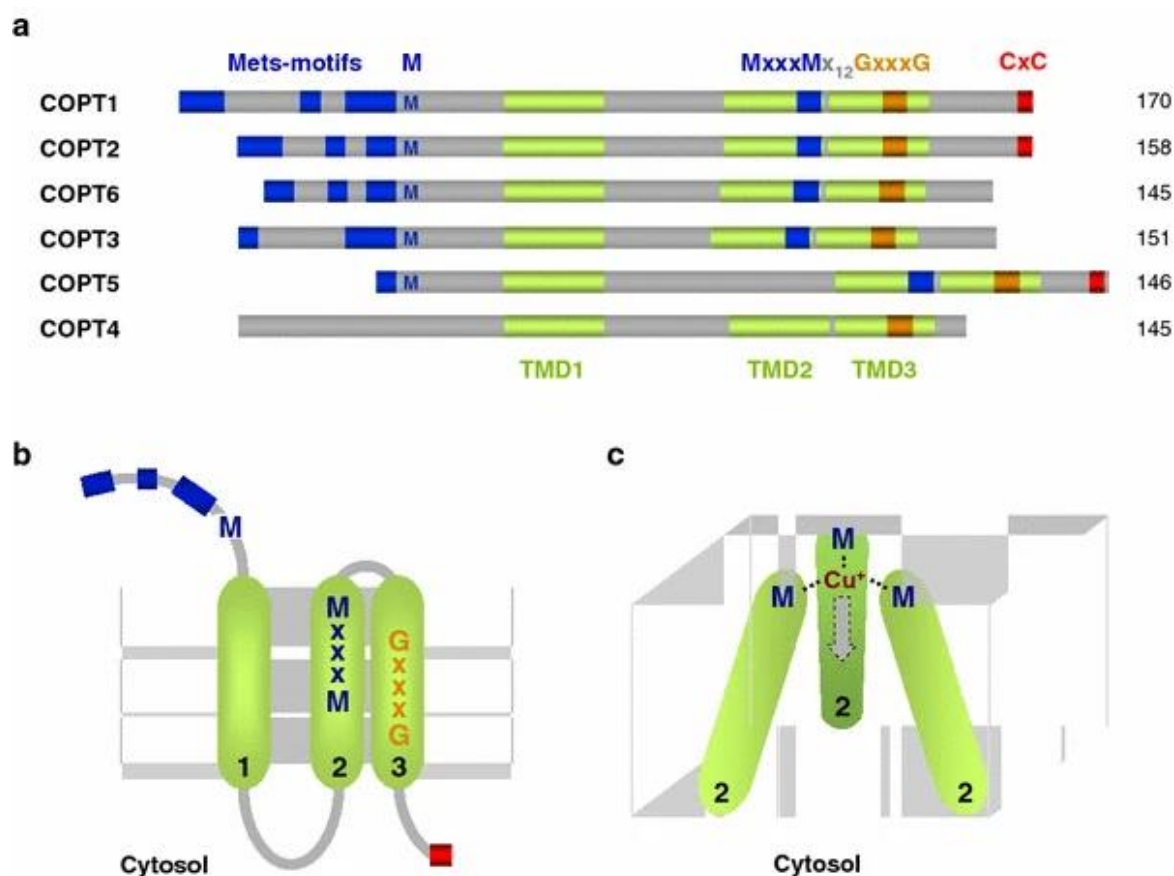
Figure 1.12 The Arabidopsis COPT family of Cu transport proteins. (a) Alignment of the COPT family of Cu transporters. The conserved features include three transmembrane domains (TMD1, TMD1, TMD3 in green), methionine rich motifs (Mets-motifs; consisting of methionine and histidine residues separated by two or fewer amino acids) and MxxxM motifs (in blue), GxxxG motifs (in orange) and CxC motifs (in red). The predicted amino acid length is shown on the right. (b) The proposed topological structure of the COPT proteins. (c) The spacial disposition of TMD2 in the human Ctr1 homotrimer complex. Crucial methionines from different monomers could coordinate Cu^+ during its transport towards the cytosol. Reprinted by permission from Springer Nature: JBIC Journal of Biological Inorganic Chemistry, Peñarrubia et al, 2009 (76)

Three of the six members of the Arabidopsis COPT family reside in the plasma membrane (COPT1, COPT2 and COPT6). These COPT family members regulate the acquisition of Cu from the external surroundings. Of the three other COPT family proteins, COPT3 and COPT5 are located in internal membranes such as the tonoplast, and regulate Cu exit from intracellular stores, while the function of COPT4 is unknown (76–79). Figure 1.13 and Table 1.1 show the localisation of the COPT family members and their roles.
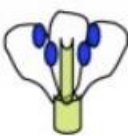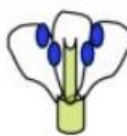
Figure 1.13. Characterisation of Arabidopsis COPT family members COPT1, COPT2, COPT5 and COPT6. COPT3 and COPT4 have not been included due to the small amount of data at the time of this figure being published. Blue highlights on the figure represent expression localisation. (a) Subcellular localisation in Arabidopsis protoplasts, *COPT2*-GPF localisation indicated in green. (b) Transcript regulation in response to Cu deficiency. (c) Expression pattern in flowers. (d) Expression pattern in roots and shoots. (e) Parameters affected in copt lines upon Cu scarcity. Figure reproduced from Puig et al (2014) (80)

Table 1.1. Localisation and role of COPT family members in Arabidopsis

COPT protein	Localisation *in planta*	Intracellular localization	Role
COPT1	Root tips, stomata, trichomes, pollen, embryos	Plasma membrane	Cu acquisition. Increased expression in Cu deficient conditions
COPT2	Young leaves, anthers, root differentiation zones	Plasma membrane , endoplasmic reticulum	Primary COPT gene upregulated in response to Cu deficient conditions
COPT3	Pollen grains and vascular bundles	Intracellular membrane, located at a part of the secretory pathway	Cu remobilisation
COPT4	Unknown	Unknown	Unknown
COPT5	Vascular tissues, higher in roots	Tonoplast	Vacuolar Cu exporter to remobilise Cu from prevacuolar vesicles or recycling vesicles under Cu scarcity
COPT6	Aerial vascular tissues, reproductive organs	Plasma membrane	Shoot Cu redistribution under Cu-deficient conditions

The COPT2 protein was proven by Tiwari et al., (2017) to be involved in Au uptake in Arabidopsis, more details of this finding are described in chapter 3 (4). Previous studies in the Bruce lab at the University of York investigated the transcriptional response of Arabidopsis to Au to identify the in planta mechanisms of uptake and tolerance to this metal (81). As part of these studies, COPT2 was identified as one of the most downregulated genes in a microarray study in response to Au treatment (53). Recent work on COPT2 has confirmed its unique role in Au uptake in Arabidopsis and yeast (4,53,82). Of the six members of the Arabidopsis COPT family, COPT2 is most highly expressed in response to Cu deficiency, and is expressed primarily in the vasculature of the cotyledons and young leaves, apical meristems, trichomes, and in the root elongation zone (76).

1.3.2. Translocation from root to shoot tissue

As shown in Figure 1.14, there are two main pathways that ions dissolved in water travel from the root hair, via the root cortex, to the xylem: the apoplastic pathway (passive diffusion) and the symplastic pathway (active transport). The apoplast is the space outside the plasma membrane, including the cell wall and intercellular spaces. In the apoplastic pathway, ions are transported in water moved through the apoplast of the root. The symplast is made up of a cytoplasmic network of plant cells interconnected by plasmodesmata, co-axial membrane channels that cross walls of adjacent plant cells, connecting the cytoplasm, plasma membranes and endoplasmic reticulum (ER). The symplastic pathway consists primarily of the protoplasm, and the entry of water and ions is mediated by the presence of the Casparian strip and the plasma membrane.
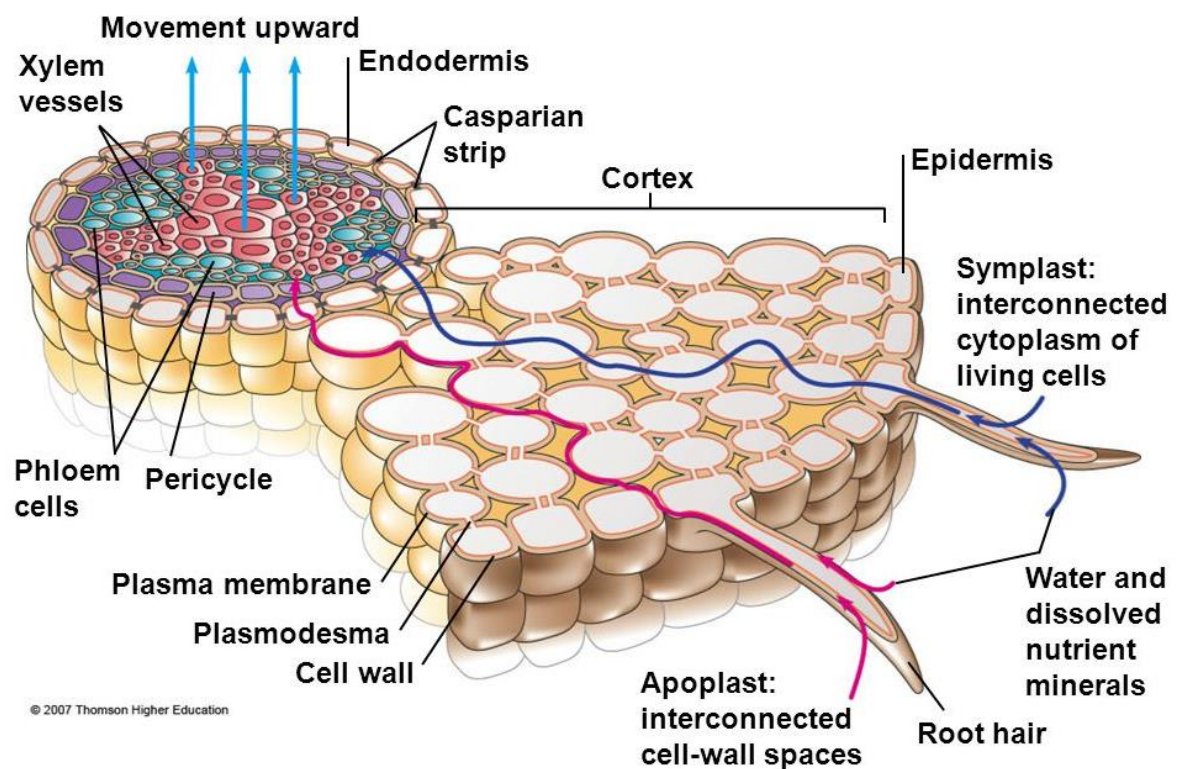
Figure 1.14. The symplastic and apoplastic pathways for water uptake in plants. Water and dissolved ions are taken up into plant tissue through one of two pathways: the symplastic or the apoplastic pathway. The apoplastic pathway involved the interconnected cell wall spaces, and the symplastic pathways involves the interconnected cytoplasm within cells. The apoplastic pathway must enter the symplastic pathway at the casparian strip for water to enter the vascular bundle, which consists of the xylem and phloem. Thompson Higher Education, 2007 .

Inside root cells, metal ions may form complexes with chelators, which can then be held in the apoplastic cellular walls or symplastic compartments (83). Metal ions that have been sequestered in the vacuoles may be transported to the stele, the central portion consisting of the vascular (xylem and phloem) and supporting tissue, and enter the xylem stream through the root symplast for translocation to the shoots (84). At the xylem, water and solutes enter the vasculature from both

pathways through the symplastic pathway, as the Casparian strip blocks movement beyond the cortex. The Casparian strip does not permit the passage of water through the apoplastic pathway, channeling it instead through other wall regions and through the plasma membrane to reach the xylem. Upon reaching the leaves, metals are distributed to extracellular compartments (cell walls) or to the vacuole to prevent the accumulation of damaging levels of free metal ions in the cytosol (85).

1.3.3. Mechanism of toxicity

Metal ions can be toxic to plants when in levels above that required for normal function. Metal cations are oxidising agents, and cause oxidation reactions to occur through their reduction. High levels of oxidizing agents result in a removal of electrons from essential organic molecules, disrupting normal cellular function (86). The reactivity of metal ions can lead to the generation of harmful reactive oxygen species (singlet oxygen ($^1O_2$), superoxide (O_2^-), hydrogen peroxides (H_2O_2) and hydroxyl radicals ($OH^{\cdot}$)) via Fenton and Haber-Weiss reactions (87). An excess of reactive oxygen species (ROS) and free radicals generates oxidative stress above the capacity of the cell to neutralise them. Plants produce ROS in several organelles as a result of the metabolic processes necessary for growth and survival, such as photosynthesis in the chloroplast and respiration in the mitochondria (86). These processes include highly oxidising reactions or a high rate of electron flow, which results in ROS production. They are also generated in plastids, peroxisomes, the cytosol and the apoplast; peroxidases and amino oxidases in cell walls, along with NADPH oxidase in the plasma membrane produce ROS in response to stressors (88).

Reactive oxygen species have a role in signal transduction, as they act as signaling molecules in plants responses to pathogens, stress, acclimation and cellular death (88). For example, in the photosynthetic tissues, $^1O_2$ may be produced by photosystem I, and O_2^-, H_2O_2 and $OH^{\cdot}$ by photosystem II due to a lack of water (86).

Plants have developed ROS detoxification mechanisms due to the continual exposure of cellular components to ROS. For example, mechanism of $^1O_2$ detoxification in plants includes carotenoids (89), ascorbate (90), vitamin B6 (91) flavonoids (92) and the water soluble chlorophyll binding protein (WSCP) (93) . These molecules detoxify $^1O_2$ by themselves being oxidised, reducing the $^1O_2$, and then they are reduced by reduction reactions (86).

1.3.4. Detoxification adaptations

There are multiple mechanisms that plants use to balance the concentrations of metals. The first line of defense against the uptake of toxic metal concentrations lies in the ability of plants to restrict the uptake into root tissue and limit their translocation to tissues where they could cause damage. Processes for uptake avoidance include adherence to extracellular root components, precipitation of metal ions through root exudates, and metal exclusion (94). The mechanism of action of root exudates includes acting as ligands to form stable metal complexes or altering the rhizosphere pH to precipitate metals. Cell wall pectins, which consist of negatively charged carboxylic groups of polygalacturonic acid, can bind to positively charged metal ions to restrict their entry into the cell (95). The second line of defense includes detoxification mechanisms to mitigate the toxic effects of high concentrations of metals accumulating in the cytosol. Complexing agents can function as ligands to metal ions, reducing the free metal ion concentration. Some of the organic components involved in detoxification through the mechanism of chelation include organic acids, amino acids, phytochelatins (PCs), metallothioneins (MTs), and cell wall components such as proteins, pectins and polyphenols (96,97).

1.3.4.1. Organic acids

Organic acids act by complexing with the metal ions to reduce their toxicological bioavailability; for instance, acetic and citric acids chelate cadmium (Cd) in *Solanum nigrum* (potato) leaves and malate chelates Zn in the Zn HA *A. helleri* (98)*.* Citrate and malate have been shown to complex Zn in the roots of the grass *Deschampsia caespitosa* (tussock grass) accounting for some of the high tolerance to Zn demonstrated by the grass (99,100) and later studies have confirmed the complexation of Zn by citrate in the cytosol (101). After exposure to 45 µM Cd for four hours, ~10 % of Cd in tobacco suspension cells was in the form of Cd-peptide (102), with a higher proportion complexed by malate and citrate. Only 6 % of the total Cd was free in the cell (101). The proportion of Cd complexed to different organic acids depends on the cellular pH; a pH higher than 5.0 resulted in more citrate ligand binding and decrease the influence of malate (101). In two species of Ni Has, 80 % of Ni was present bound to citrate and malate; in five others, there was only the citrate complex (103).

1.3.4.2. Peptides

Peptides have also been shown to be induced under the presence of metals. Exposure to Cd was shown to induce the expression of Cd-binding peptides, which are involved in sequestering Cd in vacuoles (101). Complexation with Cd-specific peptides is thought to be a response to high Cd concentrations, as at low concentrations it was suggested that the presence of vacuolar citrate would effectively complex cellular Cd (101,104). Comparisons between Ni HAs and non-HAs showed an increase in histidine in the xylem sap following Ni exposure in the HAs, with chelation occurring with histidine (19%), glutamine (15%), citrate (9%) and malate (3%) (105).

1.3.4.3. Metallothioneins

Metallothioneins (MT) are cysteine rich molecules which provide thiols for metal chelation when in their reduced state. Plants contain the MT-II and MT-III types of MTs, which differs to the mammalian MT-Is (106). There are 58 genes in plants which predict MT-like proteins, with a small number partly characterised. The MT-IIIs differ from the MT-IIs in that they are atypical, non-translationally synthesised polypeptides based on repeating units of γ-glutamylcysteine (107). Cadmium has been shown to displace Zn from some MT-IIs in plants, and bind in a similar manner (108), and these molecules have been suggested to play a role in Zn detoxification and homeostasis (109). The upregulation of this MT is induced in the presence of abscisic acid (109). It has been suggested that the role of MTs is to scavenge metal ions released from protein degradation during leaf senescence, or to protect DNA from oxidative damage due to the metal-mediated formation of free radicals (110). Metallothioneins have a disparate response to metals, with no one-size-fits-all response (107), and there has been little progress in identifying metal regulatory elements in the promoter regions of *AtMT1* and *AtMT2,* though some ethylene regulatory elements have been found in an MT-II present in leaves (111,112). A Cd-responsive sequence has been identified, *pas*, and is present on the auxin-regulated gene *parA*, which regulates the transcript of downstream genes (113). Multiple MTs have been expressed in *E. coli* and yeast as GSH-fusion proteins (114–118). In one of these experiments, despite being exposed to Cu, Cd, Fe and Zn, only Cu or Cd bound the fusion protein, and it was only when Zn was present alone that the metal bound to the fusion protein (118). The expression of *AtMT1* and *AtMT2* in MT-deficient *E. coli* or yeast mutants complemented the mutants, allowing cells to tolerate otherwise harmful concentrations of Cu (116) or Zn (117). The importance of MT-IIs in metal tolerance has been assessed in Arabidopsis. The transcript abundance of *MT2a*, but not *MT1a*, increased in more tolerant Arabidopsis ecotypes in response to Cu, and this pattern was reflected in the protein abundance (119). In yeast, three proteins have been shown to be involved in cellular trafficking of Cu to specific sites: *ATX1*, *LYS7* and *COX17* (120,121). In plants it is suggested that MTs act either as stores of metal, or as chaperones to metalloenzymes.

1.3.4.4. Phytochelatins

Phytochelatins are γ-Glu-Cys peptides, and are made up of five families, based on the C-terminal amino acid (107). Following Cd exposure, PCs were induced in a range of plants from vascular and nonvascular plant, mosses, and algae (122–124). Yeasts have also been shown to produce PCs in response to Cd (125). Many plants treated with metals, produce PCs, and often other peptides of (γ-Glu-Cys)$_n$ (122–124). Various metal treatment of plant cells has been shown to induce the expression of these peptides, including Cd, Zn, lead, silver (Ag), arsenate, mercury (Hg), Cu, Ni, selenate, gallium, Pd, indium, and tin (122,126). Phytochelatin synthase was purified by Loeffler et al (1989) and shown to perform the transpeptidation of the γ-Glu-Cys moiety of glutathione (GSH) onto another GSH to form an n+1 oligomer of (γ-Glu-Cys)$_2$-Gly, and shown to stop its activity when there was sufficient ligand to bind all Cd at a molar ration of 1Cd:2Cys (127). The synthesis of phytochelatins synthase has been shown to be induced by Cd, Ag, Pd, Cu, Zn, Au, Hg and Fe (128). Glutathione

was used with a crude PC synthase preparation from pea to produce PCs in the presence of Cu and Cd (129). Demand for Glu in Cd-treated maize root results in increased presence of the enzyme phosphoenol-pyruvate carboxylase and glutamine synthase (130). The γ-Glu-Cys ligand is thought to be involved in Cd chelation, and more Cd resistant tomato cell lines had higher activity of the γ-Glu-Cys synthetase (131), resulting in higher GSH synthesis and PC synthase activity. Alternatively, the messenger RNA (mRNA) for γ-Glu-Cys synthetase was not changed in roots by the presence of Cd (132). In *Rauvolfia serpentina* (Indian snakeroot) cells under Cu and Zn treatment, PCs accumulated rapidly until both metals were depleted after which the PC content reduced (133). Complexes of Zn- or Cd- PC have been demonstrated to increase the metal tolerance of metal sensitive enzymes ribulose-1,5-bisphosphate carboxylase/oxygenase, nitrate reductase, glyceraldhyde-3-phosphate dehydrogenase, alcohol dehydrogenase and urease by 10-150-fold when the Cd or Zn was supplied to the PC (134).

1.3.4.5. Sequestering ions in vacuoles

Vacuoles are the sites of storage of most of the solutes present in cells (62). Accumulation of solutes in the vacuole is necessary for turgor pressure in cells, which is the main force of growth for plants. The major components of the vacuole are sugars, K, Ca, Mg, and Ni ions, but this varies widely depending on the species and environment. The vacuole can help to compartmentalise metal ions when they are present in excess, and engineering plants with a more efficient system of vacuolar compartmentalisation has been suggested for the development of phytoremediation (85). In plants, PCs accumulate in the vacuole in response to Cd treatment, with PC-metal complexes thought to be concentrated in the vacuole (135). Some HAs have been shown to use vacuolar metal compartmentalisation as part of their detoxification mechanisms: Krämer, et al. (2004) identified that *Thlaspi geosingense* is able to sequester the leaf-located Ni into the vacuole to enhance Ni tolerance (136).

1.3.4.6. Efflux

Another strategy to reduce metal excess and toxicity is in the active removal of metal ions at the plasma membrane to decrease the cellular concentration. The metal efflux pumps in plants include the P-type ATPases and the ATP-binding cassette (ABC) transporters, with the subfamilies MRP (Multidrug Pleiotropic Drug Resistance) and PDR (Pleiotropic Drug Resistance) playing a vital role in metal chelation (137,138). The Arabidopsis *DTX1* is thought to localise to the plasma membrane and mediate the efflux of metal ion such as Cd^{2+}, and therefore improving tolerance (139).

1.4. Thesis objectives

Phytomining has the potential to provide a bridge between the loss of precious, finite metals into the environment and their reuse. Phytomining can be cost-effective, by targeting high value metals such as Au and Pd, and environmentally friendly, promoting the remediation of contaminated sites. Ideal phytomining plants would be fast growing, able to produce high biomass; but also, be tolerant to the target metal, and able to accumulate a metal concentration in the shoot tissue higher than exists in the substrate (140). The accumulation and tolerance in these plants is reliant on high uptake and efficient detoxification mechanisms. To round out the process, it would be beneficial to control the formation of NPs within the plant tissue, so that the NP-containing biomass can be used in downstream catalytic reactions. There is potential to use synthetic biology to engineer plants with improved metal uptake and tolerance and transfer this knowledge to plant species capable of advantageous physiological features, such as high biomass and fast growth.

The objectives of this work were to gain a fundamental understanding of Au and Pd uptake and NP formation in Arabidopsis and to use synthetic biology to engineer plants more suited to phytomining:

1. Contribute to the current understanding of Arabidopsis Au uptake by COPT2 through studies with yeast and Arabidopsis *copt2* mutants. Utilise the knowledge gained to investigate the potential of *COPT2* overexpression in Arabidopsis towards the goal of increased Au uptake. Explore the potential of the GP towards the enrichment of 10 nm AuNPs *in planta*, and the combination of *COPT2* overexpression and the GP towards Arabidopsis lines capable of increased Au uptake and 10 nm AuNP formation.

2. Build upon the knowledge gained in Au uptake and NP formation by COPT2 and the GP by exploring the interaction between COPT2 and GP with Pd. Use previously established tools, e.g., transgenic yeast mutants, Arabidopsis *copt2* mutants, *COPT2* overexpression lines, GP-producing lines, and double transgenic lines overexpressing *COPT2* and the GP, to characterise the involvement of COPT2 and the GP with Pd.

3. Using RNA-sequencing, expand the current understanding of Pd uptake and tolerance in Arabidopsis. Identify key genes involved in uptake, including the response of *COPT2*, translocation, sequestration, efflux, and detoxification, looking towards to how these genes might be utilised in future work to genetically engineer plants suitable for Pd phytomining.

2. Materials and methods
2.1. Experimental materials
2.1.1. Reagents and suppliers

All reagents were obtained, unless stated, from: Formedium Ltd. (Norfolk, UK), New England Biolabs Ltd. (NEB UK) (Hitchin, UK), Promega UK (Southampton, UK), QIAGEN Ltd. (Manchester, UK), Merck (London, UK), Thermo Fisher Scientific (Loughborough, UK) and VWR International (Leicestershire, UK). Water used in experiments, unless otherwise stated, was sterile, distilled water obtained using the Milli-Q water filtration system (Merck Millipore, Germany). DNA primers were synthesised by Integrated DNA Technologies (Leuven, Belgium).

2.1.2. Yeast and bacterial strains

Yeast and bacterial strains used in this study are listed in Table 2.1 and Table 2.2, respectively. Five yeast strains were used in this work: Y00000 (BY4741), DTY165, MPY17 (*Δctr1ctr3*), Y03629 (*Δccc2*) and Y04533 (*Δace1*). BY4741 is a WT, parental strain to *Δccc2* and *Δace1,* and DTY165 is a WT, parental strain to *Δctr1ctr3.* The BY4741, *Δccc2* and *Δace1* strains were purchased from Euroscarf (Frankfurt, Germany); the DTY165 and *Δctr1ctr3* strains were gratefully received from Dr Aaron Smith and Professor Dennis J. Thiele from the Thiele Lab (Duke University, USA). For plasmid expression and purification, TOP10F' chemically competent *Escherichia coli* (*E. coli*) cells were purchased from Invitrogen; for Arabidopsis transformation, *Agrobacterium tumefaciens* (*Agrobacterium*) GV301 electrocompetent cells were purchased from GoldBio (Au Biotechnology, Inc. Saint Louis, MO).

2.1.3. Arabidopsis lines

Arabidopsis Columbia-0 (Col0) is the background ecotype for all Arabidopsis genotypes used, which are listed in Table 2.3. References to the Arabidopsis WT line refer to this ecotype.

2.1.4. Plasmids and vectors

In the yeast work, pYES2 (*Ura3 Ap^r pGal1 ColE1 ori and 2 µm ori;* Invitrogen, Figure 2.1) was used as the plasmid backbone for: pYES2-yEGFP, which was kindly received from Professor Frans Maathuis (University of York) and is comprised of the pYES2 sequence fused to the yeast-enhanced GFP protein (yEGFP); and for pYES2-*COPT2y* (synthesised by GeneArt). The Arabidopsis *COPT2* sequence was codon optimised for a yeast expression system prior to being cloned into pYES2.1V5-His TOPO. The resultant pYES2-*COPT2y* plasmid (6361 bp) contained the codon-optimised *COPT2y* sequence (481 bp) under the control of a *GAL1* and T7 promoter; it also contained a V5 epitope, a His-tag, a CYC1 transcription termination signal, a pUC origin of replication (ori), the *Amp-R* sequence (an ampicillin resistance gene), the *URA3* gene (for selection in yeast), a URA3 promoter, 2micron ori and an F1 ori. Optimisation was performed using ThermoFisher GeneArt software and involved the conversion of codon sequences less favoured or 'low quality' by the yeast

translational machinery, to synonymous codons biased toward 'high quality' expression within a yeast system, and a reduction in the spread of guanine and cytosine content.
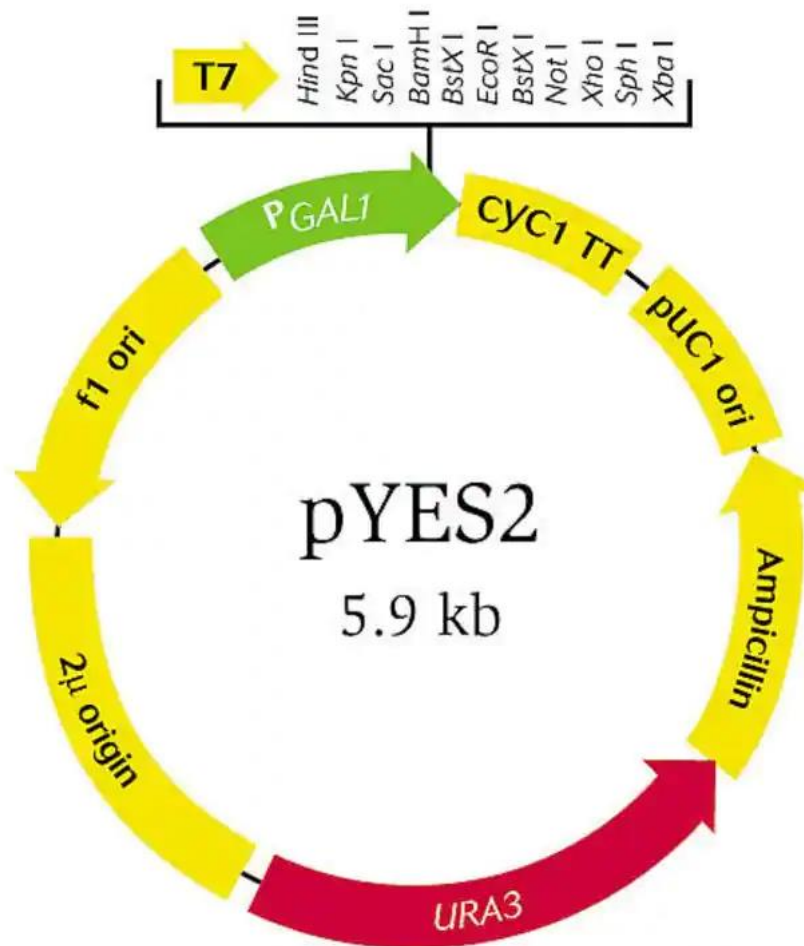
Figure 2.1. Vector map of pYES2 containing the GAL1 promoter, Amp[R], a pUC1 origin of replication (ori), and a multiple cloning site containing a T7 ori. (141)

Table 2.1. Yeast strains used in this study

Strain	Background	Genotype	Reference	Selectable marker(s)
BY4741 (WT)		MATa; his3D1; leu2D0; met15D0; ura3D0	Brachmann et al, 1997	Sensitive to SD-U
DTY165 (WT)		MATα, ura3-52, his6, leu2-3-112, his3-D200, trp1-901, lys2-801, suc2-D	Li et al, 1996	Sensitive to SD-U
MPY17	DTY165	MATα, ctr1::ura3::KanR, ctr3::TRP1, his3, lys2-801, CUP1	Peña et al, 1998	Sensitive to SD-U, Kanamycin resistant
Y03629	BY4741	BY4741; MATa; his3Δ1; leu2Δ0; met15Δ0; ura3Δ0; YDR270w::kanMX4	Winzeler et al, 1999	Sensitive to SD-U, Kanamycin resistant
Y04533	BY4741	BY4741; MATa; his3Δ1; leu2Δ0; met15Δ0; ura3Δ0; YGL166w::kanMX4	Winzeler et al, 1999	Sensitive to SD-U, Kanamycin resistant

Table 2.2. Bacterial strains used in this study

Strain	Genotype	Reference	Selectable marker(s)
TOP10F' chemically competent *E. coli*	F'[lacIq Tn10(tetR)] mcrA Δ(mrr-hsdRMS-mcrBC) φ80lacZΔM15 ΔlacX74 deoR nupG recA1 araD139 Δ(ara-leu)7697 galU galK rpsL(StrR) endA1 λ-	Casadaban and Cohen, 1980	Tetracycline, Streptomycin resistant
Agrobacterium GV301	C58 (rif R) Ti pMP90 (pTiC58DT-DNA) (gent R) Nopaline	Clough and Bent, 1998	Rifampicin, gentamycin resistance

Table 2.3. Arabidopsis genotypes used in this study

Line	Line ID	Details	Background	Reference	Resistance
Col0	NASC ID: N1092	WT line	Col0	Meinke and Scholl, 2003	NA
copt2-1	NASC ID: N416069 GABI-kat line ID: 168D01-013363	T-DNA mutant in *COPT2*; *copt2* mutant genotype	Col0	Rosso et al, 2003 ; Kleinboelting et al, 2012	Sulfadiazine
copt2-2	NASC ID: N655195 ABRC stock number: SALK_147451.31.40. x	T-DNA Mutant in *COPT2; copt2* mutant genotype	Col0	Alonso et al, 2003	Kanamycin
copt2-3	GABI-kat line ID: 314H06.1	T-DNA mutant in *COPT2; copt2* mutant genotype	Col0	Kleinboelting et al, 2012	Sulfadiazine resistant
35S-COPT2A	NA	Arabidopsis optimised *COPT2* under the control of CaMV35S	Col0	Generated in this work	Glufosinate ammonium
35S-COPT2B	NA	Arabidopsis optimised *COPT2* under the control of CaMV35S	Col0	Generated in this work	
35S-COPT2C	NA	Arabidopsis optimised *COPT2* under the control of CaMV35S	Col0	Generated in this work	
35S-GPA	NA	GP sequence until the control of CaMV35S	Col0	Generated in this work	Kanamycin
35S-GPB	NA	GP sequence until the control of CaMV35S	Col0	Generated in this work	
35S-GPC	NA	GP sequence until the control of CaMV35S	Col0	Generated in this work	
35S-GPCA	NA	GP sequence until the control of CaMV35S, plus Arabidopsis optimised *COPT2* under the control of CaMV35S	Col0	Generated in this work	Kanamycin, Glufosinate ammonium
35S-GPCB	NA	GP sequence until the control of CaMV35S, plus Arabidopsis optimised *COPT2* under the control of CaMV35S	Col0	Generated in this work	
35S-GPCC	NA	GP sequence until the control of CaMV35S, plus Arabidopsis optimised *COPT2* under the control of CaMV35S	Col0	Generated in this work	

2.2. Microbiology methods
2.2.1. Preparation of media

The reagents used in yeast growth media are detailed in Table 2.4. The composition of the Murashige and Skoog (MS) medium utilised for plant culture is shown in Table 2.4. Components were dissolved in water, mixed with a magnetic stirrer, and autoclaved (121 °C, 15 minutes) to sterilise before use. For solid media, agar (A) was added prior to autoclaving (1.5 %). Heat labile reagents (antibiotics, glucose/galactose) were sterilised by passing through a 0.2 µM filter, then added to autoclaved media following cooling (~ 60 °C). A list of the antibiotic and herbicide stocks and working concentrations are shown in Table 2.6. When necessary, glucose (glu) or galactose (gal) were added after being filter-sterilised at 2 %.

2.2.2. Metal additions to growth media

Media were augmented with Au (as $KAuCl_4$) or Pd (as K_2PdCl_4) from a filter sterilised (0.2 µm) 50 mM stock solution and adjusted to pH 5.7 (using 0.5 M NaOH). Copper was added (as $CuSO_4$) from a filter sterile (0.2 µm) 30 mM stock solution and altered to pH 5.7 (1 M NaOH). Stock solutions were kept at -20 °C for long term storage.

2.2.3. Buffer preparation

Buffers were prepared according to lab protocols: the recipes used are listed in Table 2.7.

2.2.4. Microbial culture

Microbial cultures grown 'overnight,' refer to a 16-hour period; a day refers to a period of 24 hours. On solid media, yeast was grown for 2-3 days at 30 °C until distinct colonies were seen, *E. coli* and *Agrobacterium* cultures were grown overnight at 37 °C or 28 °C respectively; liquid cultures were shaken at 180 rpm. The microbial culture media used in this study are detailed in Table 2.4.

Table 2.4. Growing media used in this study. For the preparation of solid media, agar was added prior to autoclaving (1.5%). Throughout this work, the addition of agar is shown by the presence of (A) in the media name e.g., YPD(A).

Culture media	Organism	Reagents	pH
Yeast peptone dextrose (YPD)	Yeast	2% Bacto-peptone, 2% D-Glucose, 1% yeast extract	5.7 (NaCl)
Synthetic complete (SC)	Yeast	As supplied	5.7 (NaCl)
Synthetic defined medium without Uracil (SD-U)	Yeast	1.7% Yeast Nitrogen Base Without Amino Acids and Ammonium Sulfate, 5% Ammonium sulfate, 1.92% Yeast Synthetic Drop-out Medium Supplements without uracil	5.7 (NaCl)
Luria broth (LB)	E. coli and Agrobacterium	10 g / L tryptone, 10 g / L NaCl, 5 g / L Yeast extract	7.5
MS (half strength)	Arabidopsis	2.2 g / L water (½ strength used)	5.7 (NaCl)

Table 2.5. The composition of MS medium used for plant growth in this study

Components	Molecular weight	Concentration (mg/L)	mM
Myo-Inositol	180.0	100.0	0.5556
Nicotinic acid (Niacin)	123.0	0.05	0.0004
Pyridoxine hydrochloride	206.0	0.05	0.0002
Thiamine hydrochloride	337.0	0.1	0.0003
Ammonium Nitrate (NH_4NO_3)	80.0	1650.0	20.6250
Boric Acid (H_3BO_3)	62.0	6.2	0.1000
Calcium Chloride ($CaCl_2$) (anhyd.)	111.0	332.2	2.9928
Cobalt Chloride ($CoCl_2$-$6H_2O$)	238.0	0.025	0.0001
Cupric Sulfate ($CuSO_4$-$6H_2O$)	250.0	0.025	0.0001
Ferric sulfate ($FeSO_4$-$7H_2O$)	278.0	27.8	0.1000
Magnesium Sulfate ($MgSO_4$) (anhyd.)	120.0	180.7	1.5058
Manganese Sulfate ($MnSO_4$-H_2O)	169.0	16.9	0.1000
Potassium Iodide (KI)	166.0	0.83	0.0050
Potassium Nitrate (KNO_3)	101.0	1900.0	18.8119
Potassium Phosphate monobasic (KH_2PO_4)	136.0	170.0	1.2500
Sodium Molybdate (Na_2MoO_4-$2H_2O$)	243.0	0.25	0.0010
Zinc sulfate ($ZnSO_4$-$7H_2O$)	288.0	8.6	0.0299
Glycine (Free Base)	75.0	2.0	0.0267
Sodium EDTA (Na_2-EDTA)	372.0	37.26	0.1002

Table 2.6. Antibiotic/herbicide stock and working concentrations used in this study

Antibiotic/herbicide	Stock solution	Working concentration
Glufosinate ammonium	20 mg / mL (0.2 µM filter sterilised)	20 µg/mL
Kanamycin	50 mg / mL (0.2 µM filter sterilised)	50 µg/mL
Gentamycin	30 mg / mL (0.2 µM filter sterilised)	30 µg/mL
Spectinomycin	50 mg / mL (0.2 µM filter sterilised)	50 µg/mL
Carbenicillin	50 mg / mL (0.2 µM filter sterilised)	50 µg/mL

Table 2.7. Buffers and recipes used in this study

Buffer	pH	Reagents	Used for
Tris-acetate-EDTA (TAE)	8.0	For 50X stock: 242 g/L tris base, 57.1 mL/L glacial acetic acid, 100 mL/L 0.5 M ETDA solution (pH 8.0)	1X TAE used for Agarose gel electrophoresis
Phosphate-buffered saline (PBS)	7.4 (HCl)	For 10X stock: 80 g/L NaCl, 2 g/L KCl, 14.4 g/L Na_2PO_4, 2.4 g/L KH_2PO_4	
Cetyltrimethylammonium bromide (CTAB)	8.0	2% w/v CTAB reagent, 100 mM Tris–Cl buffer (pH 8.0), 2 M NaCl, 25 mM EDTA (pH 8.0)] containing 2% w/v PVPP and 2% v/v beta-mercaptoethanol (added just before use)	Used in total RNA extraction

2.2.5. Microbial storage

For short term microbial storage (< 2 years) stab and slant cultures were generated as follows: cells were streaked onto solid media appropriate to the specific microorganism: SD-U(A) for transformed yeast, SC(A) for non-transformed yeast, LB(A) containing appropriate antibiotic(s) for non-transformed and transformed *E. coli* and *Agrobacterium*. Yeast, *E. coli* or *Agrobacterium* cultures were grown at 30 °C, 37 °C or 28 °C respectively until distinct colonies were identified. For stab cultures, a single colony was picked using a sterile pipette tip from a freshly streaked plate and stabbed into a 2 mL screw-cap vial containing 1 mL solid media. For slant cultures, 1 mL of molten solid media was added to a 2 mL screw-cap vial and left to cool at a 45 ° angle with the lid slightly loosened. A single colony was picked from a freshly streaked plate using a sterile loop, and material transferred to the surface of the LB(A) slant. Stab and slant cultures were incubated with lids loosened slightly at 28 °C overnight for *Agrobacterium,* 37 °C overnight for *E. coli*, and 30 °C for 2-3 days for yeast cultures. Following the formation of a cloudy white formation on the surface of slants or within the stab, these were stored at 4 °C. For long term storage of yeast and bacterial strains (> 2 years), liquid cultures (using media defined above) containing material picked from a single, distinct colony using a sterile loop, were grown at 30 °C for yeast, 37 °C for *E. coli* and 28 °C for *Agrobacterium*, and 15 % v/v glycerol stocks prepared in sterile cryogenic vials and stored at -80 °C.

2.2.6. DNA purification from microbial cells

Purification of DNA from microbial cells was performed using a QIAprep Spin Miniprep Kit (QIAGEN) according to the manufacturer's instructions.

2.2.7. Polymerase chain reaction (PCR)

The GoTaq® Green Master Mix (Promega UK Ltd) was used for PCR with the components as per Table 2.8. Reactions for PCR were run in a thermocycler (PTC-200 Peltier Thermal Cycler, MJ Research), with the lid preheated to 100 °C to prevent condensation in the PCR tubes. The cycling conditions are detailed in Table 2.9, and the primers used in PCR reactions are shown in Table 2.10.

2.2.8. Agarose gel electrophoresis

Agarose gel electrophoresis was used to analyse DNA samples by the molecular weight following PCR. A 1.2 % (w / v) gel was prepared by mixing high grade agarose powder in 1 X TAE buffer solution (Table 2.7). The mixture was heated in a microwave to dissolve the agarose powder, then cooled to 60 °C before the addition of Ethidium bromide to a final concentration 0.3 µg / mL. The molten agarose was then poured into the gel tray, sealed at the ends with autoclave tape and containing a gel comb to provide wells for the samples. Once the gel had set, the comb and tape were removed and the gel was placed into an electrophoresis tank containing 1 X TAE, after which DNA samples were loaded into each well. Samples loaded from PCR did not require addition of loading dye as this was included in the PCR components. To determine DNA fragment size, samples were loaded alongside a 1 kb DNA ladder (Promega Corporation, UK), unless otherwise stated,

containing fragments with sizes ranging from 250 bp – 10,000 bp (Figure 2.2). A BioRad PowerPac 3000 generated an electric current which was applied across the tank at 120 Vs for 30 minutes, migrating the negatively charged nucleotides to the positively charged cathode. Gels were visualised using an ultraviolet (UV) transilluminator imaging system (UVItec gel documentation system) and molecular weight estimated by comparison with the known weight bands on the ladder included.
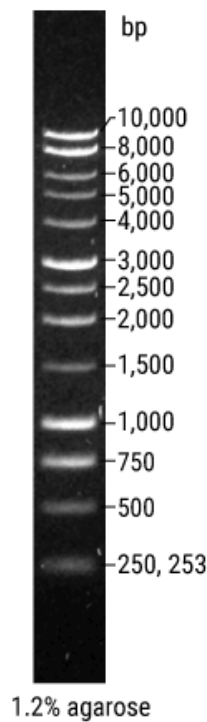
Figure 2.2. DNA ladder used in PCR reactions. Distribution of bands of known size on a 1.2 % agarose gel.

Table 2.8. PCR reaction components

Component	Volume (µL)	Final concentration
GoTaq® Green Master Mix, 2X	10	1X
Upstream primer (10 µM)	0.4	200 nM
Downstream primer (10 µM)	0.4	200 nM
DNA template	4 / colony pick	<250 ng
Nuclease -free water	20	N. A.

Table 2.9. PCR cycling conditions

Reaction stage	Temperature (ºC)	Duration
Initial denaturation	95	2 minutes
Denaturation	95	30 seconds
Annealing	50 – 65	30 seconds
Extension	72	1 minute
Repeat stages 2-4, 35 times	-	-
Final extension	72	5 minutes

Table 2.10. PCR primers used in this study

Used in	Primer label	Sequence (5' to 3')
PCR confirmation of *pYES2*	YTE_L1_URA3	CGCTGFTGAGATCCAGTTCG
	YTE_R1_URA3	CAGAAAAGCAGGCTGGGAAG
PCR confirmation of *COPT2y*	YTE_L1_*COPT2*y	GCCTCCACCATCTCCATCTT
	YTE_R1_*COPT2*y	AATAGAGCTGCTGGTTTGGC
PCR confirmation of *copt2-1*	GKAT-PCR(s)	CCCATTTGGACGTGAATGTAGACAC
	COPT2LP1	TCAATTGTTCAACAAACGCAG
	COPT2RP1	GATTTTTCATAACATTTCAAACCAC
PCR confirmation of *copt2-2*	LBb1.3	ATTTTGCCGATTTCGGAAC
	COPT2LP2	CTGTGTCGTGAGGTTTTGAGG
	COPT2RP2	TCTTGAGTGTGTACACAGCGG
PCR confirmation of *copt2-2*	o8474	ATAATAACGCTGCGGACATCTACATTTT
	COPT2LP3	GAACCTTCTATGGACAGCATTTG
	COPT2RP3	GACGAAGAGGCATGGAGTTG
PCR confirmation of GP sequence	pART7-R	GAATGAACCGAAACCGGCG
	GP-PCR	GGTGGTCTGAAAAGTTGTAATGA

Table 2.11. Quantitative PCR (qPCR) primers used in this study

Used in	Primer description / label	Sequence (5' to 3')
Arabidopsis *COPT2* **primer efficiency tests (qPCR)**	Upstream Left Primer 1 (C2Ups1LP)	ACCAACGCAAAGAAGATTAGACG
	Upstream Right Primer 1 (C2Ups1RP)	ACAACATTACAACTCCATGCCTCT
	Upstream Left Primer 2 (C2Ups2LP)	TACCAACGCAAAGAAGATTAGACG
	Upstream Right Primer 2 (C2Ups2RP)	ACAACATTACAACTCCATGCCTCT
	Upstream Left Primer 3 (C2Ups3LP)	ATACCAACGCAAAGAAGATTAGACG
	Upstream Right Primer 3 (C2Ups3RP)	TACAACATTACAACTCCATGCCTCT
	Downstream Left Primer 1 (C2Ups1LP)	CCTACGTGTCAGTGGCTCAA
	Downstream Right Primer 1 (C2Ds1RP)	GGACATAACAGCGAGCATCA
	Downstream Left Primer 2 (C2Ds2LP)	CCACCATCACCATCATCATC
	Downstream Right Primer 2 (C2Ds2RP)	CTCCGTGTTCTTACCCCAAA
	Downstream Left Primer 3 (C2Ds3LP)	TGATGCTCGCTGTTATGTCC
	Downstream Right Primer 3 (C2Ds3RP)	CGATAGCGACGATGAAAACA
ACTIN2 (qPCR)	q-ACTINF	TACAGTGTCTGGATCGGTGGTT
	q-ACTINR	CGGCCTTGGAGATCCACAT
COPT2 **(qPCR)**	C2Ds1RP	GGACATAACAGCGAGCATCA
	C2Ds2LP	CCACCATCACCATCATCATC
GP (qPCR)	GP-F	ATGGGAGCTTCTCTTTGGTGGTCTGAAAAGTTGTAATGA
	Universal reverse primer	NA
GP (qPCR)	optGP-F	GGTGGTCTGAAAAGTTGTAATGA
	Universal reverse primer	NA

2.2.9. DNA clean-up from PCR

Products were purified directly following PCR using the Wizard® SV Gel and PCR Clean-up System (Promega), using the centrifugation method option as per the manufacturers protocol, and eluted into 30 µL nuclease-free water.

2.2.10. Quantification of nucleotides

Both DNA and RNA were quantified using a Nanodrop 1000 Spectrophotometer (Thermo Fisher Scientific). Both DNA and RNA absorb at 260 nm, and the ratio of absorbance at 260 nm and 260 nm was used to assess sample purity. A ratio of around 1.8 was considered as acceptable for DNA, and a ratio of 2.0 as acceptable for RNA, as lower ratios indicate the presence of protein, phenol or other contaminants absorbing near 280 nm. Samples were assessed in triplicate.

2.2.11. DNA sanger sequencing

The DNA samples were sequenced using the LightRun service (Eurofins Genomics). Sample submission required a total sample amount of 10 µL in 1.5 mL Eppendorf tubes: containing 5 µL of purified template DNA (at 80 – 100 ng / µL) in water along with 5 µL primer (at 5 µM) (Table 2.10). The PCR products were purified prior to sequencing.

2.2.12. Generation of *pYES2-COPT2y*

Arabidopsis *COPT2* was optimised for expression in yeast to accommodate the codon bias of a yeast expression system, rather than the original Arabidopsis by GeneArt (Thermo Fisher Scientific). The resulting *COPT2y* sequence was cloned into the *pYES2.1V5-His TOPO* and synthesised by GeneArt (Thermo Fisher Scientific) and will be referred to as *pYES2-COPT2y* hereafter.

2.2.13. Heat shock transformation of *pYES2-COPT2y* into *E. coli*

The *pYES2-COPT2y* was transformed into XL10-Gold Ultracompetent *E. coli* cells via heat shock transformation. The plasmid (1 µL) was added to 50 µL of *E. coli* cells and chilled on ice (4 °C) for five minutes. Cells were then placed in a 42 °C water bath for one minute, and 500 mL of LB media added immediately for the outgrowth step (37 °C, one hour with shaking at 180 rpm); 50 µL of the culture was plated onto LB(A) containing 50 µg / µL Carbenicillin, and the remaining culture spread onto a second plate. Culture plates were incubated overnight at 37 °C and positive transformants confirmed by PCR (2.2.7) and sequencing (2.2.11), using primers specific for the *COPT2y* sequence, shown in Table 2.10. Each PCR reaction included a single colony which was sampled from these plates by contact with a sterile pipette tip and added to the reaction. A glycerol stock of *E. coli* was generated as per 2.2.5 and stored at -80 °C.

2.2.14. Purification of *pYES2-COPT2y*

A section of the frozen *E. coli pYES2-COPT2y* glycerol stock was transferred to SD-U(A) plates using a sterile loop, then cultured for 2-3 days (30 °C) until distinct colonies were seen. The *pYES2-COPT2y* DNA was isolated as per 2.2.6. The plasmid concentration was quantified as per 2.2.10, and confirmed by PCR using primers specific to *COPT2y* for *pYES2-COPT2y* strains (Table 2.10) as per 2.2.7.

2.2.15. Transformation of yeast strains with *pYES2-COPT2y*

Yeast strains were transformed with *pYES2-COPT2y*, using the Frozen-EZ Yeast Transformation II Kit (Zymo Research) as per the manufacturers protocol. Transformed cultures were plated onto SD-U plates for selection (37 °C, 48 hours). Colonies were assessed by PCR to confirm the presence of *pYES2-COPT2y* using primers as described above.

2.2.16. Yeast studies on COPT2 involvement in Au or Pd uptake

Yeast cell cultures of all *pYES2-COPT2y* transformed strains (2.1.2) were grown overnight (30 ^{o}C) in SD-U media, containing 2 % (w / v) glu, 6.7 g / L yeast N base without amino acids, and 1.9 g / L yeast synthetic drop-out medium supplements without uracil (Sigma-Aldrich) unless otherwise stated, as shown in Table 2.12. Overnight cultures were centrifuged (3000 rpm, five minutes) and washed twice with water before being redissolved. Cultures were serially diluted with SD-U media containing either 2 % gal or 2 % glu to an OD600 of 1. As SD-U medium contains metals (Table 2.12), metals that were added in the spot dilution assay are referred to hereafter as 'additional' or 'added' metals, and are separate from the base composition of SD-U as described in Table 2.12. The culture was spotted (3 µl) using a pipette onto SD-U(A) media containing either 2 % (w / v) gal or glu, and additional metals (100 µM Cu, 500 µM Au.100 µM Cu + 500 µM Au, 500 µM Pd or.100 µM Cu + 500 µM Pd). Plates were incubated at 30 ^{o}C and images taken after five days using an Epson Perfection V370 Photo Flatbed scanner.

Table 2.12. The composition of SD-U medium used to select for *pYES2-COPT2y* transformed yeast strains in this study

Component	Name	Concentration (mg / L, unless otherwise stated)
Yeast N base without amino acids	Ammonium sulphate	5 (g/L)
	Potassium phosphate	1 (g/L)
	Magnesium sulphate	500
	Ca chloride	100
	Sodium chloride (NaCl)	0.1
	Inositol	2.0
	Boric acid	0.5
	Niacin	0.4
	Thiamine hydrochloride	0.4
	Pyridoxin hydrochloride	0.4
	Ca pantothenate	0.4
	Manganese sulphate	0.4
	Zinc sulphate	0.4
	p-Aminobenzoic acid	0.2
	Iron chloride	0.2
	Riboflavine	0.2
	Sodium molybdate	0.2
	Potassium iodide	0.1
	Cu sulphate	0.04
	Biotin	0.002
	Folic acid	0.002
Agar		15 (g / L)
Yeast Synthetic Drop-out Medium supplements		1.92 (g / L)
Glu or gal		20
pH value (5.4 + 0.2)		

2.3. Plant cultivation methods
2.3.1. Growth media

For use in hydroponic growth systems, ½ MS medium (Merck) (142) was used as plant growth media as per the manufacturer's instructions (2.2 g / L added to water prior to autoclaving). The ½ MS media were adjusted to pH 5.7 using sodium hydroxide (NaOH; Merck) prior to autoclaving (121 °C, 15 minutes). When it was necessary to use ½ MS media in a solid state, agar for plant culture (9 g / L) (Merck) was also added (½ MS(A)). These were added to sterile plates and allowed to cool and solidify for 20 minutes. When using soil, the compost used was Levington Seed & Modular F2 compost (ICL Professional Horticulture).

2.3.2. Seed sterilisation by chlorine gas

Seeds were added to 1.5 mL Eppendorf tubes to a third of the tube volume and placed with lids open into racks. Racks were placed into a plastic box within a fume cupboard, and 3 mL 37 % hydrochloric acid added to 100 mL sodium hypochlorite in a volumetric flask which had been placed into the plastic box. The box was sealed at once to prevent the release of chlorine gas produced by the

resulting chemical reaction. After three hours, the lid of the box was removed to allow the gases to escape for half an hour prior to using the seeds.

2.3.3. Seed stratification

Seeds were stratified at 4 $^{\circ}$C in the dark for 48 hours.

2.3.4. Growth environment

Plants were grown under a 16-hour constant light (80 µmol / m^2 / s), 8-hour dark cycle at 21 $^{\circ}$C day temperature, 18 $^{\circ}$C night temperature, unless otherwise stated. To reduce light-induced stress of germinating and young seedlings in the hydroponic experiment, plants were germinated on ½ MS(A) under these conditions. After seven days, seedlings were moved to a growth cabinet at 12-hour constant light (180 µmol / m^2 / s), 12-hour dark cycle at 21 $^{\circ}$C day temperature, 18 $^{\circ}$C night temperature. Seeds were placed on top of water saturated soil to germinate, and a clear lid used to maintain humidity until seedlings were a week old. Soil was kept moist by watering from below.

2.3.5. Hydroponic system, growth conditions

For the hydroponic system, plants were first sterilised as per 2.3.2, stratified (2.3.3) then transferred to ½ MS(A) and grown as per 2.3.4. Tweezers were used to lift seedlings off the surface of the ½ MS(A) at the ten-day stage and transfer them into the hydroponic set up. The hydroponic set up consisted of a p1000 pipette tip box (Starlab, UK); 200 mL ½ MS media; a polystyrene 'raft' containing six holes cut to fit within the box; and flat, circular sponges sized to these holes, with a cut down the middle. One seedling was placed in the centre of each sponge, so that the root and the shoot were on separate sides. These were placed into the polystyrene rafts, which floated on the ½ MS media within the box. Each box contained six seedlings of one line with five boxes prepared per line. At twelve-days-old, the health of transferred seedlings was reviewed and those that were wilting were replaced with twelve-day-old seedlings from the ½ MS(A) plates. Growth media (½ MS) was replaced weekly to mitigate contamination with fungal pathogens, and seedlings kept in the growth cabinet (2.3.4).

2.3.6. Growth and storage of Arabidopsis

Arabidopsis seeds were sown onto F2 soil alongside WT seeds of the same genetic background as per 2.3.6. Seeds were stratified (2.3.3) prior to being moved to a growth cabinet (2.3.4). At two weeks old, two to three rosette leaves were cut from each seedling, placed into Eppendorf tubes, and snap-frozen in liquid nitrogen (N). These samples were stored until needed (-80 $^{\circ}$C). If needed, DNA was extracted from these samples as per 2.4.1 and quantified as per 2.2.10.

2.4. Molecular biology methods for plant studies
2.4.1. DNA extraction from plant tissue

The DNeasy PowerPlant Pro kit was used for DNA extraction (QIAGEN) from plant tissue. Around 50 mg of Arabidopsis tissue was placed in a 1.5 mL Eppendorf tube and flash frozen in liquid N for 30 seconds prior to disruption. Tissue was moved to a PowerBead Tube (QIAGEN) containing stainless steel ball bearings (2.38 mm). A kit-supplied homogenisation solution was added to the tube prior to homogenisation. The tissue was homogenised by bead-beating using a Tissue-Lyser II (QIAGEN) for 2 minutes at speed 25 / s. Tubes and holders were then rotated to ensure even homogenisation and returned to the Tissue-Lyser II for a further 2 minutes at 25 / s. Samples were processed according to the manufacturer's protocol.

2.4.2. RNA extraction from plant tissue

Two techniques were used to extract RNA from Arabidopsis tissue, dependent on the RNA content required. The method of RNA extraction depended on the focus of the downstream applications; if the level of *COPT2* was being investigated the EasyPure Plant RNA kit (Transgen Biotech co. LTD) was used. This is a filter-based method of RNA purification and does not capture small nucleotide sequences. If the GP sequence was being investigated, which is a short, 30 nt sequence (GGAGCTTCTC TTTGGTGGTC TGAAAAGTTG) (2.4.14), the total RNA, cetyltrimethyl ammonium bromide (CTAB) extraction process was used. The method of tissue preparation was common to both techniques: Arabidopsis leaf and root tissue was harvested, placed inside a 1.5mL Eppendorf tube and snap-frozen in liquid N for 30 seconds. Tissue was either processed directly or stored at -80 °C for future processing. To homogenise the plant tissue, a pestle and mortar was used. Liquid N was added often to the mortar to ensure the tissue remained frozen, and the pestle was used to disrupt and homogenise the tissue until it resembled a fine powder. Homogenised samples were stored in 1.5 mL Eppendorf tubes at -80 °C for further processing. To ensure the extraction of total RNAs, including small (>18 nt) RNAs, the RNA was extracted using the CTAB extraction buffer method as follows: firstly 1 mL of the extraction buffer containing CTAB was added to 100 mg of ground sample, and samples incubated in a water bath (65 °C, 20 minutes), and tubes inverted every 5 minutes. An equal volume of chloroform-isoamyl alcohol (24:1) was added, and samples agitated before being centrifuged (4 °C, 15 000 g, 15 minutes). The supernatant was then collected and an equal volume of phenol-chloroform-isoamyl alcohol (25:24:1, saturated phenol of pH 5) was added, mixed gently, then centrifuged (4 °C, 15, 000 g, 15 minutes). The phenol-chloroform-isoamyl step was repeated if the supernatant was not clear. The supernatant was collected and transferred to 1.5 mL microcentrifuge tubes, and 0.25 volume of 10 M lithium chloride added. Tubes were then gently inverted and stored overnight (4 °C). The tubes were then centrifuged (4 °C, 15 000 g, 15 minutes), the pellet washed with 4 M NaCl, then 75% ethanol, before being centrifuged a final time (4 °C, 12, 000 g, 15 minutes). The pellet was then dissolved in nuclease free water and stored at -80 °C for further use. For all other RNA extractions, the *EasyPure* Plant RNA kit was used. In both cases, contaminating DNA was removed using the DNase Max® kit (QIAGEN).

2.4.3.   Synthesis of cDNA for qPCR

Arabidopsis lines were grown to two-weeks old as per 2.3.6, RNA extracted as per 2.4.2. The method of RNA extraction depended on the focus of the qPCR; if the GP peptide sequence was being investigated, the total RNA, CTAB extraction process was used, if the level of *COPT2* was being investigated the *EasyPure* Plant RNA kit was used instead. Synthesis of cDNA was performed from DNAse-treated RNA using two methods: one for *COPT2* expression analysis and the second for GP expression analysis. For *COPT2* expression analysis, SuperscriptTM (II) Reverse Transcriptase (RT) (Invitrogen) was used as per the manufacturer's protocol. Total RNA (1 µg), Invitrogen Oligo (dT) 12-18 primers (10 mM) and dNTP mix (10 mM) was added to PCR tubes, then water added to a total of 12 µL. Samples were incubated at 65 $^\circ$C for five minutes in a thermocycling machine (PTC-200 Peltier Thermal Cycler, MJ Research), then held at 4 $^\circ$C for one minute, then 4 µL of 5 X Reverse Transcription Buffer, 2 µL DTT (0.1 M) and 1 µL of Invitrogen RNase Out (40 u / µL) was added. The reaction mix was incubated at 42 $^\circ$C for two minutes and 1 µL of SuperscriptTM (II) RT (200 u / µL) added to a total of 20 µL. Tubes were incubated at 42 $^\circ$C for two hours, followed by an enzyme inactivation step at 70 $^\circ$C for 15 minutes.

For GP expression analysis, the RNA was transcribed to cDNA using the miRNA 1st-strand cDNA synthesis kit (Agilent), as per the manufacturer's instructions. This kit contains a polyA tail extension step; a longer polyA tail means that it was possible to detect in qPCR the otherwise-short GP sequence using a universal reverse primer, which anneals to the cDNA sequence tag added to the 5' end of all cDNA species by the RT adapter primer during 1st-strand cDNA synthesis. Samples were kept on ice during the following steps: samples were serially diluted to the final concentrations for the primer efficiency tests, and cDNA was stored at -20 $^\circ$C until ready to use. Figure 3.12 and Figure 3.13 illustrate the location of the primers used in the primer efficiency tests against the *COPT2* sequence in the T-DNA mutant lines. The results of the primer efficiency tests are shown in Figure 3.14 - Figure 3.20.

2.4.4.   Confirmation of the T-DNA insertion in *copt2* mutant genotypes

To identify the location of the T-DNA insertion in all three Arabidopsis *copt2* mutant lines, PCR primers were selected that were specific to each line: a primer that was specific to the T-DNA sequence, as well as gene specific primers. Primers were selected from Nottingham Arabidopsis stock centre (NASC) (T-DNA specific primers), designed using Primer3 software, or taken from Perea-García et al, 2013 (143) in the case of *copt2-1* specifically (Table 2.10). The PCR reactions were performed using the DNA extracted as above (2.4.1), and reactions run as previously described (2.2.7). Three primers were used in each reaction to confirm the presence of the T-DNA insertion: one T-DNA specific primer, and two gene-specific primers (Table 2.10). Using three primers in the reaction generates various products depending on whether the samples were homozygous for *COPT2* or the T-DNA insertion sequence, or heterozygous. Reaction products were run on a 1.2 % Agarose gel as per 2.2.8. Products were then purified, quantified, and sequenced as previously

described. The "BLAST Sequence Analysis Tool" (144) was used with the results of the sequencing to determine the location of the T-DNA insertions in each Arabidopsis line.

2.4.5. Primer efficiency tests

Primers for qPCR were designed using the primer design software Primer3 (145,146) and synthesised by Integrated DNA Technologies and Sigma Aldrich. Specification for primer design included a product size range of 50 – 200 bps, a primer length of ~20 bps, an ideal Tm range of 58 – 60 °C with a Tm max of 70 °C, and a GC % range of 50 – 60 %, with some flexibility allowed. The qPCR reactions contained 4 μL WT cDNA (undiluted, 10^{-1}, 10^{-2}, or 10^{-3}), 200 nM primers, 10 μL FAST SYBR Green PCR Master Mix (Thermo Fisher Scientific) and nuclease free water to a final volume of 20 μL, in three technical replicates. In all qPCR reactions, nuclease free water was added in the place of cDNA in the negative control, and *ACTIN2* used as the endogenous control. Reactions were conducted in a sealed 96-well plate, which was centrifuged at 5000 g for 2 minutes prior to loading the plate into the qPCR machine (StepOnePlus™ Real-Time PCR System, cat no 4376600, Applied Biosystems). All qPCR reactions were conducted with the following cycle conditions: two minutes at 50 °C, ten minutes at 95 °C, forty cycles of 95 °C for 15 seconds and 60 °C for one minute. The primers used in the primer efficiency test are included in Table 2.11. Primers were investigated to determine their primer efficiencies using the following calculation, considering the slope of the standard curve calculated by plotting the cycle threshold (CT) value of primers used in qPCR reactions containing serial dilutions of WT DNA:

$$Efficiency\ (\%) = \left(\frac{-1}{10^{Slope} - 1}\right) x\ 100$$

Primers were selected using the following criteria: an efficiency of between 90 and 110 %, production of a single amplicon indicated by melt curve analysis (multiple peaks indicate more than one amplicon), and an absence of a large peak at 65 °C (which can indicate prominent levels of primer dimerisation).

2.4.6. Analysis of expression level by qPCR

The qPCR experiments were performed with a 4 μL undiluted sample from the cDNA synthesis reaction (2.4.3), alongside 200 nM of each primer. The reaction conditions were as described above for the primer efficiency tests (2.4.5), with the primers used (Table 2.11) selected due to their efficiency in the primer efficiency tests. Five technical replicates were performed per cDNA sample, and three biological replicates included in the qPCR analysis. StepOne Plus Real-Time PCR system (Applied Biosystems) and StepOne Software v2.2.2 (Thermo Fisher Scientific) was used to calculate CT values, and relative expression calculated by normalisation to the endogenous control, and then to the WT expression level by the Pfaffl method, which allows incorporation of the primer efficiencies into the calculation (147).

2.4.7. Arabidopsis root characterisation in the presence of Cu, Au or Pd

To identify phenotypic variations between Arabidopsis genotypes and WT in the presence of Cu, Au or Pd, seeds were sterilised (2.3.2) prior to stratification (2.3.3) as described previously. Seeds were then placed onto ½ MS(A) media which had been prepared as per 2.3.1, with Cu (0, 30, 40, 48 µM), Au (0, 50, 100, 150, 200 µM), or Pd (0, 5, 10, 15, 20 µM) (2.2.2) having been added to the ½ MS(A) media prior to cooling. Root length and number of branches was measured when plants were twelve days old, using ImageJ to measure the length on plates against a scale measurement (148). Root architecture was calculated as branches per mm (branches / length), as it was noted that some lines maintained high numbers of lateral branches despite shorter roots.

2.4.8. Analysis of element concentration in root and shoot tissue of Arabidopsis genotypes

Seeds were sterilised using the Cl-gas method (2.3.2), and 30 seeds placed in a single line across a square, twelve cm by twelve cm petri-dish filled with ½ MS (A) (2.3.1). These were stratified as per 2.3.3. Following stratification, plates were removed from the aluminium foil used to exclude light, and placed into a rack to stand vertically, so that the roots grew down along the surface of the solid media. Plates were kept within a plant growth room (16-hour day at 23 °C, eight-hour night at 20 °C) for ten days, allowing the seeds to germinate and produce root and shoot tissue. Tweezers were used to lift seedlings off the surface of the ½ MS(A) at the ten-day stage and transfer them into the hydroponic set up (2.3.5). At five-weeks old, ½ MS media was replaced with ½ MS media containing 1 mM Au (2.2.2, 2.3.1), five samples of each genotype and condition were collected after 24 hours, including the control condition with did not include any metal. The 1 mM concentration was used as optimisation experiments had determined that lower concentrations, more like those in mine waste tailings, did not result in an Arabidopsis shoot concentration above the detection limit for ICP-OES after 24 hours of exposure. A 1 mM concentration was detectable by ICP-OES in the WT lines in these optimisation experiments.

Samples were washed three times with 50 mL water and patted dry with blue roll. Additionally, root samples were submerged in a root desorption solution (2 mM $CaSO_4$ and 10 mM ethylenediaminetetraacetic acid) for ten minutes and shaken (180 rpm) to remove metals bound to the outside of the root tissue. Samples were then washed three times with 50 mL water and patted dry with blue roll. Samples were weighed (wet weight (g)) and placed in an oven at 90 °C for 72 hours, after which they were weighed again (dry weight (g)). The electronic scale utilised in the dry weight measurements was more accurate than that used in the wet weight measurements, and therefore the dry weight was used in element concentration calculations.

Tissue samples were broken down mechanically using a glass rod, the surface of which was then washed into the sample vial (EPA 40 mL screw vial with Chromacol 24-ST3-EPA PTFE lined screw caps, Thermo Scientific) with 10 mL methanol, and samples sonicated for 20 minutes. Following the sonication stage, samples were placed in a heating block and heated until the methanol had evaporated (100 °C, eight hours), leaving the sample in a dry, powdered form. Samples were digested overnight in 500 µL hot acid (aqua regia) in a fume cupboard (110 °C). Aqua regia is a

mixture of nitric acid and hydrochloric acid at a molar ratio of 1:3. The lids of the sample vials were screwed on tightly to reduce the escape of gases and generate a convection current as the gas heated at the bottom of the vial, vapourised, and cooled at the top. After cooling for at least an hour, samples were diluted with water to a final volume of 10 mL in a 10 mL volumetric flask, then filtered using glass microfibre filters (1.6 µM pore Whatman Glass microfibre filters, GF/A Grade, Cytivia) to remove particulates. Samples were run on an iCAP 7000 series (Thermo Fisher) to determine the concentration of Au, Pd, Cu or Fe by Inductively coupled plasma optical emission spectroscopy (ICP-OES). A standard curve for these elements was calculated using serial dilutions of Periodic table mix 1 and Periodic table mix 2 for ICP (Merck, UK); from 10,000 ppb to 1 ppb. Concentration (ppm) was multiplied by the dilution factor (0.1 L) to calculate the total mass of each element per sample (mg), then normalised by dry weight (g). Per element, concentration was initially measured using two wavelengths in case of interfering spectra or differences in sensitivity. Gold was measured at 242.795 nm and 267.595 nm, Pd was measured at 340.269 nm and 324.584 nm, Cu was measured at 213.598 nm and 324.754 nm, and Fe was measured at 239.562 nm and 259.940 nm.

2.4.9. Analysis of oxidative stress in root tissue

Metal or abiotic stress tends to elicit the generation of ROS within plant tissue. The metals Cu and Au are toxic in high concentrations to plant tissue and have previously been shown to result in an increase in cellular ROS production. Arabidopsis plants were grown on ½ MS(A) plates in conditions as described in section 2.3.6, then at two-weeks-old, four seedlings were transferred to each well in a six-well plate (STARLAB), containing ½ MS with either 30 µM Cu, 25 µM Au or 50 um Au. After 24 hours of metal exposure, seedlings were transferred to new wells and washed once with 1 X PBS.

A stock solution of 2',7'-dichlorodihydrofluorescein diacetate (H$_2$DCFDA) (Sigma-Aldrich) was produced by dissolving H$_2$DCFDA in dimethyl sulfoxide (DMSO) (10 mM). The stock solution was diluted to 10 µM (in PBS buffer) in a dark, 1.5 mL Eppendorf tube. Arabidopsis WT or *copt2-1* root samples were submerged in the liquid for 30 minutes as this resulted in the inner structures taking up the dye, then washed four times with 1 X PBS buffer in the dark. In the reaction shown in Figure 2.3, when oxidised by peroxides, which are involved in the production of ROS, H$_2$DCF is converted into a green, fluorescent product, dichlorofluorescein (DCF), which can be measured (149). Samples were exposed to peroxides in the root tissue for 24 hours before fluorescence measurement.
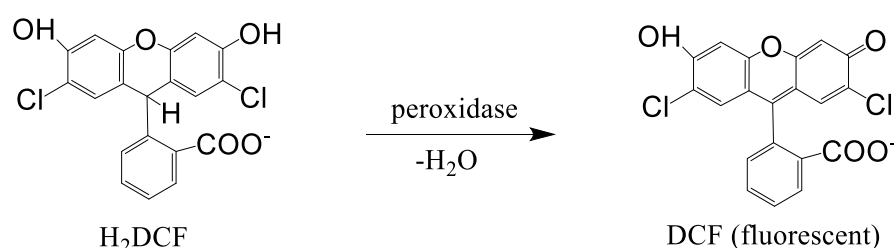
Figure 2.3. Reaction of 2',7'-dichlorodihydrofluorescein (H$_2$DCF) to generate the fluorescent product dichlorofluorescein (DCF)

The sample was mounted on a microscopic glass slide with 10 % glycerol solution. Images were captured using the ZEISS LSM 710 Epifluorescence microscope (Zeiss, Germany). Roots naturally emit auto fluorescent, and to mitigate this the lambda filter was selected at 9 % laser exposure, laser at 488 and gain master at 812. The dye had an emission wavelength of 522 nm, and a peak was identified at this wavelength. For images, a FITC filter (range 493 – 560 nm) was used (3 % laser exposure, laser at 488, gain master at 820). To maintain the consistency of fluorescence among images, common default exposure time was set for all the captured images. Images were quantified in ImageJ (148).

2.4.10. The *pART7* and *pMLBART* binary vector system

A binary vector system, shown in Figure 2.4, was used to generate *35S-COPT2* lines. The *COPT2* sequence was codon optimised for expression in Arabidopsis to distinguish between the endogenous and introduced version of the gene (optimisation performed on GeneArt) as the *COPT2* gene does not contain introns. This version of the sequence will be referred hereafter to as *optCOPT2*. The *XhoI* [CTCGAG] and *BamHI* [GGATCC] restriction enzyme sites were added to the beginning and end of *optCOPT2*, respectively, which contained the Cauliflower mosaic virus 35S promoter (CaMV35S) sequence upstream of *optCOPT2*. The *XhoI* and *BamHI* sites were used for ligation of the *optCOPT2* sequence into *pART7*. The *pMLBART-optCOPT2* was then created by *NotI* digestion to remove the flanking CaMV35S and ocs 3' sequences, and ligation into *pMLBART*. The gene cassette construction was performed by Dr Liz Rylott (Centre for Novel Agricultural Products, University of York) prior to the commencement of this project. The *pMLBART* contains spectinomycin resistance for *bacterial* selection, glufosinate ammonium resistance for plant selection, and a *NotI* cloning site between the right- and left-border. Binary vectors were laboratory stocks. The GV301 Electrocompetent *Agrobacterium* strain (GoldBio) (Table 2.2) strain contains a C58 chromosomal background with rifampicin resistance and the Ti plasmid pmp90 (pTiC58Dt-DNA) which contains rifampicin and gentamycin resistance on the Ti plasmid. The GV301 Ti plasmid has the T-DNA region sequences deleted and transformation with the binary vector containing the missing T-DNA region results in a functional T-DNA binary system that allows for the transfer of genetic material into a host plant S genome, such as in Arabidopsis.
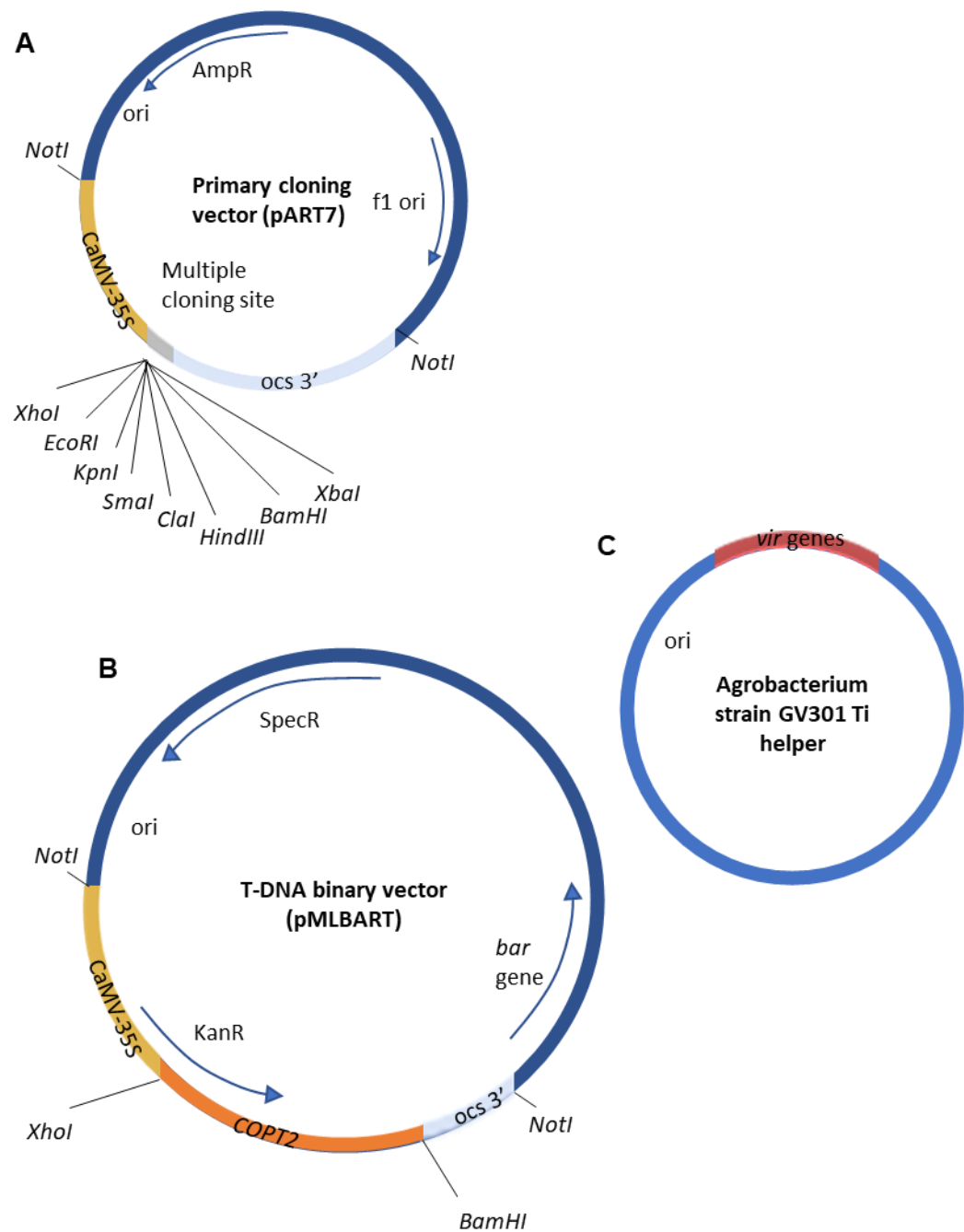
Figure 2.4. Schematic diagram of the T-DNA binary vector system (*pART7* and *pMLBART*) used in this study the generation of *35S-COPT2* and *35S-*GP*C* Arabidopsis lines A: Primary cloning vector containing the CaMV35S promoter and a multiple cloning site for insertion of the opt*COPT2* and *NotI* cloning sites for transfer into the binary vector; B: The opt*COPT2* gene is maintained within the T-DNA region of a binary vector, containing the Basta gene for selection against the non-selective herbicide glufosinate ammonium; C: Vir proteins encoded by genes on a separate replicon (*vir* helper) mediate T-DNA processing from the binary vector and T-DNA transfer from the bacterium to the host cell.

2.4.11. Heat shock transformation of *Agrobacterium*

The *pMLBART-optCOPT* was transformed into *Agrobacterium* (Table 2.2) by the heat shock technique. *Agrobacterium* were thawed on ice (250 µL per transformation reaction), and 100 ng of plasmid (in a volume up to 10 µL) added to the thawed culture. The mixture was kept on ice (4 °C) for five minutes, and then transferred to liquid N for five minutes. The mixture was incubated for an additional five minutes in a 37 °C water bath, then 250 µL cells transferred to a 15 mL falcon tube containing 1 mL of LB and shaken (180 rpm, 28 °C) for two hours. Cells were pelleted (2 minutes, 5000 rpm), the supernatant discarded, and cells resuspended in 150 µL LB before 50 µL or 100 µL was spread onto two LB(A) plates containing the selection antibiotic (untransformed: gentamycin 30 µg/mL; transformed: spectinomycin 50 µg / mL) and cultured at 28 °C overnight. Successful transformants were identified as single colonies that grew on LB(A) containing antibiotic, and these were re-streaked onto a fresh LB(A) plate containing antibiotic prior to use in the floral dip transformation of Arabidopsis.

2.4.12. Floral dip transformation of Arabidopsis with *Agrobacterium*

Six weeks prior to transformation, Arabidopsis seeds were grown as in 2.3.6. The propagator dome was removed after five days, and seedlings thinned to ten per pot (in p15, 3 X 5, cell propagator trays) after three weeks. Successfully transformed *Agrobacterium* was streaked onto a fresh LB(A) plate containing antibiotics for both the Ti plasmid (gentamicin 30 µg / mL) and the transgene construct (spectinomycin 50 µg / mL) and grown overnight at 28 °C. A 50 mL falcon tube containing 10 mL culture of LB (containing both previously mentioned antibiotics) was inoculated with a single culture picked from the *Agrobacterium* LB(A) plate and grown overnight at 28 °C with shaking (180 rpm). The overnight culture was then transferred to a 2 L Erlenmeyer flask containing LB (with both antibiotics) and grown overnight at 28 °C with shaking (180 rpm). The culture was then split evenly between two sterile, balanced 250 mL centrifuge bottles, and the *Agrobacterium* culture pelleted by centrifugation (5000 rpm, three minutes). The supernatant was discarded, and pellets resuspended in the same volume of 5 % sucrose in sterile, distilled water. The suspension was then poured into a large beaker and 0.05 % Silwet added to the suspension. Arabidopsis plants were inverted and placed into the suspension, ensuring that the buds and base of the leaf rosette were submerged in the liquid. The suspension and plant were agitated by manual shaking for 30 seconds. Following agitation, plants were transferred into an autoclave bag, and returned to the plant growth room (2.3.4). Plants were removed from these bags twenty-four hours later, and seeds allowed to develop and mature. Upon the formation of siliques, watering was stopped, plants left to dry, and seeds collected.

2.4.13. Confirmation of transformation of T1 seeds, and homozygous seed selection

Arabidopsis transformants containing the selectable marker gene (*bar* gene) were picked as those able to successfully produce secondary leaves on plant selection media (½ MS(A) containing 20 mg / mL glufosinate ammonium herbicide). Resistant seedlings were put to F2 compost and allowed to propagate seeds. To establish segregation ratios, 100 T2 seeds were sown onto ½ MS(A) (20 mg/mL glufosinate ammonium). The T2 lines with 3:1 resistant:sensitive segregation ratios, indicative of single insertional events, were again transferred to soil. Following this, stable, non-segregating, homozygous T3 transgenic lines were detected by identifying lines with 100% resistance to glufosinate ammonium. Three independent, homozygous lines, referred to as *35S-COPT2A, B* or *C* from this point forward were identified for subsequent analysis.

2.4.14. Generation of Arabidopsis *35S*-GP lines

The AuNP forming peptide (GP) (amino acid sequence GASLWWSEKL) has been shown to aid the *in vitro* formation of AuNPs when in solution with $KAuCl_4$ (59). Prior to the commencement of this project, Dr Liz Rylott had generated and established homozygous *35S*-GP expressing Arabidopsis lines. These lines were generated using the *pART7* and pART27 binary vector system (150), and expression is under the control of the near-constitutive CaMV35S promoter (Figure 2.5, Figure 2.6).

Figure 2.5. The GP sequence present in the Arabidopsis *35S*-GP lines. Highlighted are the following features: *Xho*I site (blue), start codon (red), GP coding sequence (yellow), stop codon (black), *Nde*I site (pink), *Hind*III site (green)

The *Xho*I and *Hind*III sites at the beginning and end of the GP sequence respectively were used for ligation into *pART7*, which has ampicillin/carbenicillin resistance. The sequence containing the flanking CaMV35S and ocs 3' sequences was removed from *pART7* using the *Not*I digestion sites and cloned into pART27 (pART27-*35S*-GP), which has spectinomycin, streptomycin and kanamycin resistance (50 µg/mL) (Figure 2.6). The pART27 was introduced into the *Agrobacterium* GV301 strain (which contains rifampicin and gentamycin resistance on the Ti plasmid) by heat shock transformation. Arabidopsis WT lines were transfected with *Agrobacterium* containing *pART27-35S-*GP by floral dip (2.4.12), and transformants identified using selection media (½ MS containing 50 µg/mL kanamycin). Lines segregating with 3:1 resistant to sensitive ratios, indicative of single insertional events, were selected and subsequently homozygous T3 lines were identified on selection media, then five homozygous seedlings for each line put to soil to be used in future experiments (*35S*-GP*A*, *35S*-GP*B*, *35S*-GP*C*).
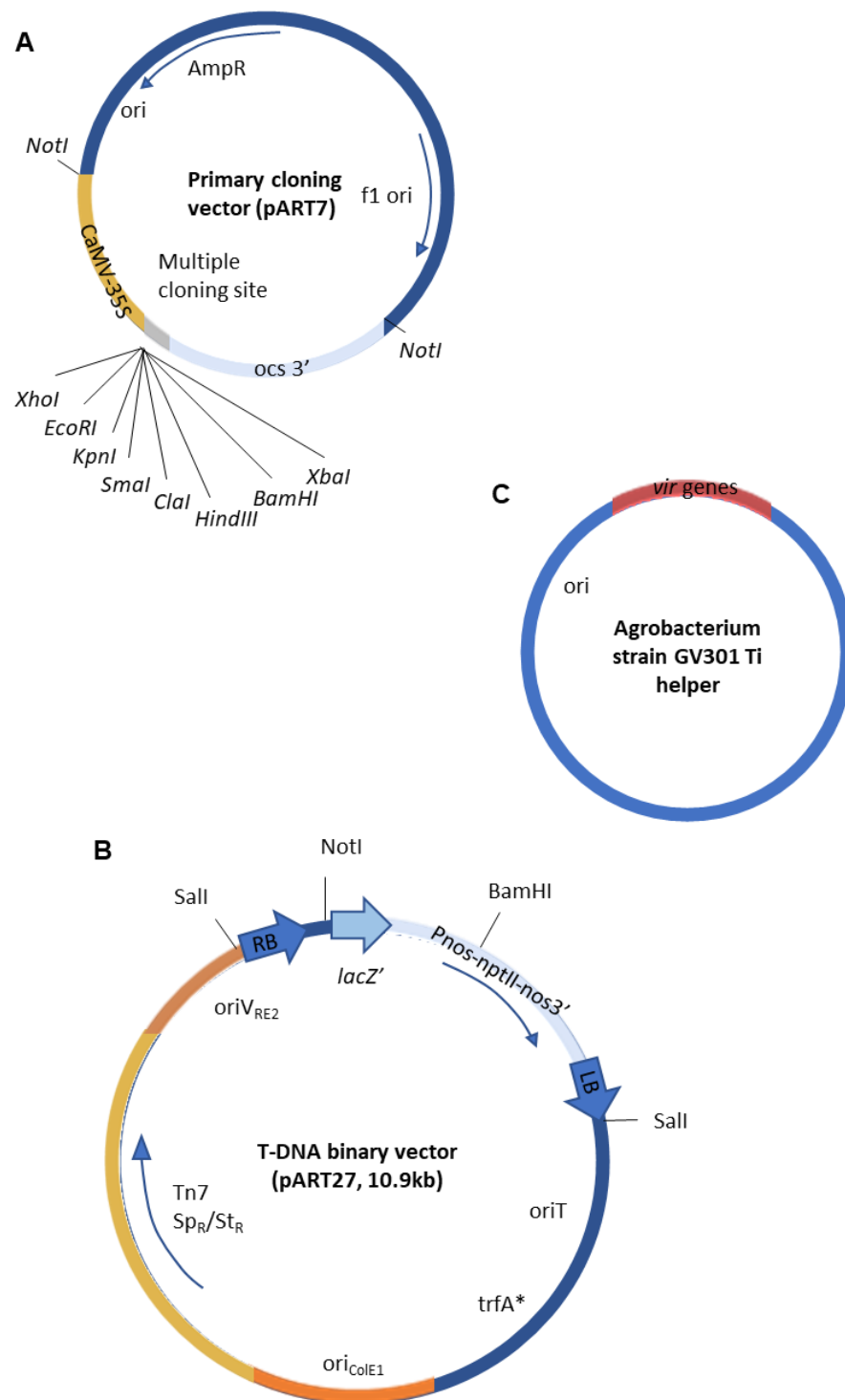
Figure 2.6. Schematic diagram of the T-DNA binary vector system (*pART7* and pART27) used in this study for the generation of *35S*-GP Arabidopsis lines. Schematic diagram of the T-DNA binary vector system used in the generation of Arabidopsis *35S*-GP lines. A: Primary cloning vector containing the CaMV35S promoter and a multiple cloning site for insertion of the optimised *COPT2* sequence (*optCOPT2)* and *NotI* cloning sites for transfer into the binary vector; B: The *pART27* binary vector; C: Vir proteins encoded by genes on a separate replicon (*vir* helper) mediate T-DNA processing from the binary vector and T-DNA transfer from the bacterium to the host cell.

2.4.15. Confirmation of Arabidopsis *35S*-GP lines by diagnostic PCR

For diagnostic PCR, DNA was extracted (2.4.1) from two-week-old rosette leaves of soil-grown WT, *35S*-GP*A, 35S*-GP*B,* and *35S*-GP*C* lines grown as previously described (2.3.6). The RNA extraction was performed using the CTAB method as previously described (2.4.2). An additional DNase treatment was performed as per 2.4.2. The RNA was transcribed to cDNA using the miRNA 1st-strand cDNA synthesis kit as described previously. The manufacturers protocol stated that "the custom forward primer should be identical in sequence and length to the target". Primers for qPCR were initially designed within the insert sequence, however as the GP sequence is 30 bases long, the products produced would be short (~ 30 nucleotides)**.** Ideally, the parameters of the primer should be as follows: Tm between 50-55 ^{o}C**;** avoid the formation of hairpins more negative than -2**;** avoid 3' end self-dimers more negative than -5 and internal self-dimers more negative than -6 kcal / mol. The parameters of the GP sequence primer (GP-F) are shown in Table 2.13. The sequence was then optimised to fit the parameters of recommended primer design. The optimization included shortening the sequence to reduce the Tm and reducing the 3' self-dimers.

Table 2.13. Parameters of the primers used in RT-PCR and qPCR reactions for genotyping Arabidopsis *35S*-GP lines

Primer name	Sequence (5' – 3')	Length (nt)	Tm (oC)	GC (%)	Hairpin ΔG (kcal/mol)	Self-dimer ΔG
GP-F	ATGGGAGCTTCTCTTTGGTGGT CTGAAAAGTTGTAATGA	39	64	41	-0.8	-9.28 3'
optGP-F	GGTGGTCTGAAAAGTTGTAATG A	23	53	39	-0.48	-1.94

2.4.16. Primer efficiency tests and qPCR in *35S*-GP lines

The primer pair efficiency was established as previously described in 2.4.5, using primers detailed in Table 2.11. Analysis of expression level was performed by qPCR as per 2.4.6. The optGP-F and universal reverse primer were used to estimate the GP transcript abundance relative to the endogenous control gene (*ACTIN2*). As the GP sequence is a synthetic peptide that is not present in the Arabidopsis WT lines, these values could not be normalised to WT expression so was instead normalised to *ACTIN2*. Excluding this step, the Pfaffl method was used, which accounts for specific primer efficiency, and Arabidopsis WT cDNA was utilised in the qPCR reaction as a control.

2.4.17. Generation of transgenic plants lines (*35S*-GP*C*) using the *pART7* and *pMLBART* binary vector system

The *pMLBART* T-DNA binary vector system was used to introduce the *optCOPT2* sequence (2.4.10) into previously established Arabidopsis *35S*-GP using *Agrobacterium* mediated transformation as previously described (2.4.12), to generate double-transgenic *35S*-GP*C* lines.

2.4.18. Confirmation of transformation of T1 *35S*-GP*C* seeds, and homozygous seed selection

Positive transformants containing the selectable marker gene were selected as those that were able to successfully produce secondary leaves on plant selection media (½ MS containing 20 mg / mL glufosinate ammonium herbicide and 20 mg / mL kanamycin). Resistant seedlings were put to F2 compost and allowed to propagate seeds. To establish segregation ratios, 100 T2 seeds were sown onto ½ MS(A) (20 mg / mL glufosinate ammonium). The T2 lines with 3:1 resistant: sensitive segregation ratios indicative of single insertional events, were again transferred to soil. Following this, stable, non-segregating, homozygous T3 transgenic lines were detected by identifying lines with 100% resistance to glufosinate. Three independent, homozygous lines, referred to as *35S*-GP*CA, B* or *C* from this point forward were identified for subsequent analysis.

2.4.19. Quantitative PCR on *COPT2* and GP sequence in *35S*-GP*C* lines

Analysis of expression level was performed by qPCR as per 2.4.6. The level of *COPT2* expression was established as described previously (2.4.6), as was the level of GP (2.4.16).

3. The role of Arabidopsis *COPT2* and expression of the gold-nanoparticle-forming peptide (GP) in Au uptake and NP formation

3.1. Introduction

As outlined in section 1.3.1.1, COPT2 is plasma-membrane located Cu uptake transporter that also transports Au in Arabidopsis (4). In this chapter, the interaction between COPT2, Au and the gold-nanoparticle-forming peptide (GP) is investigated to determine their involvement in Au uptake and NP formation. To investigate this, a range of yeast and Arabidopsis, mutant and transgenic lines were utilised. In section 3.2 methods, the *pYES2-COPT2y* and *pMLBART-optCOPT2* are described, and their subsequent transformation into yeast or Arabidopsis to generate transgenic yeast strains or Arabidopsis *COPT2* over-expression (*pMLBART-COPT2*) lines. The *pART*27-GP was transformed into Arabidopsis, and then into the *COPT2* over-expression lines. The yeast and Arabidopsis lines were then investigated for the influence of COPT2 and GP on Au uptake and tolerance.

3.1.1. Au

Gold is widely recognized as a metal of significance for ornamental objects, jewelry and investment (151), and more recent applications in technology and the manufacture of electronics (152). The diverse applications of Au are a result of the unique properties of the metal. Gold is an efficient electrical conductor, resistant to corrosion, has high malleability, when alloyed with other metals can have increased durability and strength, and altered optical properties (152). In developing countries, Au has an important role in socio-economic development; Au mines often operate in remote locations and result in the creation of employment, infrastructure and investment from foreign sources (46). Anthropogenically generated AuNPs enter the environment through the degradation of waste products, or through the process of abrasive wear in industry. The usefulness of Au is applicable in surprising research areas; AuNPs are used in rapid medical diagnostic test kits, including the Covid-19 antigen and antibody tests (153).

Many industrial applications utilise Au in tiny amounts, and this results in a gradual loss of this element into the environment by disposal through routes that do not allow for metal recycling. There is also an untapped resource of Au in the waste materials, or tailings, from mining activities. Mine tailings, generated as a waste product of Au mining contain a mix of elements. The composition of the mine tailings is determined by the method used to extract the metal, as well as the components that were present in the ore. For instance, cyanidation tailings, produced as part of the cyanidation leaching process in Au mining, consist of hazardous solid waste containing Au, cyanides (which are highly toxic), and other elements including Ag, Fe, S, Cu, lead and Zn (154). Around 90% of Au is recovered from ore through the cyanidation process, which has led to hundreds of millions of tons of cyanide tailings worldwide (155).

3.1.2. Studies of heterologous COPT2 expression in the presence of Au in yeast

The yeast strains utilised in this study were: *Δace1*, *Δccc2* and *Δctr1ctr3*, along with their parental strains BY4741 and DTY165. These mutant yeast strains are part of the Cu uptake and detoxification pathway in yeast, as shown in Figure 3.1.
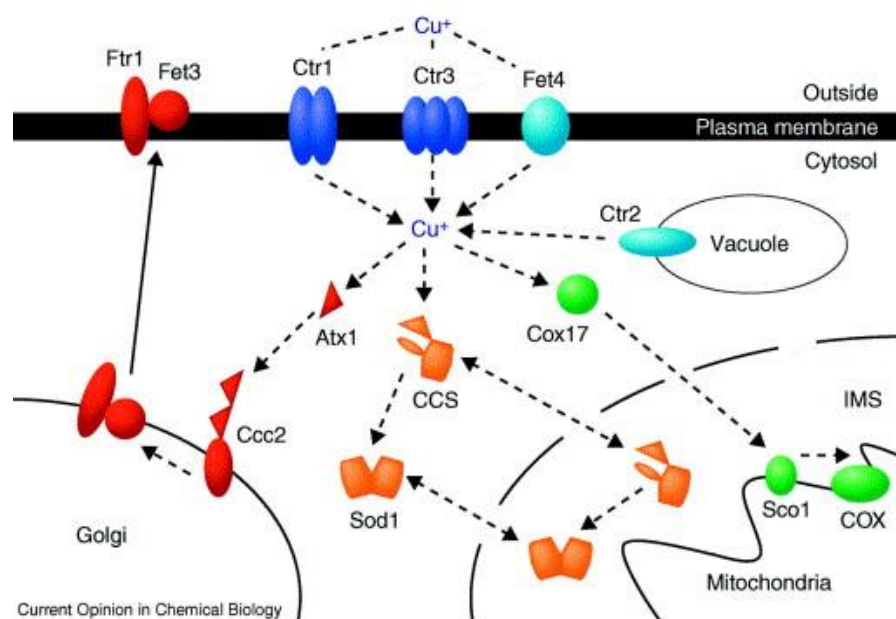
Figure 3.1. Cu transport and distribution in yeast as shown by Puig et al (2002). Depending on extracellular Cu concentrations, Cu is transported inside the cell by two high-affinity Cu transporters *Ctr1* and *Ctr3*, or by a low-affinity Cu/Fe-transporter *Fet4*. *Ctr2* could be involved in Cu efflux from the vacuole. Cu is distributed by an unknown mechanism to three different metallochaperones: *Atx1*, *CCS* and *Cox17*. Delivery of Cu to the secretory compartment (pathway shown in red) involves the metallochaperone *Atx1* that shuttles Cu to *Ccc2*, a P-type ATPase located in the trans-golgi network and is responsible for Cu translocation. Once Cu is in the lumen of the secretory pathway, it is loaded onto Fet3, a multi-Cu-ferroxidase essential for high-affinity Fe uptake that partners with the *Ftr1* subunit. The delivery of Cu to *Sod1* is mediated by the Cu chaperone for *SOD*, *CCS* (pathway shown in orange). The CCS protein contains three different domains: an Nt domain I similar to *Atx1*, a central domain II with homology to *Sod1* and an essential Ct domain III. *CCS* directly interacts with *Sod1* through the central domain and contacts from domain III to form a heterodimer. The pathway for delivery of Cu to the mitochondria is shown in green. The metallochaperone *Cox17* delivers Cu to *Sco1*, and other proteins, located in the inner mitochondrial membrane. Then Cu is transferred to specific subunits of *COX*. Figure reproduced from Puig et al (2002), with permission from Elsevier (73)

Whilst an essential metal to many enzymes, in high quantities Cu can be toxic, and therefore Cu homeostasis is tightly controlled. Copper is able to participate in Fenton-like reactions which can generate extremely reactive $OH^{.}$, capable of causing cellular damage such as protein oxidation, DNA and RNA cleavage and membrane damage due to lipid peroxidation (87). A high concentration of Cu can also cause toxicity due to its incorporation into proteins that do not require the metal. For example, Cu has been shown to replace Zn in the Zn-finger DNA binding domain of the human estrogen receptor, resulting in a disruption of the protein function (156). The *Δctr1ctr3* mutant strain is the first part of the Cu uptake and detoxification pathway investigated in this work. The *Δctr1ctr3*

strain contains a double deletion of *CTR1* and *CTR3* by PCR mutagenesis of the *URA3* marker, replaced in part by the kanamycin resistance cassette (167). In yeast, extracellular Cu^{2+} is reduced to Cu^+ by cell surface located Fre1p and Fre2p reductases (69,157), then Cu^+ is transported into the cell by two independent high affinity Cu uptake transporter proteins, Ctr1 and Ctr3 (158,159).

The distribution of Cu to specific target enzymes is mediated by Cu chaperones, for instance Atx1, a metallochaperone which mediates Cu delivery to proteins in the secretory pathway (e.g. Ccc2), as shown in Figure 3.1 (160). The *Δccc2* strain, used in this work, lacks a functional yeast Ccc2, which encodes a P-type ATPase pump localised in the golgi compartment in the secretory pathway (169), regulating Cu delivery from the cytosol to multi-Cu oxidase Fet3p. The post-translational insertion of four Cu ions into Fet3p is essential for its activity as a multiCu-containing glycoprotein, which catalyses the oxidation of Fe^{2+} to Fe^{3+}, coupled to the reduction of O_2 to H_2O. The Fet3p-bound Fe^{3+} can then permeate the membrane facilitated by Ftr1p (161).

The third yeast mutant used in this study is the *Δace1 s*train, which lacks the functional Cu-binding transcription factor, Ace1p, which activates the transcription of the MT genes *CUP1* and *CUP2*, involved in Cu detoxification, and the O_2^- dismutase gene, *SOD1* (169). The Ace1p binds Cu through specific cysteine residues within the amino-terminal DNA binding domain (162,163). Copper resistance in yeast is strongly influenced by the *CUP1* locus, and the level of Cu resistance is tied to the copy number of this locus (164,165). Expression of *CUP1* is increased 10 – 20 fold in response to elevated Cu concentration, and *CUP2* influences the expression of *CUP1,* acting as a trans-regulator (165). Reduced expression of *CUP1* results in Cu sensitivity at otherwise non-toxic levels (164).

The copper transporter family of proteins (COPTs) in Arabidopsis were described by Sancenón et al (2003), in part by heterologous expression in yeast (76). The COPTs (COPT1/2/3/5) were used in functional complementation analysis performed in the *Δctr1ctr3* yeast mutant (76). The functional complementation assay, or spot dilution assay, was also utilised in the work described here. Yeast strains are grown in selection media (SD-U) to an $OD_{600} = 1.0$. A serial dilution is performed for each strain, and then an equal volume of each non diluted or diluted culture placed sequentially onto SD-U(A) plates. The growth of yeast strains under different conditions can be assessed qualitatively by assessing the level of growth at each dilution on SD-U(A) plates containing different metal additions. As shown in Figure 3.2, in work performed by Sancenón et al., the COPTs were expressed in yeast under the control of the constitutive glyceraldehyde-3-phosphate dehydrogenase gene promoter. The *Δctr1ctr3* line lacks the ability to survive under Cu-limiting conditions with a non-fermentable carbon source because of the defective high-affinity plasma membrane transporters (168). Lack of growth in ethanol/glycerol media for the mutant containing the negative control was restored when transformed with the same plasmid expressing yeast *CTR1* (as a positive control), *COPT1* and *COPT2,* as did 100 μM Cu (76).
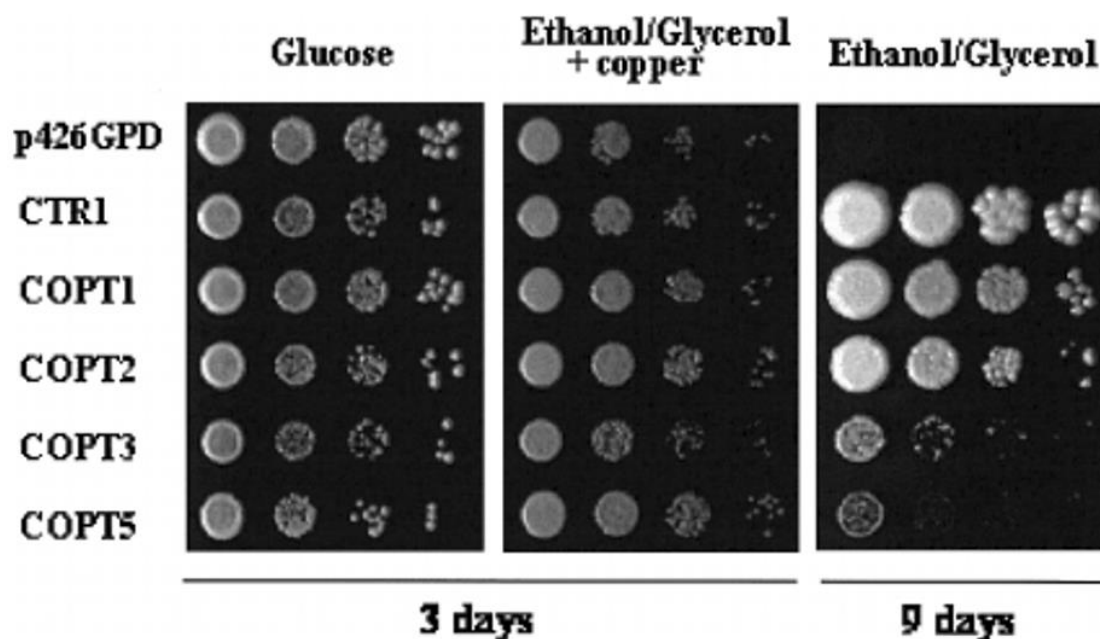
Figure 3.2. Functional complementation of *Δctr1ctr3* yeast mutant by COPT1, COPT2, COPT3 and COPT5. The *Δctr1ctr3* mutant was transformed with vector p426GPD (expression vector, negative control), the same vector expressing yeast CTR1 (yeast, positive control) or the predicted open reading frame (ORF) for COPT1 (plant positive control), COPT2, COPT3 or COPT5. Cells were grown at 30 °C on glucose (glu) (SC-ura) or on ethanol/glycerol plus copper (YPEG + 100 µM CuSO$_4$) plates for three days, and on ethanol/glycerol (YPEG) for 9 days. Reprinted with permission from Springer Nature: Plant Molecular Biology, Sancenón et al (2003) (76)

In 2017, Tiwari et al (4) demonstrated the activity of *COPT2* in Au uptake in Arabidopsis, by showing that the heterologous expression of *COPT2* leads to Au sensitivity in yeast. To measure the toxicity caused by Au uptake, the growth kinetics of *COPT2*-expressing yeast cells were investigated in liquid media. Yeast cultures were inoculated with Cu (as a positive control) and Au and the growth measured by spectrophotometer (OD) at 12, 16 and 20 hours post addition of Cu or Au as shown in Figure 3.3A. The liquid growth studies showed that there was a growth inhibition of the COPT2-expressing yeast strain after 12 hours compared to the vector transformed cells in the presence of Cu and Au. Following elemental profiling using ICP-OES, the concentration of Cu and Au in the COPT2-expressing yeast cells was higher than in the vector transformed controls, suggesting that COPT2 can function with Au as well as Cu (4).
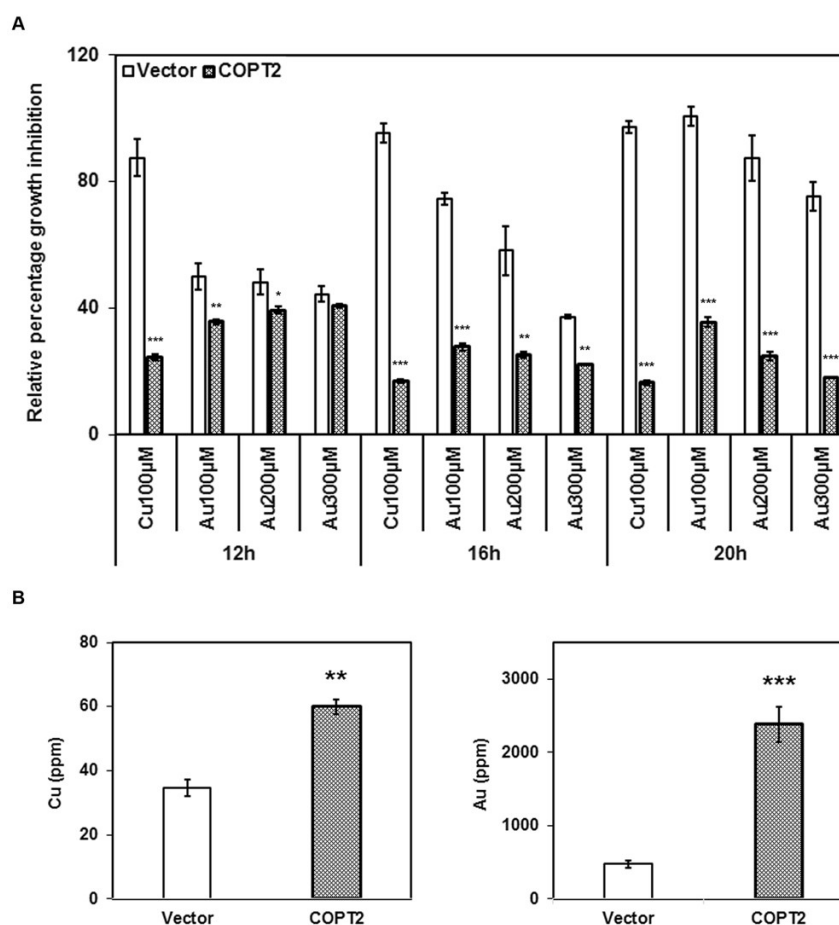
Figure 3.3. The Au-induced growth inhibition and uptake ability of COPT2 in yeast, as demonstrated by Tiwari et al (2017) (4). (A) The precultures (O. D.1.0) of vector and COPT2-transformed clones were inoculated in SC-URA medium with and without mentioned concentrations of Cu and Au and were monitored for growth. The data shows the relative percentage growth inhibition of three individual replicates. (B) Overnight grown cultures (O. D.1.5) were fed with Au (100 µM) and allowed to grow for 4 h. Cells were harvested and washed with nanopure water many times. Elemental profiling was performed using ICP-OES. Asterisks *, ** and *** denote significant difference P > 0.01, P > 0.001 and P > 0.0001 compared to vector transformed yeast cells. Figure reproduced from Tiwari et al (2017) (4)

In the work presented in this chapter, the five yeast strains described above have been transformed to express a version of the Arabidopsis *COPT2* where the sequence has been codon optimised for expression in yeast. The expression of *COPT2* is under the control of the GAL1 promoter and therefore only expressed in the presence of galactose as the sole carbon source. These strains were grown in a spot dilution assay (as per Sancenón et al., Figure 3.2) on SD-U plates containing Cu, Au or Cu and Au, at non-toxic concentrations, to determine the impact of *COPT2* expression on growth.

3.1.3. Studies of Au in Arabidopsis, using *copt2* mutant lines

Studying genetic mutants are a central tool for understanding the biological impacts of genes, permitting the study of the loss of an individual gene on the organism's function. In this work, Arabidopsis *copt2* mutants are used to study the activity of COPT2 by assessing the root phenotype in the presence of Au in comparison to the WT. Such *in vivo* characterisation is preferable to gene characterisation by sequence homology to other genes, as this may provide misleading information. A high degree of sequence similarity between proteins doesn't necessarily indicate shared function, for example, the *AtABCC7* is not orthologous or functionally equivalent to *OsABCC7* from *Oryza sativa* or *HsABCC7* from humans (166). The three Arabidopsis *copt2* mutants utilised in this work were generated by T-DNA insertion, as part of a collection of sequence-indexed insertion lines in Arabidopsis (167). *Agrobacterium* T-DNA-induced insertion mutant collections were generated in the late 1990's and early 2000's (167). These lines were generated by the insertion of a T-DNA fragment randomly into the plant host genome by a transformation process mediated by *Agrobacterium* infection. The DNA fragment that is introduced into the genome is flanked by a 25 bp border sequence from a heavily modified tumour inducing Ti plasmid. The location of the randomly inserted T-DNA can be identified using the known DNA border sequence, utilising primers from the left border of the T-DNA, and mapping this sequence to the genome to identify the insertion location (168), as shown in Figure 3.4.
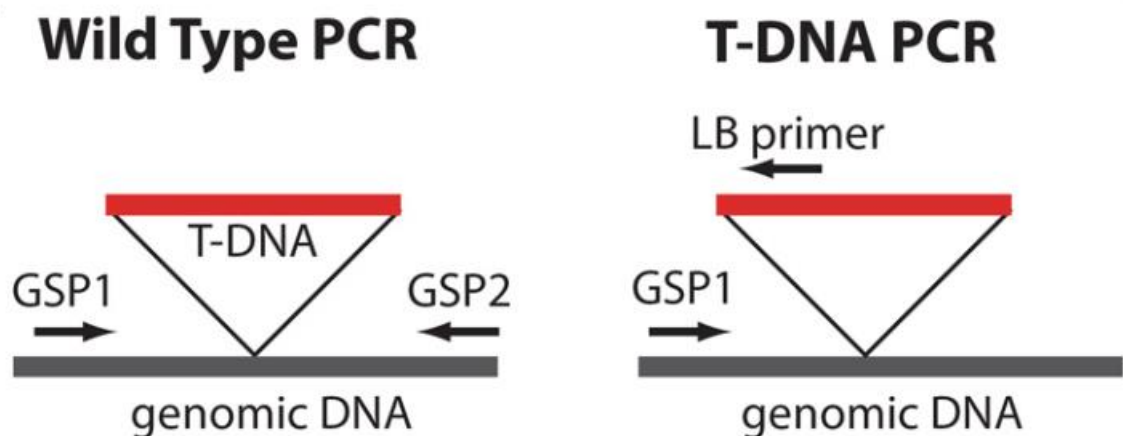
Figure 3.4. Schematic showing the process of identifying the location of a T-DNA insertion. A collection of Arabidopsis T-DNA insertion mutants were generated using this technique, and the insertion locations identified using a primer that is designed against the known left border (LB) of the T-DNA sequence.

The *copt2-1* mutant line was characterised by Perea-García et al. (2013) (143). The *copt2-1* mutant line was established in this work as a knockout under all conditions evaluated (Figure 3.5). In the WT line under Cu and Fe sufficient conditions, there is basal *COPT2* expression. Expression is increased slightly under Fe-deficient conditions, further under Cu-deficient conditions, and expressed at the highest level in WT under both Fe- and Cu- deficient conditions, as shown in Figure 3.5.
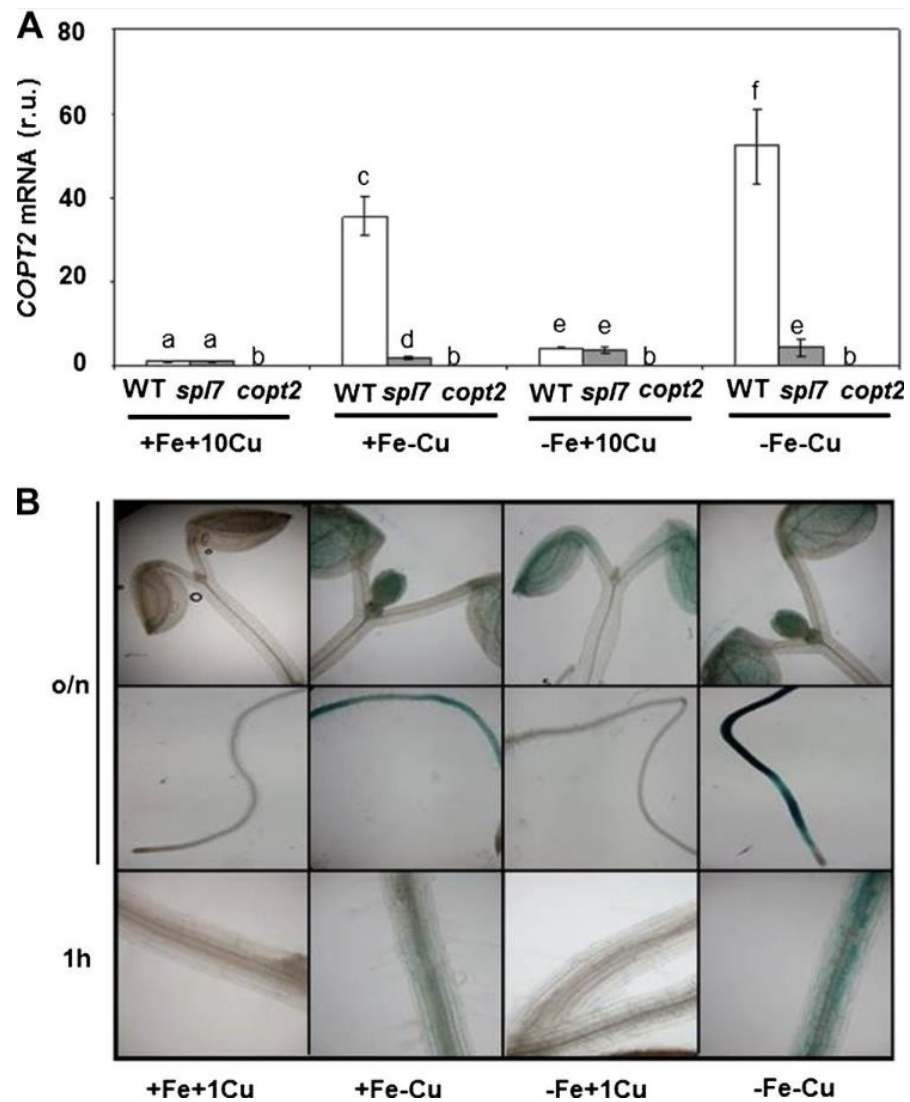
Figure 3.5. *COPT2* expression in Arabidopsis under Cu and Fe deficiencies. (A) *COPT2* expression analysis by qPCR in WT (WT; white bars), *spl7* (gray bars), and *copt2-1* (*copt2*; dark gray bars) seedlings. Total RNA from 7-day-old seedlings grown under the control (+Fe+Cu; supplemented with 10 µm CuSO$_4$), Cu deficiency (+Fe−Cu), Fe deficiency (−Fe+Cu; supplemented with 10 µm CuSO$_4$), or Fe and Cu deficiency (−Fe−Cu) conditions was isolated and retrotranscribed to complementary DNA. *UBQ10* gene expression was used as a loading control. Values are means ± sd of three biological replicates. r. u. , Relative units. Different letters above the bars represent significant differences among all the means ($P < 0.05$). (B) GUS staining in 7-d-old seedlings from the PCOPT2:GUS transgenic lines grown under control (+Fe+Cu; supplemented with 1 µm CuSO$_4$), Cu deficiency (+Fe−Cu), Fe deficiency (−Fe+Cu; supplemented with 1 µm CuSO$_4$), or Fe and Cu deficiency (−Fe−Cu) conditions at different incubation times at 37°C (overnight [o/n] and 1 hour). Figure reproduced from Perea-García et al. (2013) (143)

In their study linking Arabidopsis *COPT2* with Au uptake in root tissue, Tiwari et al. demonstrated that the *copt2-1* mutant line had reduced Au uptake (4). The concentration of Au in the root and shoot tissues of *copt2-1* was measured using ICP-OES following exposure to 10 ppm Au for four days in a liquid growth system. The Au content in the roots of the *copt2-1* line was significantly lower than in the roots of the WT line, but not in the shoot tissue, as shown in Figure 3.6. As the authors anticipated, the Cu level was significantly reduced in *copt2-1* root tissue in the presence of Au compared to the WT, but higher in the shoot tissue.
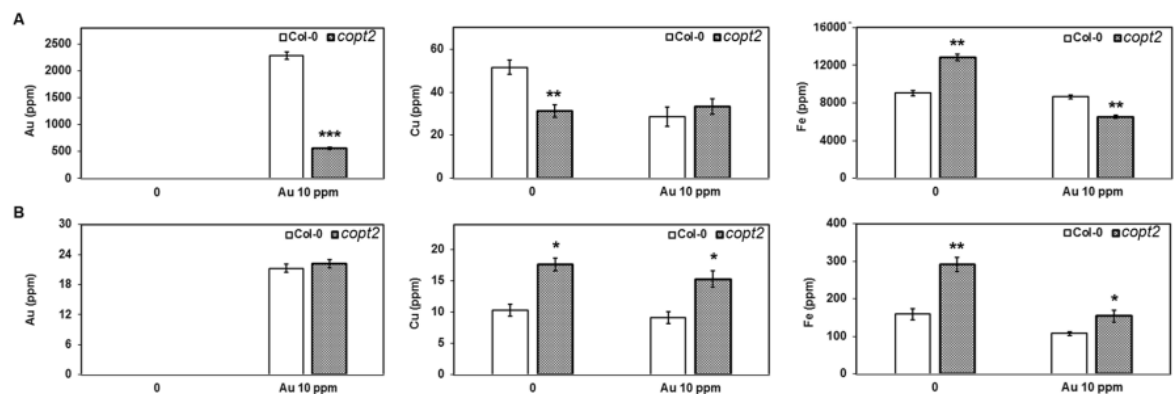
Figure 3.6. Element measurement in root and shoot of Arabidopsis by Tiwari et al. (2017). (A) Elemental profiling under control and Au (10 ppm) treated conditions through ICP-OES in root and (B) shoot. Data are a mean of three independent biological replicates and presented as $\pm$SEM. Asterisks (*, ** and ***) represent significant difference: $p > 0.01$, $p > 0.001$ and $p > 0.0001$ compared to the WT (Col-0). Figure reproduced from Tiwari et al., (2017) (4)

There are several methods to measure the concentration of elements in plant tissue, including optical methods (flame emission spectroscopy (FAS), atomic absorption spectroscopy (AAS), graphite-furnace AAS (GF-AAS), ICP-OES), mass spectrometry methods (ICP mass spectrometry (ICP-MS)), X-ray fluorescence (XRF) or using ion-specific electrodes or ion chromatography (169). In ICP-OES, used in the work presented here, a solution of sample is sprayed into a stream of argon that flows into a 'torch' where the gas stream is heated to 10,000 ºC. At this temperature, a plasma forms, where the atoms are present in an ionized state, and the elemental composition is determined using optical emission spectroscopy (OES). The spectrophotometer is used to separate the emission spectra of elements present in the sample to identify the concentration against a standard curve. Solid samples, such as plant tissue, are converted into a liquid state prior to analysis using acid digestion to dissolve the plant material. There are numerous advantages of using ICP-OES over other elemental analysis techniques, such as AAS:

- A wide linear dynamic range
- A high matrix tolerance
- Improved ease and speed of analysis (170)

In the work presented here, five-week-old Arabidopsis plants were exposed to 1 mM Au for four hours, before being converted to a liquid state using aqua-regia. Aqua regia is formed of nitric acid (HNO_3) and hydrochloric acid (HCl), and is used to dissolve Au, Pd and Pt, as shown in Figure 3.7 (171). The samples were diluted, and the concentration of Au, Cu and Fe analysed by ICP-OES to determine whether there was a difference in element concentration between the *copt2* mutant lines and the WT.

A

$$HNO_3\ (aq) + 3HCl\ (aq) \longrightarrow NOCl\ (g) + 2H_2O\ (l) + Cl_2(g)$$

B

$$Au(s) + 3NO_3^-\ (aq) + 6H^+\ (aq) \leftrightarrows Au^{3+}\ (aq) + 3NO_2\ (g) + 3H_2O\ (l)$$
$$Au^{3+}\ (aq) + 4Cl^-\ (aq) \leftrightarrows AuCl_4^-\ (aq)$$
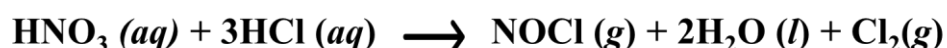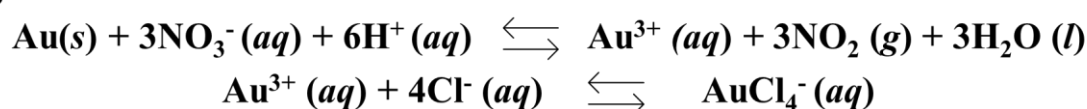
Figure 3.7. Aqua regia, a mixture of nitric acid (HNO_3) and hydrochloric acid (HCl). (A) The chemical reaction that occurs following the mixing of HNO_3 and HCl: nitrosyl chloride (NOCl), water (H_2O) and chloride (Cl_2) are formed, with NOCl and Cl_2 released as gases. (B) The chemical reactions which represent the reaction between Au and aqua regia. The reduction of the concentration of Au^{3+} ions shift the equilibrium towards the oxidised form, resulting in the gold dissolving completely to form chloroauric acid ($HAuCl_4$).

Plants respond to metal induced stress in several ways, but one of the most common is the generation of ROS and oxidative stress. The cell H_2DCF is a chemically reduced form of fluorescein used as an indicator for ROS in cells (172). The non-fluorescent H_2DCF is converted to the highly fluorescent DCF following cleavage of the acetate groups by intracellular esterases and oxidation as shown in Figure 3.8. The fluorescent product, DCF, can then be visualised to qualitatively establish the level of ROS. Quantification of the ROS can be performed by measuring the area of coverage of the fluorescence in a sample.
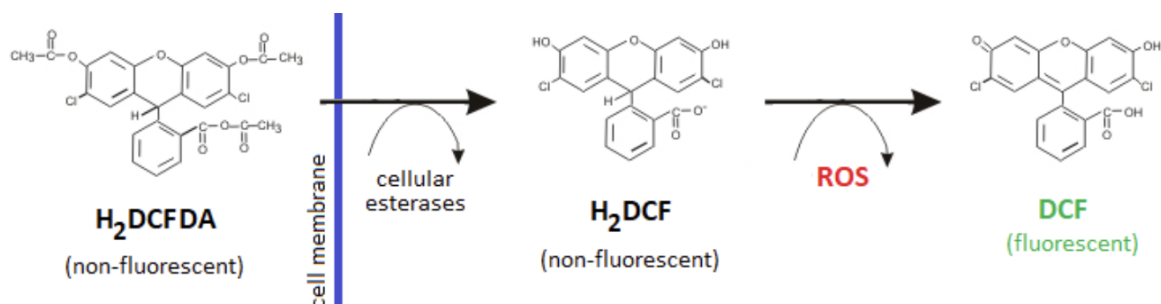
Figure 3.8. The principle of ROS level measurement using H_2DCF in cells. 2´,7´-dichlorofluorescin diacetate (H_2DCFDA) is a non-fluorescent, cell-permeable reagent which is deacetylated by cellular esterases to a non-fluorescent 2'7'-dichlorofluorescin (H_2DCF) after diffusion into the cell. H_2DCF is then oxidizied by ROS into a highly fluorescent 2',7'-dichlorofluorescein (DCF). ROS-reactive oxygen species. Figure reproduced from Nová et al. (2020) (173)

Tiwari et al. (2017) determined that a high uptake of Au generates oxidative stress in the WT, but not in *copt2-1*, as shown in Figure 3.9. The level of ROS was measured in this work indirectly by visualising the fluorescence produced after staining with H_2DCF in the root tip of three-week-old plants exposed to 10 ppm Au for 48 hours.
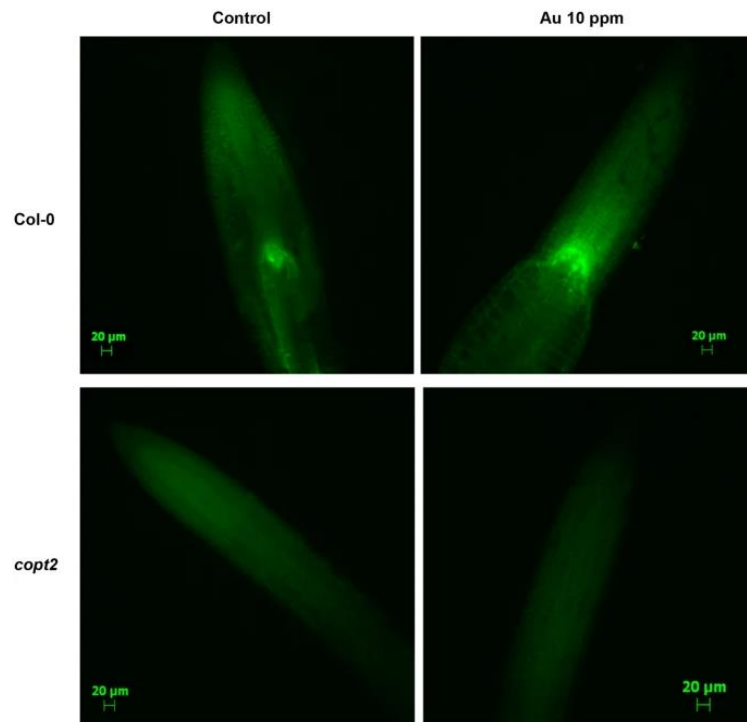
Figure 3.9. Gold-induced ROS production at the root tip of Arabidopsis. The H_2DCF staining of the root tip was performed under control and 48 hours of Au exposure. The upper panels showing the Col-0 (WT) and the *copt2* mutant is in lower panels. The scale bars are equivalent to 20 µM. Figure reproduced from Tiwari et al. (2017) (4)

3.1.4. Studies of Au in Arabidopsis, using *35S-COPT2* lines

Previous work demonstrated that *copt2-1* lines have reduced Au content in the root tissue compared to the WT when plants were exposed to Au (4). The work presented here investigated whether increased expression of *COPT2* would result in altered Au content and root morphology, using the techniques described above. The *COPT2* sequence was introduced into Arabidopsis WT using the floral dip technique, which is an *Agrobacterium* mediated transformation developed by Clough and Bent in 1998 (168). *Agrobacterium* is a soil pathogenic bacterium, which causes crown-gall disease or hair root disease in infected plants (174). In this technique, plants that are developing floral tissues are dipped into a solution containing *Agrobacterium*, 5 % sucrose and 500 µL / L of the surfactant Silwet L-77 (168). The *Agrobacterium* used for transformation contains a Ti plasmid, and this is transferred into the plant genome via horizontal gene transfer (174). In *Agrobacterium* strains not used for transformation, the Ti plasmids are large, low copy number, and hard to isolate, as well as lacking a multiple cloning site or promoters for use in *E. coli*. The use of a T-DNA binary vector system is used instead to overcome these challenges. The T-DNA binary vector system is made up

of the T-binary vector and the *vir* helper plasmid. The T-binary vector contains T-DNA repeats from the Ti-plasmid and a gene of interest to be inserted into the plant genome, whilst lacking the tumor-associated gene sequences and *vir* genes. The vir helper plasmid contains *vir* genes which encode proteins that promote the integration of the T-DNA into the plant genome. The gene of interest is cloned into the T-binary vector, and the vector transformed into *Agrobacterium* competent cells for transformation into plants (174).
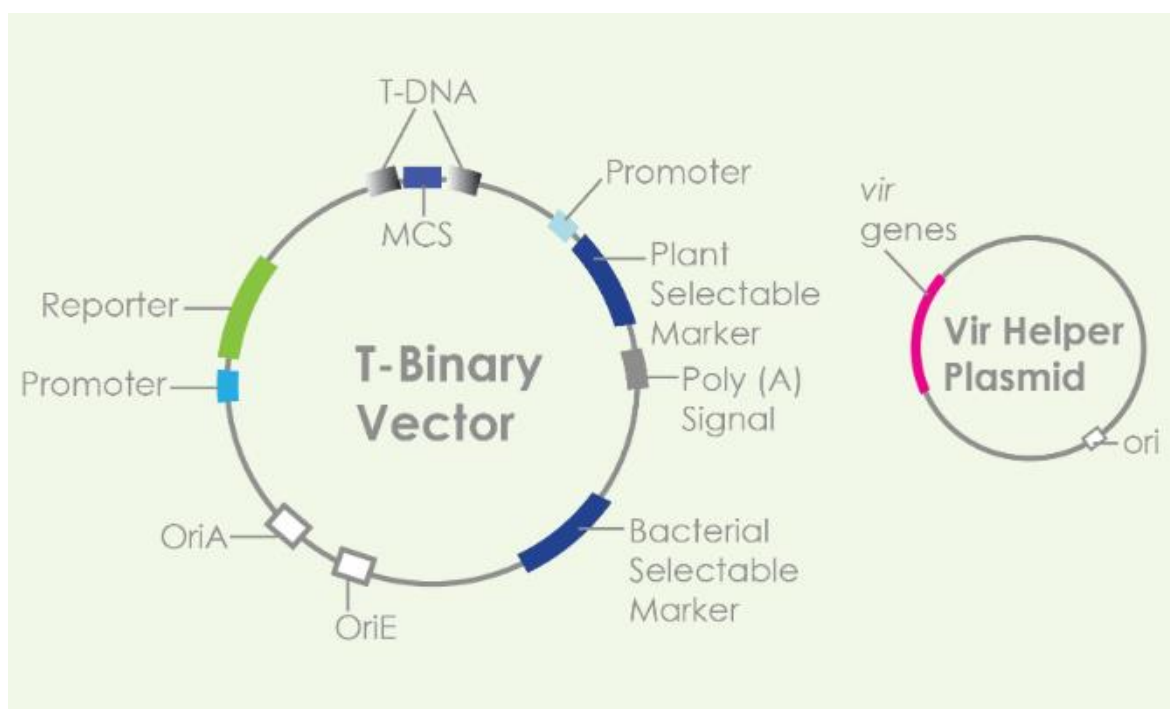
Figure 3.10. The T-DNA binary system used in *Agrobacterium* mediated transformation (GoldBio). The T-DNA binary vectors usually contain: an origin of replication or ori for *E. coli* or OriE (an element on the plasmid for replication and maintenance in *E.* coli), an origin of replication or ori for *Agrobacterium* or OriA (a site on the plasmid for replication in *Agrobacterium*), a multiple cloning site or MCS (this region contains restriction enzyme sites to allow for the insertion of the gene of interest), a plant selectable marker (to allow for selection of transgenic plants), a bacterial selectable marker (to allow for selection in the transformed bacteria), a promoter (to drive transcription of the gene of interest), poly(A) signals (an element containing poly-A for protein production), a reporter (a sequence encoding a particular protein with a specific function for monitoring the recombinant protein, such as β-glucuronidase or GUS, luciferase or LUC, or Green Fluorescent Protein or GFP) Image reproduced from GoldBio (175).

Generation of the T-DNA binary vectors used in this work was performed prior to the commencement of this project by Dr Liz Rylott at the University of York. The *COPT2* sequence was introduced into the T-binary vector under the control of the CaMV35S promoter. The cauliflower mosaic virus is an aphid-spread plant pathogen that affects plants in the *Brassicaceae* family. It is a reverse transcribing virus, replicating through an RNA intermediate. In 1985, Odell et al. reported that fragments of the CaMV35S promoter could direct transgene expression in tobacco and demonstrated non-specific expression throughout the plant tissue (176). The CaMV35S promoter is a regulatory sequence that is widely used to direct the near-constitutive expression of transgenes in plants. Characterisation of

the homozygous, T3 35S-*COPT2* lines generated through this method were performed as described above for the *copt2* mutant lines.

3.1.5. Studies of Au in Arabidopsis, using *35S*-GP and 35S-GPC lines

The properties, uses, and synthesis of NPs has been discussed in section 1.2. Based on work performed by Tan et al (2010) (59), the generation of Arabidopsis lines expressing the GP is described in section 3.2. The *35S*-GP lines express the GP under the control of the near-constitutively expressing CaMV35S promoter. Preliminary, unpublished studies by Dr. Liz Rylott have shown that plants expressing these short, synthetic peptides can be used to seed the formation of size controlled AuNPs *in planta*. The plant material exposed to Au became a brown/purple colour, indicating the formation of AuNPs in the tissue. The WT plants demonstrated a wide range of AuNP sizes. With the expression of peptides shown to seed the formation of *X-large, Large, Medium* or *Small* NPs, the distribution of NP sizes is altered in these plant lines, as discussed previously in chapter 1 (Figure 1.9a and b) . The plants expressing the *X-large* peptides had a smaller distribution of NPs below 10 nm in diameter ($p < 0.05$), and a larger distribution of NPs above 30 nm in diameter compared to the WT ($p < 0.01$).

Manipulating the NP formation in aerial tissues using this method could potentially be used to increase uptake, translocation, and NP deposition, and improve catalytic ability. In the work presented here, the *35S*-GP lines were characterised for growth on Au and Au uptake as described previously for the *copt2* mutant lines. Finally, the generation and characterisation of double transgenic lines is described; using Arabidopsis *35S*-GP as the parental background, *COPT2* was transformed into these lines by *Agrobacterium* mediated floral dip (168) to generate double transgenic lines that were theoretically capable of altered Au uptake and NP formation.

3.1.6. Summary

The interaction of *COPT2* and/or the GP with Au was investigated using a yeast spot dilution assay on Cu and Au, characterisation of Arabidopsis *copt2* mutants and *35S-COPT2, 35S*-GP or *35S*-GP*C* transgenic lines by analysis of root architecture, ROS production, and element concentration. The work presented here was performed towards the synthesis of plants lines capable of increased Au uptake, tolerance, and production of AuNPs of a valuable morphology (~ 10 nm in diameter) for industry.

3.2. Methods
3.2.1. Yeast studies

The Arabidopsis *COPT2* sequence was codon optimised for a yeast expression system prior to being cloned into *pYES2.1V5-His TOPO*. The resultant *pYES2-COPT2y* (6361 bp) contained the codon-optimised *COPT2y* sequence (481 bp) under the control of a *GAL1* and T7 promoter, a V5 epitope, a His-tag, a *CYC1* transcription termination signal, a pUC ori, *AmpR* (an ampicillin resistance gene), a *URA3* promoter and *URA3* gene (for selection in yeast), 2micron ori and an f1 ori (Figure 3.11A). Optimisation was performed using ThermoFisher GeneArt software and involved the conversion of 'low quality' codon sequences, less favoured by the yeast translational machinery, to synonymous codons biased toward 'high quality' expression within a yeast system, and a reduction in the spread of guanine and cytosine content. As a result of this optimisation, the *COPT2y* sequence contained a higher percentage of codons of a higher quality class, demonstrated by a shift in the codon quality distribution towards higher percentages shown in Figure 3.11C. In Figure 3.11D, the quality value of the most frequently used codons for a given amino acid in a yeast expression system is set to 100, with the remaining codons scaled accordingly. The codon-quality plot demonstrates the quality of the used codon at the indicated codon position, showing a shift in the *COPT2y* related plot towards codons of a higher quality for yeast expression (Figure 3.11D). The optimisation step also resulted in a stabilisation of the percentage guanine-cytosine content; Figure 3.11E shows the change in guanine-cytosine content in a 40 bp window centred at the indicated nucleotide position (section 2.2.12).

To investigate the involvement of COPT2 in Au uptake, the five *pYES2-COPT2y* expressing yeast strains (BY4741, the parental strain to *Δccc2* and *Δace1*, DTY165, the parental strain to *Δctr1ctr3*) were used in growth assays on SD-U(A) media containing Cu, Au, or both metals.
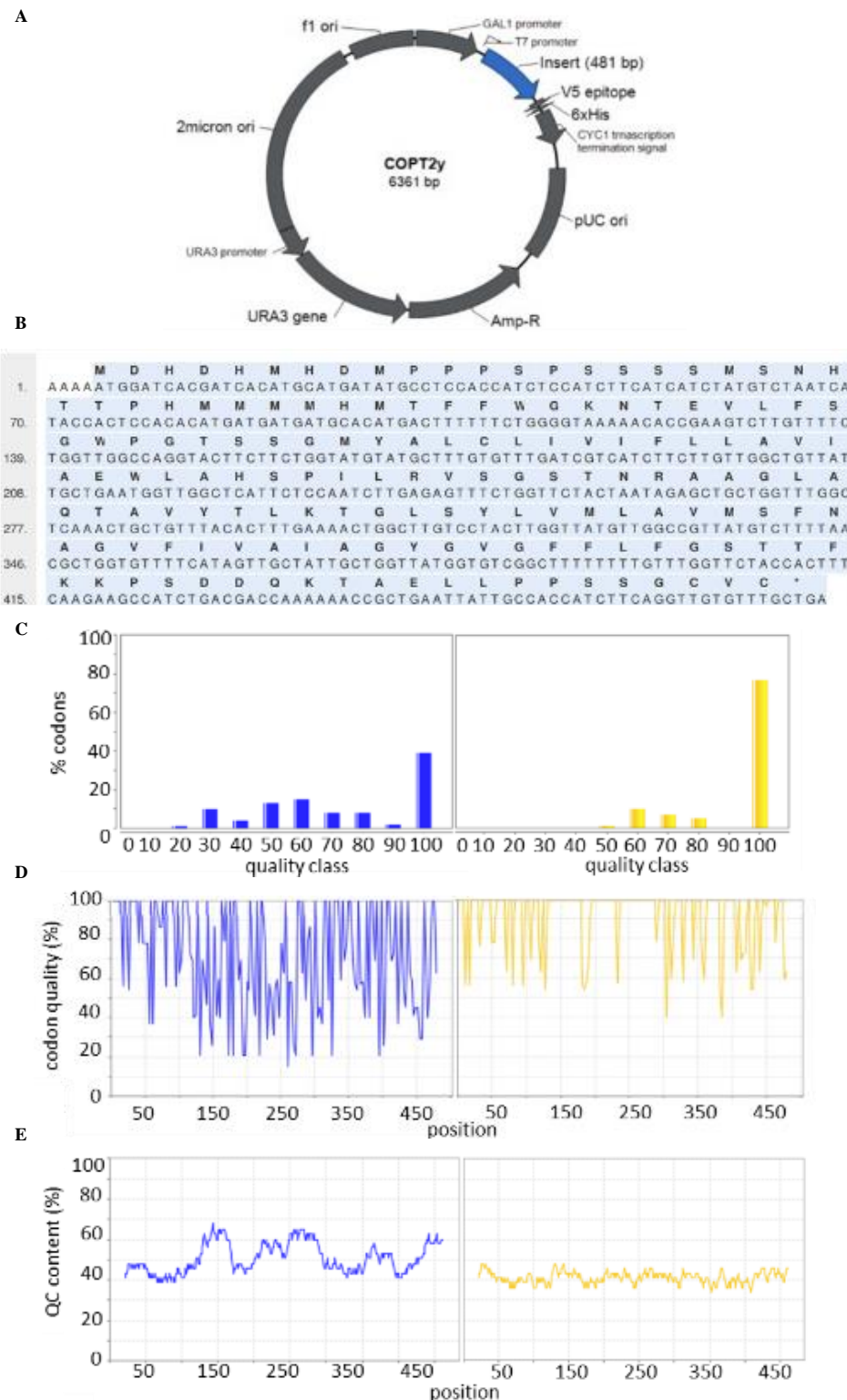
Figure 3.11. The pYES2-*COPT2y* and analysis of codon distribution for expresion in a yeast system; (A) Vector map of pYES2-*COPT2y*; (B) *COPT2y* sequence. Sequence analysis of (C-E) *COPT2* (blue) or *COPT2y* (yellow): (C) Codon quality distribution; (D) Codon quality plot; (E) guanine-cytosine content in a 40 bp window centered at the indicated nucleotide position (figures produced in GeneArt).

3.2.2.   Arabidopsis studies
3.2.2.1. Floral dip transformation and confirmation of Arabidopsis *35S-COPT2* lines

The *COPT2* sequence was codon optimised for expression in Arabidopsis to distinguish between the endogenous and introduced version of the gene (optimisation performed on GeneArt) as the *COPT2* gene does not contain introns; this version of the sequence will be referred to as *optCOPT2*. The *XhoI* [CTCGAG] and *BamHI* [GGATCC] restriction enzyme sites were added to the beginning and end of *optCOPT2*, respectively, which contained the CaMV35S promoter sequence upstream of *optCOPT2*. The optimised *COPT2* sequence (*optCOPT2*) differed to the endogenous Arabidopsis *COPT2* sequence by 33%. The *pART7* and *pMLBART* binary vector system was used for transformation (150), and binary vectors were laboratory stocks. The *pMLBART* contains a kanamycin resistance gene for bacterial selection (*KanR*), glufosinate ammonium resistance gene (*bar)* for plant selection, and a *NotI* cloning site between the right- and left-border (Figure 2.4, Materials and methods pg. 49). The *pMLBART*-opt*COPT2* was created by *NotI* digestion and ligation and confirmed prior to the commencement of this project by Dr. Liz Rylott.

For overexpression studies, Arabidopsis WT plants were transfected by *Agrobacterium* containing *pMLBART*-optC*OPT2* using the floral dip method. Positive transformants containing the selectable marker gene (*bar* gene) were selected as those that were able to successfully produce secondary leaves on plant selection media (½ MS containing 20 mg/mL glufosinate ammonium herbicide). Prior to further study, PCR-based techniques were used to confirm the authenticity of the mutant and overexpression lines.

3.2.2.2. The Arabidopsis *copt2* mutant lines

For the *copt2-1*, *copt2-2,* or *copt2-3* lines (the *copt2* mutant lines), the presence and location of the T-DNA inserts was analysed on two-week-old Arabidopsis rosette tissue using PCR, as described in section 2.3.

Primer efficiency tests were performed which utilised three up- and down-stream primer pairs, as shown in Table 3.1 and Table 3.2. The TAIR SeqViewer (177) was used to visualise the primer location (Figure 3.12, Figure 3.13). Primer efficiency tests and qPCR analysis was performed as per section 2.4. The *COPT2* cDNA sequence was obtained from Ensembl (178), and the sequences up- or downstream of the T-DNA insertion locations were obtained from The Arabidopsis Information Resource (TAIR) (177). The most efficient primer pair was used in downstream qPCR analysis.

Table 3.1. Arabidopsis qPCR primers upstream of the T-DNA locations in *copt2-1, copt2-2, copt2-3.* Up- and down-stream primer pairs, labelled by the *copt2* line (C1/2/3), their location up- or down-stream (Ups/Ds), the primer type (LP/RP) and then the primer number (1/ 2/3), e.g., C2UpsLP1 refers to the up-stream primer on the left-hand side of the sequence in *copt2-2*, part of primer pair one.

	Sequence (5' - 3')	Template strand	Length	Tm	GC %	Self-complementarity	Self-3' complementarity
C2UpsLP1	ACCAACGCAAAGAAGATTAGACG	Plus	23	59.57	43.48	2	2
C2UpsRP1	ACAACATTACAACTCCATGCCTCT	Minus	24	60.52	41.67	4	0
Product length	48						

Primer pair 2

	Sequence (5' - 3')	Template strand	Length	Tm	GC %	Self-complementarity	Self-3' complementarity
C2UpsLP2	TACCAACGCAAAGAAGATTAGACG	Plus	24	59.38	41.67	2	2
C2UpsRP2	ACAACATTACAACTCCATGCCTCT	Minus	24	60.51	41.67	4	0
Product length	48						

Primer pair 3

	Sequence (5' - 3')	Template strand	Length	Tm	GC %	Self-complementarity	Self-3' complementarity
C2UpsLP3	ATACCAACGCAAAGAAGATTAGACG	Plus	25	59.71	40	2	2
C2UpsRP3	TACAACATTACAACTCCATGCCTCT	Minus	25	60.28	40	4	0
Product length	51						

Table 3.2. Arabidopsis qPCR primers downstream of the T-DNA locations in *copt2-1, copt2-2, copt2-3.* Up- and down-stream primer pairs, labelled by the *copt2* line (C1/2/3), their location up- or down-stream (Ups/Ds), the primer type (LP/RP) and then the primer number (1/ 2/3), e.g., C2UpsLP1 refers to the up-stream primer on the left-hand side of the sequence in *copt2-2*, part of primer pair one.

Primer pair 1

	Sequence (5' - 3')	Template strand	Length	Tm	GC %	Self-complementarity	Self-3' complementarity
C2DsLP1	CCTACGTGTCAGTGGCTCAA	Plus	20	59.68	55.00	4.00	0.00
C2DsRP1	GGACATAACAGCGAGCATCA	Minus	20	58.06	50.00	2.00	1.00
Product length	106						

Primer pair 2

	Sequence (5' - 3')	Template strand	Length	Tm	GC %	Self-complementarity	Self-3' complementarity
C2DsLP2	CCACCATCACCATCATCATC	Plus	20	55.95	50.00	4.00	2.00
C2DsRP2	CTCCGTGTTCTTACCCCAAA	Minus	20	57.45	50.00	2.00	0.00
Product length	93						

Primer pair 3

	Sequence (5' - 3')	Template strand	Length	Tm	GC %	Self-complementarity	Self-3' complementarity
C2DsLP3	TGATGCTCGCTGTTATGTCC	Plus	20	58.06	50.00	2.00	0.00
C2DsRP3	CGATAGCGACGATGAAAACA	Minus	20	56.38	45.00	4.00	0.00
Product length	51						
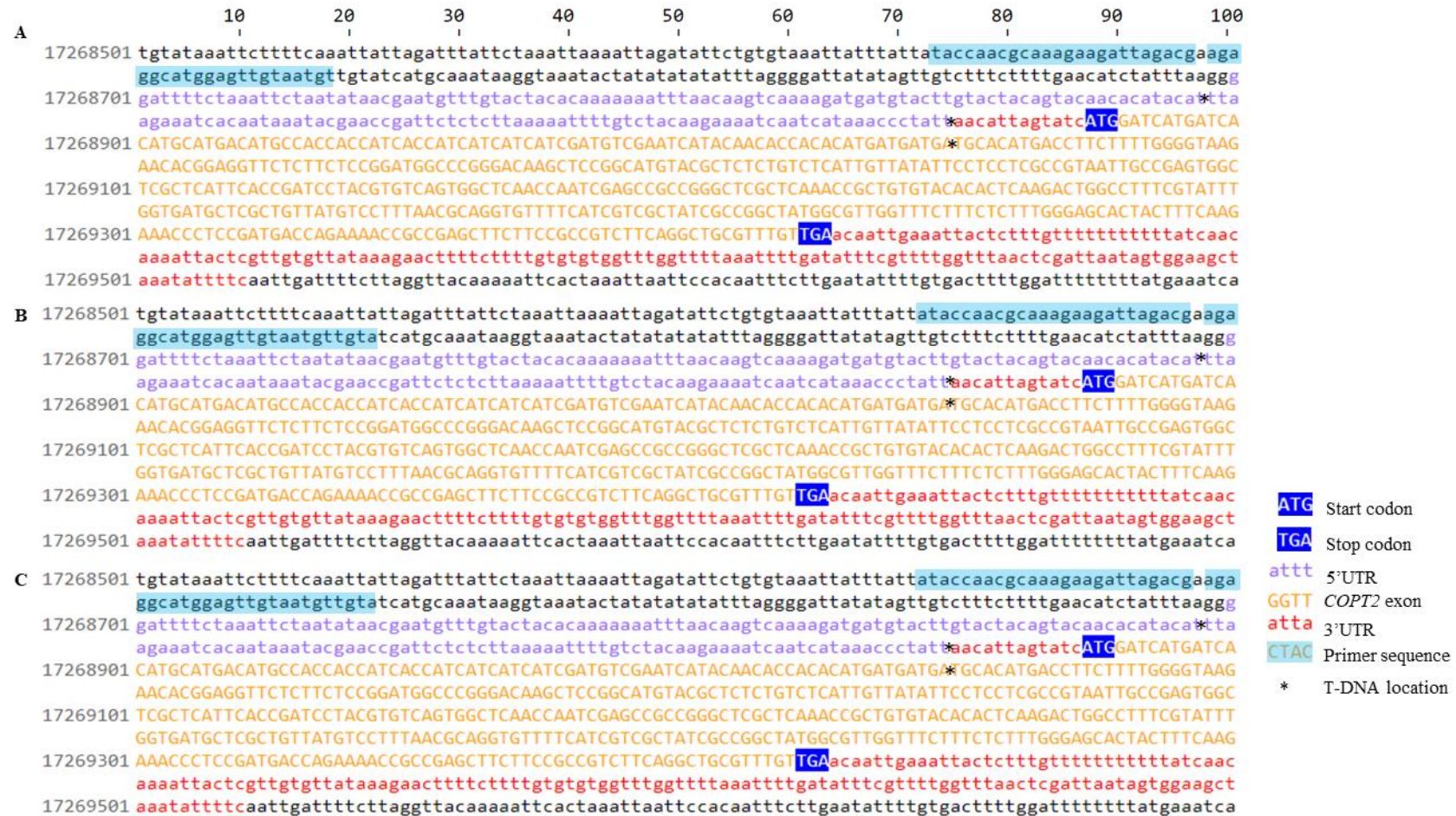
Figure 3.12. Quantitative PCR primers tested for the study of *COPT2* transcript abundance in Arabidopsis *copt2* mutants. Primer pairs A, B and C are located upstream of all three *COPT2* T-DNA locations identified in Arabidopsis *copt2-1, copt2-2, copt2-3.*

Figure 3.13. Quantitative PCR primers tested for the study of *COPT2* transcript abundance in Arabidopsis *copt2* mutants. Primer pairs A, B and C are located downstream of all three *COPT2* T-DNA locations identified in Arabidopsis *copt2-1, copt2-2, copt2-3.*
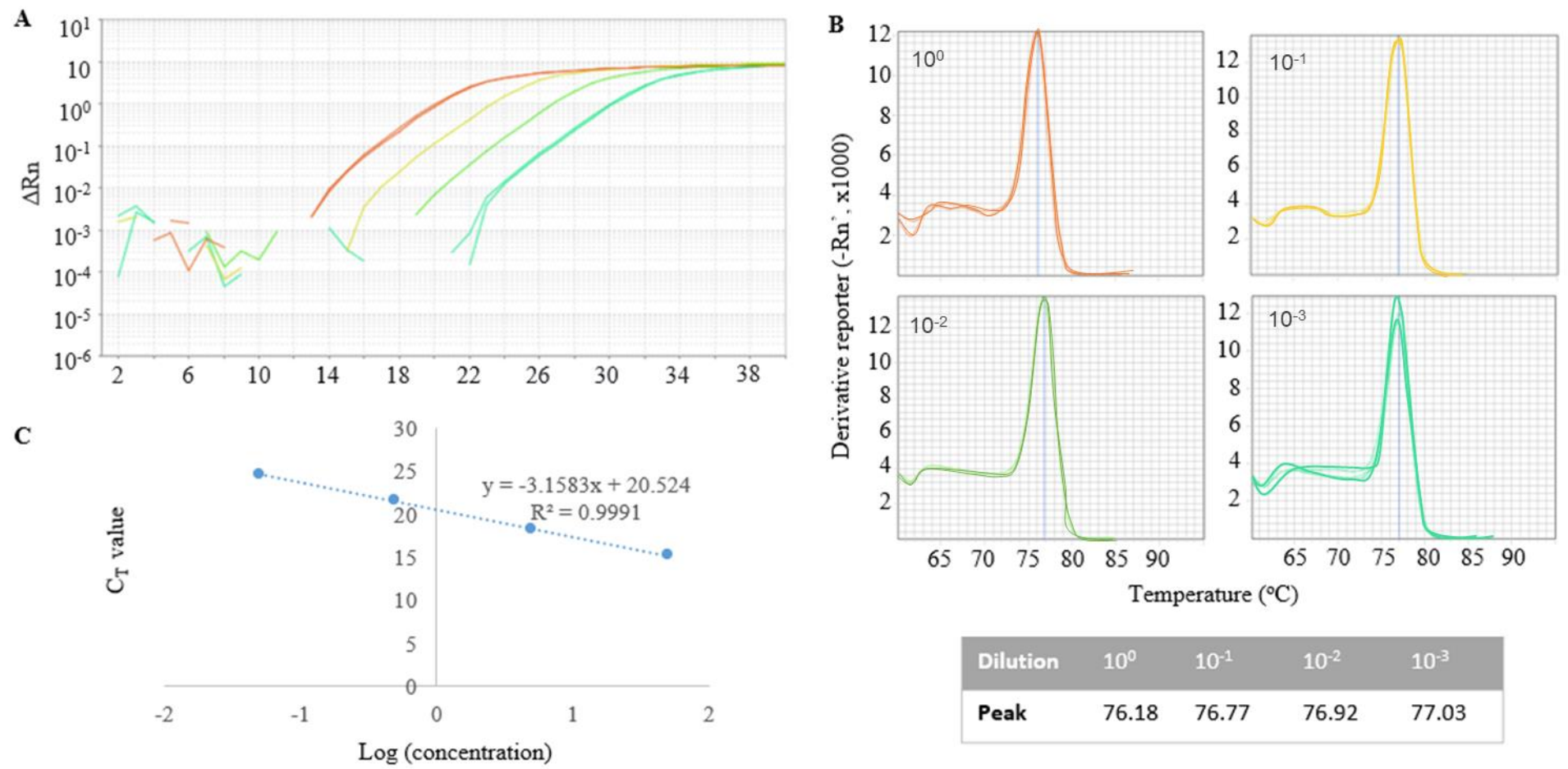
Figure 3.14. Primer efficiency test results for primer pair *ACTIN2* with undiluted (red), 10^{-1} (yellow), 10^{-2} (green), 10^{-3} (turquoise) WT cDNA; A: Amplification plot; B: Melt curves that correspond to the amplification plot; C: Primer efficiency standard curve. Each PCR reaction was run in triplicate.
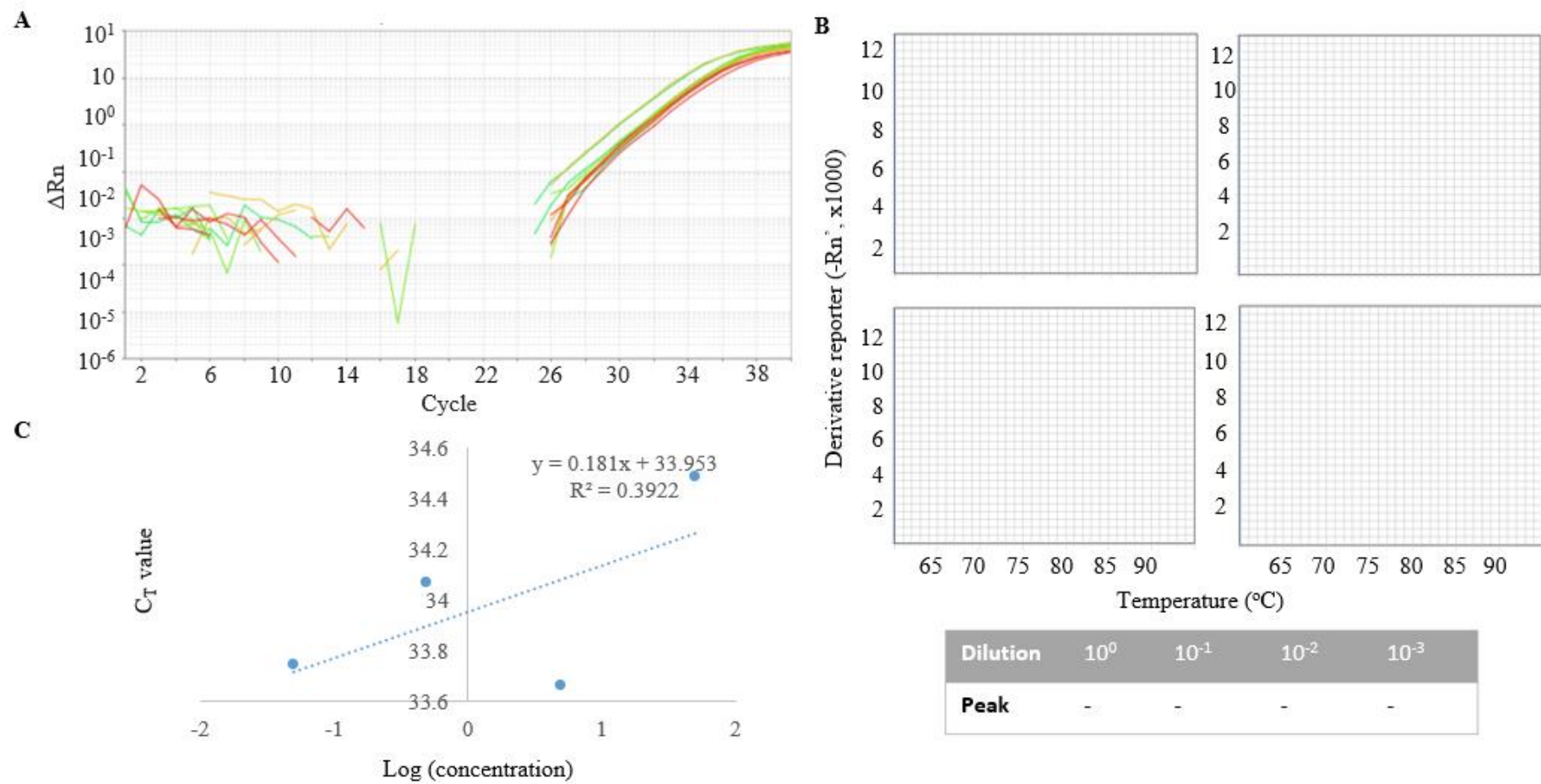
Figure 3.15. Primer efficiency test results for primer pair C2Ups1 with undiluted (green), 10^{-1} (yellow), 10^{-2} (turquoise), 10^{-3} (red) WT cDNA; A: Amplification plot; B: Melt curves that correspond to the amplification plot; C: Primer efficiency standard curve. Each PCR reaction was run in triplicate. Melt curves were missing from the StepOne analysis.
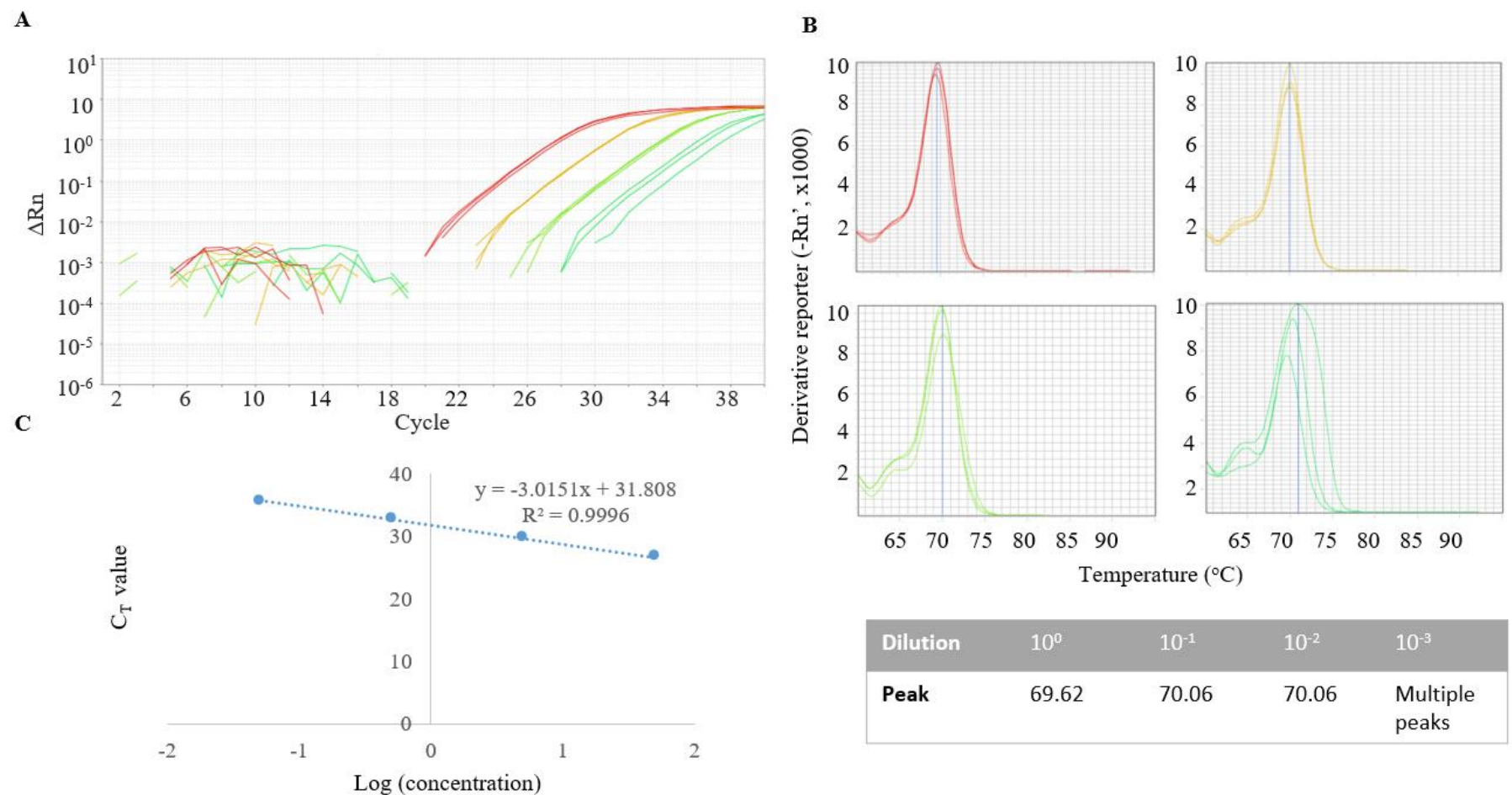
Figure 3.16. Primer efficiency test results for primer pair C2Ups2 with undiluted (red), 10-1 (yellow), 10-2 (green), 10-3 (turquoise) WT cDNA; A: Amplification plot; B: Melt curves that correspond to the amplification plot; C: Primer efficiency standard curve. Each PCR reaction was run in triplicate.
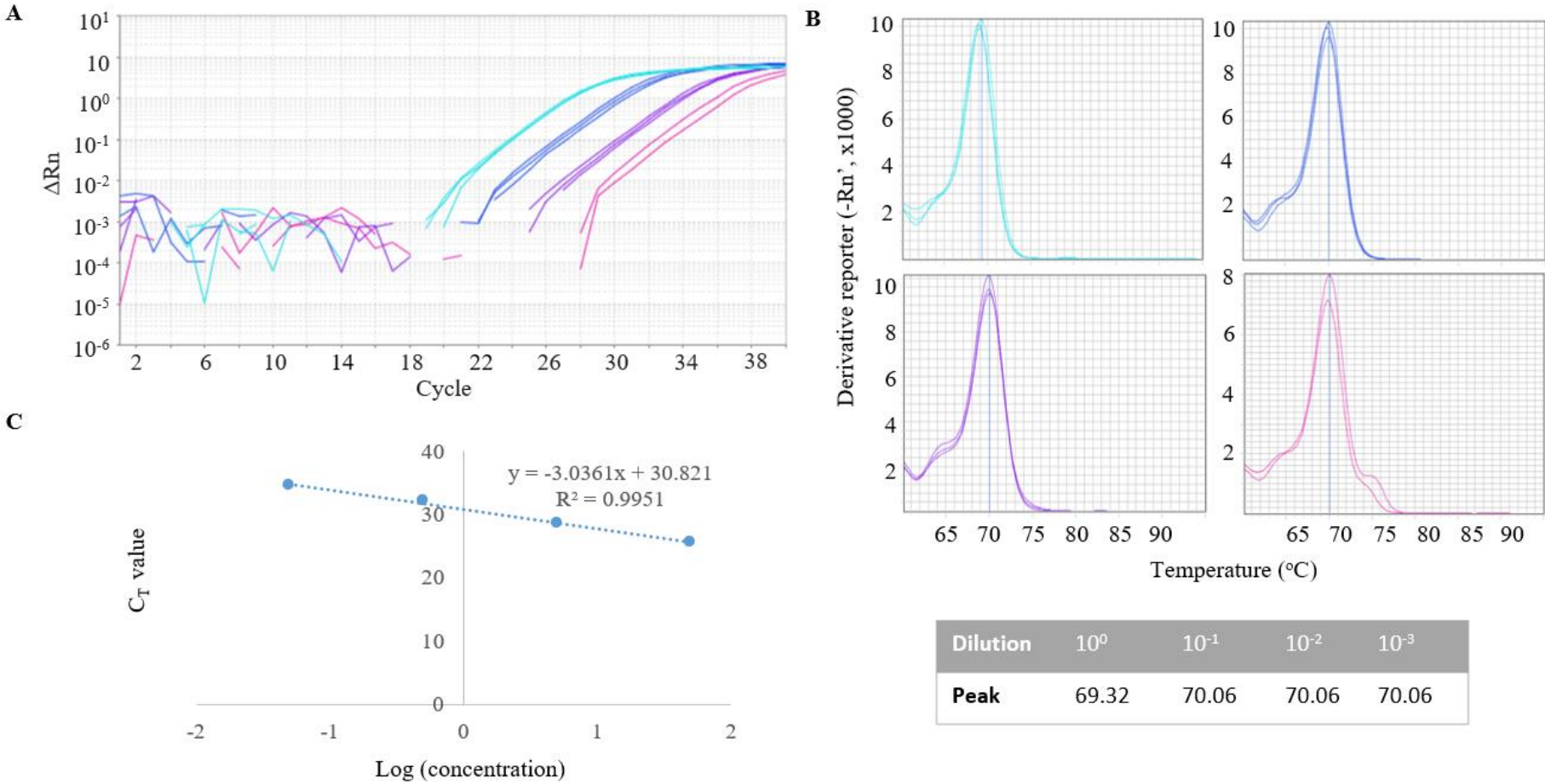
Figure 3.17. Primer efficiency test results for primer pair C2Ups3 with undiluted (light blue), 10^{-1} (navy), 10^{-2} (purple), 10^{-3} (pink) WT cDNA; A: Amplification plot; B: Melt curves that correspond to the amplification plot; C: Primer efficiency standard curve. Each PCR reaction was run in triplicate.
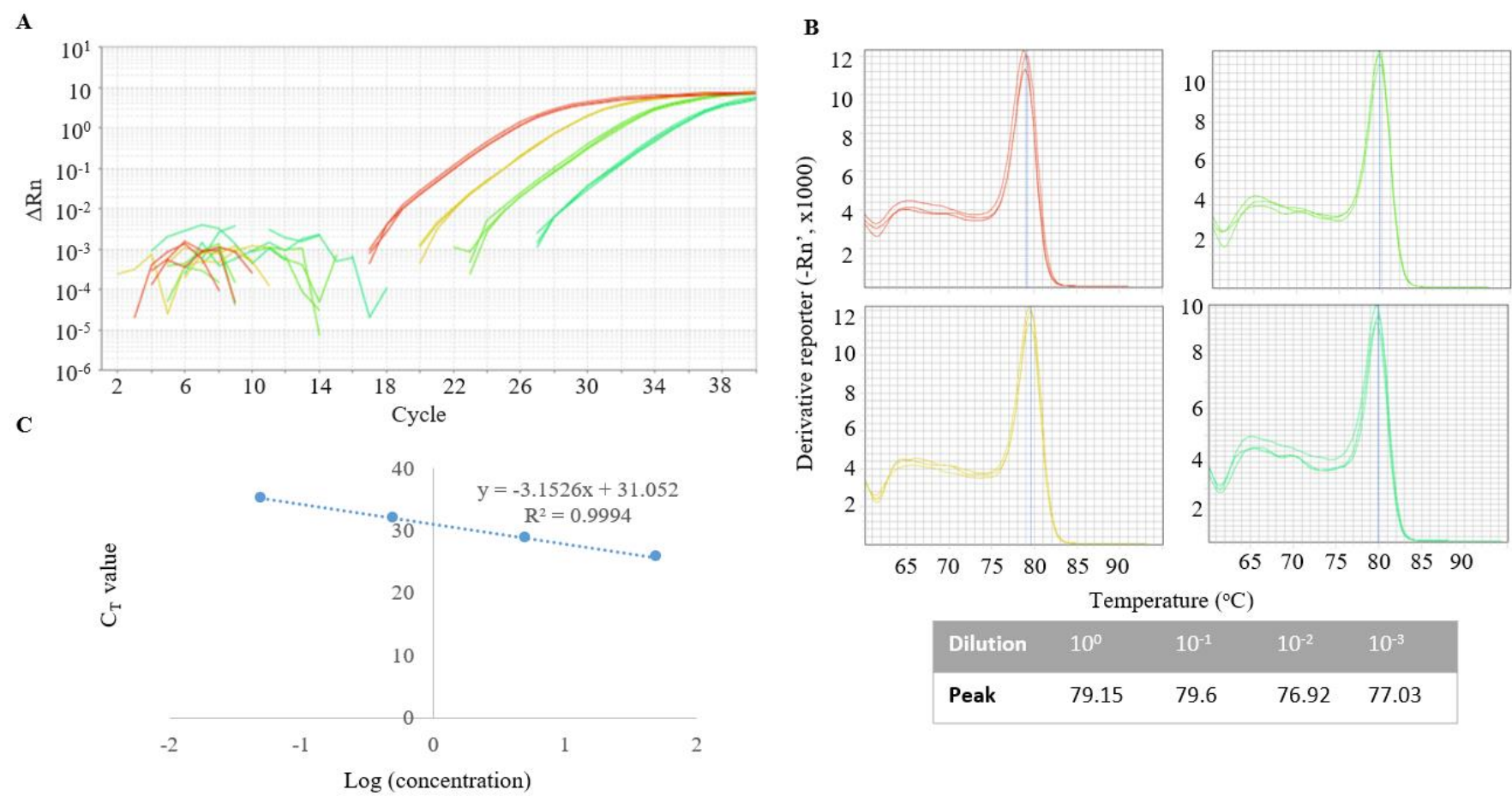
Figure 3.18. Primer efficiency test results for primer pair C2Ds1 with undiluted (red), 10^{-1} (yellow), 10^{-2} (green), 10^{-3} (turquoise) WT cDNA; A: Amplification plot; B: Melt curves that correspond to the amplification plot; C: Primer efficiency standard curve. Each PCR reaction was run in triplicate.
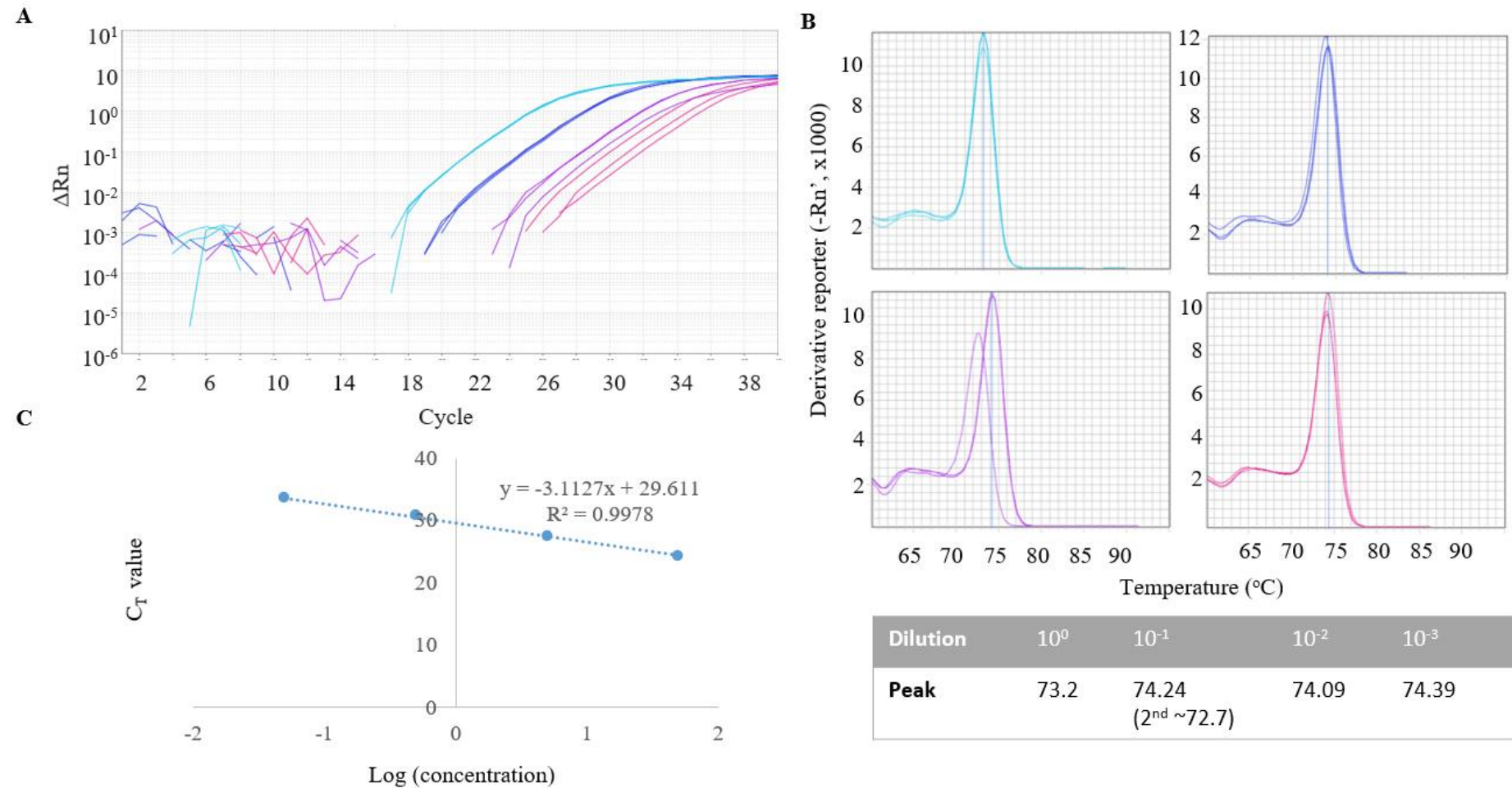
Figure 3.19. Primer efficiency test results for primer pair C2Ds2 with undiluted (light blue), 10^{-1} (navy blue), 10^{-2} (purple), 10^{-3} (pink) WT cDNA; A: Amplification plot; B: Melt curves that correspond to the amplification plot; C: Primer efficiency standard curve. Each PCR reaction was run in triplicate.
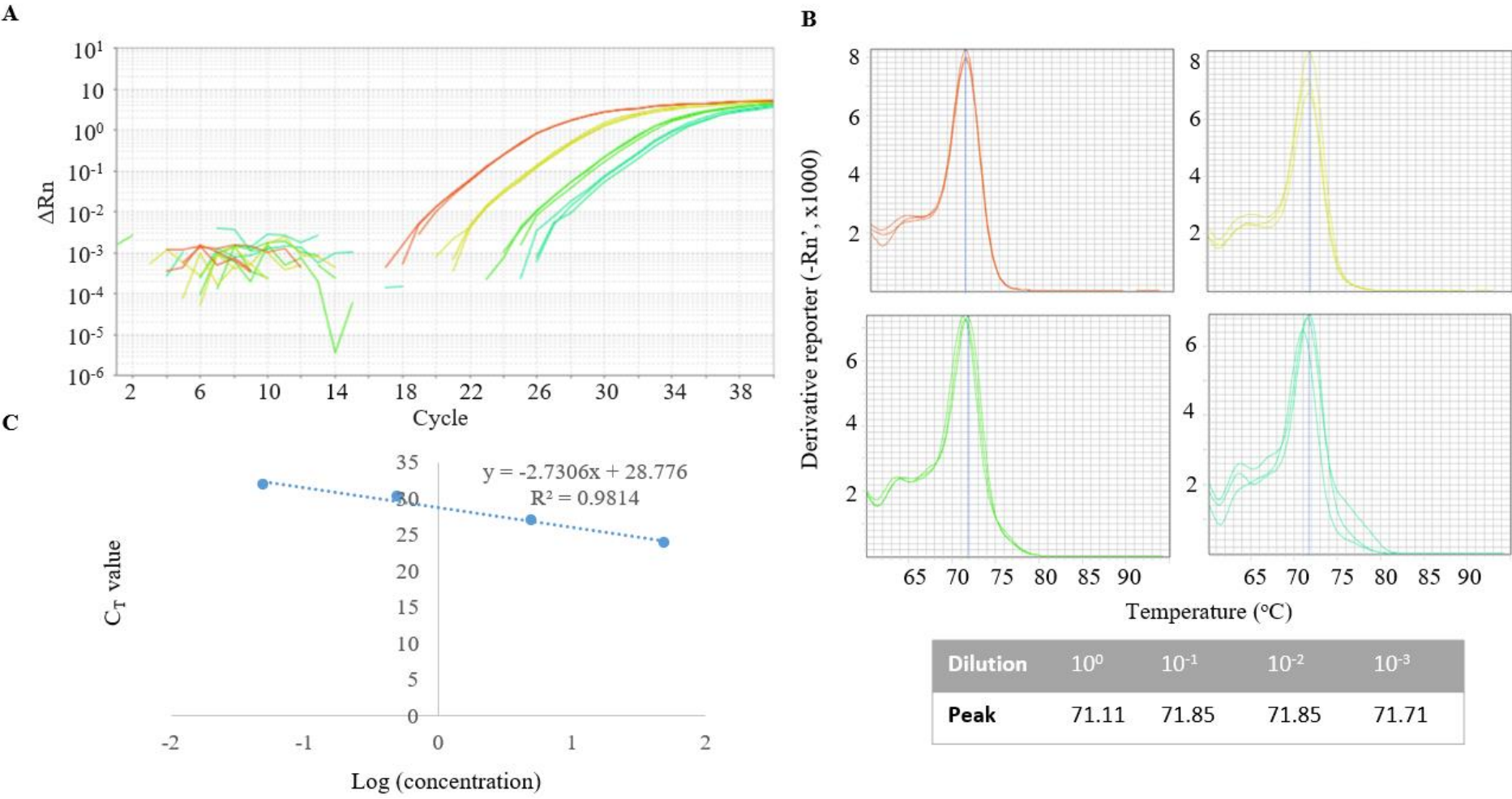
Figure 3.20. Primer efficiency test results for primer pair C2Ds2 with undiluted (red), 10^{-1} (yellow), 10^{-2} (green), 10^{-3} (turquoise) WT cDNA; A: Amplification plot; B: Melt curves that correspond to the amplification plot; C: Primer efficiency standard curve. Each PCR reaction was run in triplicate.

3.2.2.3. The Arabidopsis *35S-COPT2,* OE lines

To investigate the effect of increased *COPT2* expression on metal uptake in Arabidopsis, the *pMLBART-COPT2* was transformed into Arabidopsis by Dr Liz Rylott using *Agrobacterium* mediated floral dip transformation prior to this work. As the endogenous *COPT2* does not contain introns, primers spanning an intron-exon boundary could not be designed for qPCR analysis. However, prior to transformation, *COPT2* was further codon optimised using GeneArt software (*optCOPT2*) enabling a distinction between the endogenous and introduced version of *COPT2.*
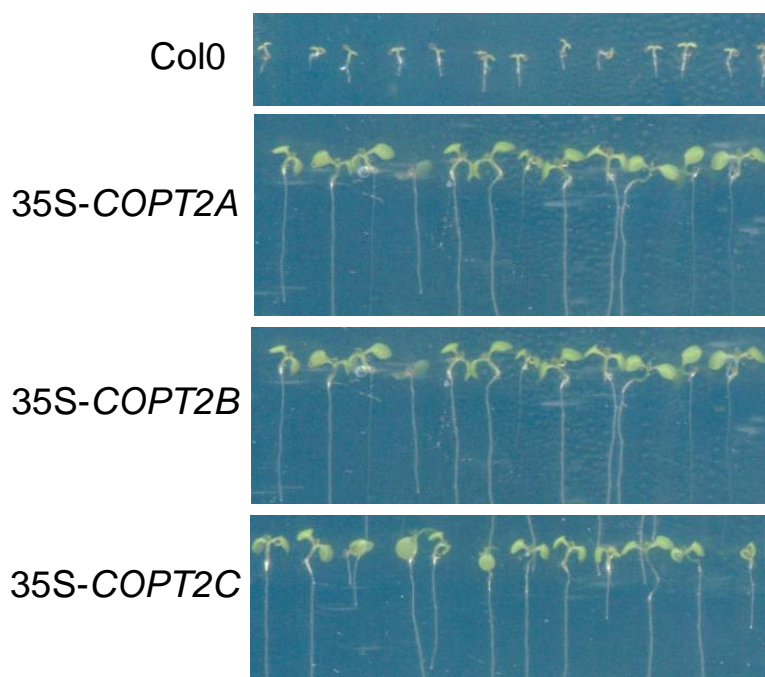
Figure 3.21. Images of the growth of twelve-day-old Arabidopsis WT (Col0) and the T3 *35S-COPT2A, 35S-COPT2B, 35S-COPT2C* lines grown for twelve days on ½ MS(A) media containing 20 mg/mL glufosinate ammonium for selection of plants lines that containin the *bar* gene (part of the *pML-COPT2y* for positive selection. There were sixteen seeds sown for each line, and if all sixteen produced secondary leaves, as was demonstrated by the *35S-COPT2A, B* and *C* lines in this figure, they were considered to be homozygous for the *pML-COPT2y* insertion.

These plants (the T1 generation) were transferred to soil, and T2 seeds harvested and screened on selective medium. The T2 lines with 3:1 resistant: sensitive segregation ratios indicative of single insertional events, were again transferred to soil. Following this, stable, non-segregating, homozygous T3 transgenic lines were detected by identifying lines with 100% resistance to glufosinate (Figure 3.21). Eventually, three independent, homozygous lines, referred to as *35S-COPT2A, B* or *C* from this point forward were identified for subsequent analysis. Expression levels of *COPT2* were determined using qPCR, with the primers shown in Table 2.11.

3.2.2.4. Arabidopsis *35S*-GP lines

Prior to the commencement of this project, Dr Liz Rylott (Centre of Novel Agricultural Products, University of York) generated and established homozygous 35S-GP expressing Arabidopsis lines. These lines were generated using the pART7 and pART27 binary vector system (150), and expression is under the control of the near-constitutive CaMV35S promoter (Figure 2.5, Figure 2.6, Materials and methods pg. 52).

Ligation into *pART7* used the *Xhol* and *HindIII* sites at the beginning and end of the GP sequence, which has ampicillin/carbenicillin resistance. The sequence containing the flanking CaMV35S and ocs 3' sequences was removed from *pART7* using the *NotI* digestion sites and cloned into pART27 (pART27-*35S*-GP), which has spectinomycin resistance (50 µg/mL) (Figure 2.6). Heat shock transformation was used to introduce the pART27 into the *Agrobacterium* GV301 strain, which contains rifampicin and gentamycin resistance on the Ti plasmid. The floral dip method was used to transfect the Arabidopsis WT lines with *Agrobacterium* containing *pART27-35S*-GP (2.4.12), and transformants identified using selection media (½ MS containing 50 µg/mL spectinomycin). The ½ MS(A) plates containing spectinomycin were used to screen for homozygous T2 lines, and those with segregation ratios indicative of single insertional events (sensitive: resistant; 1:3) were selected, and for analysis, three, independently transformed, homozygous lines (*35S*-GP*A, 35S*-GP*B, 35S*-GP*C*) were used.

3.2.2.5. Identification of three homozygous 35S-GP lines by PCR and visualisation

For diagnostic PCR, DNA was extracted from two-week-old rosette leaves of soil-grown WT, *35S*-GP*A, 35S*-GP*B,* and *35S*-GP*C* lines. The CTAB method was used to extract RNA for gene expression level analysis (qPCR). Analysis of peptide expression levels was performed using the primers shown in Table 2.13 (Materials and methods, pg. 53). The parameters of the GP sequence primer (GP-F) are shown in Table 2.13 and this primer, alongside the universal reverse primer did not produce PCR products. The sequence was optimised to fit the parameters of recommended primer design. The optimisation included shortening the sequence to reduce the Tm and reducing the 3' self-dimers (Table 2.13). The optimised primer (optGP-F) generated RT-PCR products in all three *35S*-GP lines (Figure 3.22).
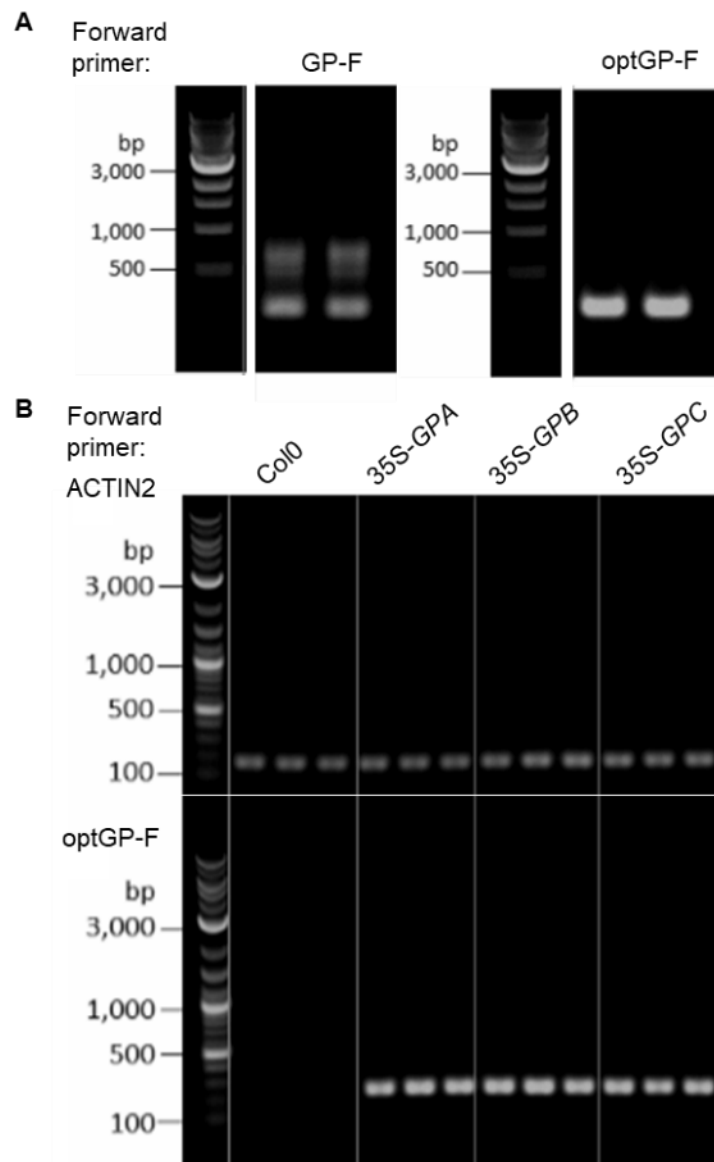
Figure 3.22. The efficacy of forward primers against the GP sequence in RT-PCR reactions alongside the *pART7* reverse primer on DNA extracted from two-week-old Arabidopsis *35S*-GP rosette leaves. A: Testing genotyping primers GP-F (the entire GP sequence used as the forward primer) and optGP-F (shorter, optimised GP sequence as forward primer). Not shown: single band with ACTIN2 primers; B: Genotyping three biological replicates of the three *35S*-GP lines (*35S*-GP*A*, *35S*-GP*B*, *35S*-GP*C*) using the ACTIN2 primer pair as control, and the optGP-F forward primer alongside the *pART7* reverse primer.

3.2.2.6. Primer efficiency tests on primers specific to the GP transcript

The primer efficiency of the 35S-optGP forward and the miRNA universal reverse primer were tested, in triplicate, using cDNA synthesised from RNA extracted from two-week-old Arabidopsis *35S*-GP*A* rosette leaves (Figure 3.23). The primer efficiency of the optGP-F primer pair was established at 102.56 %, within the acceptable range previously described in section 2.4.5. The melt curves contained single peaks for all dilutions tested, but the peak of the curve differed between dilutions. In the undiluted sample, the peak of the melt curve occurred at 77.68 ^{o}C, whereas in the other three dilutions the peak of the melt curve occurred at 77.06 ^{o}C (Figure 3.23B). A peak at 77.68 ^{o}C was also demonstrated when the optGP-F primer pair were used in a qPCR reaction alongside Arabidopsis WT cDNA, indicating non-specific binding at lower concentrations of cDNA. As the cDNA synthesis kit used recommends using cDNA straight from synthesis, and as the undiluted cDNA generated the only melt curve peak unique to the *35S*-GP cDNA, undiluted cDNA was used in the expression analysis. The efficiency of the endogenous primer pair, ACTIN2, had already been established at 107.31 %.
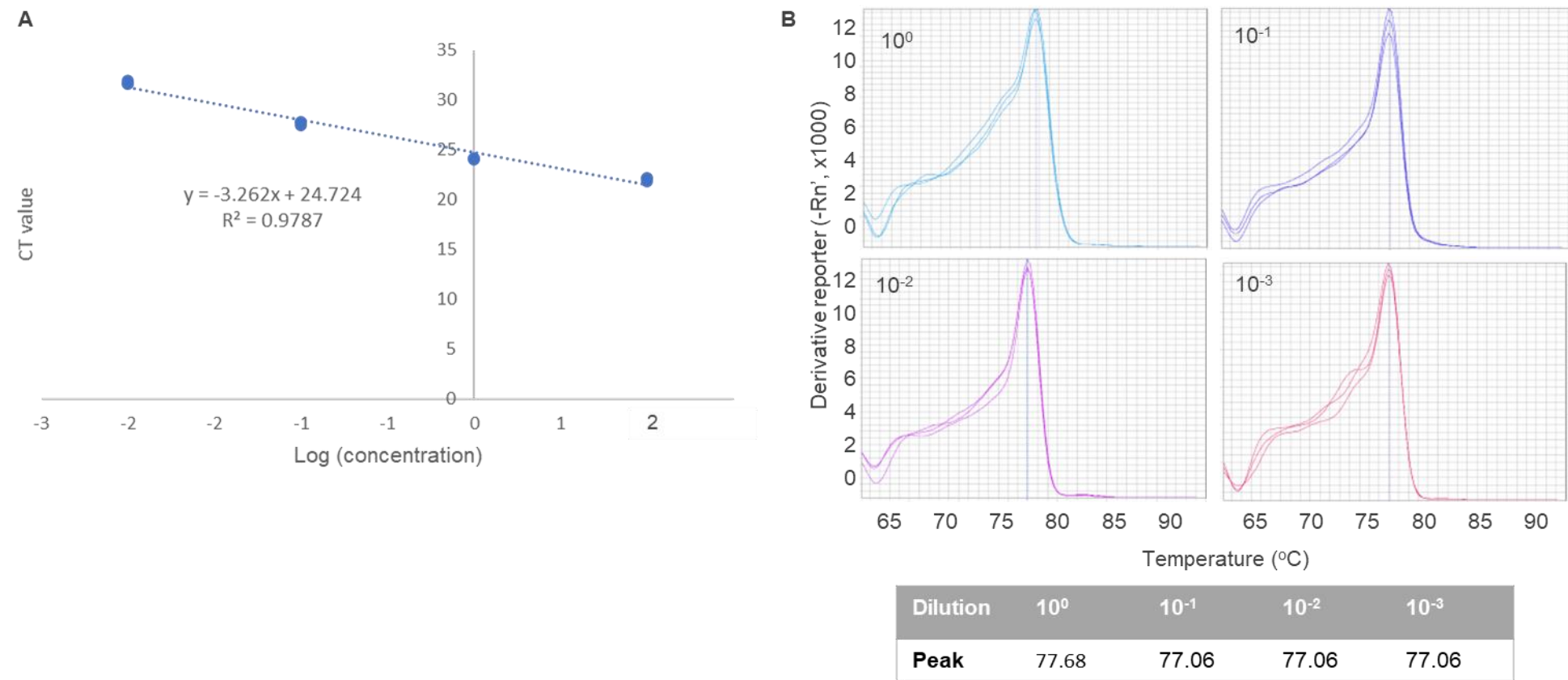
Figure 3.23. Primer efficiency test results for the optGP-F and universal miRNA reverse primers, on undiluted (light blue), 10^{-1} (navy), 10^{-2} (purple), 10^{-3} (red) cDNA synthesised from RNA extracted from rosette leaves of two-week-old *35S-GPA* Arabidopsis lines. A: Primer efficiency standard curve; B: Melt curve analysis for all dilutions tests. Each PCR reaction was performed in triplicate.

3.2.2.7. Arabidopsis *35S*-GP*C* lines

To investigate the combined effect of the expression of the GP sequence alongside increased *COPT2* expression, *pMLBART-COPT2* was introduced into the previously characterised Arabidopsis *35S*-GP lines. The homozygous T2 lines were screened on glufosinate ammonium and spectinomycin, those with segregation ratios indicative of single insertional events (sensitive: resistant; 1:3) were selected, and for analysis three, independently transformed, homozygous lines (*35S*-GP*CA, 35S*-GP*CB, 35S*-GP*CC*) were used.

3.2.2.8. Arabidopsis *COPT2* and transgenic genotypes studies with Cu or Au

To identify phenotypic variations between Arabidopsis *copt2* mutants*, 35S-COPT2*, *35S*-GP*, 35S*-GP*C* and WT seeds were grown on ½ MS(A) media containing Cu or Au (pg. 46, 2.4.7). Root length and number of lateral root branches were measured when plants were twelve days old, using ImageJ to measure the length of roots against a scale measurement (148). Root architecture was calculated as branches per mm (branches / length). The concentration of Cu, Au, and Fe in *copt2* mutant lines, transgenic and WT genotypes was investigated through a hydroponic system, with 1mM Au added to ½ MS media when plants were five-weeks old and harvested after 24 hours of exposure. Following an acid digest step to prepare samples for analysis, ICP-OES was used to establish the concentration of these metals in Arabidopsis shoot or root tissue (2.4.8). Metal or abiotic stress tends to elicit the generation of ROS within plant tissue. The metals Cu and Au are toxic in high concentrations to plant tissue, and have previously been shown to result in an increase in cellular ROS production (4,179). To measure ROS production, Arabidopsis *copt2* mutants and WT lines were exposed to H_2DCF, which produces a fluorescent product, DCF, in the present of peroxides, and imaged using an ZEISS LSM 710 Epifluorescence microscope (Zeiss, Germany) after 24 hours of exposure.

3.3. Results
3.3.1.   Yeast studies
3.3.1.1. Transformation of *pYES2-COPT2y* into *E. coli*

The *pYES2-COPT2y* was transformed into XL10-Gold Ultracompetent *E. coli* cells via heat shock transformation as per 2.2.13. Successful transformants were selected as those that formed an individual colony on LB plates containing kanamycin (50 µg/mL), then confirmed by colony PCR using primers specific to *COPT2y,* with the correctly sized amplicon identified at 371 bps for all individual *E. coli* colonies tested (Figure 3.24).
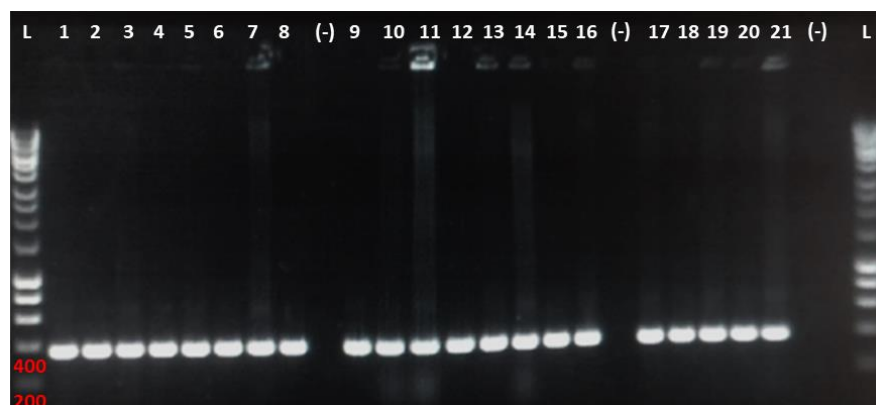
Figure 3.24. Amplicons generated by PCR using primers specific to *COPT2*y on individual *E. coli* colonies following heat shock transformation by pYES2-*COPT2y* on a 1.2% agarose gel.

3.3.1.2. Confirmation of transformation of *pYES2-YeGFP* and *pYES2-COPT2y* into yeast

Following transformation of yeast (strains: BY4741, *Δccc2*, *Δace1*, DTY165, *Δctr1ctr3*) with *pYES2-YeGFP* and *pYES2-COPT2y*, colonies that grew on SD-U(A) selection media were evaluated using PCR to confirm the presence of the plasmid sequences. All five strains were successfully transformed with *pYES2-YeGFP* and *pYES2-COPT2y*, as evidenced by PCR product visualisation, using primers specific to *pYES2* (Figure 3.25A, C) or to the *COPT2*y sequence (Figure 3.25B).
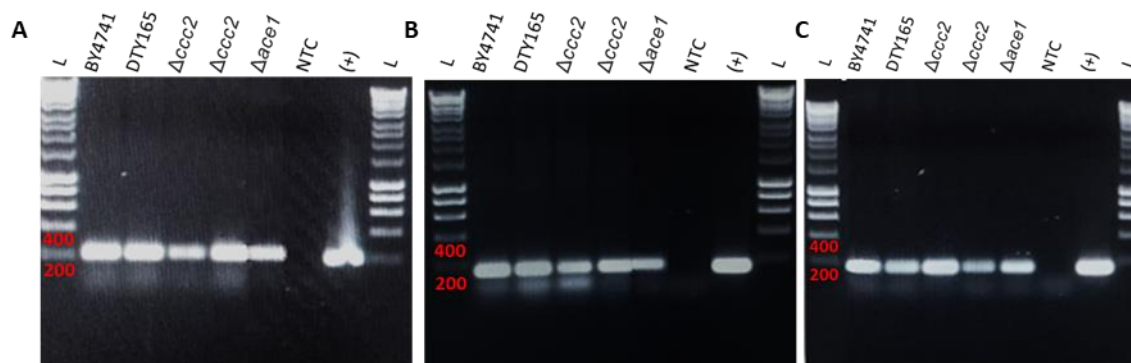
Figure 3.25. Visualisation of colony PCR products following transformation of five yeast strains with *pYES2-YeGFP* or *pYES2-COPT2y* on a 1.2 % agarose gel; A: Using *pYES2-YeGFP* specific primers in PCR reactions containing yeast strains transformed with *pYES2-COPT2y*; B: Using *COPT2y* specific primers in PCR reactions containing yeast strains transformed with *pYES2-COPT2y*; C: Using *pYES2-YeGFP* specific primers in reactions containing yeast strains transformed with *pYES2-YeGFP.*

3.3.1.3. Yeast studies on *COPT2* involvement in Au uptake

To confirm and further characterise the involvement of COPT2 in Cu and Au uptake, five *pYES2-COPT2y* expressing yeast strains (BY4741, *Δccc2, Δace1,* DTY165, *Δctr1ctr3*) were utilised in growth assays on SD-U(A) media containing either Cu, Au, or both, as per section 2.2.16, pg. 40 (Figure 3.26). As shown in Figure 3.26, due to the *GAL1* promoter upstream of *COPT2y*, *COPT2y* is only expressed in strains carrying *pYES2-COPT2y* with gal as the sole carbon source (Figure 3.26, left panel).

On SD-U(A) media containing glu as the sole carbon source, there is no expression of *COPT2y* (Figure 3.26, right panel). Figure 3.26 demonstrates that for all strains, excluding *Δace1*, there was significant growth for all serial dilutions (10^0, 10^{-1}, 10^{-2}, 10^{-3}, 10^{-4}) when strains were grown on SD-U with glu, regardless of the metal added. There was significant growth for all serial dilutions of *Δace1* when grown on SD-U(A) and glu media containing Au (Figure 3.26B); however, in the presence of Cu alone, or Cu and Au, there was complete loss of the *Δace1* strain at all dilutions (Figure 3.26A and C). The *Δace1* strain lacks the Cu binding transcription factor which results in the activation of the MT genes *CUP1* and *CUP2* and *SOD1*. Reduced expression of *CUP1* results in increased sensitivity to Cu, and increased Cu uptake by the expression of *COPT2y* is likely to result in lowered resistance to Cu. If the Au detoxification mechanisms in yeast utilise the Ace1 regulated proteins, then the same pattern will be shown when the *Δace1* strain is grown on SD-U(A) media containing

Au. Comparisons between the *Δace1* strain expressing *COPT2y* or not expressing *COPT2y* on Au suggest that the genes controlled by Ace1 are not involved in Au detoxification in yeast.
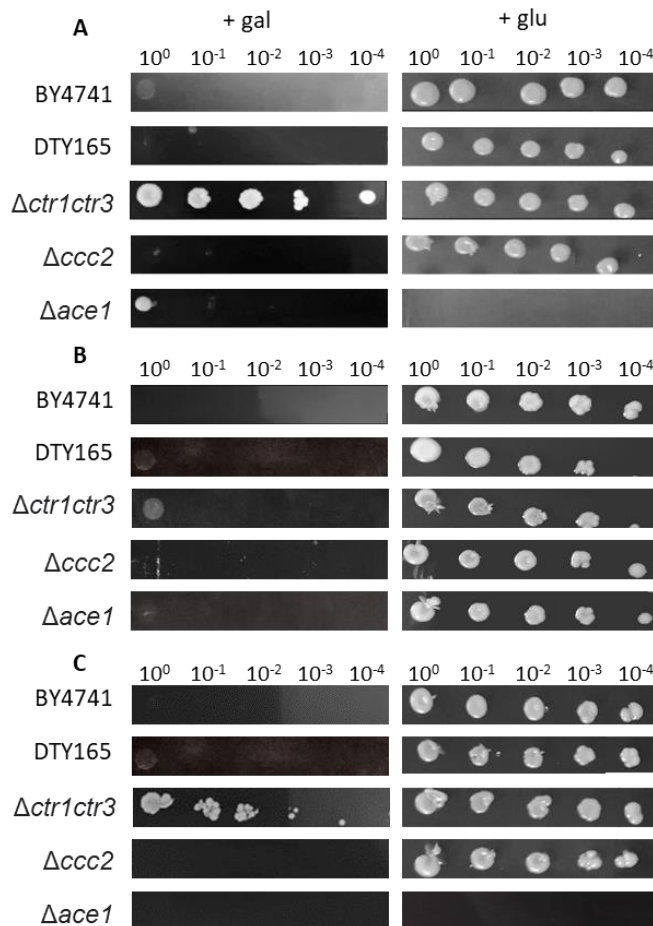
Figure 3.26. Spot dilution growth assay on SD-U(A) media containing Cu, Au or both, using yeast strains containing pYES2-*COPT2y*. Figures A, B and C contain different metal additions to the SD-U(A) media: (A) 100 µM Cu (B) 500 µM Au or (C) 100 µM Cu and 500 µM Au. The *COPT2y* sequence is under the control of the GAL1 promoter and therefore expression of *COPT2y* only occurs with galactose (gal) as the available carbon source. The SD-U(A) media (used for positive selection of yeast colonies containing *pYES2-COPT2y)* contained either gal (resulting in *COPT2y* expression) or glucose (glu) (no expression of *COPT2*y). Cultures were grown to an OD600 of 1, and serially diluted by a factor of 10 (10^0, 10^{-1}, 10^{-2}, 10^{-3}, 10^{-4}). Each row shown in the figure is a single strain and each 'spot' is a serial dilution of the one before, moving from left to right. There were five technical replicates of each condition, and the images included are representative of the trends seen across these replicates.

The *Δctr1ctr3* strain lacks the expression of the high affinity Cu uptake transporters in yeast, *CTR1* and *CTR3*. The expression of *COPT2y* in the *Δctr1ctr3* strain is expected to result in an increased sensitivity to Cu (or Au) compared to the growth of the strain not expressing *COPT2y.* On SD-U plates containing gal, with Cu as the additional metal, there was complete or near complete lack of growth of strains excluding *Δctr1ctr3*. The *Δctr1ctr3* strain produced colonies at all serial dilutions (Figure 3.26A). On SD-U plates containing gal and Au as the additional metal, there was complete or near complete lack of growth of all strains compared to growth on SD-U with glu and Au (Figure

3.26B). With both Cu and Au added to SD-U and gal there was a significant rescue of growth in *Δctr1ctr3* compared to growth on medium containing Au as the sole additional metal (Figure 3.26C). In the presence of Au and Cu, the *Δctr1ctr3* strain had a visible reduction in colony growth after the first dilution, compared to strong growth at all dilutions when Cu was present alone (Figure 3.26C compared to Figure 3.26A). The *Δccc2* strain lacks the P-type ATPase located in the trans-golgi secretory pathway, and links Cu homeostasis with Fe uptake in yeast. In *Δccc2* mutants, increased Cu content in the yeast cells via the expression of *COPT2* would be expected to result in increased sensitivity as less of the free Cu would be trafficked to the golgi apparatus, leading to increased free Cu ions and metal induced stress, as well as Fe deficiency.

3.3.2. Arabidopsis studies
3.3.2.1. Identification of homozygous T-DNA insertion lines by PCR and visualisation

To confirm the presence and identify the location of the T-DNA insertion in *copt2* mutant lines, PCR primers specific to each line were selected. Three primers were used in each PCR reaction: one T-DNA-specific primer and two gene-specific primers. The PCR products were visualised on a 1.2 % agarose gel as per section 2.4.4, pg. 44. The WT DNA samples were isolated from four individual plants (Figure 3.27A, 1-4) and were tested alongside Arabidopsis *copt2-1* samples from four individual plants (Figure 3.27A, 5-8). Bands were observed at the expected location following PCR reactions using the WT plants (979 bp) and the *copt2-1* plants (750 bp). Faint bands, likely to be non-specific background reactions, were observed for both WT and *copt2-1* samples (Figure 3.27A). Sample five also contained the WT band (979 bp), suggesting that this sample is heterozygous for the T-DNA insertion, and that the seed population received was a mix of homozygous or heterozygous seeds. Seeds were obtained from Arabidopsis plants 6, 7 and 8, and these seed stocks were used in future work (Figure 3.27A).

In the reactions using the *copt2-2* and *copt2-3* DNA, five WT DNA samples (1-5) were assessed alongside five Arabidopsis *copt2* mutant samples (6-10). Bands were observed at the expected location following PCR reactions using the WT (1155 bp using *copt2-2* primers; 1141 bp for *copt2-3* primers) and *copt2* mutant line DNA samples (496 - 796 bp for *copt2-2* samples 6, 7 and 8; 516 bp for *copt2-3* samples) (*copt2-2:* Figure 3.27B; *copt2-3*: Figure 3.27C). Faint bands were observed resulting from reactions using the *copt2-2* primers; however, these are likely to be non-specific background reactions (Figure 3.27B). The *copt2-2* samples 9 and 10 contained the WT band (1155 bp) indicating that these samples are WT lines, and that the seed population received was a mix of homozygous WT and *copt2-2* seeds. Seeds were obtained from *copt2-2* plants 6, 7 and 8, and used in future work.
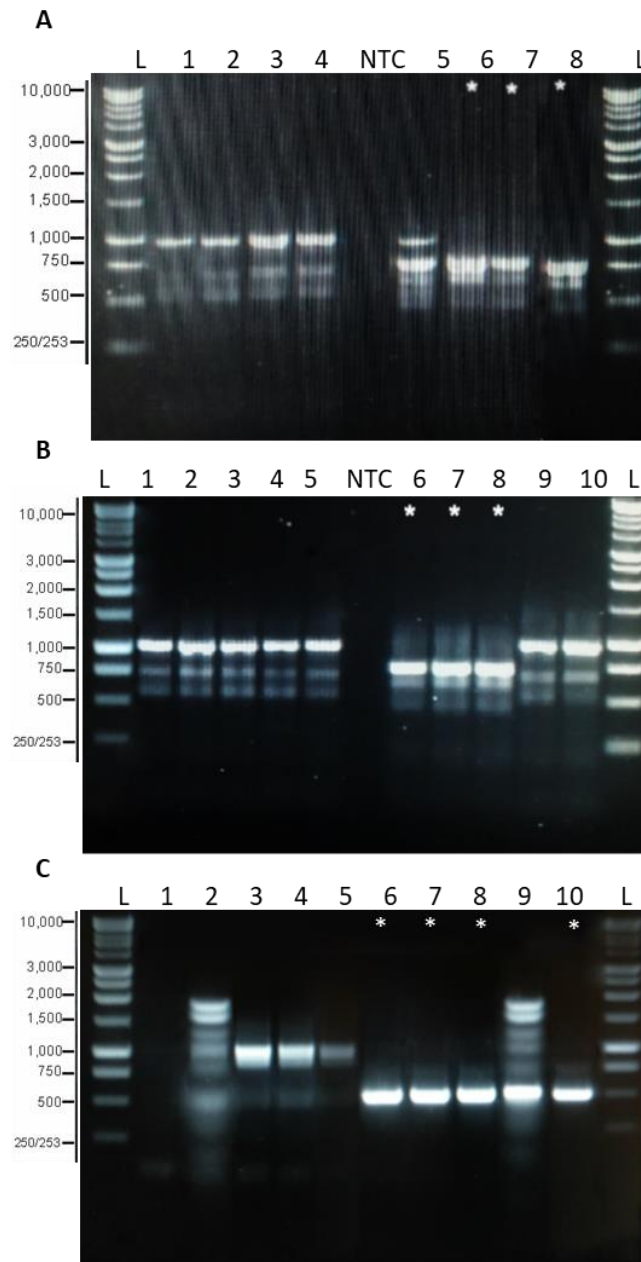
Figure 3.27. PCR products on a 1.2 % agarose gel, performed on DNA extracted from rosette leaves of two-week old Arabidopsis *copt2* plants to identify lines that were homozygous for the T-DNA insertion. For each reaction, three DNA primers were used: two gene-specific primers and a T-DNA border primer; (A): PCR performed on WT DNA (1-4) and *copt2-1* DNA (5-8), using the *COPT2*LP1, *COPT2*RP1 and GKAT-PCR(s) DNA primer sequences. The endogenous *COPT2* amplicon was expected at 979 bp and the T-DNA amplicon was expected between 750 bp; (B) PCR performed on WT DNA (1-5) and *copt2-2* DNA (6-10), using *COPT2*LP2, *COPT2*RP2 and LBb1.3 DNA primer sequences. The endogenous *COPT2* amplicon was expected at 1155 bp and the T-DNA amplicon was expected between 496 – 796 bp; (C) PCR performed on WT DNA (1-5) and *copt2-3* DNA (6-10), using *COPT2*LP3, *COPT2*RP3 and o8474 DNA primer sequences. The endogenous *COPT2* amplicon was expected at 1141 bp and the T-DNA amplicon was expected between 516 bp.

Visualisation of *copt2-3* sample one did not produce any PCR products, and there was a smear of products in sample 2. There were multiple bands in sample nine, indicative of DNA degradation, and therefore it was unclear whether these lines are homozygous for the T-DNA insertion. As a result, the Arabidopsis *copt2-3* seeds were subsequently obtained from plants 6, 7, 8 and 10, which were confirmed as homozygous T-DNA insertion lines as these samples produced a single PCR product at the expected location and these seed stocks used in future work (Figure 3.27C).

3.3.2.2. Identification of T-DNA insertion location by sequencing in Arabidopsis *copt2* lines

To establish the exact location of each T-DNA within the *COPT2* sequence for each of the three *copt2* mutant lines, and thus the effects on transcription and subsequent translation, the PCR products were sequenced so the sequence could be used to match the location on the Arabidopsis genome. The location of the T-DNA insertion impacts the level of expression of the affected gene (180). In a study performed by Wang (2008), just over 1000 published Arabidopsis T-DNA insertion mutants were investigated to determine the location of the T-DNA insertion and the expression of the affected gene (180). The author found that insertion in the protein-coding region of a gene generated a knockout 90 % of the time. If the insertion is present before the start codon, a knockout will be generated in 25 % of cases, or a knockdown will be generated 67 % of the time. Insertion after the stop codon did not affect the transcription of the upstream gene in 17 % of samples evaluated.

The T-DNA insertion in Arabidopsis *copt2-1* lies in chromosome three at the 17,268,874 bp position, at the 17,268,798 bp position in *copt2-2*, both within the promoter region of *COPT2*: 13 bp and 89 bp upstream of the translation start site located at position 17, 268, 887 bp, respectively. In Arabidopsis *copt2-3,* the T-DNA insertion is at the 17,268,977 bp position, 90 bp downstream of the translation start site, within the *COPT2* coding region (Figure 3.28).
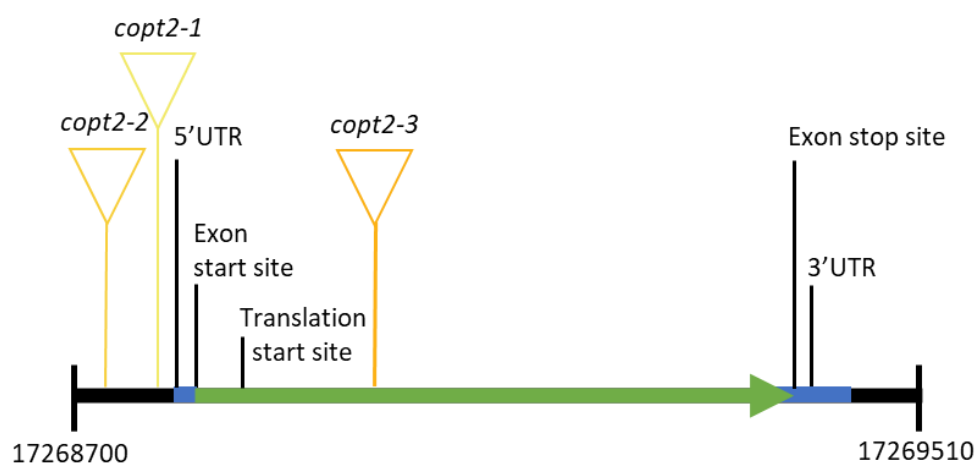
Figure 3.28. Location of the T-DNA insertion sequences in the three Arabidopsis *copt2* lines: *copt2-1, copt2-2,* and *copt2-3*. The locations of the T-DNA insertions in these lines were identified by PCR, sequencing, and comparison of sequences to the Arabidopsis genome. All T-DNA sequences are located within chromosome three.

3.3.2.3. The expression of *COPT2* in Arabidopsis *copt2* mutant lines

Levene's test was used to confirm homogeneity of variances (Levene's test: F = 1.8397, p = 0.1863). However, the assumption of normality was not met (Shapiro-Wilk: W = 0.84677, p < 0.05). Based on this outcome, analysis was performed using a Kruskal-Wallis test (the non-parametric alternative to the one-way ANOVA), and the median with the interquartile range used to summarise the data. The statistical analysis determined that there was a significant effect of genotype on the transcript abundance of *COPT2* in two-week old rosette leaves (Kruskal-Wallis: X_2 = 10.686; d. f. = 3; p-value < 0.05).
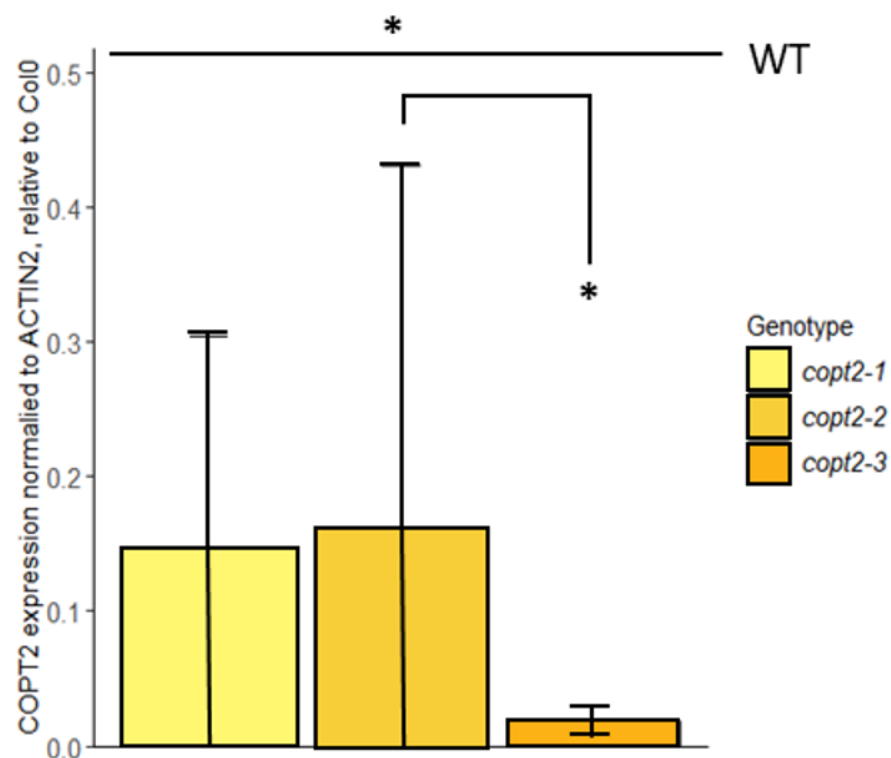
Figure 3.29. The *COPT2* transcript abundance in rosette tissue relative to *ACTIN2*. The C2Ds1 primer pair was used to estimate COPT2 transcript abundance relative to the endogenous control ACTIN2 gene and normalised to WT expression. The Pfaffl method was used to calculate gene expression level, which considers the primer efficiency of the primers used (ACTIN2: 107.31%; C2Ds1: 107.59%) (6). The expression level was analysed by qPCR using the primer pair C2Ds1LP and C2Ds1RP which is situated downstream of the T-DNA insertion in *copt2-1, copt2-2, copt2-3.* Values are a mean of five biological replicates + SD. Results of a one-way ANOVA are indicated on the graph; asterisks indicate the level of significant difference to the WT expression level (not shown) (* = p < 0.05; ** = p < 0.01; *** = p < 0.001).

Summary statistics for the data are shown in Table S1. The transcript abundance of *COPT2* was significantly higher in WT samples than in the three *copt2* mutant genotypes. The *copt2-2* had significantly higher expression of *COPT2* transcript compared to *copt2-3,* but there were no other significant differences noted (Table S2).

3.3.2.4. Characterising effect of Au on roots

Previously, *copt2-1* had been shown to have drastically reduced *COPT2* transcript in shoot and root tissue compared to WT (143). When grown hydroponically the mutant also exhibited significantly decreased levels of Cu in the root compared to the WT (143). The reduced Cu uptake led to longer root length of the *copt2-1* mutant seedlings grown on 10 µM CuSO$_4$ (143). To verify the interaction of COPT2 and Au, the root length, number of lateral root branches and root architecture of the three *copt2* mutant lines were analysed on Au.

Arabidopsis WT and the three *copt2* mutant genotypes were grown on undosed ½ MS(A) plates, and ½ MS(A) plates containing a range of Cu or Au concentrations. Tests for homogeneity of variances and normal distributions were performed for each concentration evaluated (Levene's and Shapiro-Wilk test, respectively) and used to inform statistical analysis. Comparisons were made using a two-way ANOVA test to investigate whether the interaction of concentration and genotype influenced root length, number of lateral root branches and root architecture. Root architecture was calculated by dividing the number of lateral root branches by the root length to calculate the number of branches per mm of root. All values were normalised to the 0 µM mean value to evaluate differences in the root phenotype in response to the metal treatment.

Levene's tests on the Cu dataset established that neither the length, number of lateral root branches nor root architecture data were normally distributed (Length: d. f. = 19, 504; F = 1.628; p-value < 0.05; Lateral root branches: d. f.19, 504; F = 1.746; p-value < 0.05; Architecture: d. f.19, 504, F = 7.9789; p-value < 0.05). The Shapiro-Wilk tests established that the length data had equal variances (W = 0.9953; p-value < 0.1135) but the number of lateral root branches and root architecture did not (Lateral root branches: W = 0.9194; p-value < 0.05; Architecture: W = 0.9578; p-value < 0.05). The two-way ANOVA test was used to establish significant differences, but with a more stringent probability value (0.02). There were no significant differences in the root length, number of lateral root branches or root architecture between WT and the three *copt2* mutant genotypes (Length: d. f. = 12, 504; F = 1.628; p-value > 0.02; Lateral root branches: d. f. = 4, 504; F = 1.746; p-value > 0.02; Architecture: d. f.12, 504; F = 1.905; p-value > 0.02).

Figure 3.31 shows the results of the root characterisation on Cu (left panel) or Au (right panel). With increasing concentrations of Cu, there was a general decrease in root length for all lines except *copt2-3*, in which case the root length increased slightly relative to the undosed, 0 µM condition. The number of lateral root branches decreased sharply at concentrations of Cu above 10 µM, which is likely to be linked to the shorter roots at these higher concentrations. At the higher Cu concentrations, there are fewer root branches per mm of root length. The 10 µM Cu concentration is an exception; the number of lateral root branches is higher on 10 µM Cu than it is on 0 µM for the *copt2-1, copt2-2,* and *copt2-3* genotypes.
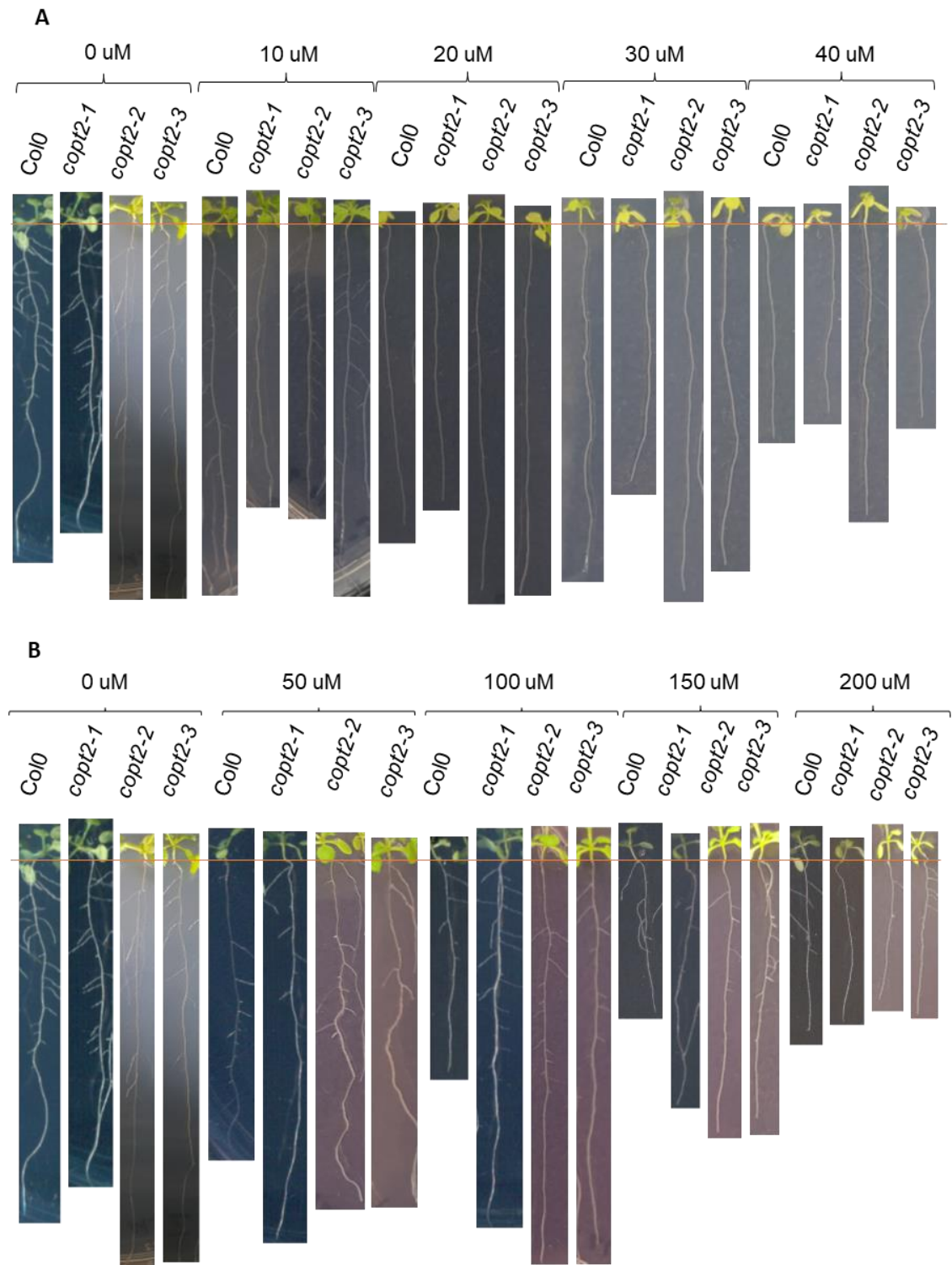
Figure 3.30. Representative images (plates scanned using an Epson Perfection V370 Photo Flatbed scanner for consistency of scale) of the growth of twelve-day-old Arabidopsis WT (Col0) and the three *copt2* mutant lines on ½ MS(A) media containing a range of added Cu or Au. (A) Cu (as CuSO₄) or (B) Au (as KAuCl4). The orange line indicates the initiation of the root length measurement at the junction between root and shoot. Measurements of root length and number of lateral root branches were performed from these images using ImageJ. Images are representative of the growth of between 10 – 63 biological reps, across three technical reps.
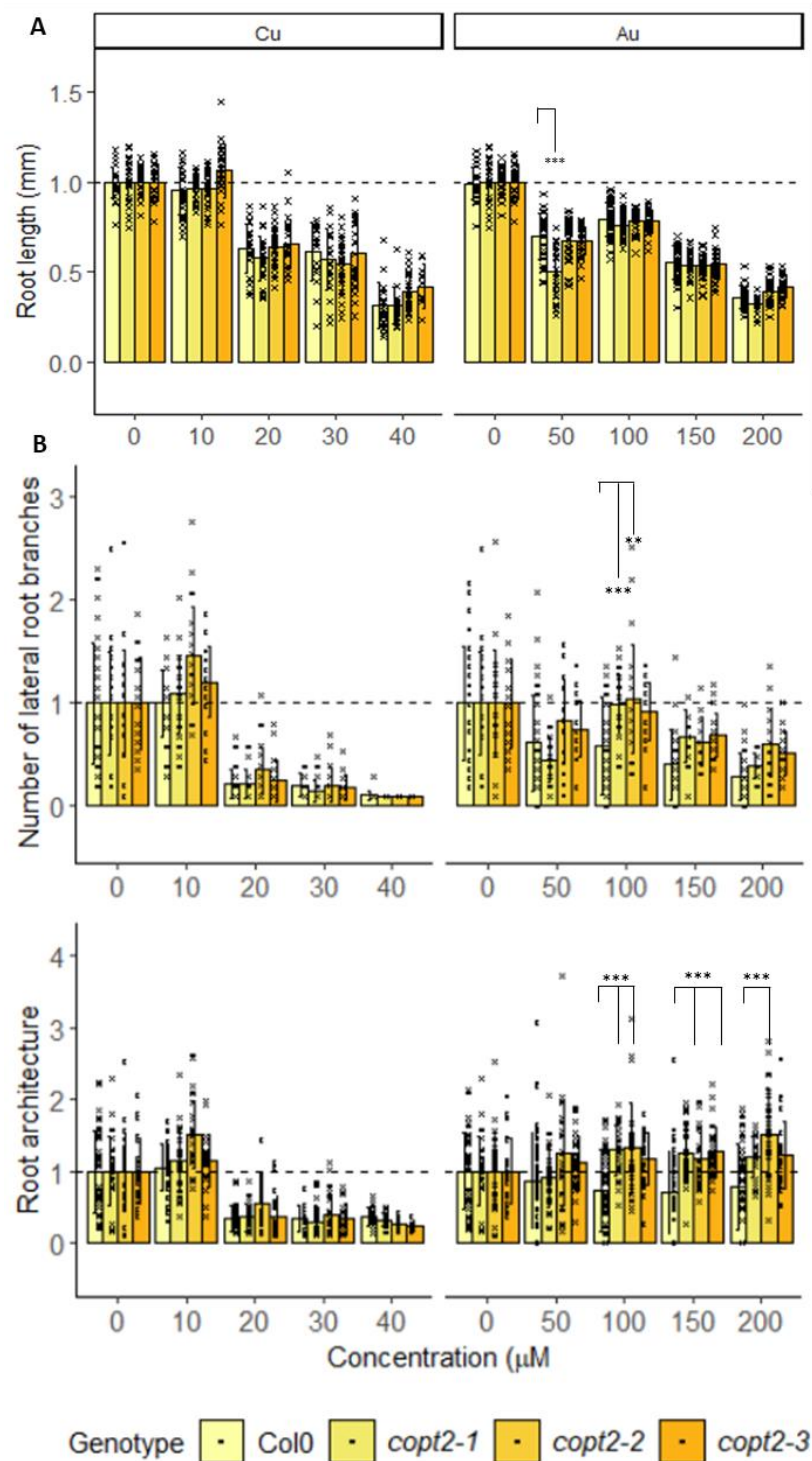
Figure 3.31. Root characterisation of two-week-old seedlings (Arabidopsis WT (Col0) and three *copt2* mutant genotypes) grown on ½ MS(A) media containing Cu or Au. Data are normalised to the values at 0 µM. Statistical significance was calculated by a two-way ANOVA test and a Tukey's HSD test. Levene's test for homogeneity of variances and a Shapiro Wilk for data normality were used for test assumptions. Asterisks mark significant differences in each concentration (p-value: * < 0.02; ** < 0.01; *** < 0.001). A: Root length; B: Number of lateral root branches; C: Root architecture. Values are a mean of between 10 - 63 biological reps, across three technical reps. Higher concentrations resulted in fewer measurable seedlings. The exact number of reps for each condition is shown in Table S3 – Table S5. Black bars are + SD.

Levene's test for homogeneity of variances showed that for root length, number of lateral root branches and architecture that the data did not have equal variances (Length: d. f. = 19, 642; F = 3.7806; p < 0.05; Lateral root branches: d. f. = 12, 630; F = 6.241; p-value < 0.05; Architecture: d. f. = 19, 630; F = 3.2027; p < 0.05). Shapiro-Wilk's test for normal distribution showed that none of the three datasets has normal distribution (Length: W = 0.9855; p < 0.05; Lateral root branches: W = 0.9804; p < 0.05; Architecture: W = 0.9777; p-value < 0.05). As before, the two-way ANOVA was performed with a more stringent test statistic (0.02). It was determined that there was a significant influence of the interaction between genotype and concentration on the root length, number of lateral root branches and root architecture of Arabidopsis WT and *copt2* mutant lines (Two-way ANOVA, Length: d. f. = 12, 646; F = 6.045; p-value < 0.001; Lateral root branches d. f. = 12, 630; F = 3.029; p-value < 0.001; Architecture d. f. = 12, 630; F = 2.741; p-value < 0.01).

Surprisingly, the Au results showed that the roots of the *copt2* mutants differed in morphology compared to the WT when grown on Au than Cu. Figure 3.31A shows that the root length of all lines initially showed a sharp decrease in root length and branching on 50 µM Au compared to the 0 µM control. At 100 µM Au the root length and branching for all lines increased compared to the 50 µM, before dropping at the higher Au concentrations. With the addition of increasing concentrations of Au, the root architecture of the WT and *copt2* mutant lines remain stable; there are fewer lateral root branches per mm of root length for all lines, but the *copt2* mutant lines consistently have more branches per mm of root length than the WT, and this is significant in *copt2-1* and *copt2-2* at 100 µM Au (p < 0.001), *copt2-1* and *copt2-3* at 150 µM Au (p < 0.001) and *copt2-2* at 200 µM Au (p < 0.001) (Table S8).

3.3.2.5. Analysis of element uptake in Arabidopsis *copt2* mutant lines grown in the presence of Au

Seeds were stratified, germinated and seedlings grown for ten to twelve days before being moved to the hydroponic system, then grown until five-weeks old. The plants were then dosed by replacing ½ MS media with ½ MS media containing 1 mM Au (as K_2AuCl_4). Five samples were collected after 24 hours, washed, and weighed. Samples were dried before being weighed again. Additionally, root samples were submerged in a root desorption solution (2 mM $CaSO_4$ and 10 mM ethylenediaminetetraacetic acid) for ten minutes before being dried. Samples were prepared for ICP-OES as described (2.4.8). Plants were grown in a liquid culture, rather than soil, to better control the metal exposure, and to be able to clean the root samples more effectively than if they had been in soil.

A standard curve for these elements was generated using serial dilutions of Periodic table mix 1 and Periodic table mix 2 for ICP (Merck, UK); from 10,000 ppb to 1 ppb. Concentration (ppm) was multiplied by the dilution factor (0.1 L) to calculate the total mass of each element per sample (mg), then normalised by dry weight (g).

Per element (Au, Cu or Fe), concentration was measured using two wavelengths in case of interfering spectra or differences in sensitivity. For the samples shown as NA values in Table 3.3, the intensity of light emitted saturated the detector. These samples contained a concentration of elements which were above the detectable range. The number of NA values were used to decide which wavelengths could be used to analyse the element concentration.

Table 3.3. Count of 'NA' values per wavelength (nm) for Au, Cu or Fe

Element	Wavelength (nm)	Values as na	
		Shoot	Root
Au	242.795 (axial)	0	1
	267.595 (axial)	0	18
Cu	213.598 (axial)	0	5
	324.754 (radial)	0	2
Fe	239.562 (radial)	0	5
	259.940 (axial)	6	4

Both Au specific wavelengths were used to graph concentration in the shoot tissue (242 nm and 267 nm), whereas only the measurements taken at 267.595 nm (267 nm) were graphed for the root Au concentration due to the high number of NA values (Table 3.3). There was an unknown, interfering element present ~ 213.6 nm, which impaired the accuracy of the Cu 213.598 nm (213 nm) intensity reading. Therefore, the Cu specific 324.754 nm (324 nm) wavelength was selected for further analysis. Due to the presence of six NA values in the Fe 259.940 nm (259 nm) shoot tissue analysis, the Fe 239.562 nm (239 nm) reading was selected for further analysis (Table 3.3). These wavelength selections were utilised for all subsequent ICP-OES analyses.

Comparisons were made using a one-way ANOVA (for data that fit the assumptions) or a Kruskal-Wallis test (the non-parametric alternative to the one-way ANOVA) (Table S10). These were followed by post-hoc tests to determine the direction of any significant differences (Table S11).

Surprisingly, as shown in Figure 3.32, the *copt2-2* demonstrated a significantly increased concentration of Au compared to the WT. The reduced expression of *COPT2* did not result in an alteration in the Fe content in shoot or root tissue; however, Cu content was significantly higher in the *copt2* mutant genotypes (excluding the shoot *copt2-1* samples) in both shoot and root tissue. There were no significant differences in the Au concentration between root samples, potentially due to the binding of Au ions organic components (such as aquaporins). It is also possible that the root tissue was saturated due to the high concentration of Au present in the medium.
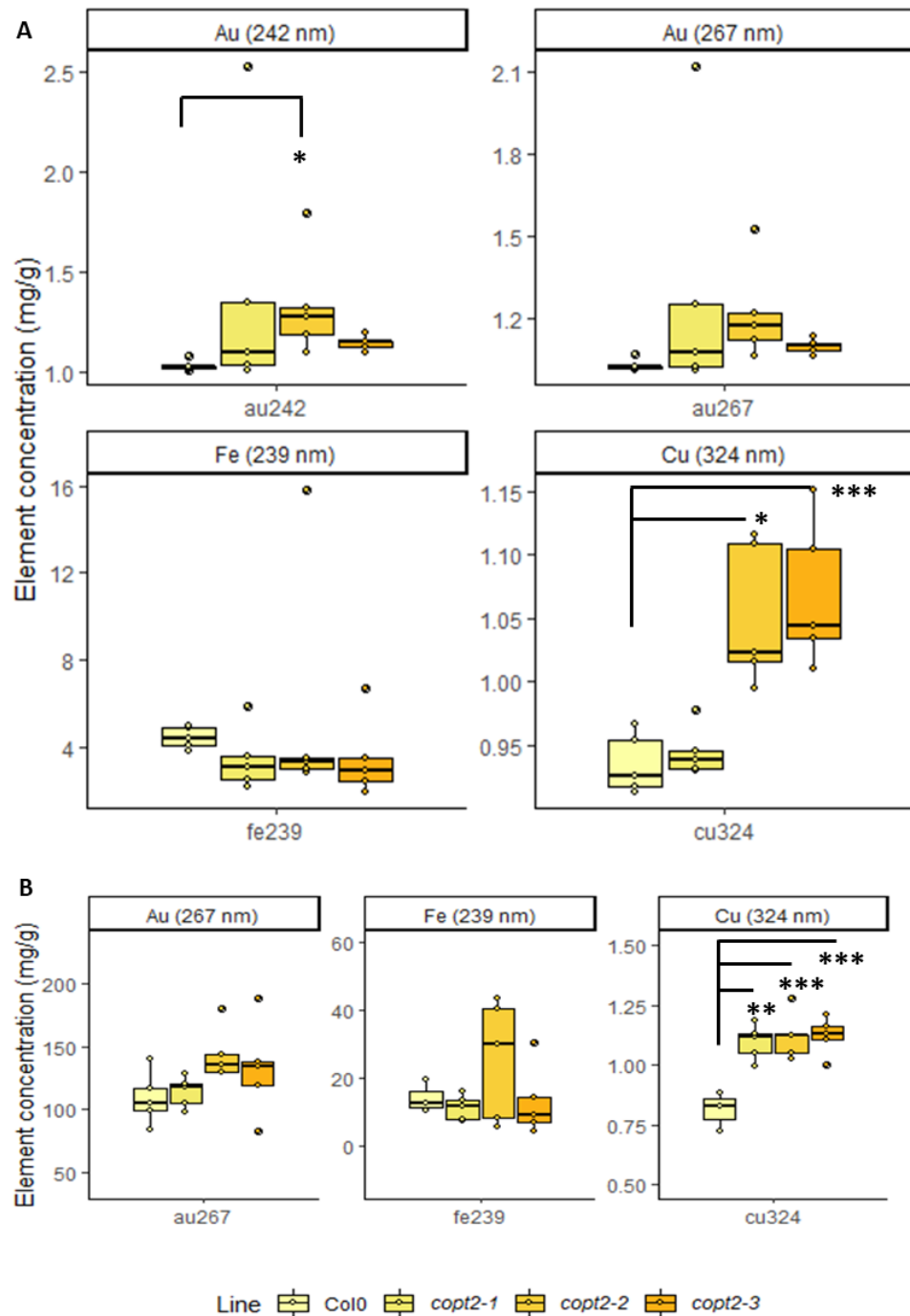
Figure 3.32. Element (Au, Cu, or Fe) concentration (mg/g) in WT (Col0) and three T-DNA insertion *copt2* mutant lines *(copt2-1, copt2-2* and *copt2-3*) 24 hours after the addition of 1 mM Au to hydroponically grown, five-week-old Arabidopsis. (A) Shoot tissue; (B): Root tissue. Five biological replicates were analysed by ICP-OES and normalised by dry weight (g). Homogeneity of variances was determined by Levene's test, and normality of data was determined by the Shapiro-Wilk test. Normally distributed data were analysed by one-way ANOVA and Tukey's HSD test; otherwise, data were analysed by a Kruskal-Wallis and Wilcoxon rank sum test for multiple comparisons. Significant differences between WT (Col0) and *COPT2* are indicated on plots as asterisks (*: $p < 0.05$, **: $p < 0.01$, ***: $p < 0.001$). Circular dots indicate the distribution of raw data, 'whiskers' inducate the upper and lower quartiles.

3.3.2.6. Measurements of ROS accumulation in Arabidopsis WT and *copt2* mutant line root tips

Tiwari et al. (2013) reported an unquantified decrease in ROS production in Au-dosed root tips of *copt2* mutant lines compared to WT (4). To investigate the effect further, the fluorescent indicator H$_2$DCF was used in our study to visualise the presence of ROS in response to metal treatment. Roots were submerged in Cu or Au (25 µM Cu; 25 µM or 50 µM Au), then treated with H$_2$DCF for 30 minutes. Samples were exposed to peroxides in the root tissue and the fluorescence signal measured by epifluorescence microscopy. ImageJ was used to quantify the fluorescence.
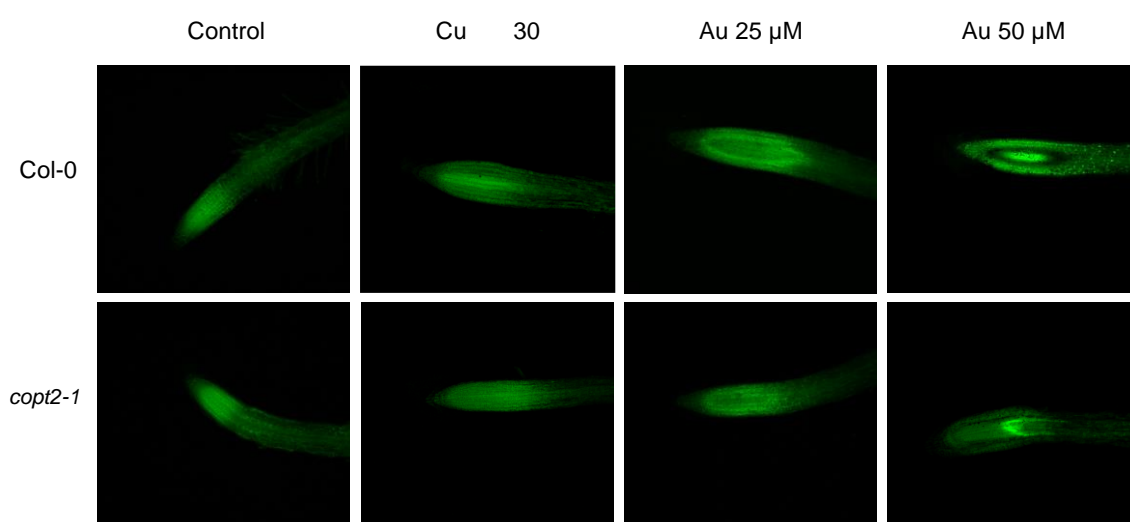
Figure 3.33. Metal (Cu or Au) induced ROS production at the root tip of Arabidopsis WT (Col0) or *copt2-1* lines. The staining by H$_2$DCF was performed for 30 minutes after 24 hours of the root tip being submerged in a metal containing solution, and fluorescence images taken 24 hours following treatment. Upper panels show the WT (Col0) images, and the lower panels show the Arabidopsis *copt2-1* images. Images were taken with an epifluorescence microscope with FITC filter at 3 % exposure.

Whilst the work described here was able to utilise three *copt2* mutant lines, Tiwari et al only had access to the *copt2-1* to demonstrate the activity of *COPT2* in Arabidopsis Au uptake, and therefore this allele was selected for ROS analysis (4). Root tips treated with Cu or Au had an increased fluorescence, marking an increase in ROS production in the root tip (Figure 3.33). The fluorescence intensity was brighter in the Arabidopsis WT root tips dosed with Au 50 µM comparative to 25 µM Au; fluorescence appeared less bright in the root tip of Arabidopsis *copt2-1* lines when compared to the WT, for both Cu and Au treatments (Figure 3.33).
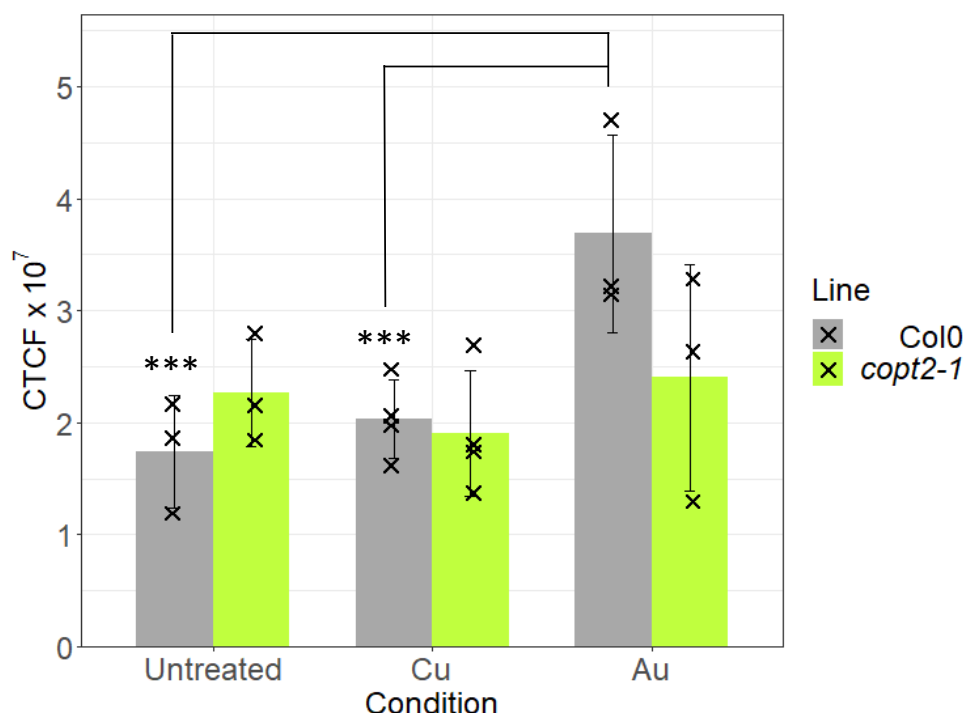
Figure 3.34. Mean corrected total cell fluoresence (CTCF) in Arabidopsis WT (Col0) and *copt2-1* root tips after 24 hour exposure to 30 µM Cu (Cu) and 25 µM Au. Bar plots are the mean of three or more replicates ± sd. Analysis was performed by a two-way ANOVA (signif. codes: '***' 0.001 '**' 0.01 '*' 0.05). Individual data points are denoted by crosses on the graph.

The results of the fluorescence quantification is shown in Figure 3.34. Fluorescence was quantified on a minimum of three images from the untreated, 30 µM Cu, and 25 µM Au conditions. The data had homogeneity of variances (Levene's test: F = 0.3323, d. f. = 5, 14, p-value = 0.8851) and were normally distributed (Shapiro-Wilk: W = 0.9677, p-value = 0.7057). There was not a statistically significant interaction between the metal concentration and Arabidopsis genotype on fluorescence (Two-way ANOVA: F = 3.013, d. f. = 2, p-value = 0.0814). Simple main effects analysis showed that the metal (Cu or Au) did have a statistically significant effect on the corrected total cell fluorescence (CTCF) (ANOVA: F = 5.643, d. f. = 2, p-value < 0.05), but genotype did not (ANOVA: F = 0.933, d. f. = 1, p-value = 0.3504). A post-hoc test was performed as the small sample size may have had an impact on these results, and post-hoc tests have more power to find differences between groups. There were significant differences between the untreated and Au-treated conditions (Tukey's HSD test: p-value < 0.05), and between the Au- and Cu-treated conditions (p-value < 0.05) (Table S12). But critically, there was no difference between WT and *copt2-1* with either metal treatment. It is likely that there are other Au uptake transporters in Arabidopsis alongside COPT2, as many transporters have multiple targets. The presence of other transporters may have masked any phenotypic differences in response to Au.

Tiwari et el. demonstrated that the *copt2-1* genotype accumulated less Au than the WT, and that *COPT2* can transport Au in Arabidopsis (4). There were no significant differences in the root length of the *COPT2* genotypes compared to WT, but two of the three *copt2* mutants demonstrated a higher

number of lateral root branches at 10 μM Au. In the analysis of element concentration, only the *copt2-2* genotypes demonstrated a significantly higher Au accumulation in shoot tissue compared to the WT. As the significantly higher Au concentration in the *copt2-2* mutant line was only present when Au concentration was measured at 242 nm, not 267 nm, this may not be accurate. It is possible that there is an interaction of *COPT2* with Au, but in the knock-down genotypes we have used, the differences are not clear cut.

3.3.2.7. Investigating *COPT2* expression in Arabidopsis *35S-COPT2* lines by qPCR

To monitor expression of *COPT2,* qPCR was performed using the previously characterised C2Ds1 primers on cDNA from soil-grown rosette leaves, prepared as described in 3.2. A one-way ANOVA was used to evaluate differences between lines, including WT (Col0, not shown on graph). As before, outliers and whether data met the assumptions were calculated as above (3.3.2.3). All three *35S-COPT2* Arabidopsis genotypes contained significantly higher *COPT2* transcript abundance compared to Arabidopsis WT (ANOVA: F value = 27.31, d. f. = 3, 25; p-value < 0.001) (Figure 3.35). A Tukey's HSD test was performed to identify the direction of the significant differences (Table S13).
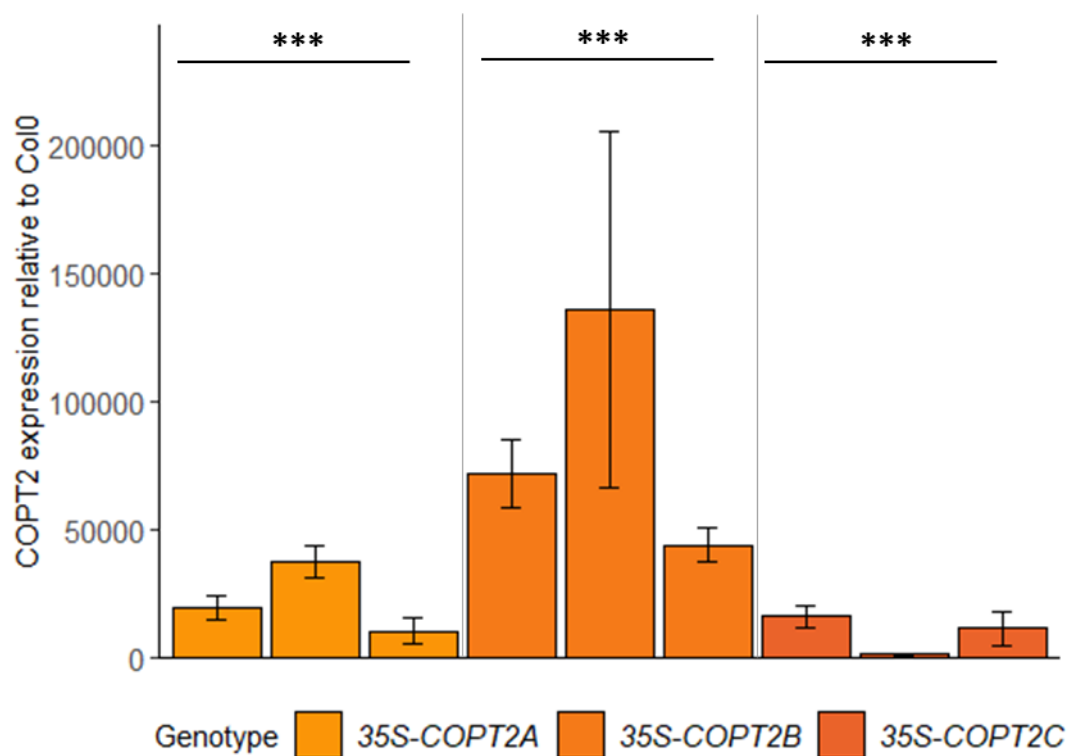
Figure 3.35. The *COPT2* transcript abundance in the rosette tissue of three independent, homozygous *35S-COPT2* lines normalised to *ACTIN2*, relative to the *COPT2* expression level in Arabidopsis WT (Col0), indicated by the primer pair C2Ds1LP and C2Ds1RP. Values are a mean of five biological replicates $\pm$ SD. Results of a one-way ANOVA are indicated on the graph; asterisks indicate the level of significant difference to the WT expression level (not shown) (* = p < 0.05; ** = p < 0.01; *** = p < 0.001).

3.3.2.8. Root characterisation using three Arabidopsis *35S-COPT2* genotypes on Cu and Au

To examine whether increased expression of Arabidopsis *COPT2* changes the phenotypic response of plants to Au, the *35S-COPT2* overexpression lines and WT, were grown on ½MS(A) media containing a range of Cu or Au concentrations, and the primary root length, number of lateral root branches and root architecture investigated (Figure 3.36).

Levene's test for equal variances showed that the root length, number of lateral root branches and architecture on Au datasets did not have equal variances (Length: d. f.19, 825; $F = 7.982$; p-value < 0.05; Lateral root branches: d. f. = 19, 769; $F = 10.082$; p-value < 0.05; Architecture: d. f.19, 742; $F = 5.4566$; p-value < 0.05), and the Shapiro-Wilk tests demonstrated that these datasets did not follow a normal distribution (Length: $W = 0.9600$; p-value < 0.05; Lateral root branches: $W = 0.8591$; p-value < 0.05). The two-way ANOVA test was performed with a more conservative test statistic (p = 0.02). The statistical analysis showed that the interaction of concentration and genotype had a significant effect on the root length, number of lateral root branches and root architecture of WT and *35S-COPT2* lines grown in the presence of Au (Two-way ANOVA, Length: 12, 825; $F = 9.418$; p-value < 0.001; Lateral root branches: d. f. = 12, 769; $F = 5.244$; p-value < 0.001; Architecture: d. f. = 12, 742; $F = 2.713$; p-value < 0.01). As Figure 3.37 shows, with the presence of Au in the growth media, the root length and number of lateral root branches were reduced for all lines assessed. Whilst there were significant differences between WT and the *35S-COPT2* lines, these were inconsistent across the *35S-COPT2* genotypes. For example, at 100 µM Au, all the *35S-COPT2* lines had shorter roots than the WT. However, the phenotypic response at 100 µM Au is the only concentration of Au where the response of the *35S-COPT2* lines were consistent with respect to WT.
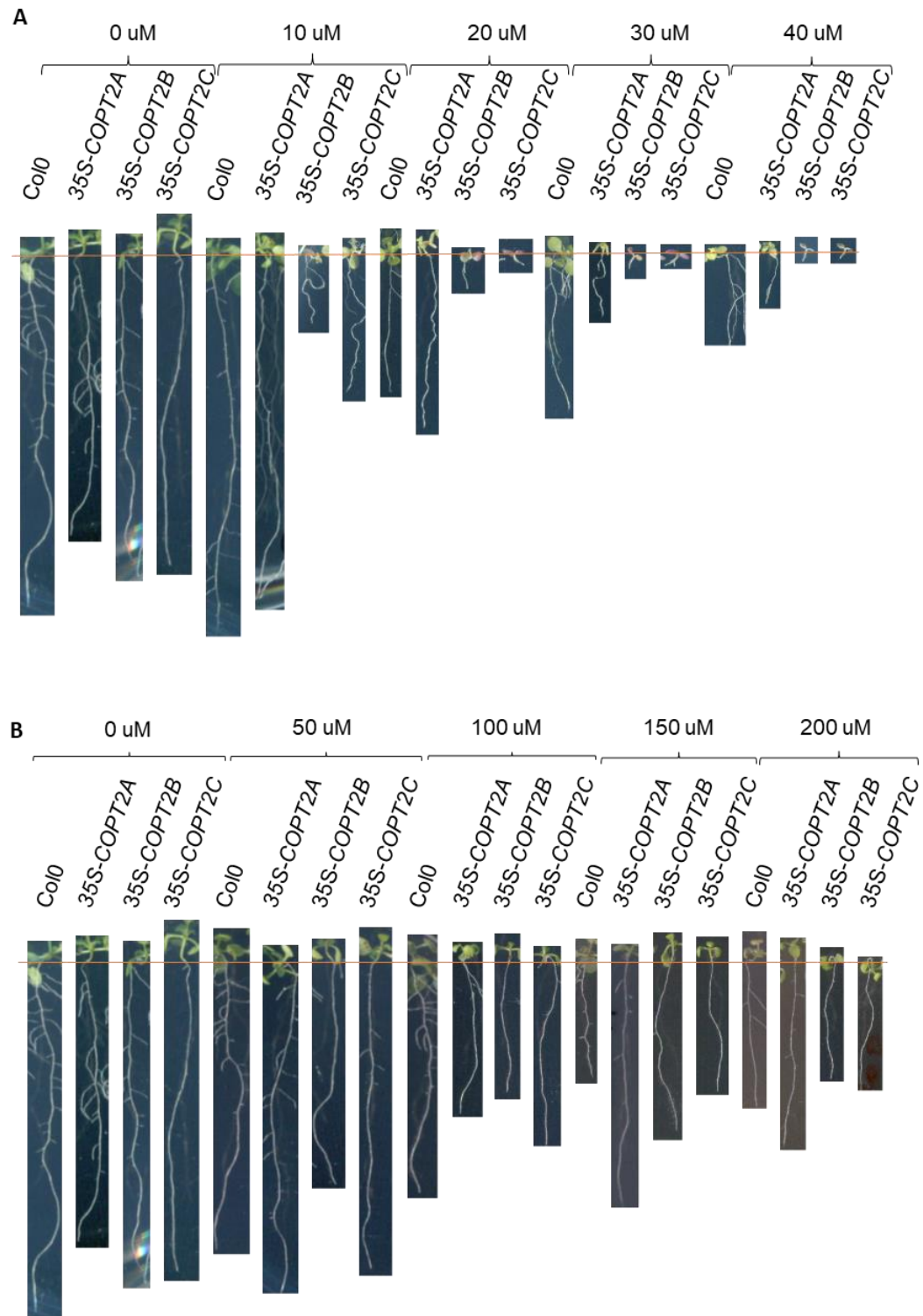
Figure 3.36. Representative images (plates scanned using an Epson Perfection V370 Photo Flatbed scanner for consistency of scale) of the growth of twelve-day-old Arabidopsis WT (Col0) and the three *35S-COPT2* lines (A, B or C) on ½ MS(A) media containing a range of added Cu or Au concentrations, with (A) Cu (as CuSO₄) or (B) Au (as KAuCl4). The orange line indicates the initiation of the root length measurement at the junction between root and shoot. Measurements of root length and number of lateral root branches were performed from these images using ImageJ. Images are representative of the growth of between 12 – 56 biological reps, across three technical reps.
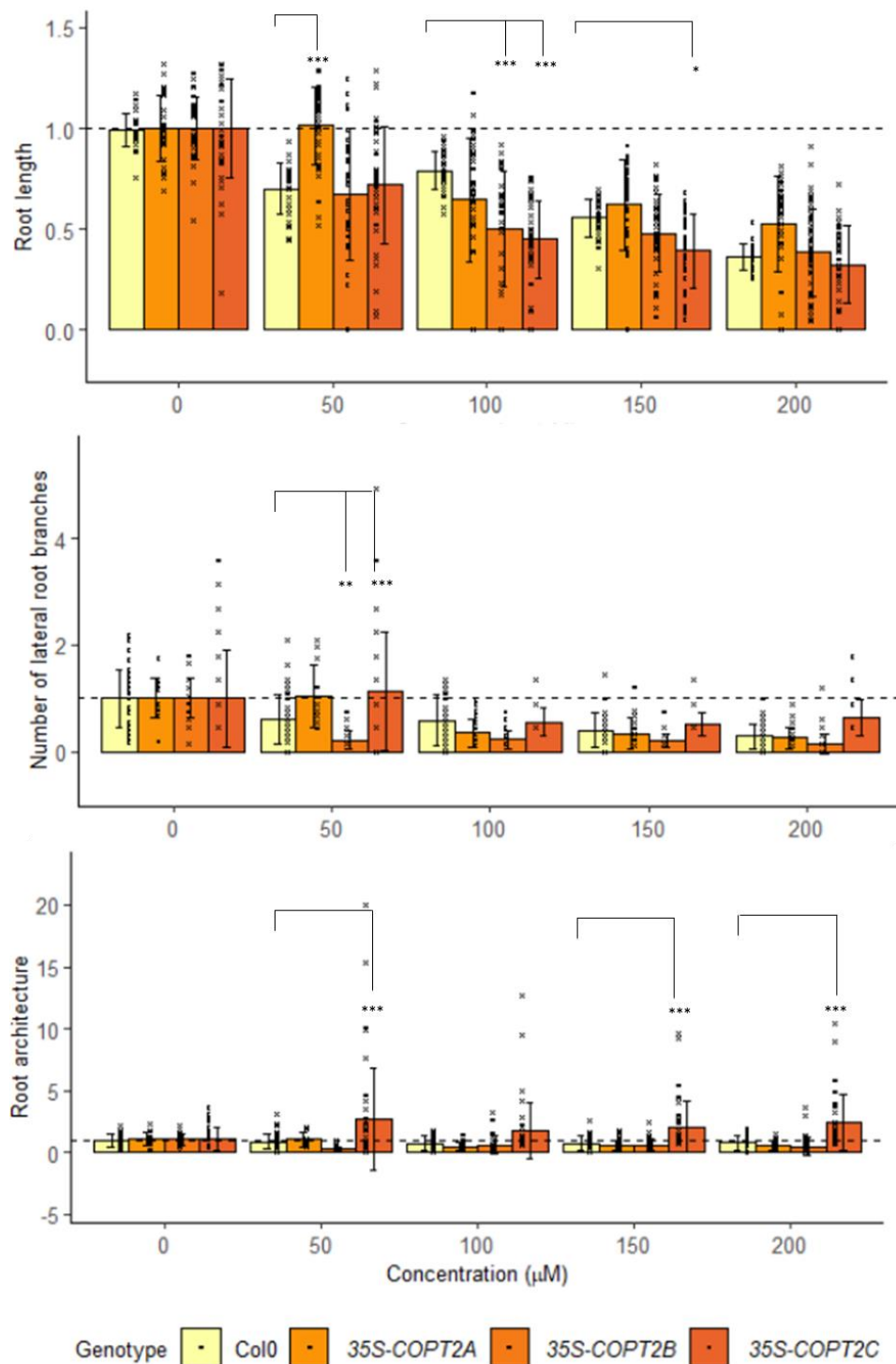
Figure 3.37. Root characterisation of two-week-old Arabidopsis WT (Col0), *35S-COPT2A*, *35S-COPT2B* and *35S-COPT2C* seedlings grown on ½ MS(A) media containing a range of Cu or Au concentrations. Assumptions tests used were Levene's for homogeneity of variances and Shapiro Wilk for data normality. Statistical significance was calculated by two-way ANOVA test and a Tukey's HSD test. Asterisks mark significant differences between concentrations or between *COPT2* genotypes and the WT (Col) in each concentration, normalised to 0 µM (p-value: * < 0.02; ** < 0.01; *** < 0.001). Values are a mean of between 12 - 56 biological reps, across three technical reps. Higher concentrations resulted in fewer measurable seedlings. The exact number of reps for each condition is shown in Table S14 – Table S16. Black bars are + SD.

3.3.2.9. Analysis of element uptake in three Arabidopsis *35S-COPT2* genotypes grown in the presence of Au

Following the analysis of the *35S-COPT2* overexpression lines on ½MS(A) plates containing Cu and Au, the lines were grown hydroponically (with roots submerged in 1mM Au containing media) to assess metal uptake as in section 3.3.2.5. The results are presented in Figure 3.38. Statistical analysis was performed as in section 3.3.2.6 (Table S20 – Table S22). Figure 3.38A shows that compared to the WT the *35S-COPT2B* and *35S-COPT2C* lines exhibited significantly higher ($p < 0.05$ and $p < 0.05$, respectively) shoot Au concentrations (Table S22). There were no significant differences in the levels of Fe between the shoots of the WT and *35S-COPT2* lines. In the root tissues, shown in Fig.3.3.41B, there was no significant difference in the levels of Au or Fe between WT and *35S-COPT2* overexpression lines. However, the *35S-COPT2* overexpression lines all exhibited higher levels of Cu than WT; this was significant for *35S-COPT2A* and *B* ($p < 0.05$ and $p < 0.01$ respectively (Table S22).
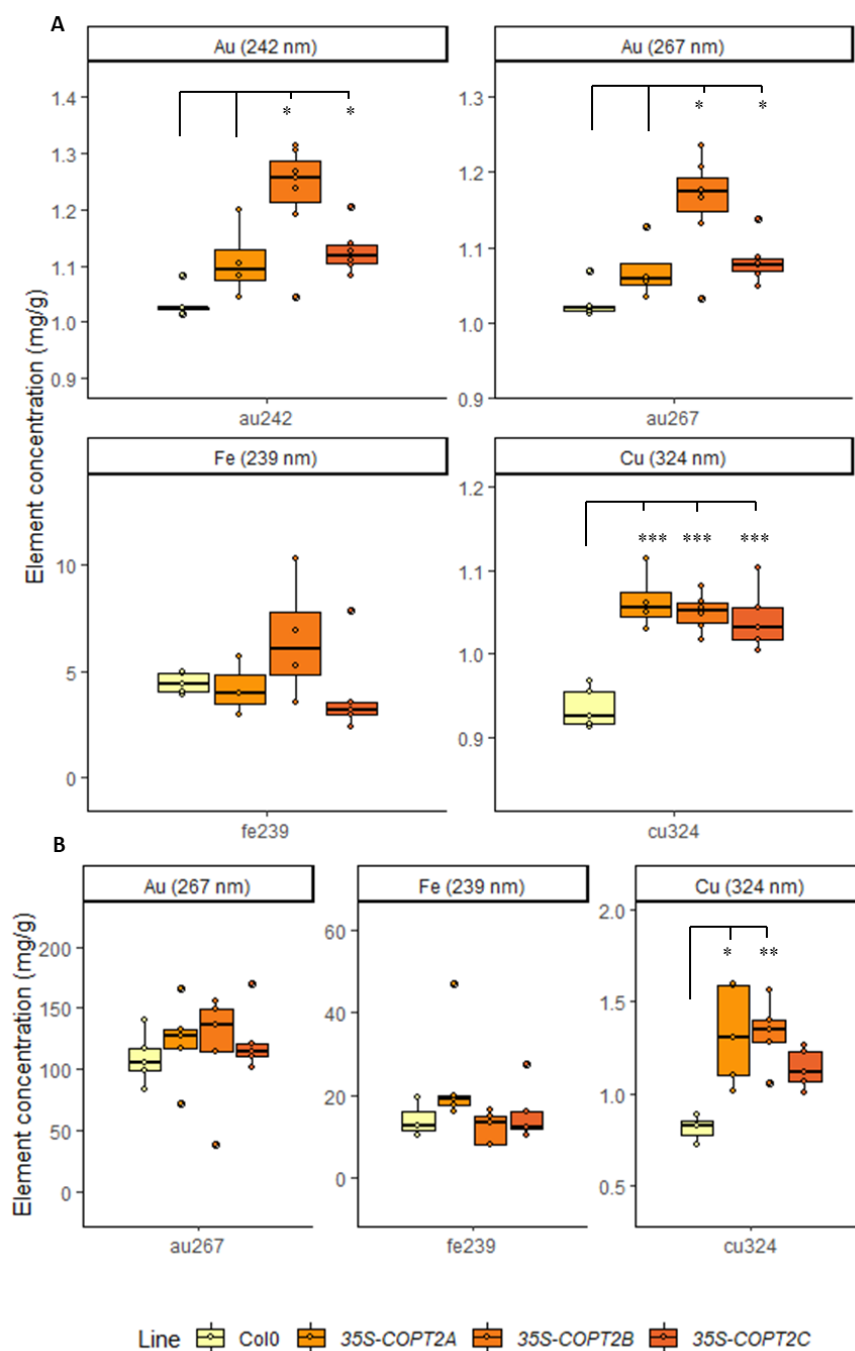
Figure 3.38. Element (Au, Cu, or Fe) concentration (mg/g) in WT (Col0) and three *35S-COPT2* lines 24 hours after the addition of 1 mM Au to hydroponically grown, five-week-old Arabidopsis. (A) Shoot tissue; (B) Root tissue. Five biological replicates were analysed by ICP-OES and normalised by dry weight (g). Homogeneity of variances was determined by Levene's test, and normality of data was determined by the Shapiro-Wilk test. Normally distributed data were analysed by one-way ANOVA and Tukey's HSD test. Data that did not meet the assumptions of a one-way ANOVA were analysed by a Kruskal-Wallis and Wilcoxon rank sum test for multiple comparisons. Significant differences are indicated on plots as asterisks (*: $p < 0.05$, **: $p < 0.01$, ***: $p < 0.001$). Circular dots indicate the distribution of raw data, and 'whiskers' are upper and lower quartiles. The Au 242 measurements were excluded as there were a high number of NA values due to the high concentration.

3.3.2.10.　Investigating the expression of the GP sequence in Arabidopsis *35S*-GP lines by qPCR

The optGP-F and universal reverse primer were used to estimate the GP transcript abundance relative to the endogenous control gene (*ACTIN2*). As the GP sequence is a synthetic peptide that is not present in the Arabidopsis WT lines, these values could not be normalised to WT expression. Excluding this step, the Pfaffl method was used, which accounts for specific primer efficiency (ACTIN2: 10.31 %; optGP-F: 102.56 %). Arabidopsis WT was utilised in the qPCR reaction as a control, but the GP sequence was undetected in the Arabidopsis WT cDNA and is not shown (Figure 3.39).
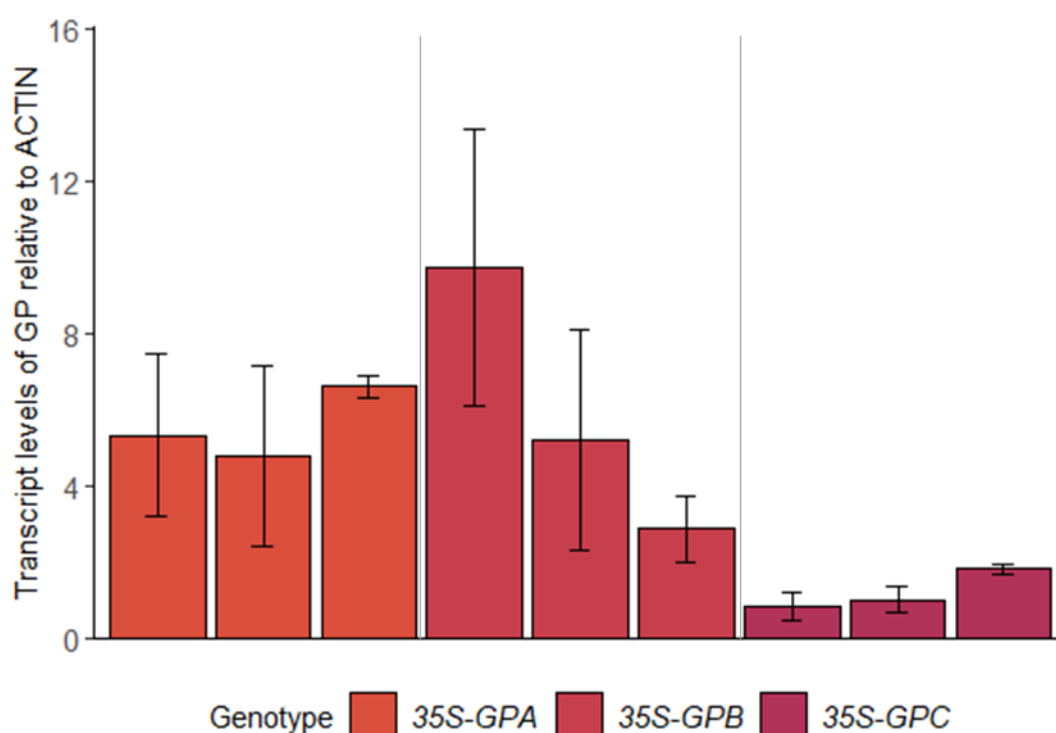
Figure 3.39. The GP transcript abundance in Arabidopsis *35S*-GP*A*, *35S*-GP*B* and *35S*-GP*B* two-week old rosette leaves normalised to the endogenous *ACTIN2* level, as indicated by primer pair optGP-F and the universal reverse primer. Values are a mean of five biological replicates $\pm$ SD. Primers were also used in qPCR reactions against Arabidopsis WT (Col0) but as the sequence was undetected.

3.3.2.11. Root architecture characterisation of Arabidopsis *35S*-GP lines on Cu or Au

To examine whether the expression of the short, synthetic GP would change the phenotypic response of plants to Au due to increased NP formation, Arabidopsis WT, *35S*-GP*A*, *35S*-GP*B* and *35S*-GP*C* lines were grown on ½MS(A) media containing Au (0, 50, 100, 150 or 200 µM) and the primary root length, number of lateral root branches and the interaction between length and branching investigated, as shown in Figure 3.40 and Figure 3.41.

Levene's test for equal variances showed that the root length, number of lateral root branches and architecture on Au datasets did not have equal variances (Length: d. f.17, 533; F = 6.613; p-value < 0.05; Lateral root branches: d. f. = 17, 519; F = 12.045; p-value < 0.05; Architecture: d. f.17, 519; F = 5.2975; p-value < 0.05), and the Shapiro-Wilk tests demonstrated that these datasets did not follow a normal distribution (Length: W = 9498; p-value < 0.05; Lateral root branches: W = 0.9901; p-value < 0.05; Architecture: W = 0.9759; p-value < 0.05). The two-way ANOVA test was performed with a more conservative test statistic (p = 0.02). The statistical analysis showed that the interaction of concentration and genotype had a significant effect on the root length, number of lateral root branches and root architecture of WT and *35S*-GP lines grown in the presence of Au (Two-way ANOVA, Length: 10, 533; F = 18.62; p-value < 0.001; Lateral root branches: d. f. = 10, 519; F = 6.317; p-value < 0.001; Architecture: d. f. = 10, 519; F = 9.519; p-value < 0.001). As Figure 3.41 shows, with increasing concentrations of Au above 100 µM, the *35S*-GP lines had shorter roots and fewer lateral root branches than at 0 µM. At 50 µM Au, *35S*-GP*A* and *35S*-GP*B* had significantly longer roots than the WT (p < 0.001), but the *35S*-GP*C* lines were similar to the WT. The number of lateral root branches of *35S*-GP*A* and *35S*-GP*B* lines were higher than WT, but this difference was only significant at *35S*-GP*A* (p < 0.001). There were no significant differences in the root architecture at the lower concentrations of Au (50, 100 µM). At the higher concentrations (150, 200 µM) the *35S*-GP results were inconsistent between the three transgenic genotypes. At 150 µM Au *35S*-GP*C* had more complex root architecture than the WT (p < 0.001), but at 200 µM Au, *35S*-GP*A* had less complex root architecture than the WT (p < 0.001).
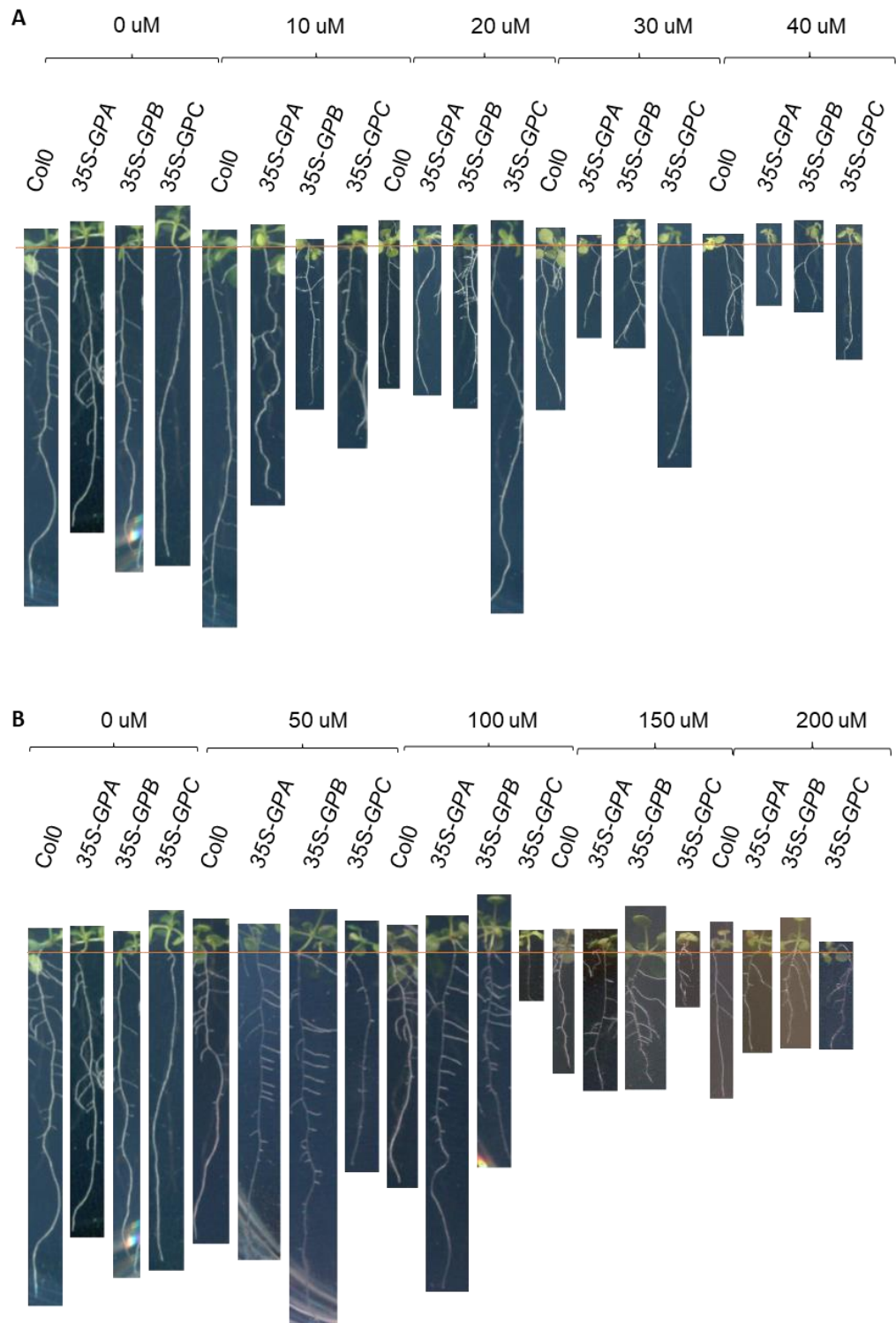
Figure 3.40. Representative images (plates scanned using an Epson Perfection V370 Photo Flatbed scanner for consistency of scale) of the growth of twelve-day-old Arabidopsis WT (Col0) and the three *35S*-GP (A, B or C) lines on ½ MS(A) media containing a range of added Cu or Au concentrations, with (A) Cu (as $CuSO_4$) or (B) Au (as $KAuCl4$). The orange line indicates the initiation of the root length measurement at the junction between root and shoot. Measurements of root length and number of lateral root branches were performed from these images using ImageJ. Images are representative of the growth of between 3 – 56 biological reps, across three technical reps.
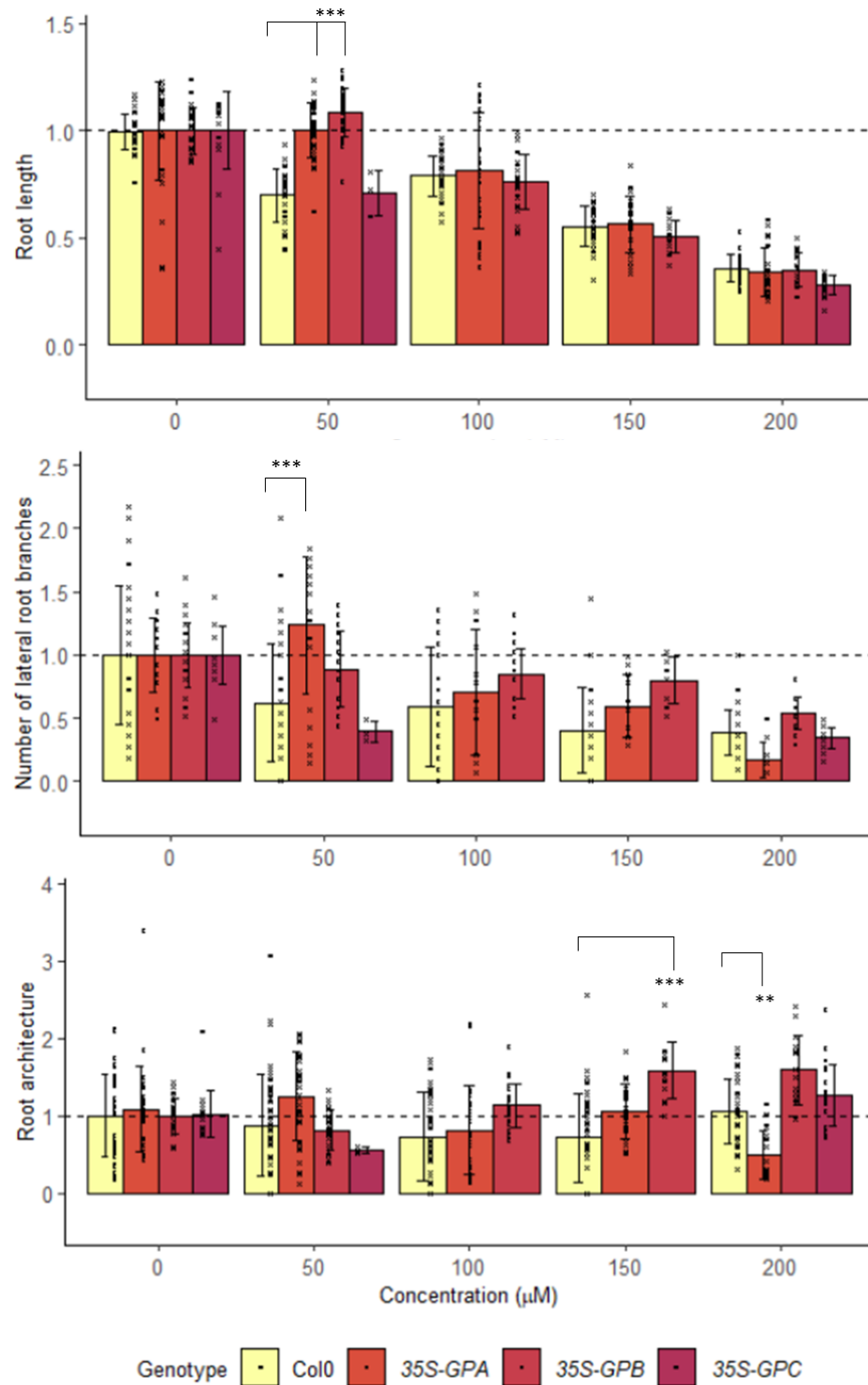
Figure 3.41. Root characterisation of two-week-old Arabidopsis WT (Col0), *35S*-GP seedlings grown on ½ MS(A) media containing a range of Cu or Au concentrations. Assumptions tests used were Levene's for homogeneity of variances and Shapiro Wilk for data normality. Statistical significance was calculated by two-way ANOVA test and a Tukey's HSD test. Asterisks mark significant differences between concentrations or between *COPT2* genotypes and the WT (Col) in each concentration, normalised to 0 µM (p-value: * < 0.02; ** < 0.01; *** < 0.001). Values are a mean of between 3 - 56 biological reps, across three technical reps. Higher concentrations resulted in fewer measurable seedlings. The exact number of reps for each condition is shown in Table S23 – Table S25. Black bars are + SD.

3.3.2.12.   Analysis of element uptake in Arabidopsis *35S*-GP lines grown in the presence of Au

Following the analysis of *35S*-GP lines on ½ MS(A) plates containing Au and having established that the root phenotype of *35S*-GP lines differs to the WT root phenotype, these lines were grown hydroponically as in section 3.3.2.5. Figure 3.42 shows the results of the ICP-OES analysis of element concentration. Figure 3.42 shows that, measured at 267 nm, the *35S*-GP lines showed a higher concentration of Au in both shoot (*35S*-GP*C* $p < 0.05$) and root (*35S*-GP*B* $p < 0.01$; *35S*-GP*C* $p < 0.001$), compared to WT. There were no significant differences between *35S*-GP and WT Fe concentration in either shoot or root tissue. The *35S*-GP lines had significantly higher Cu concentrations than the WT in the shoot ($p < 0.001$ all *35S*-GP lines) and root (*35S*-GP*A* and *35S*-GP*C* $p < 0.001$; *35S*-GP*B* $p < 0.01$) tissue.

In summary, compared to WT, the *35S*-GP lines had increased root branches in the presence of Au or Cu; and when grown in liquid culture, accumulated significantly more Au and Cu in their aerial tissues.
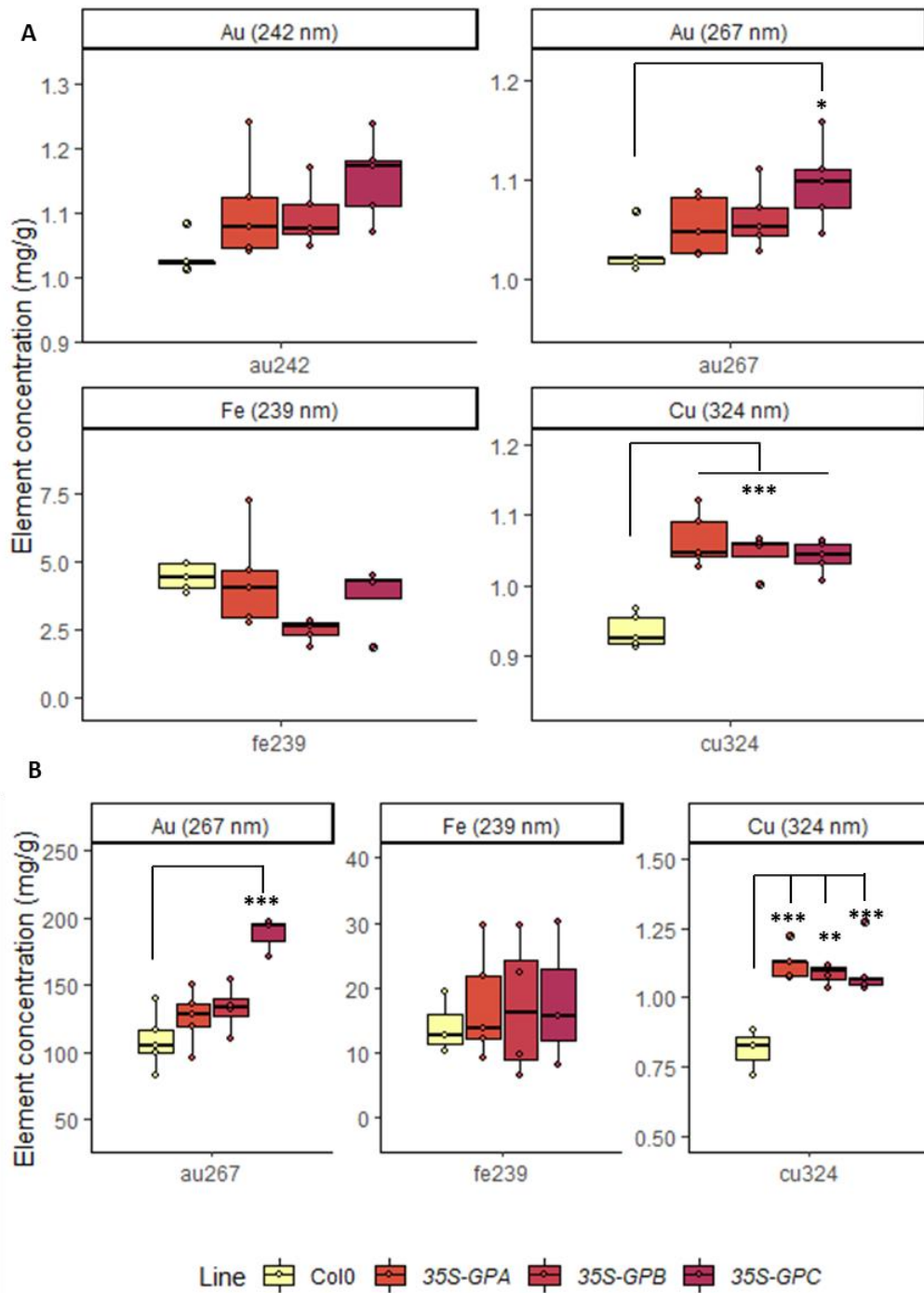
Figure 3.42. Element (Au, Cu, or Fe) concentration (mg/g) in WT (Col0) and three *35S*-GP expressing lines (*35S*-GP*A, 35S*-GP*B* and *35S*-GP*C*) 24 hours after the addition of 1 mM Au to hydroponically grown, five-week-old Arabidopsis. (A) Shoot tissue; (B) Root tissue. Five biological replicates were analysed by ICP-OES and normalised by dry weight (g). Homogeneity of variances was determined by Levene's test, and normality of data was determined by the Shapiro-Wilk test. Normally distributed data were analysed by one-way ANOVA and Tukey's HSD test. Data that did not meet the assumptions of a one-way ANOVA were analysed by a Kruskal-Wallis and Wilcoxon rank sum test for multiple comparisons. Significant differences are indicated on plots as asterisks (*: $p < 0.05$, **: $p < 0.01$, ***: $p < 0.001$). Circular dots indicate the distribution of raw data, and 'whiskers' are upper and lower quartiles.

3.3.2.13.   Floral dip transformation and confirmation of Arabidopsis *35S*-GP*C* genotypes

Previously established Arabidopsis *35S*-GP genotypes were used as the background genotype and transformed with *pMLBART-optCOPT2* to generate the *35S*-GP*C* genotypes. Transformants containing both selectable marker genes (*pMLBART-optCOPT2*: *bar* gene; pART27-*35S*-GP: SpR/StR) were selected on ½ MS(A) and both 50 µg / mL spectinomycin and 20 mg / mL glufosinate ammonium. Three independent genotypes were confirmed, as described in section 2.4.14, and referred to as *35S*-GP*CA, B* or *C* from this point forward.

To assess transgene expression, primers for the *COPT2* and GP sequences in Arabidopsis *35S-COPT2* and *35S*-GP genotypes listed in Table 2.10 (3.3.2.10) were used. Transcript abundance was calculated relative to the endogenous control gene *ACTIN2*. In the *COPT2* primer reactions, the relative transcript abundance was then normalised to the WT expression level, whereas in the GP primer reactions this was not performed as the WT samples do not express the GP sequence. Nonetheless, in the GP primer reactions the Arabidopsis WT samples were utilised as a negative control, and the GP sequence was undetected in these reactions, and is not shown in the figures (Figure 3.43).
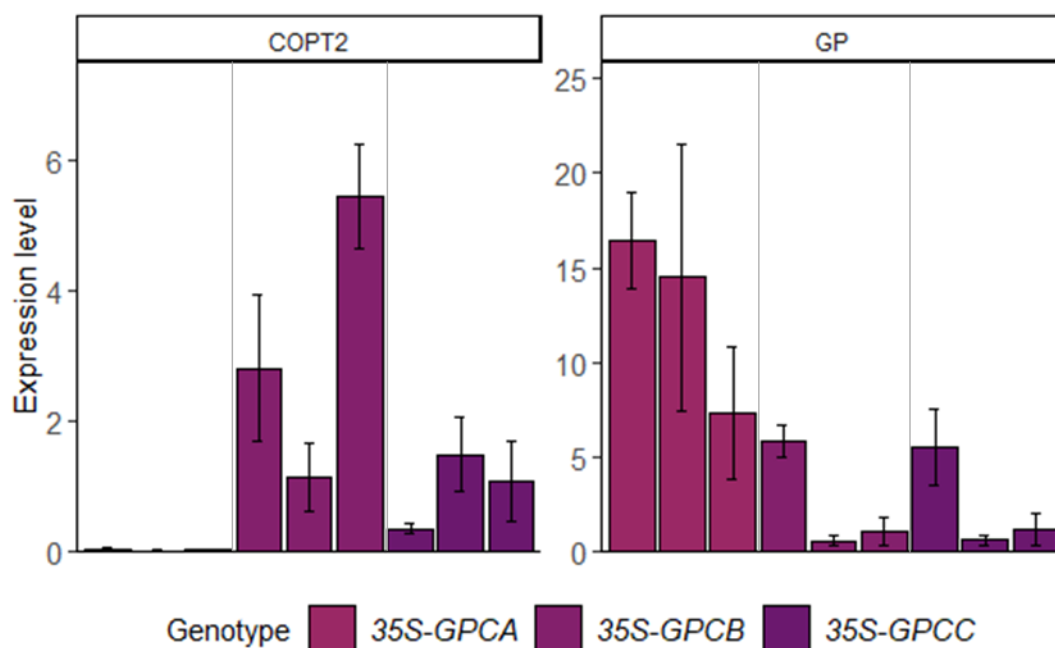
Figure 3.43. The transcript abundance of the *COPT2* or GP sequence in the rosette tissue of three independent, homozygous *35S*-GP*C* Arabidopsis lines, normalised to ACTIN2. The *COPT2* graph shows the expression level in *35S*-GP*C* genotypes relative to the *COPT2* expression level in Arabidopsis WT (Col0), indicated by the primer pair C2Ds1LP and C2Ds1RP. The GP transcript abundance in Arabidopsis *35S*-GP genotypes as indicated by primer pair optGP-F and the universal reverse primer. Values are a mean of five biological replicates $\pm$ SD. Primers were also used in qPCR reactions against Arabidopsis WT, but the sequence was undetected.

Figure 3.43 shows abundance of *COPT2* and GP in the transgenic Arabidopsis lines. Only *35S*-GPCB and *35S*-GPCC had *COPT2* expression higher than the Arabidopsis WT. The *35S*-GPA genotype had levels of *COPT2* expression comparable to the Arabidopsis WT, suggesting that there may be silencing of the gene in this genotype. All three *35S*-GP*C* genotypes expressed the GP sequence, in comparison to the Arabidopsis WT genotype, which had no detectable GP product in the qPCR reactions with the optGP-F primer pair (WT data not shown, Figure 3.43: GP).

3.3.2.14.   Root characterisation of *35S*-GP*C* genotypes grown on Cu or Au

To examine whether the combination of a higher expression of Arabidopsis *COPT2* combined with the expression of the synthetic AuNP forming peptide (GP) resulted in an altered phenotypic response to Au, Arabidopsis WT and *35S*-GPC genotypes were grown on ½MS(A) media containing a range of Au concentrations and the number of root length and lateral root branches recorded (Figure 3.44).

Levene's test for equal variances showed that the root length, number of lateral root branches and architecture on Au datasets did not have equal variances (Length: d. f.18, 500; F = 18.598; p-value < 0.05; Lateral root branches: d. f. = 18, 445; F = 7.0688; p-value < 0.05; Architecture: d. f.18, 445; F = 2.2908; p-value < 0.05), and the Shapiro-Wilk tests demonstrated that these datasets did not follow a normal distribution (Length: W = 0.9296; p-value < 0.05; Lateral root branches: W = 0.97035; p-value < 0.05; Architecture: W = 0.9865; p-value < 0.05). The two-way ANOVA test was performed with a more conservative test statistic (p = 0.02). The statistical analysis showed that the interaction of concentration and genotype had a significant effect on the root length, number of lateral root branches and root architecture of WT and *35S*-GP*C* lines grown in the presence of Au (Two-way ANOVA, Length: 11, 500; F = 16.16; p-value < 0.001; Lateral root branches: d. f. = 11, 445; F = 8.775; p-value < 0.001; Architecture: d. f. = 11, 445; F = 16.678; p-value < 0.001).

Figure 3.45 shows the results of the root characterisation, and there were no clear trends in root length, number of lateral root branches, or architecture between the *35S*-GP*C* lines and the WT. With increasing concentrations of Au, all lines demonstrated shorter root lengths, reduced branching, but the complexity of the root architecture remained stable. It was hypothesized that the increased uptake by expression of *35S-COPT2* and therefore sensitivity was being balanced out by the reduced toxicity of Au ions by the formation of AuNPs (*35S*-GP*)*, and therefore the concentration of Au was analysed to determine if there was an increase in Au content in the *35S*-GP*C* lines.
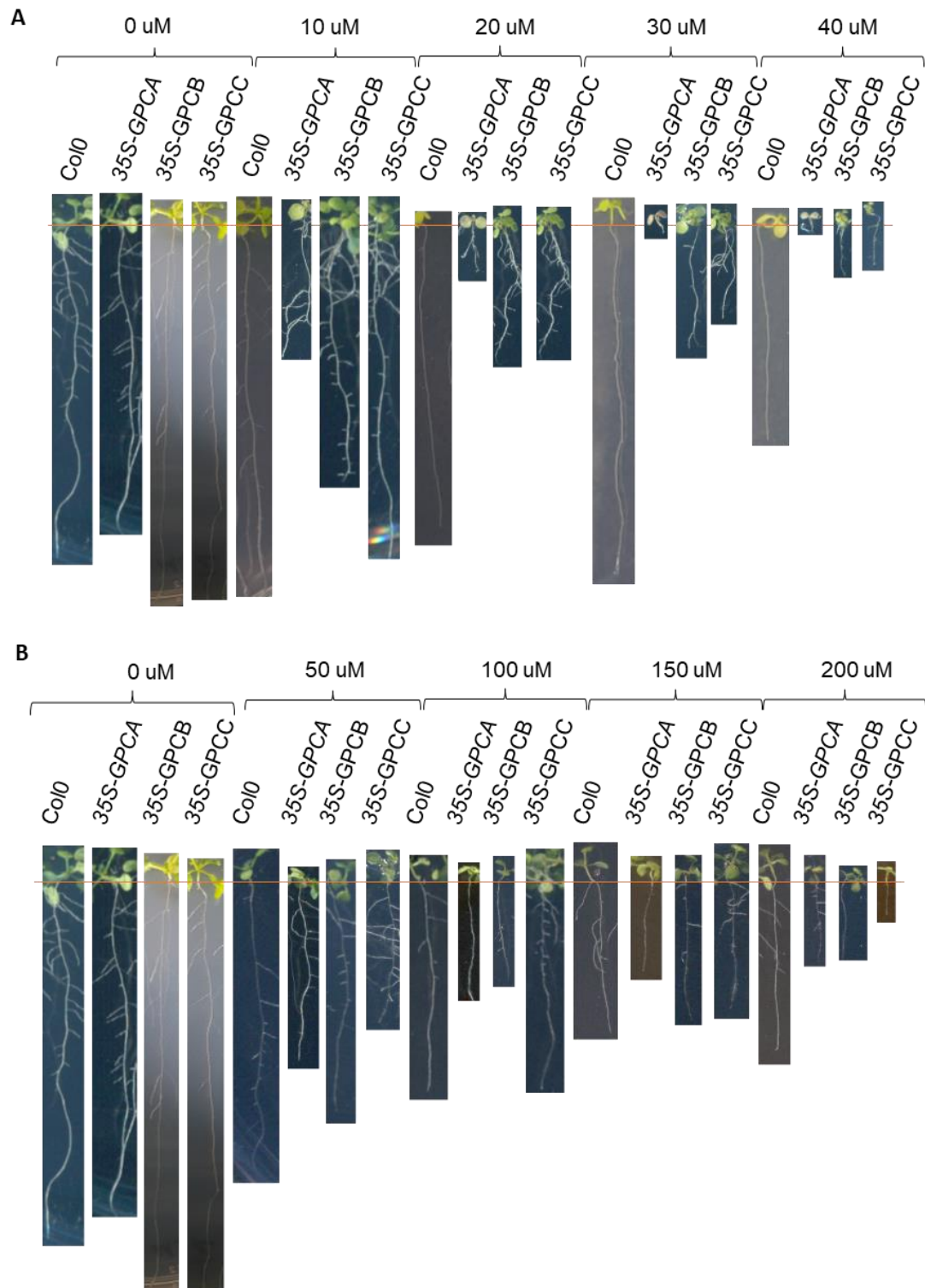
Figure 3.44. Representative images (plates scanned using an Epson Perfection V370 Photo Flatbed scanner for consistency of scale) of the growth of twelve-day-old Arabidopsis WT (Col0) and the three *35S*-GP*C* lines on ½ MS(A) media containing a range of added Cu or Au concentrations, with (A) Cu (as CuSO₄) or (B) Au (as KAuCl4). The orange line indicates the initiation of the root length measurement at the junction between root and shoot. Measurements of root length and number of lateral root branches were performed from these images using ImageJ. Images are representative of the growth of between 9 - 60 biological reps, across three technical reps.
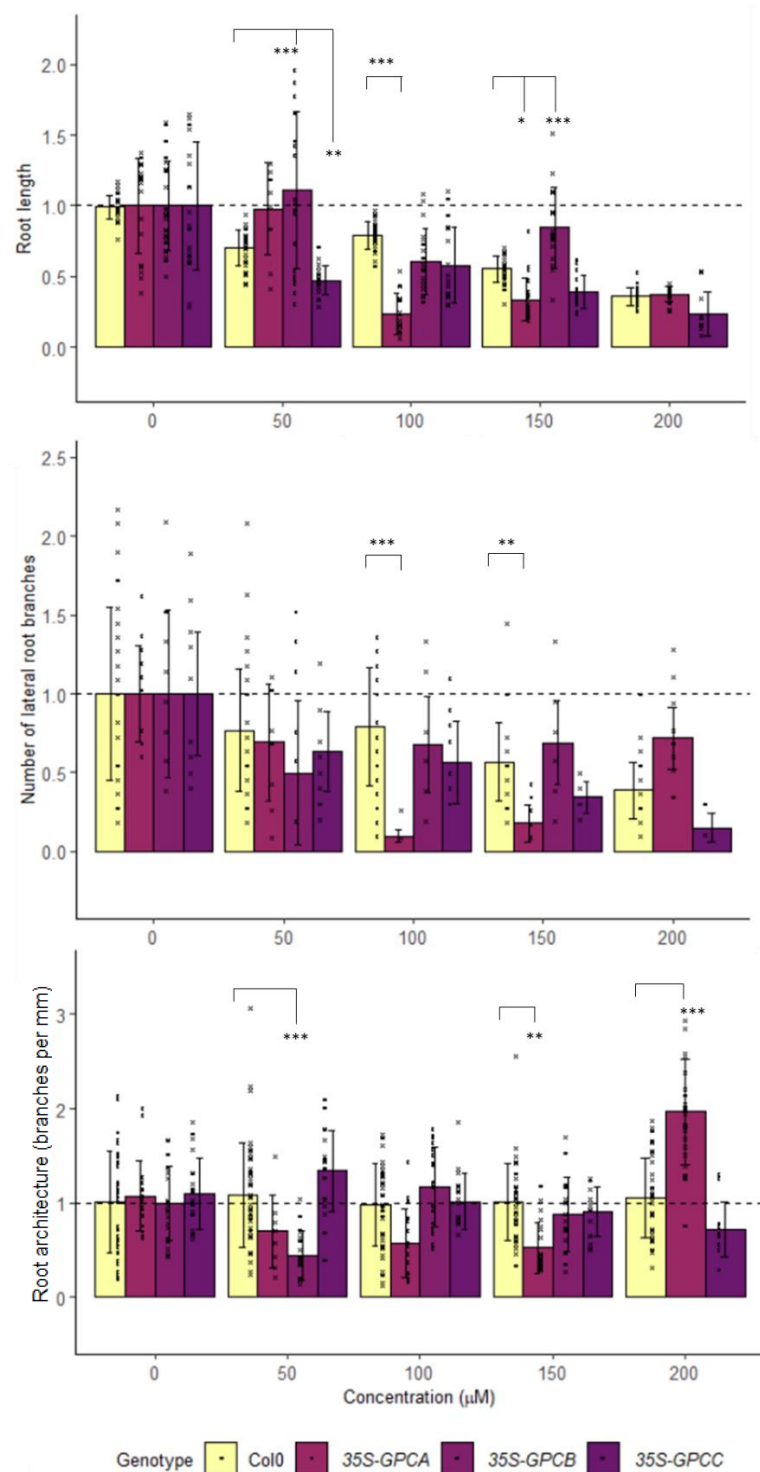
Figure 3.45. Root characterisation of two-week-old Arabidopsis WT (Col0), *35S*-GP*C* seedlings grown on ½ MS(A) media containing a range of Cu or Au concentrations. Assumptions tests used were Levene's for homogeneity of variances and Shapiro Wilk for data normality. Statistical significance was calculated by two-way ANOVA test and a Tukey's HSD test. Asterisks mark significant differences between concentrations or between *COPT2* genotypes and the WT (Col) in each concentration, normalised to 0 μM (p-value: * < 0.02; ** < 0.01; *** < 0.001). Values are a mean of between 9 - 60 biological reps, across three technical reps. Higher concentrations resulted in fewer measurable seedlings. The exact number of reps for each condition is shown in Table S32 – Table S34. Black bars are + SD.

3.3.2.15. Analysis of element uptake in Arabidopsis 35S-GPC lines grown in the presence of Au

Following up from the phenotypic response of *35S*-GP*C* lines to growth on Au compared to the WT, an analysis of element uptake was performed as before (3.3.2.5). Results of the analysis of element concentration is shown in Figure 3.46, and the results of the statistical analysis are shown in Table S38 – Table S40.

In summary, the *35S*-GP*C* lines had significantly shorter roots compared to the WT when grown on Au, and in a hydroponic system containing Au, there was significantly more Au and Cu in the shoot tissue of *35S*-GP*C* lines compared to WT.
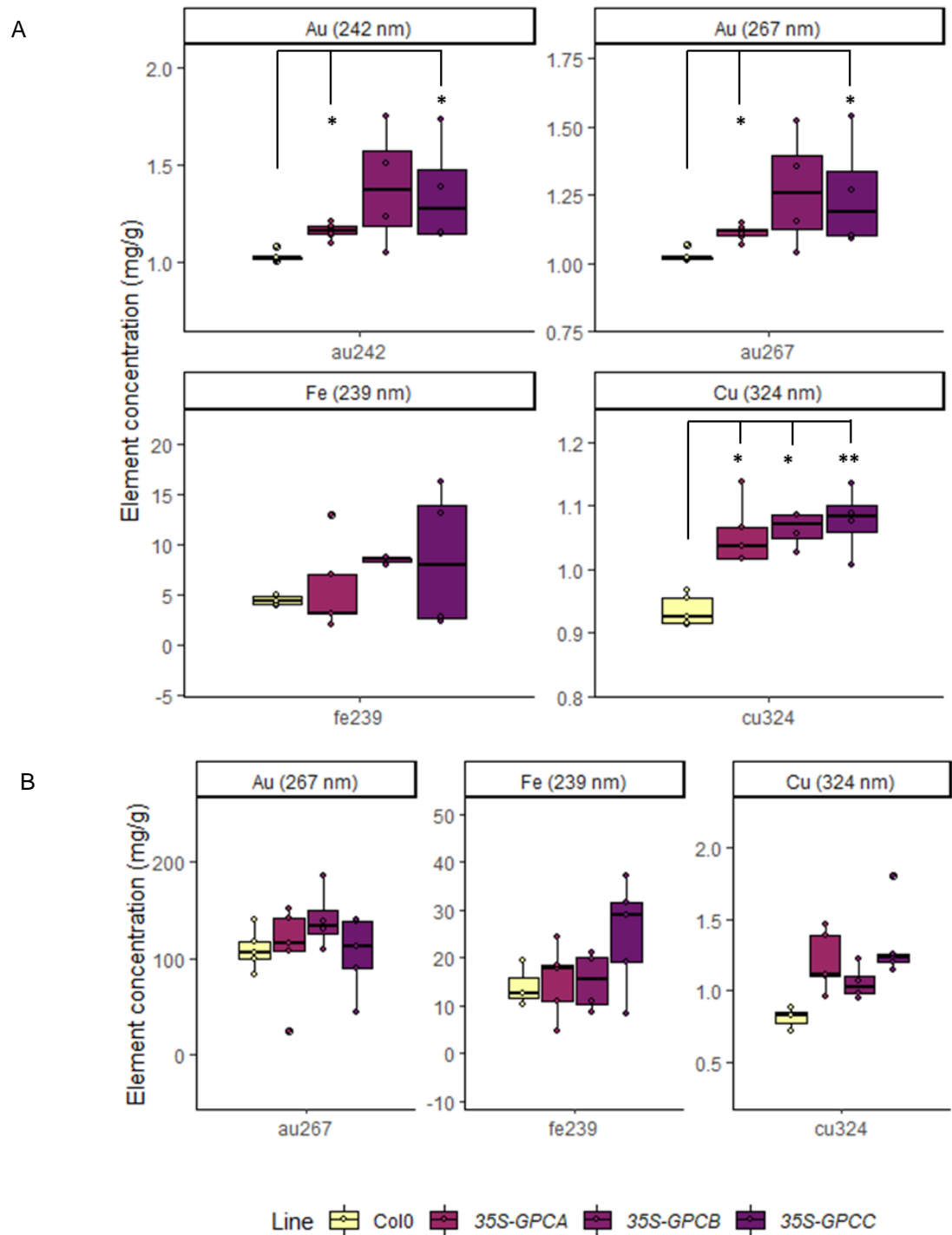
Figure 3.46. Element (Au, Cu, or Fe) concentration (mg/g) in WT (Col0) and three *35S*-GP*C* lines 24 hours after the addition of 1 mM Au to hydroponically grown, five-week-old Arabidopsis. (A) Shoot tissue; (B) Root tissue. Five biological replicates were analysed by ICP-OES and normalised by dry weight (g). Homogeneity of variances was determined by Levene's test, and normality of data was determined by the Shapiro-Wilk test. Normally distributed data were analysed by one-way ANOVA and Tukey's HSD test. Data that did not meet the assumptions of a one-way ANOVA were analysed by a Kruskal-Wallis and Wilcoxon rank sum test for multiple comparisons. Significant differences are indicated on plots as asterisks (*: $p < 0.05$, **: $p < 0.01$, ***: $p < 0.001$). Circular dots indicate the distribution of raw data, and 'whiskers' show upper and lower quartiles. The Au 242 measurements were excluded as there were a high number of NA values due to the high concentration.

3.4. Discussion

3.4.1.   Yeast strains expressing a heterologous *COPT2y* demonstrated reduced tolerance to growth on Cu and Au

The growth responses of the five *pYES2-COPT2y* expressing yeast strains were examined when strains were grown in the presence of Cu, Au, or both. The mutant strains carried mutations in genes involved in the Cu uptake and detoxification mechanisms in yeast (*Δctr1ctr3, Δccc2*, and *Δace1*) and their WT, background strains. Members of the high affinity Cu uptake transporter family, (the COPT family in Arabidopsis), the *Δctr1ctr3* strain lacks the high affinity Cu transporters Ctr1p and Ctr3p at the plasma membrane, and cannot grow on growth media containing solely non-fermentable carbon sources, such as ethanol and glycerol, lacking Cu, due to the defects in the Cu-requiring cytochrome c oxidase (73). Another part of the Cu homeostasis pathway in yeast, the *Δccc2* strain lacks a Cu-transporting ATPase which retrieves Cu from the metallochaperone ATX1 and incorporates it into trans-golgi vesicles (181), and the *Δace1* strain is deficient in the Cu binding ACE1, which activates the transcription of Cu detoxification genes when Cu is in excess (163,182,183).

As expected, the *WT pYes2-COPT2y* expressing strains did not grow on SD-U(A) media containing Cu, whilst the non-expressing strains did, presumably as the expression of *COPT2y* resulted in an increased Cu uptake to a toxic concentration within the cells. The *Δctr1ctr3 pYES2-COPT2y* expressing strain grew similarly to the non-expressing strain on the Cu containing medium, far better than the *WT pYes2-COPT2y* expressing lines, confirming the action of the Ctr1 and Ctr3 proteins in Cu uptake in yeast, as the reduced sensitivity in the mutant strain is likely a result of lower Cu uptake. There was little to no growth of the *Δccc2 pYES2-COPT2y* and *Δace1 pYES2-COPT2y* expressing strains on Cu, comparable to the *WT pYES2-COPT2y* expressing strain. The *Δace1 pYES2-COPT2y* did not grow on the Cu containing SD-U(A) media even without *COPT2y* expression, demonstrating that the survival of yeast on 100 µM Cu requires Ace1 activity. On SD-U(A) media containing Au, all strains expressing *pYES2-COPT2y* demonstrated a significant loss of growth in comparison to their growth without expression of *pYES2-COPT2y.* The complete loss of growth for all strains expressing *COPT2y* suggests that the heterologous expression of *COPT2* in yeast results in increased sensitivity, likely due to of increased Au uptake. Interestingly, when grown on SD-U(A) media containing Cu and Au, there was complete loss of all strains except for the *Δctr1ctr3 pYES2-COPT2y* expressing strain, which suggests there is competition between Cu and Au for uptake by COPT2y, as the *Δctr1ctr3 pYES2-COPT2y* expressing strain is more tolerant to growth on Au with Cu also present.

3.4.2.   Arabidopsis *copt2* mutants had reduced expression of *COPT2* compared to the WT in Cu sufficient conditions

Analysis of the expression level of *COPT2* in rosette tissue showed that for the three *copt2* mutant lines, *COPT2* expression was between 1 and 20 % of the level of WT expression in Cu sufficient conditions. In work published by Perea-García et al (2013), *copt2-1* is characterised as a knockout mutant, whilst the work published in the study presented here demonstrated a small level of

expression of *COPT2* in the *copt2-1* mutants, though the expression level was significantly lower than the WT.

Under Cu deficient conditions, *COPT2* is expressed in most tissues of seedlings (143). A more informative analysis of *COPT2* expression in the three *copt2* mutant lines may be to investigate expression level under conditions of Cu deficiency. Under the Cu sufficient conditions tested in this work, *COPT2* expression in the WT is also low, and so normalising the *copt2* mutant expression level to the WT expression level will highlight potentially insignificant differences of expression, which may have resulted from leftover genomic DNA (gDNA) despite the DNAse step. Despite this, as the *copt2-1* line had been previously characterised as a knockout mutant and the other *copt2* mutant lines had similar or less *COPT2* expression, I was confident that these lines could be used to investigate the function of COPT2.

3.4.3. Arabidopsis *copt2* mutant lines showed no phenotypic difference in root growth on Cu or Au compared to the WT

The interaction of *COPT2*y and Au in heterozygous yeast strains encouraged exploration of Au uptake capacity of Arabidopsis *copt2* mutant lines. Root characterisation on Cu of the *copt2* mutant lines, all three of which were demonstrated by qPCR analysis to have a reduced expression of *COPT2*, was used as a control to establish the Cu toxicity phenotype. Increasing concentrations of Cu resulted in decreased root length, branching, and a lower branches per mm ratio for all lines; however, there were no significant differences in root length, branching or architecture between WT and the *copt2* mutant lines grown on Cu ranging from 0 µM to 40 µM. Despite COPT2 having been previously established as a Cu uptake transporter, there was no phenotypic difference between *COPT2* lines and WT. The same pattern was shown in the root characterisation between *COPT2* lines and WT grown on ½ MS(A) media containing Au ranging from 0 µM to 200 µM. As with Cu, with increasing Au there was a decrease in the root length and number of lateral root branches. The ratio of root branches per mm remained stable for all concentrations, whereas with Cu shorter roots had fewer root branches.

3.4.4. Transporters other than COPT2 may play a more significant role in Au uptake in Arabidopsis.

The concentration of Au in Arabidopsis WT, *copt2-1, copt2-2,* and *copt2-3* shoot tissue was ~100 times lower than in root tissue. The Arabidopsis *copt2* mutant lines had a higher concentration of Au in shoot and root tissue than the WT, but this difference was only significant in *copt2-2* shoot tissue measured at 242 nm. Reduced expression of *COPT2* did not result in reduced Au accumulation, despite the hypothesis put forward by Tiwari et al., (2017), that *COPT2* is an Au transporter in Arabidopsis. It is possible that the high concentration of Au in the growth medium overshadowed any differences in Au uptake in the *copt2* mutant lines, and that a more nuanced approach would be necessary to tease out differences between the WT and *copt2* mutant lines. The mechanism of uptake has been studied for other metals more thoroughly in Arabidopsis than Au, and many of these

metals are taken up into plant tissue by a range of transporters. Other Au transporters must be acting to bring Au into the root tissue in the absence of *COPT2.*

3.4.5. Reduced *COPT2* expression resulted in lower root ROS in response to Au treatment

The production of ROS is stimulated indirectly by excess metal ions. Tiwari et al (2017) established COPT2 as an Au transporter in Arabidopsis and noted a qualitative increase in ROS production in Au-dosed root tips of the WT compared to the undosed control. In contrast, in the *copt2-1* root tip, no increase in ROS was noted following exposure to Au (Figure 3.47).
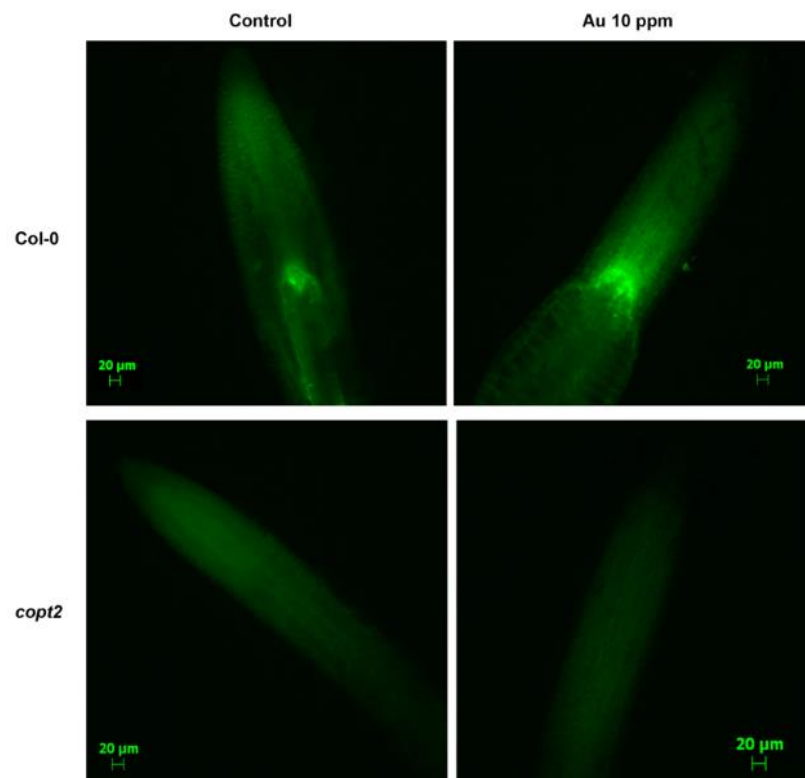
Figure 3.47. Gold-induced ROS production at the root tip of Arabidopsis as shown by Tiwari et al. (2017). The H_2DCF staining of the root tip was performed under control and 48 h of Au treatment. The upper panels showing the Col-0 and the *copt2* mutant is in lower panels. The scale bars are equivalent to 20 µm. Figure reproduced from Tiwari et al. (2017)

In the work presented in this study WT root tips demonstrated significantly increased ROS production in response to Au compared to the undosed condition. As in the Tiwari et al. work, the *copt2-1* root tips did not demonstrate an increase in ROS production following exposure to Au, likely because of reduced Au influx in the *copt2-1* line.

3.4.6.   Increased expression of COPT2 in Arabidopsis reduced growth in the presence of Au

The presence of other potential Au transporters combined with the small difference in *COPT2* expression between WT and *copt2* mutant lines under Cu sufficient conditions may have masked any phenotypic differences between WT and *copt2* mutant lines in response to Au. Clearer root phenotypic differences may be seen if the level of *COPT2* expression is more pronounced. Three Arabidopsis *35S-COPT2* lines were generated, with *COPT2* expression levels in rosette tissue varied slightly between the *35S-COPT2* lines. Root characterisation demonstrated that there were significant differences between the *35S-COPT2* lines and WT that were not seen when *copt2* mutant lines were compared to the WT. However, the root length of *35S-COPT2* lines were shorter than the WT on the undosed condition so it is unclear whether the differences seen between *35S-COPT2* and WT on ½ MS(A) media containing Au is more than a continuation of this pattern.

Nonetheless, at 50, 100 and 150 µM Au, the increased sensitivity of *35S-COPT2* to Au supports the hypothesis that *COPT2* can transport Au in Arabidopsis, and that the increased expression of *COPT2* results in reduced tolerance to growth on Au, potentially because of increased Au concentration. In conditions where transgenic plants would be used for phytoremediation or phytomining, the concentration of Au present in the environment would be much lower than conditions assessed in this experiment. High Au concentrations were tested to expose any phenotypic differences between the roots of WT and transgenic lines, and the overexpression of *COPT2* would likely not result in such significant growth reductions under real conditions.

3.4.7.   Elevated Arabidopsis *COPT2* expression increased shoot Au concentration

Element analysis using ICP-OES showed that the concentration of Au was significantly higher in the shoot tissue of *35S-COPT2* lines compared to the WT for both 242 nm and 267 nm measurements . Regulation of protein levels occurs at several points, e.g., gene expression, mRNA degradation, protein turn-over, protein activity and membrane trafficking, and *COPT2* levels are regulated at the transcriptional and posttranslational level (184,185). The transcription factor SQUAMOSA PROMOTER-BINDING PROTEIN LIKE 7 activates *COPT2* expression in response to Cu deficiency by binding to reiterative Cu deficiency-responsive elements in the promoter (185).

Numerous metal plasma membrane transporters are controlled at the posttranslational level (186,187). For *COPT2*, a recent paper by Li et al (2021) found that the *COPT2* protein is degraded in response to Cu, blocked by the proteasome inhibitor MG132 (184). Following treatment with a protein synthesis inhibitor (cycloheximide) and Cu treatment, *COPT2*-GFP levels remained stable for 30 minutes, then swiftly declined to a very low level (184). Plasma membrane proteins can be endocytosed and recycled to the cell surface or targeted to the vacuole or lysosome for degradation (188,189), but this was not shown to occur for *COPT2* in the presence of Cu (184). Instead, the 26S proteasome system is required for *COPT2* proteasome-mediated proteolysis, and this degradation is ubiquitin-independent (184). Li et al (2021) suggested that Cu exposure promotes the formation of the 26S protease, resulting in the degradation of *COPT2*.

Whilst the *35S-COPT2* lines showed significantly increased shoot Au and Cu concentrations compared to the WT, the difference was small. The effects of heightened *COPT2* expression in the *35S-COPT2* lines on Au accumulation may be being tempered by the posttranslational regulation of *COPT2* reducing the presence of *COPT2* despite increased *COPT2* expression, as *COPT2* is degraded in the presence of sufficient Cu (184). The proteasomal degradation of *COPT2* in the presence of Cu has been suggested to rely on the C-terminal Cys residue, lacking in COPT6, and modification of the Cys residue may prevent the protease mediated degradation of *COPT2* (184). Alteration of the Cys residue may impact the functionality of *COPT2* however, so this would need to be established.

3.4.8. Expression of the GP sequence may improve Au tolerance at 50 µM Au in Arabidopsis

To increase the concentration of Au in *35S-COPT2* plants, the toxicity of Au *in planta* would need to be mitigated to prevent reduced growth on Au or the efflux of Au as a detoxification mechanism. In organisms, NPs are often found in association with peptides or proteins (59,61). Free metal ions in the cell can cause cellular damage, but chelation with peptide ligands such as PCs and MTs can detoxify excess metal ions (96). Metallic Au, for instance, is relatively inert, whereas free metal ions can cause molecular damage by binding to proteins, such as aquaporins, and by increasing ROS production (190–192). Tan et al (2010) identified a AuNP forming peptide sequence that was shown to seed the formation of AuNPs *in vitro* (59), and work by Dr Liz Rylott (Centre of Novel Agricultural Products, University of York) has shown that Arabidopsis lines expressing this peptide (*35S*-GP*)* demonstrate a shift in size of NPs formed *in planta* towards smaller NPs. Expression of this peptide may have reduced the number of free Au ions in the plant tissue at the root characterisation experiment at the 50 µM concentration by the formation of AuNPs, accounting for the reduced sensitivity of the *35S*-GP lines under this condition. At the higher concentrations, it can be assumed that the peptides present in the tissue were no longer sufficient to reduce the toxic effect of the Au ions in the tissue and combined with potential reduced fitness resulting from the constitutive expression of the short, synthetic peptide sequence, meant that the *35S*-GP lines demonstrated reduced fitness when grown on higher Au concentrations.

3.4.9. The expression of GP did not result in significantly increased Au concentration in Arabidopsis

The NP forming activity of the GP was unlikely to have directly resulted in increased Au in the plant tissue, as the activity is intracellular and involved in detoxification rather than uptake. Indirectly, reduced toxicity by the formation of NPs *in planta* was hypothesised to result in increased uptake as the Au ions would be present in fewer numbers in the cytosol to result in the reduced expression of unidentified Au transporters or the increased expression of Au efflux transporters.

3.4.10. Double transgenic, *35S*-GP*C* Arabidopsis lines, had reduced tolerance to growth on Au but demonstrated a higher shoot Au concentration

Double transgenic lines expressing both 35S-GP and 35S-COPT2 had shorter roots than the WT in the undosed condition as did the 35S-GPC lines. It was hypothesised that the increased expression of *COPT2*, alongside the expression of the GP*,* would result in increased Au uptake and reduced toxicity, respectively. There are clearly more interactions at play in Au uptake and NP formation, and it is possible that the high concentration of Au in the ½ MS(A) media is exceeding the capacity of the GP present. It would be interesting to characterise the roots of the *35S*-GP*C* lines at lower, less toxic concentrations of Au.

The toxicity response of Arabidopsis to high Au may not be as prevalent in the hydroponic experiment as seedlings were exposed to 1 mM Au for a shorter period (24 hours). In the *35S-COPT2* lines the average Au shoot concentration was higher than the WT Au concentration, and in the double transgenic lines the Au concentration was higher than that of the *35S-COPT2* lines, suggesting a compound effect when the COPT2 expression level is increased alongside expression of the GP. As *COPT2* expression is induced in all tissues because of Cu deficiency, differences in expression level between WT and *COPT2* lines may be more prominent under Cu deficiency conditions. It would be interesting to examine the *COPT2* expression level in Arabidopsis shoot tissue between WT and *COPT2* lines under Cu deficient conditions to determine if there is a more significant difference between WT and *COPT2* lines.

Due to the small concentrations and high variability in the ICP-OES analysis, it would be preferable to perform this experiment with a higher starting biomass, potentially from a higher number of pooled samples or older plants.

4. Investigating the role of Arabidopsis *COPT2* and expression of the Gold-nanoparticle-forming Peptide (GP) in Pd uptake and NP formation

4.1. Introduction
4.1.1. Overview

In this chapter, the interaction between COPT2 and the GP with Pd is investigated. Building upon the knowledge gained in Au uptake and NP formation by COPT2 and the GP in chapter three, this chapter describes the use of previously established tools, e.g., transgenic yeast mutants, Arabidopsis *copt2* mutants, *COPT2* overexpression lines, GP-producing lines, and double transgenic lines overexpressing *COPT2* and the GP, to characterise the involvement of COPT2 and the GP with Pd.

4.1.2. Pd

As shown in Figure 4.1, Pd has many applications, but is mostly used in catalytic and automotive industries. Currently, about 25 % of total Pd comes from recycled automobile sources (193). Due to its use in many industries, Pd has been deemed as 'critical' to the national security and economy of the USA by the US government (194). A PGM, Pd is malleable to work with, not easily tarnished and a good electronic conductor (20), and PdNPs have applications as catalysts, drug carriers, and in cancer treatment (44). The PGM metals have comparable properties and are often found in deposits together; whilst Pd can occur as a free, non-mixed metal, it is often alloyed with Au, Pt, or other PGMs, or in Ni-Cu ore deposits. The average concentration of the PGMs in ores is between 1 ppm - 15 ppm, but occasionally mine tailings can contain higher concentrations (around 1000 to 7000 ppm) (193). The largest share (~ 40 %) of the world's known Pd deposits are located in Russia, with 36 % in South Africa, 14 % in North America and 9 % in South America, Zimbabwe, Australia, and other parts of the world (193).
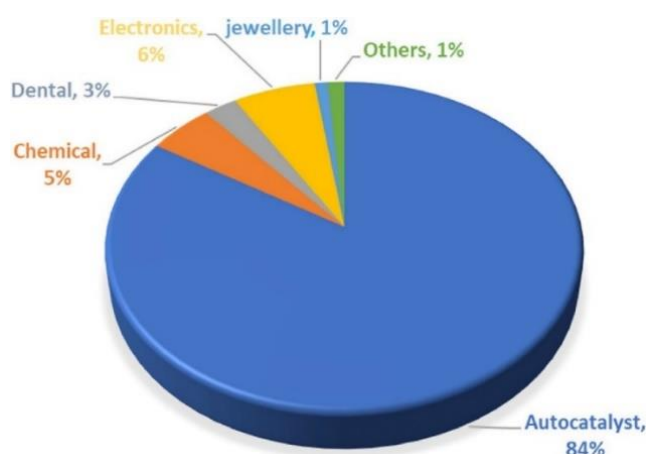
Figure 4.1. Pd demand 2021, split by sector (195)

Since 1975, Pd has been used in catalytic converters in cars, and this has directly resulted in Pd accumulation along roadsides. Over time, abrasion of the surface of catalytic converters results in Pd release alongside exhaust gases, presenting a new source of environmental pollution (196). In Sheffield (UK), Jackson et al., (2007), identified the levels of Pd and Pt from 194 environmental samples taken from around the city (196). The researchers were able to identify a route for the loss of Pt and Pd from catalytic converters to the environment, shown in Figure 4.2.
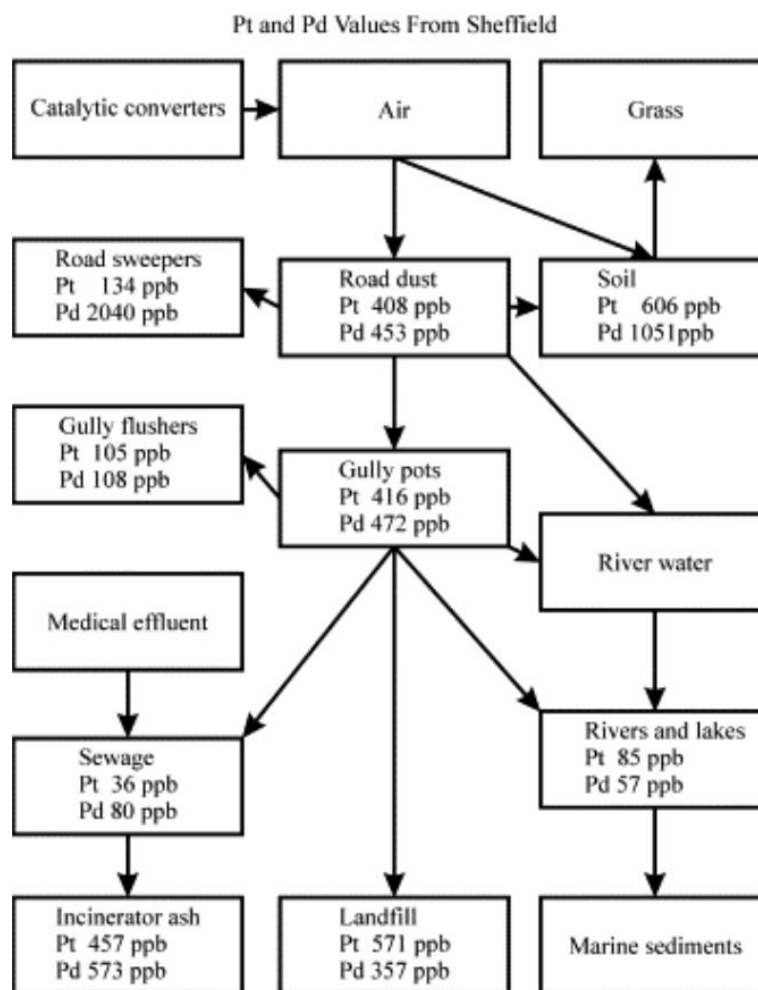
Figure 4.2. A systems diagram linking the different sample types from Sheffield and showing the maximum values of Pt and Pd for each sample type. Road dust includes motorway drainage sediment. Pt and Pd is lost from catalytic converters, and is transferred to road dust and soil. Roas sweepers accumulate the metals in the road dust. From soil, the metals are taken up into the grass growing alongside the roadways. From road dust, the metals pass into gully pots, which are the first entry point of road runoff into an urban drainage network, and then to river water, or to river water directly. From the drainage network, the metals enter sewage and sewage cleaning plants, landfill, and rivers and lakes. Figure reproduced from Jackson et al (2007) with permission from Elsevier.

Jackson et al. found that in the roadside dust, there was a mean value of 408 and 453 ppb of Pt and Pd respectively, and in the grass alongside roads there was a higher concentration of 606 and 1051 Pt and Pb respectively (Figure 4.2), though up to 2360 ppb Pd has been reported in waste incineration ash (197).

4.1.3. Downstream applications of PdNP-containing plant biomass

As outlined in section 1.2, NPs have distinct properties that distinguish them from the bulk metal, and this has resulted in the use of these particles in diverse and emerging industries (198). Nanoparticles have been synthesised using plant extracts, algae, and bacteria, but there are limitations in using bacteria to generate NPs for use as catalysts, for example (51,199–201):

- Bacteria require a reducing agent (such as H_2) to generate NPs
- Reaction conditions may cause cellular breakdown
- Cellular breakdown would release S into the reaction, rendering the catalyst ineffective (201)

Plants are capable of forming NPs in their tissues, and the common metal extraction techniques include freeze-thawing, biomass incineration, and chemical leaching (40,199,202). However, these techniques have drawbacks, and can result in destruction of the structure of the NP, alongside being laborious and energy intensive (203). Parker et al., (2014), investigated the direct use of PdNPs formed *in planta* as catalysts for a range of Suzuki-Miyaura coupling reactions (15). Palladium catalysed Suzuki-Miyaura C-C bond forming reactions are important for the synthesis of pharmaceutical intermediates and other high value molecules (204). In the work performed by Parker et al., Arabidopsis plants were grown submerged in liquid culture, and three-week old plants exposed to K_2PdCl_4 for 24 hours, and the formation of NPs confirmed by transmission electron micrograph (TEM), as shown in Figure 4.3.
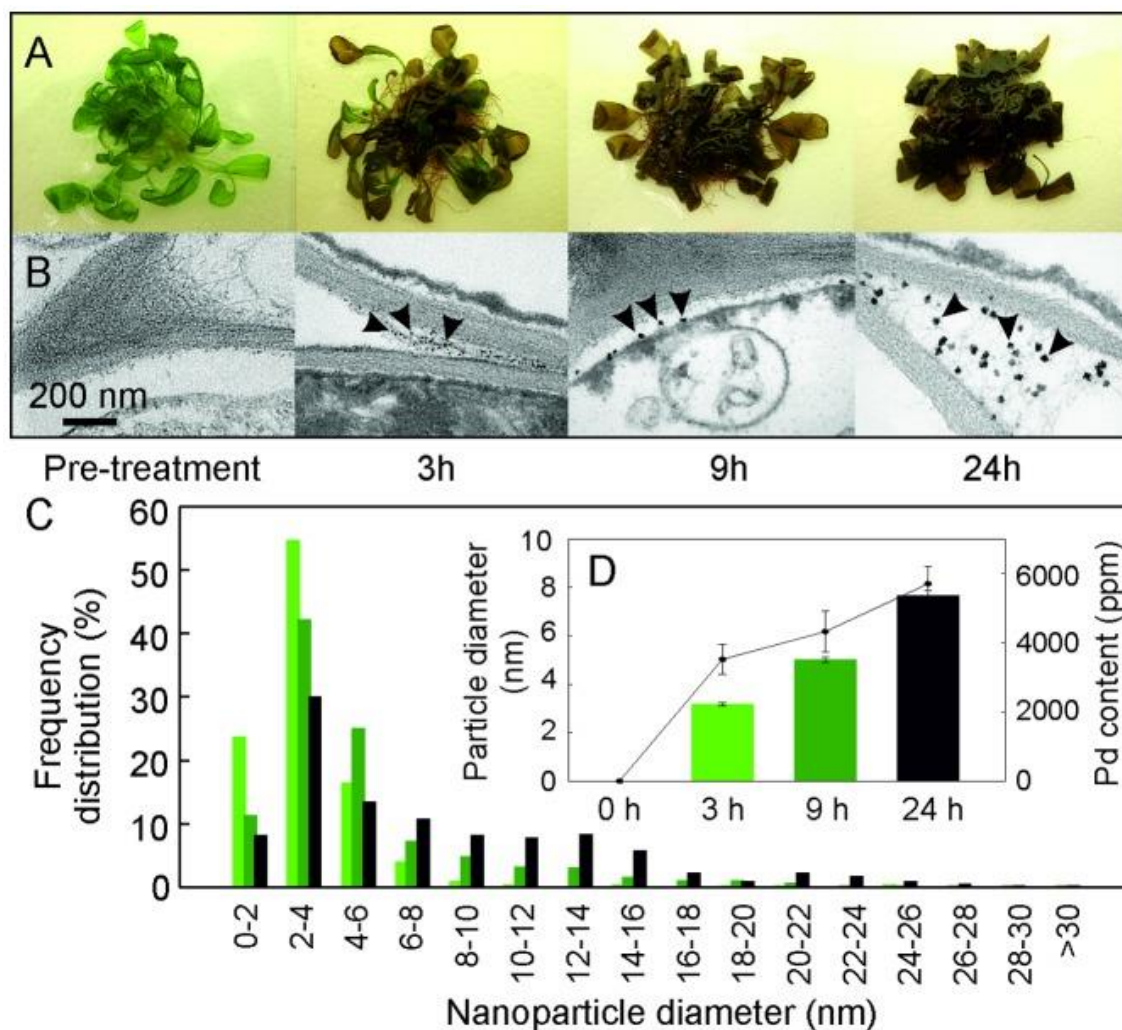
Figure 4.3. Palladium uptake and PdNP formation in Arabidopsis. (A) Appearance of 3-week-old plants 24 hours after treatment with K_2PdCl_4 (B) Transmission electron micrographs (TEMs) showing the accumulation over time of PdNPs in cell wall corners. (C) Distribution of NP sizes in leaf tissue with time. (D) Mean NP diameter and Pd concentration with time. Figure reproduced from Parker et al., (2014) (15)

The PdNP-containing plant biomass was dried, and the biomass decomposed by heating to either 300 °C (Pd-P-300) or 800 °C (Pd-P-800). The NP size distribution in the resultant products is shown in Figure 4.4.
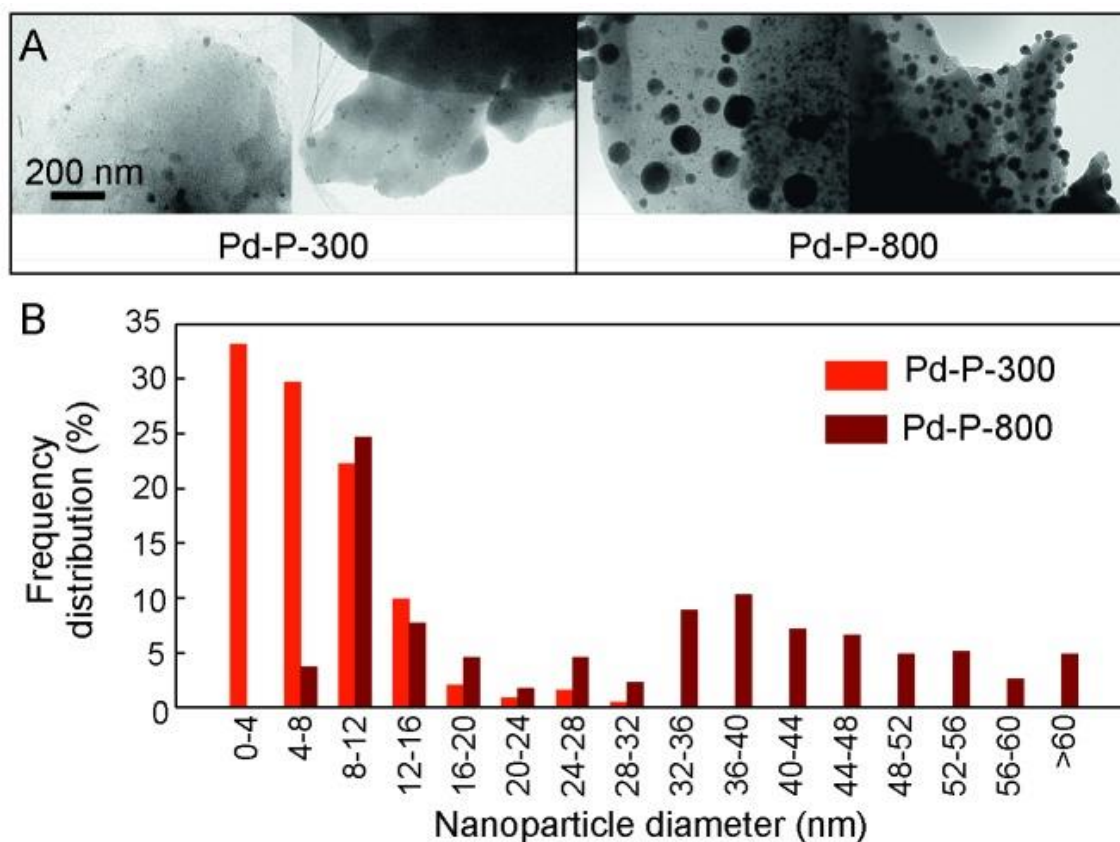
Figure 4.4. Nanoparticles in PdNP-containing plant biomass following decomposition by pyrolysis to either 300 °C (Pd-P-300) or 800 °C (Pd-P-800). (A) TEM showing PdNPs in Pd-P-300 and Pd-P-800. (B) Distribution of PdNP sizes in the plant catalysts. Figure reproduced from Parker et al., (2014) (15)

The activity of the Pd-P-300 and the Pd-P-800 catalysts were assessed in the reaction of aryl halide with phenylboronic acid, which is shown in Figure 4.5. The catalysts contained a Pd concentration of 15 %, which were identified as highly dispersed, spherical PdNPs using TEM, which are shown in Figure 4.4. Initial reactions using Pd-P-800 were unsuccessful, likely as a result of the larger NP size distribution in this catalyst. The Pd-P-300 catalysts were tested with various temperatures, bases, solvents, and mixtures of solvents to determine optimal reaction conditions; once optimised, the catalyst showed excellent catalytic activity, especially in comparison with other, non-conventional Pd catalysts. The activity of Pd-P-300 was shown to be superior to commercially available Pd catalysts (15). The work performed by Parker et al., clearly demonstrates that NPs synthesised *in planta* have promising downstream applications, with the production of PdNPs in this way reducing the requirement for toxic chemicals or energy intensive processes. With a clear downstream application, there was a strong motivation towards applying the techniques from chapter three in exploring the capability of COPT2 towards Pd uptake, and in the GP towards the formation of NPs of an industrially relevant size (10 nm).
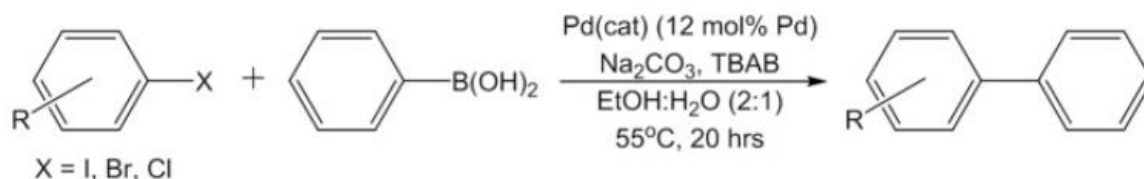
Figure 4.5. Suzuki-Miyaura C-C coupling reaction of arylhalide with phenylboronic acid. Figure reproduced from Parker et al., (2014) (15).

4.1.4. Summary

In summary, the work in this chapter focuses on the interaction of COPT2 and the GP with Pd, to determine their involvement in Pd uptake and NP formation, towards generating plants that could be used as carbon supported PdNPs in Suzuki-Miyaura reactions, which are important methods for the synthesis of pharmaceutical intermediates and other high value molecules (15). Alongside using the model plant species Arabidopsis, three yeast mutant strains were used as in the previous chapter to characterise the interaction between Pd and *COPT2*. Through characterisation of the roots in response to Pd and analysis of the Au concentration and ROS presence, Arabidopsis *copt2*, *COPT2* overexpression lines (*35S-COPT2*), GP-expressing lines (*35S*-GP) and double transgenic lines (*35S*-GP*C*) were investigated towards the fabrication of plants lines capable of increase Pd uptake and tolerance.

4.2. Methods
 4.2.1.   Yeast studies

To investigate the involvement of *COPT2* in Pd uptake, five *pYES2-COPT2y* expressing yeast strains (BY4741, *Δccc2, Δace1,* DTY165, *Δctr1ctr3*) were used in growth assays on ½ MS(A) media containing either Cu, Pd, or both, as per chapter three.

 4.2.2.   Arabidopsis *COPT2* and transgenic genotypes studies with Cu or Pd

To identify phenotypic variations between Arabidopsis *copt2, 35S-COPT2*, *35S*-GP or *35S*-GP*C* genotypes and WT in the presence of Pd, seeds were grown on ½ MS(A) media containing Pd, in the same manner as in chapter three. Root length and number of branches was measured when plants were twelve days old, using ImageJ to measure the length of roots against a scale measurement (148). Root architecture was calculated as branches per mm (branches / length). The uptake of Cu, Pd and Fe in *copt2* mutant, *35S-COPT2, 35S-GP* and *35S-GPC* genotypes was investigated in a hydroponic system, with Pd added to the growth ½ MS media when plants were five-weeks old and harvested after 24 hours of exposure. Following an acid digest step to prepare samples for analysis, ICP-OES was used to analyse the concentration of these metals in Arabidopsis root or shoot tissue.

4.3. Results

4.3.1. Yeast studies on *COPT2* involvement in Pd uptake

To investigate the involvement of *COPT2* in Pd uptake, five pYES2¬-*COPT2*y expressing yeast strains (BY4741, *Δccc2*, *Δace1*, DTY165, *Δctr1ctr3*) were utilised in a growth assay on SD-U(A) media containing Cu, Pd or a combination of Cu and Pd (Figure 1).
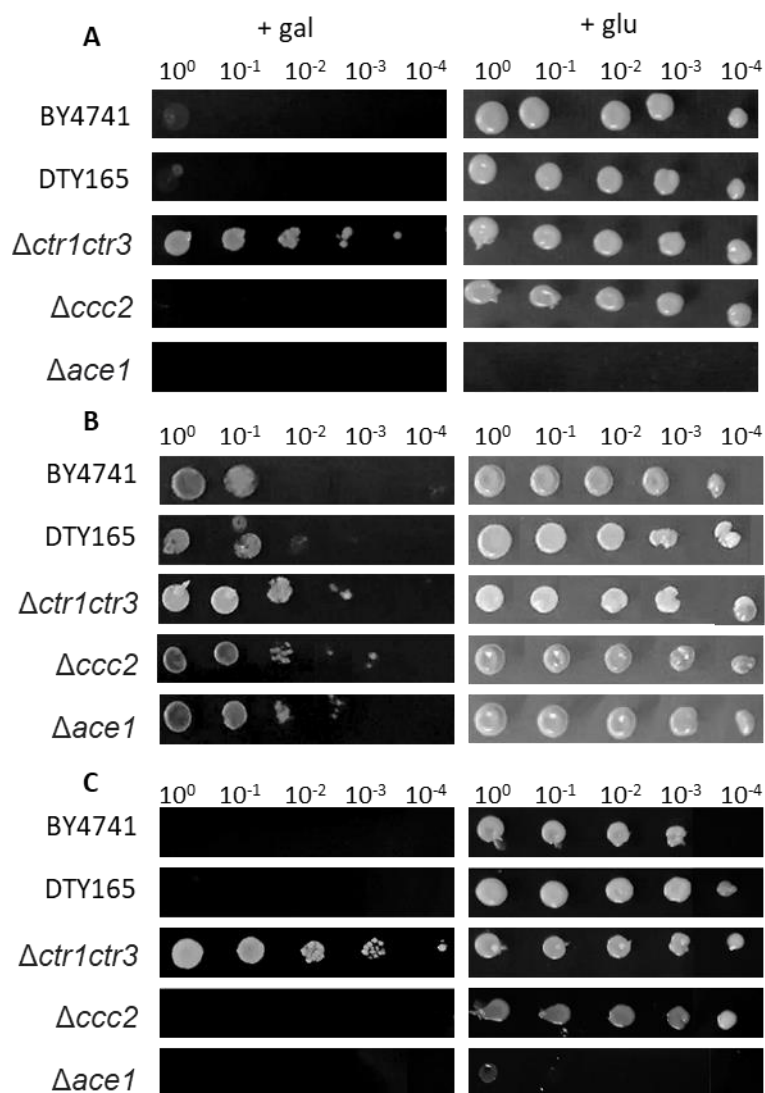
Figure 4.6. Spot dilution growth assay on SD-U(A) media containing Cu, Pd or both, using yeast strains containing pYES2-*COPT2y*. Figures A, B and C contain different metal additions to the media: (A)100 µM Cu (B)500 µM Pd or (C) 100 µM Cu + 500 µM Pd. The *COPT2y* sequence is under the control of the GAL1 promoter and therefore expression of *COPT2y* only occurs with galactose (gal) as the available carbon source. The SD-U(A) media (used for positive selection of yeast colonies containing *pYES2-COPT2y)* contained either gal(resulting in *COPT2y* expression) or glucose (glu) (no expression of *COPT2*y). Cultures were grown to an OD600 of 1, and serially diluted by a factor of 10 (10^0, 10^{-1}, 10^{-2}, 10^{-3}, 10^{-4}). Each row shown in the figure is a single strain and each 'spot' is a serial dilution of the one before, moving from left to right. Images are representative of the growth responses shown across five technical replicates.

The *COPT2*y gene is only expressed in strains carrying the pYES2-*COPT2*y sequence when grown on Sd-U(A) + gal, not glu, due to the presence of the *GAL1* promoter upstream of *COPT2y*. Figure 4.6 demonstrated that for all strains excluding *Δace1*, there was significant growth for all serial dilutions (100, 10^{-1}, 10^{-2}, 10^{-3}, 10^{-4}) when strains were grown on SD-U with glu, regardless of the metal added. In the presence of Cu alone there was a complete loss of the *Δace1* strain at all dilutions (Figure 4.6A). The *Δace1* strain does not express a functional *ACE1* transcriptional activator, required for the induction of the yeast response to toxic levels of Cu (205). Any alteration in the growth of strains when grown on SD-U(A) media containing gal can be compared to SD-U(A) media containing glu, where strains were not expressing *COPT2y*. Cu is present in all conditions at a low level as it is required for normal function; references to 'with Cu' onwards refer specifically to the added 100 μM Cu.

In the Cu condition, there was complete or near complete loss of growth in all strains excluding *Δctr1ctr3,* which demonstrated robust growth up to 10^{-3}, after which the colony size was reduced (Figure 4.6A). There was a severe reduction compared to growth on glu, suggesting an interaction between the expression of *COPT2*y and increased Cu toxicity. In the Pd condition, all yeast strains expressing *COPT2*y demonstrated significant growth reduction in all dilutions following the second serial dilution (10^{-1}). The toxicity effect was strongest in the two WT strains (BY4741 and DTY165) which had a complete loss of growth in serial dilutions 10^{-2}, 10^{-3} and 10^{-4}; *Δctr1ctr3* demonstrated significant growth reduction in dilutions 10^{-3} and 10^{-4}; the *Δccc2* strain demonstrated a reduction in growth after the second serial dilution; and the *Δace1* strain also displayed severe growth reduction after dilution 10^{-2} (Figure 1B). Although not as strong as the response to Cu, this was a severe reduction in comparison to growth on glu, suggesting an interaction between *COPT2*y Pd uptake, resulting in toxicity. In the Cu and Pd condition, there was a slight rescue of growth in *Δctr1ctr3* compared to growth on SD-U(A) media containing just Pd, suggesting some competition in binding to COPT2y by Cu and Pd, resulting in reduced Cu toxicity (Figure 4.6C). The *Δctr1ctr3* strain demonstrated a reduction in growth after the second dilution when Pd and Cu were present, with colonies present but reduced in size at all subsequent dilutions; although there was also a reduction in growth after the second dilution when just Pd was present, there was very little growth in the third dilution, and complete loss at the forth (Figure 4.6C / Figure 4.6B). All other strains demonstrated a complete loss of growth on SD-U(A) media containing both Pd and Cu (Figure 4.6).

4.3.2. Root characterisation of Arabidopsis *copt2* and *35S-COPT2* lines grown on ½ MS(A) media containing Pd

To examine the interaction of *COPT2* and Pd in Arabidopsis, root architecture characterisation was performed as detailed in chapter three, investigating root length, number of lateral root branches and the complexity of root architecture. Arabidopsis WT, three *copt2* mutant genotypes, three *35S-COPT2* genotypes, three *35S*-GP genotypes and three *35S*-GP*C* genotypes (referred to hereafter grouped as the 'Arabidopsis *copt2* and transgenic genotypes') were grown to twelve-days-old on ½MS(A) media containing Pd at 0, 5, 10, 15 or 20 µM. The root length and number of lateral branches was measured using ImageJ. Images taken from each of these analyses are shown in Figure 4.7. Comparisons between Arabidopsis WT and the *copt2* and transgenic genotypes (*35S-COPT2*, *35S*-GP and *35S*-GP*C*) have been highlighted in the following sections from these analyses.

4.3.3. Root characterisation of Arabidopsis *copt2* mutant lines grown on ½ MS(A) media containing Pd

Levene's test for equal variances showed that the root length, number of lateral root branches and architecture did not have equal variances (Length: d. f.19, 646; F = 4.3494; p-value < 0.05; Lateral root branches: d. f. = 16, 646; F = 5.8024; p-value < 0.05; Architecture: d. f.19, 646; F = 5.6517; p-value < 0.05), and the Shapiro-Wilk tests demonstrated that these datasets did not follow a normal distribution (Length: W = 0.9544; p-value < 0.05; Lateral root branches: W = 0.9023; p-value < 0.05; Architecture: W = 0.8569; p-value < 0.05). The two-way ANOVA test was performed with a more conservative test statistic (p = 0.02). The statistical analysis showed that the interaction of concentration and genotype had a significant effect on the root length, number of lateral root branches and root architecture of WT and *copt2* mutant lines grown in the presence of Pd (Two-way ANOVA, Length: 12, 646; F = 5.799; p-value < 0.001; Lateral root branches: d. f. = 12, 646; F = 2.57; p-value < 0.01; Architecture: d. f. = 12, 646; F = 3.05; p-value < 0.001).

Figure 4.12 shows the results from the root characterisation experiments on Pd with Arabidopsis WT and *copt2* lines. The most prominent differences were in the results for the root length analysis. WT lines grown on all Pd concentrations had longer roots than when grown on the control condition without Pd. The *copt2-2* and *copt2-3* lines had longer roots on 5 µM and 10 µM Pd compared to the control condition, but had shorter roots when grown on 20 µM Pd. At 5 µM Pd, *copt2-1* lines had shorter roots than the WT (p < 0.001); at the higher concentrations of Pd (10, 15, 20 µM) all *copt2* mutant lines had shorter roots than WT (*copt2-1* and *copt2-3* p < 0.001 for all concentrations; *copt2-2* p < 0.01 on 10 and 15 µM Pd; *copt2-2* p < 0.001 on 20 µM Pd).
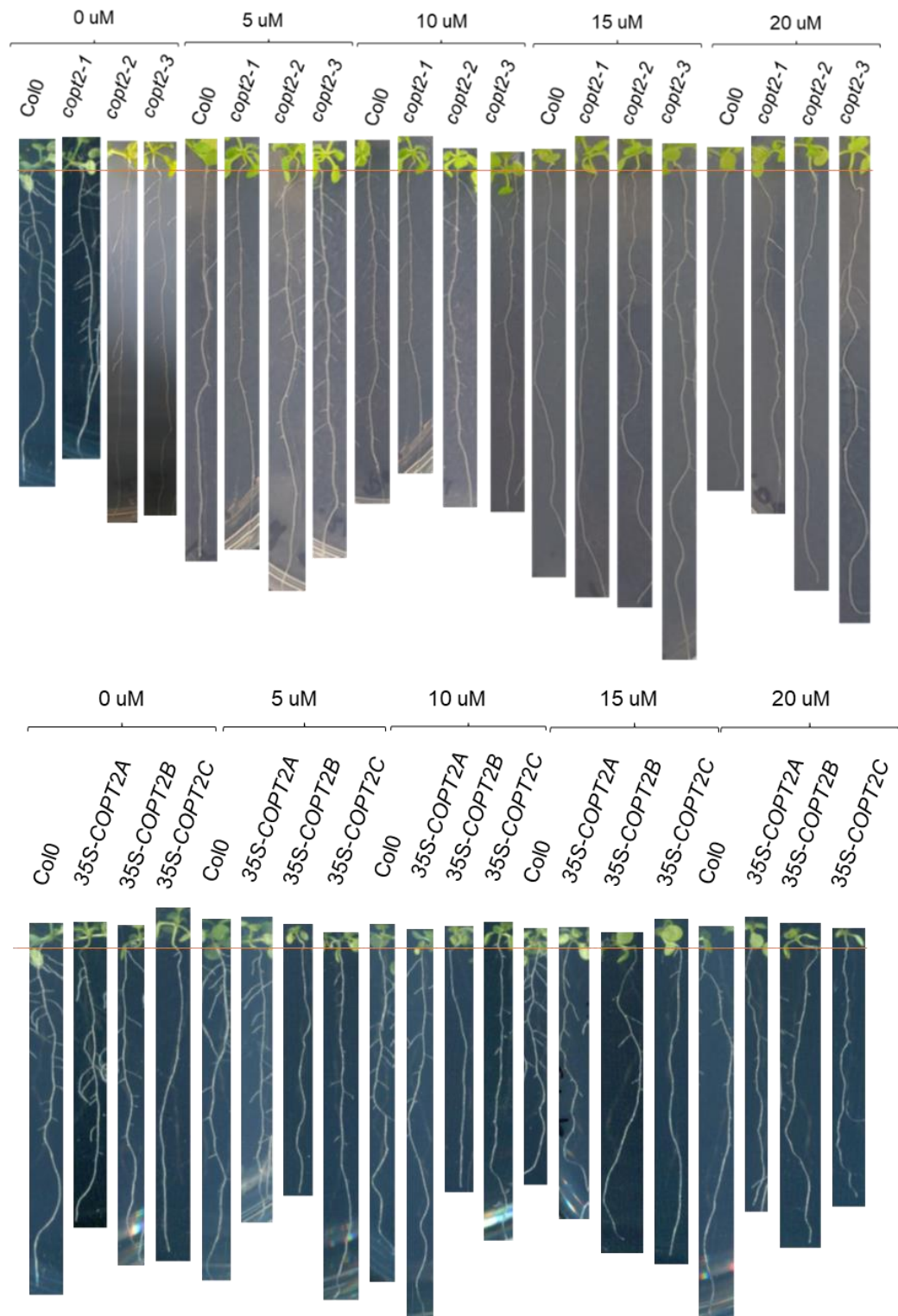
Figure 4.7. Representative images (plates scanned using an Epson Perfection V370 Photo Flatbed scanner for consistency of scale) of the growth of twelve-day-old Arabidopsis WT (Col0) and the three *copt2* mutants or the transgenic lines on ½ MS(A) media containing a range of added Pd. The orange line indicates the initiation of the root length measurement at the junction between root and shoot. Measurements of root length and number of lateral root branches were performed from these images using ImageJ. Images are representative of the growth of between 23 – 71 biological reps, across three technical reps.
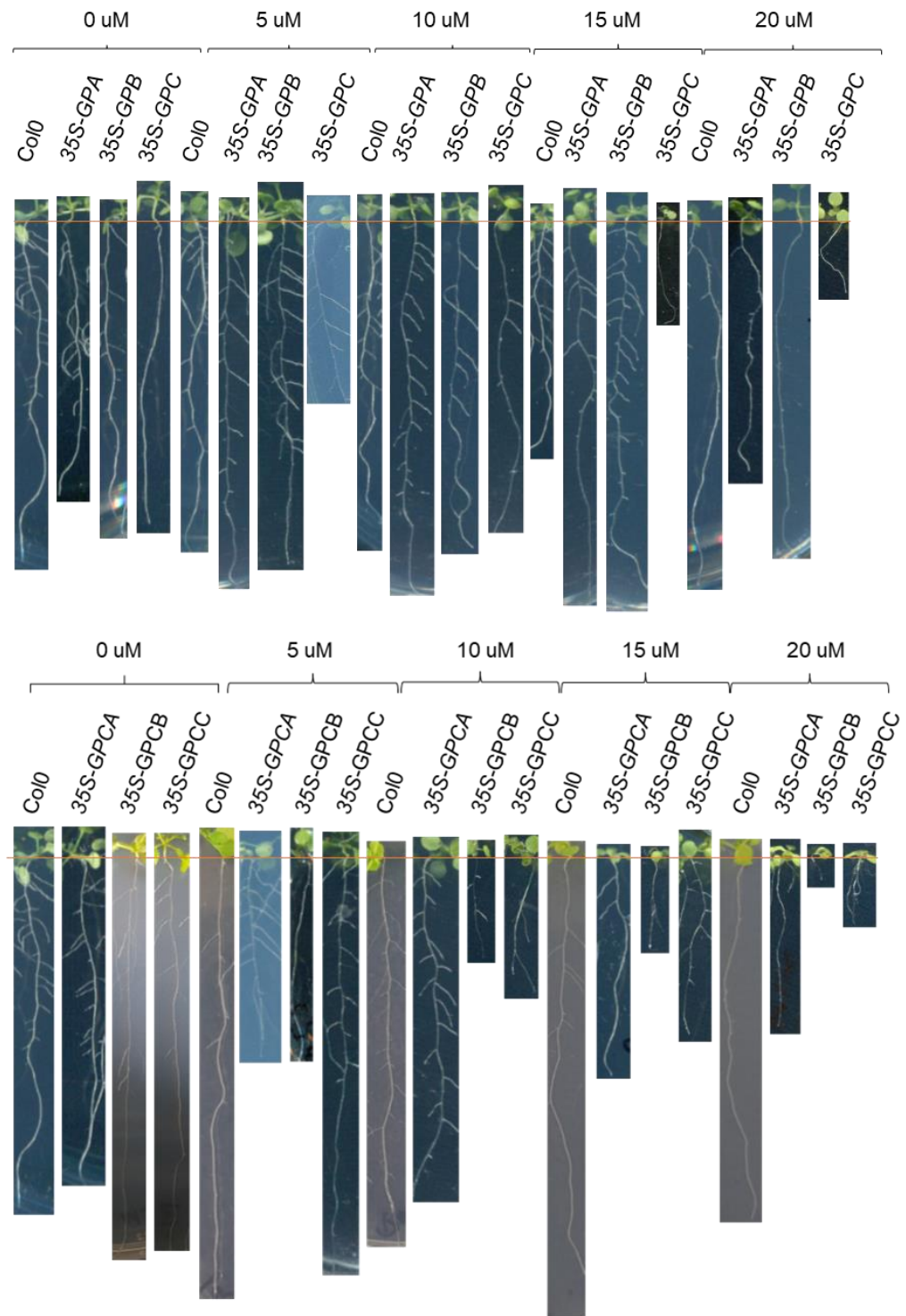
Figure 4.7 (cont) Representative images (plates scanned using an Epson Perfection V370 Photo Flatbed scanner for consistency of scale) of the growth of twelve-day-old Arabidopsis WT (Col0) and the three *copt2* mutants or the transgenic lines on ½ MS(A) media containing a range of added Pd. The orange line shows the initiation of the root length measurement at the junction between root and shoot. Measurements of root length and number of lateral root branches were performed from these images using ImageJ. Images are representative of the growth of between 23 – 71 biological reps, across three technical reps.
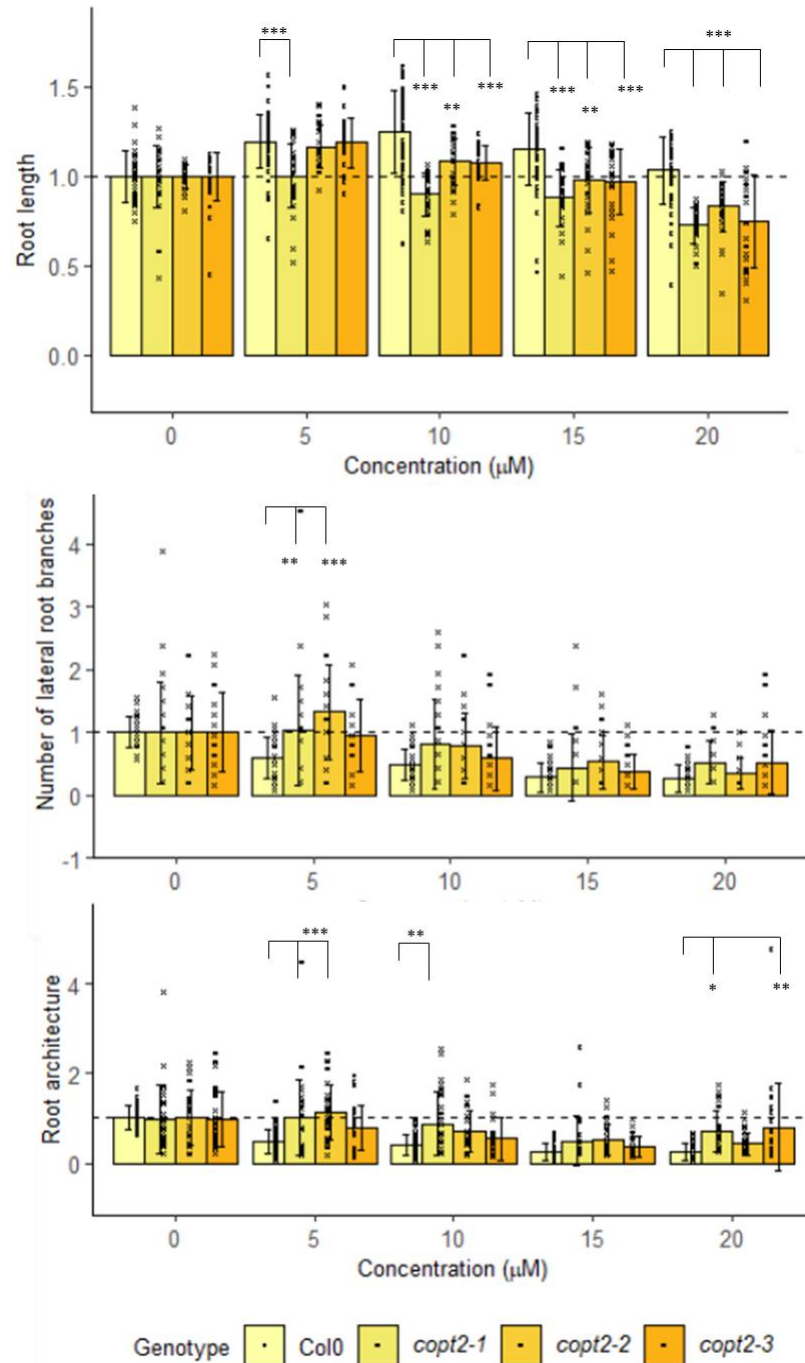
Figure 4.8. Root characterisation of two-week-old Arabidopsis WT (Col0) and the three independent *copt2* genotype (*copt2-1, copt2-2, copt2-3*) seedlings grown on ½ MS(A) media containing a range of Pd concentrations. Assumptions tests used were Levene's for homogeneity of variances and Shapiro Wilk for data normality. Statistical significance was calculated by two-way ANOVA test and a Tukey's HSD test. Asterisks mark significant differences between concentrations or between *COPT2* genotypes and the WT (Col) in each concentration, normalised to 0 µM (p-value: * < 0.02; ** < 0.01; *** < 0.001). Values are a mean of between 23 – 71 biological reps, across three technical reps. Higher concentrations resulted in fewer measurable seedlings. The exact number of reps for each condition is shown in Table S41 – Table S43. Black bars are + SD.

4.3.4. Root characterisation of *35S-COPT2* genotypes grown on Pd

Following on from the root characterisation results with the Arabidopsis *copt2* lines on Pd, the same experiments were repeated using the *35S-COPT2* lines to determine whether increased expression of *COPT2* results in phenotypic difference when lines were grown on Pd. Arabidopsis WT and *35S-COPT2* genotypes were grown on ½ MS(A) containing a range of Pd concentrations, and the root length, number of lateral root branches and root architecture recorded. The summary statistics for the root length, number of lateral root branches and root architecture are shown in Table S47 – Table S49.

Levene's test for equal variances showed that the data for root length, number of lateral root branches and root architecture on Pd did not have equal variances (Length: d. f.19, 590; F = 2.441; p-value < 0.05; Lateral root branches: d. f. = 19, 590; F = 10.005; p-value < 0.05; Architecture: d. f.19, 590; F = 7.0566; p-value < 0.05), and the Shapiro-Wilk tests demonstrated that these datasets did not follow a normal distribution (Length: W = 0.9302; p-value < 0.05; Lateral root branches: W = 0.7781; p-value < 0.05; Architecture: W = 0.7651; p-value < 0.05). The two-way ANOVA tests were performed with a more conservative test statistic (p = 0.02) (Table S50 – Table S52). The statistical analysis showed that the interaction of concentration and genotype had a significant effect on the root length, number of lateral root branches and root architecture of WT and *35S-COPT2* lines grown in the presence of Pd (Two-way ANOVA, Length: 15, 590; F = 2.435; p-value < 0.01; Lateral root branches: d. f. = 12, 590; F = 9.722; p-value < 0.001; Architecture: d. f. = 19, 590; F = 7.301; p-value < 0.001).

Figure 4.9 shows the results of the root characterisation. All *35S-COPT2* lines had shorter roots than WT when grown in the presence of Pd, except for *35S-COPT2C*, which was higher at 20 µM. These differences in root length were significant at 10 µM Pd for *35S-COPT2A* and *35S-COPT2B* (p < 0.01 and p < 0.001 respectively), and at 15 µM Pd for *35S-COPT2B* (p < 0.001) (Table S50). Except for *35S-COPT2C*, the presence of Pd in the ½ MS(A) media resulted in fewer lateral roots compared to the control lacking Pd. The *35S-COPT2C* seedlings had significantly more lateral root branches than the WT when grown on Pd at all concentrations (5 µM p < 0.01, all other concentrations p < 0.001) (Table S51). The *35S-COPT2* lines had more complex root architecture than the WT in the presence of Pd, but these differences were only significant for *35S-COPT2C* at all Pd concentrations (5 µM p < 0.01, all other concentrations p < 0.001) (Table S52).
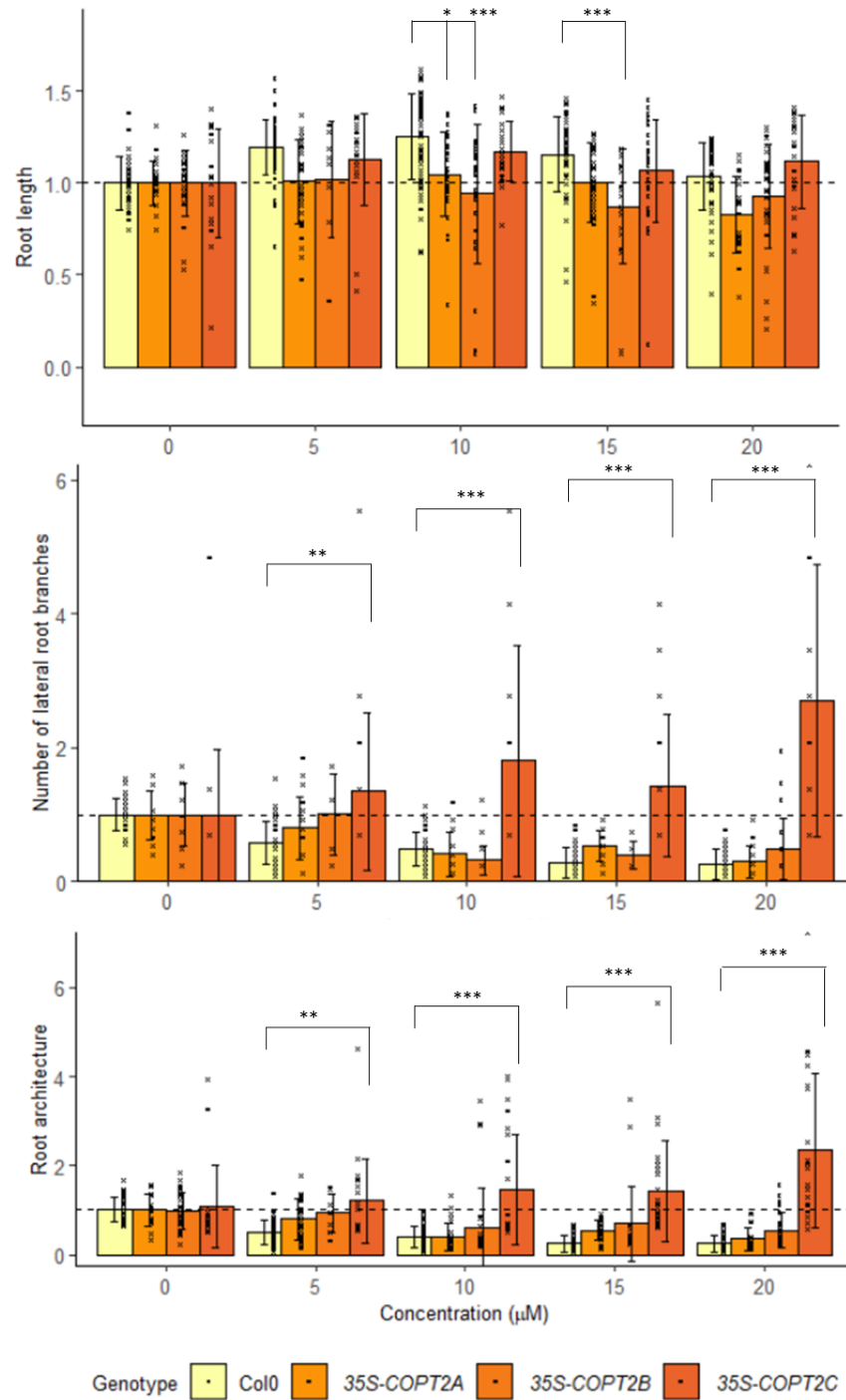
Figure 4.9. Root characterisation of two-week-old Arabidopsis WT (Col0) and three, independent, homozygous *35S-COPT2* genotype (*35S-COPT2A, 35S-COPT2B, 35S-COPT2C*) seedlings grown on ½ MS(A) media containing a range of Pd concentrations. Assumptions tests used were Levene's for homogeneity of variances and Shapiro Wilk for data normality. Statistical significance was calculated by two-way ANOVA test and a Tukey's HSD test. Asterisks mark significant differences between concentrations or between *COPT2* genotypes and the WT (Col) in each concentration, normalised to 0 µM (p-value: * < 0.02; ** < 0.01; *** < 0.001). Values are a mean of between 8 - 71 biological reps, across three technical reps. Higher concentrations resulted in fewer measurable seedlings. The exact number of reps for each condition is shown in Table S47 – Table S49. Black bars are + SD.

4.3.5. Root characterisation of *35S-GP* genotypes grown on Pd

Though the GP was originally synthesised and tested to form AuNPs around 10 nm in diameter, it may have some capacity to influence the formation of PdNPs (59). The formation of NPs in plant tissue by the expression of the *35S*-GP could help to mitigate toxicity generated in the presence of elevated level of Pd and may encourage further uptake or reduced efflux as a result. Small NPs (10 nm) are of special interest for use in catalytic industries and may result in increased catalytic efficiency in downstream applications (15). To examine the effect on the roots of the expression of the *35S*-GP, Arabidopsis WT and *35S*-GP genotypes were grown on ½ MS(A) containing a range of Pd concentrations, and the root length, number of lateral root branches and root architecture recorded. The summary statistics for the root length, number of lateral root branches and root architecture are shown in Table S53 – Table S55.

Levene's test for equal variances showed that the root length, number of lateral root branches and architecture on Pd datasets did not have equal variances (Length: d. f.19, 544; F = 7.6797; p-value < 0.05; Lateral root branches: d. f. = 16, 544; F = 11.726; p-value < 0.05; Architecture: d. f.19, 544; F = 11.015; p-value < 0.05), and the Shapiro-Wilk tests demonstrated that these datasets did not follow a normal distribution (Length: W = 0.9622; p-value < 0.05; Lateral root branches: W = 0.9567; p-value < 0.05; Architecture: W = 0.8490; p-value < 0.05). The two-way ANOVA test was performed with a more conservative test statistic (p = 0.02) (Table S56 – Table S58). The statistical analysis showed that the interaction of concentration and genotype had a significant effect on the root length, number of lateral root branches and root architecture of WT and *35S*-GP lines grown in the presence of Pd (Two-way ANOVA, Length: 12, 544; F = 16.42; p-value < 0.001; Lateral root branches: d. f. = 12, 544; F =10.65; p-value < 0.001; Architecture: d. f. = 11, 554; F = 5.523; p-value < 0.001).

The root length and number of lateral root branches of the *35S*-GP response to growth on Pd, shown in Figure 4.10, was inconsistent between the three *35S*-GP lines. The root length of *35S*-GP*B* was higher than the WT at all concentrations of Pd assessed, though only the 15 μM Pd concentration was significant (p < 0.001) (Table S56). Both the *35S*-GP*A* and *35S*-GP*C* lines had shorter roots than the WT at all Pd concentrations tested. The results comparing the WT and *35S*-GP*A* and *35S*-GP*C* lines were significantly different on 5, 15 and 20 μM Pd (p < 0.001). At 5 μM Pd, the *35S*-GP*B* and *35S*-GP*C* lines had significantly more lateral root branches than the WT (p < 0001). At 10 and 15 μM Pd, both *35S*-GP*B* and *35S*-GP*C* lines had more lateral root branches than the WT, though only *35S*-GP*C* was significant (p < 0.001) (Table S57). Excluding *35S*-GP*B* at 20 μM Pd, all *35S*-GP lines had more complex root architecture than WT at all concentrations tested (5 μM Pd *35S*-GP*C* p < 0.001; 10 μM Pd *35S*-GP*B* p < 0.01, *35S*-GP*C* p < 0.001; 15 μM Pd *35S*-GP*A* p < 0.001; 20 μM Pd *35S*-GP*A* and *35S*-GP*C* p-value < 0.001) (Table S58).
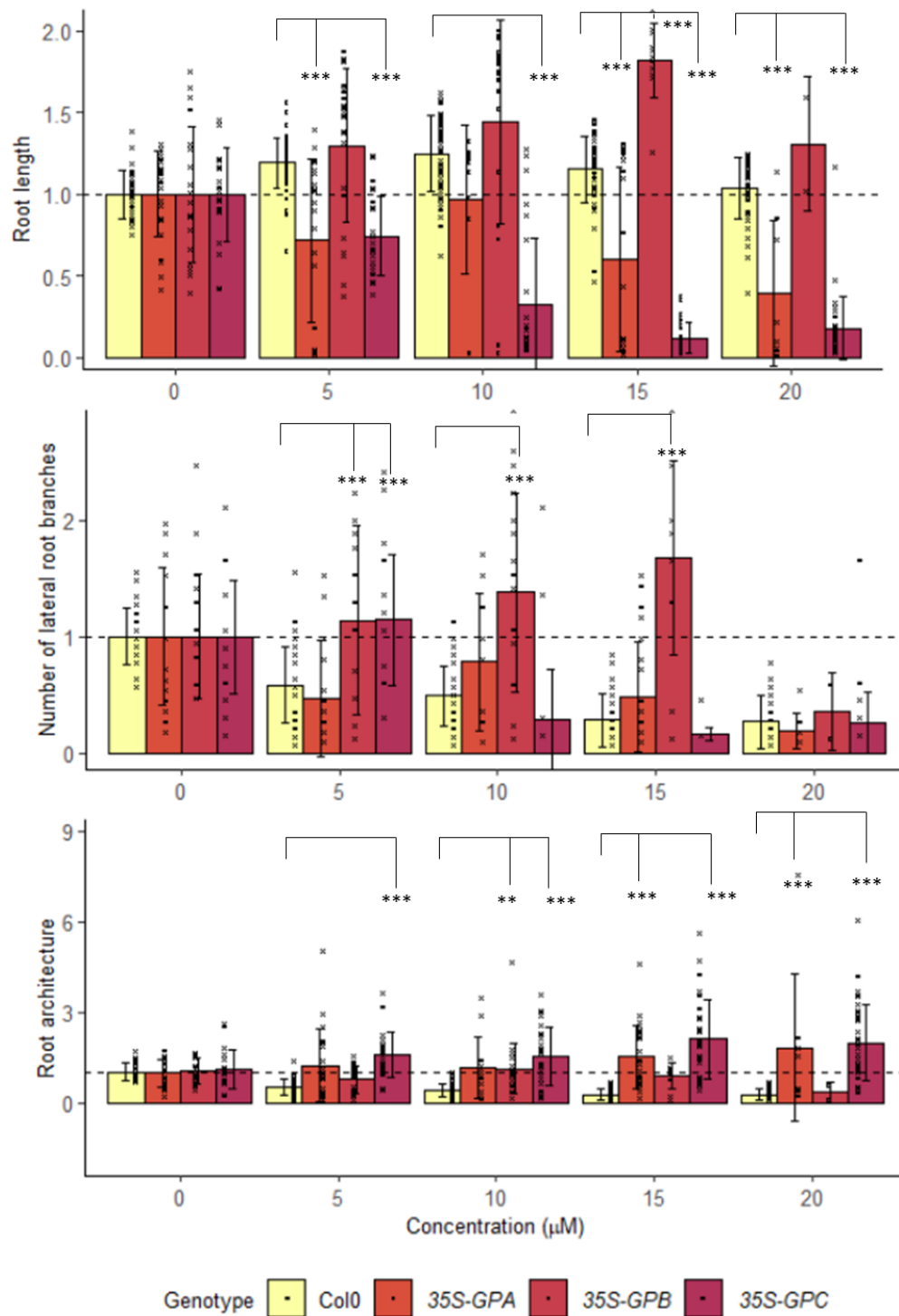
Figure 4.10. Root characterisation of two-week-old Arabidopsis WT (Col0) and three independent, homozygous *35S*-GP genotype (*35S-GPA, 35S-GPB, 35S-GPC*) seedlings grown on ½ MS(A) media containing a range of Pd concentrations. Assumptions tests used were Levene's for homogeneity of variances and Shapiro Wilk for data normality. Statistical significance was calculated by two-way ANOVA test and a Tukey's HSD test. Asterisks mark significant differences between concentrations or between *COPT2* genotypes and the WT (Col) in each concentration, normalised to 0 µM (p-value: * < 0.02; ** < 0.01; *** < 0.001). Values are a mean of between 2 - 71 biological reps, across three technical reps. Higher concentrations resulted in fewer measurable seedlings. The exact number of reps for each condition is shown in Table S53 – Table S55. Black bars are + SD.

4.3.6. Root characterisation of *35S*-GP*C* genotypes grown on Pd

To examine whether the combination of a higher expression of Arabidopsis *COPT2* combined with the expression of *35S*-GP resulted in an altered phenotypic response to Pd, Arabidopsis WT and *35S*-GP*C* genotypes were grown as above. The summary statistics for the root length, number of lateral root branches and root architecture are shown in Table S59 – Table S61.

Levene's test for equal variances showed that the root length, number of lateral root branches and architecture on Pd datasets did not have equal variances (Length: d. f.19, 645; F = 11.45; p-value < 0.05; Lateral root branches: d. f. = 19, 642; F = 12.296; p-value < 0.05; Architecture: d. f.19, 642; F = 13.715; p-value < 0.05), and the Shapiro-Wilk tests demonstrated that these datasets did not follow a normal distribution (Length: W = 0.9605; p-value < 0.05; Lateral root branches: W = 0.9171; p-value < 0.05; Architecture: W = 0.7576; p-value < 0.05). The two-way ANOVA test was performed with a more conservative test statistic (p = 0.02) (Table S62 – Table S64). The statistical analysis showed that the interaction of concentration and genotype had a significant effect on the root length, number of lateral root branches and root architecture of WT and *35S*-GP*C* lines grown in the presence of Pd (Two-way ANOVA, Length: 12, 642; F = 16.00; p-value < 0.001; Lateral root branches: d. f. = 12, 642; F = 7.839; p-value < 0.001; Architecture: d. f. = 12, 642; F = 10.509; p-value < 0.001).

The results of the root characterisation analysis of *35S*-GP*C* lines on Pd are shown in Figure 4.11. With increasing concentrations of Pd, the root length of the three *35S*-GP*C* genotype seedlings decreased while the WT root length remained stable (p < 0.001, Table S62). Excluding *35S*-GP*CA* on 5 and 10 µM Pd, there were no differences in the number of lateral root branches between WT and the *35S*-GP*C* lines at any concentration (Table S63). The root architecture of the *35S*-GP*C* lines was more complex than the WT, excluding *35S*-GP*CC* on 5 µM Pd (Table S64). The differences in root length and architecture of the *35S*-GP*C* lines compared to WT suggested there may be an interaction between *COPT2*, GP and Pd.
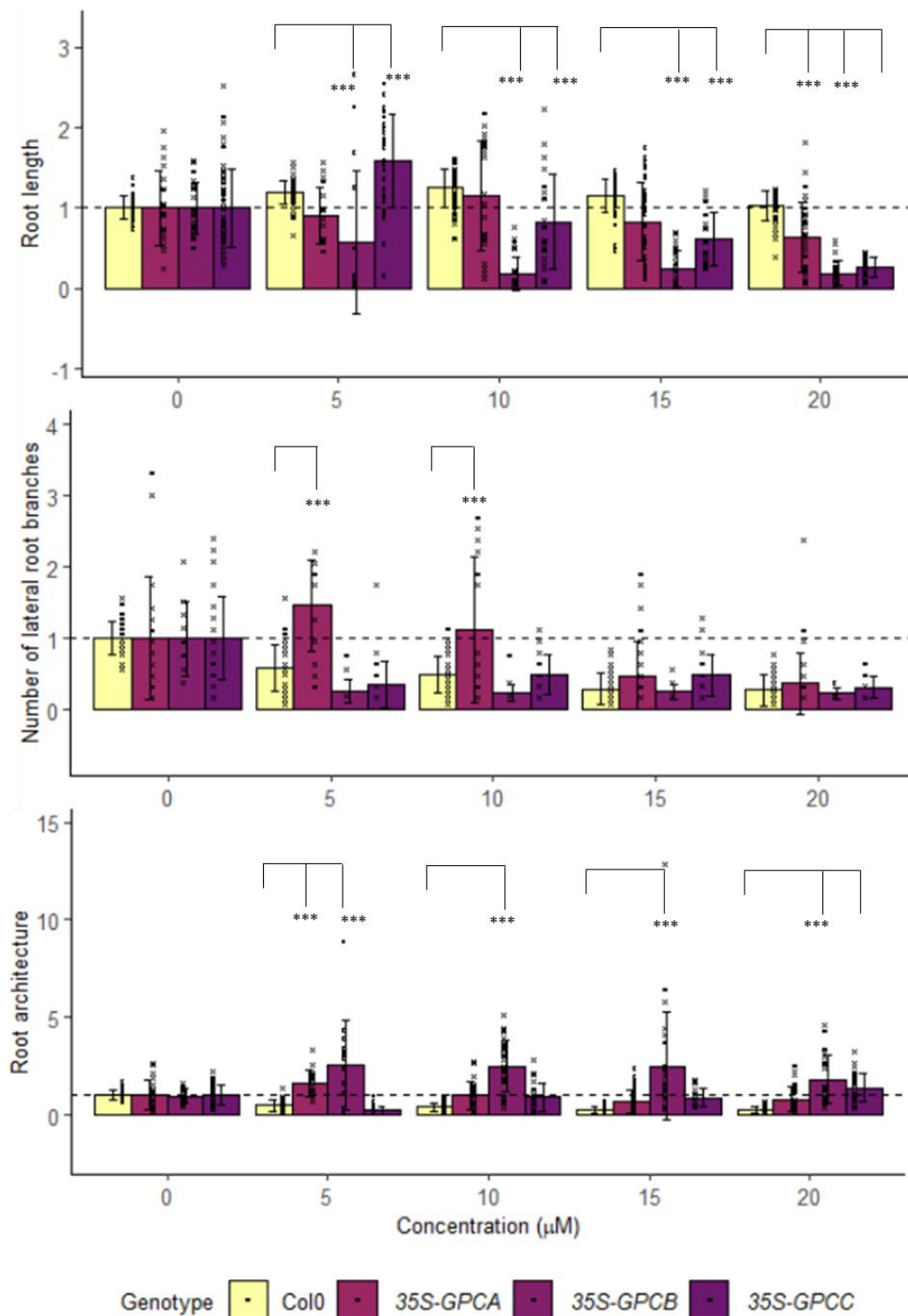
Figure 4.11. Root characterisation of two-week-old Arabidopsis WT (Col0) and *35S*-GP*C* seedlings grown on ½ MS(A) media containing a range of Pd concentrations. Assumptions tests used were Levene's for homogeneity of variances and Shapiro Wilk for data normality. Statistical significance was calculated by two-way ANOVA test and a Tukey's HSD test. Asterisks mark significant differences between concentrations or between *COPT2* genotypes and the WT (Col) in each concentration, normalised to 0 μM (p-value: * < 0.02; ** < 0.01; *** < 0.001). Values are a mean of between 16 - 71 biological reps, across three technical reps. Higher concentrations resulted in fewer measurable seedlings. The exact number of reps for each condition is shown in Table S59 – Table S61. Black bars are + SD.

4.3.7. Analysis of element uptake of Arabidopsis *copt2* mutant and *35S-COPT2* lines grown in the presence of Pd

Analysis of element uptake was performed as in chapter three, using the Arabidopsis *copt2* mutant and transgenic genotypes alongside WT. A one-way ANOVA was performed for each tissue type (shoot or root) and wavelength (Pd: 340 nm, 342 nm; Cu: 324 nm; Fe: 239 nm) (Table S65). Homogeneity of variances for each subset of data was analysed by a Levene's test, and the normality of data was investigated using a Shapiro-Wilk test on the residuals of the one-way ANOVA analysis (Table S66, Table S67). All data subsets excluding the root measurement of Pd at 342 nm were analysed by a Kruskal-Wallis test, as they did not meet the assumptions of the one-way ANOVA. The Pd measurements both produced significant results, but the subsequent Wilcoxon rank sum test did not show any significant differences in the data analysed at 340 nm (Table S68). In the Pd concentration data analysed at 342 nm, Arabidopsis WT contained a significantly higher concentration of Pd comparative to *copt2-2*, but this was the only significant difference (Table S68, Figure 4.12). Generally, the Arabidopsis *copt2* mutant lines, and the *35S-COPT2, 35S-GP* and *35S-GPC* lines resulted in a reduced Pd concentration compared to the WT. Reduced Pd concentration was expected in the *copt2* mutant lines, but not in the *35S-COPT2, 35S-GP* or *35S-GPC* lines, which had shown an increase in Au concentration when plants were exposed to Au in chapter three.
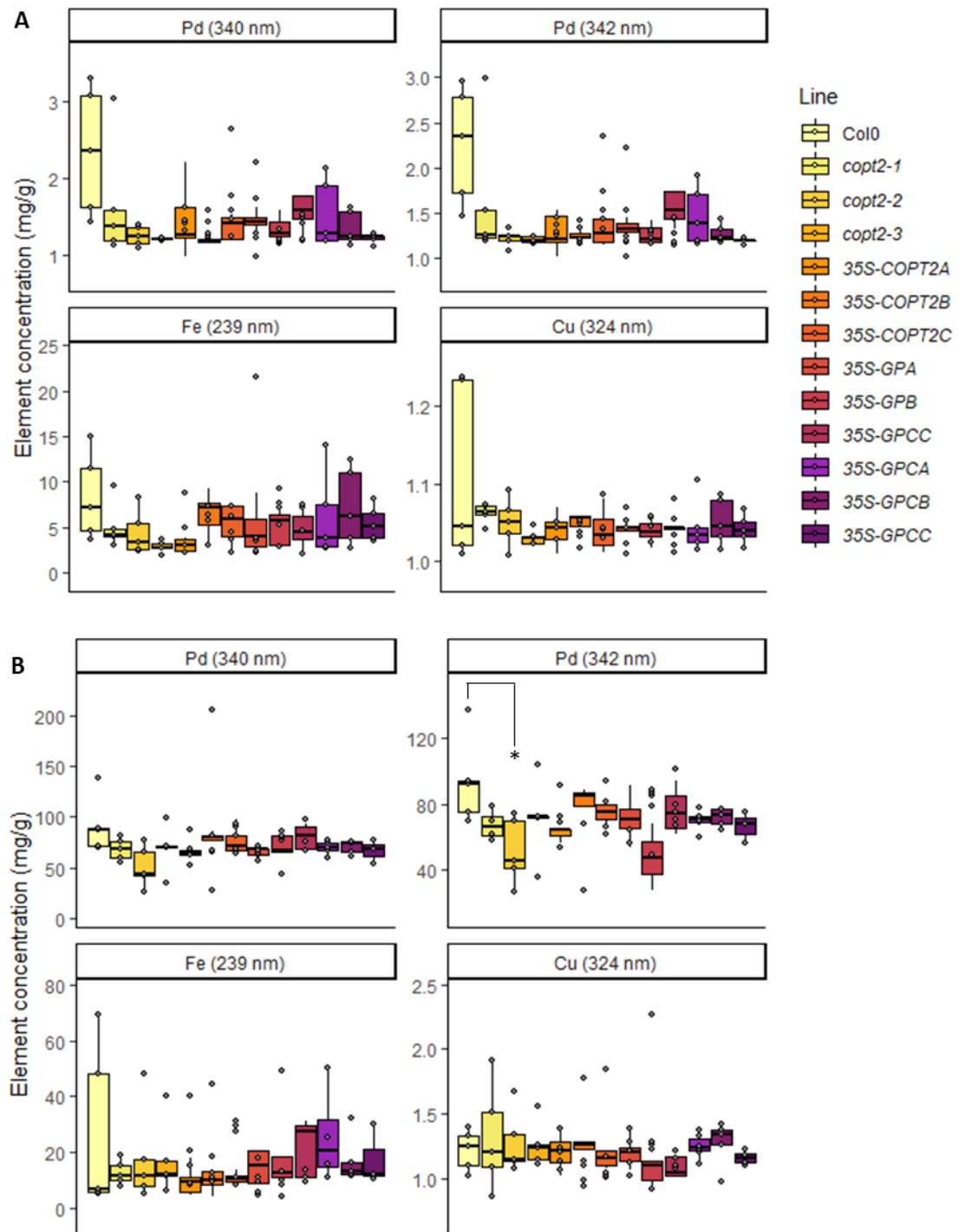
Figure 4.12. Element (Pd, Cu, or Fe) concentration (mg/g) in Arabidopsis genotypes 24 hours after the addition of 1 mM Pd to hydroponically grown, five-week-old Arabidopsis. (A) Shoot tissue (B) Root tissue. Five biological replicates were analysed by ICP-OES and normalised by dry weight (g). Homogeneity of variances was determined by Levene's test, and normality of data was determined by the Shapiro-Wilk test. Normally distributed data were analysed grouped by wavelength (nm) and tissue type by one-way ANOVA and Tukey's HSD test. Data that did not meet the assumptions of a one-way ANOVA were analysed by a Kruskal-Wallis and Wilcoxon rank sum test for multiple comparisons. Significant differences are indicated on plots as asterisks (*: $p < 0.05$, **: $p < 0.01$, ***: $p < 0.001$). Circular dots indicate the distribution of raw data, and 'whiskers' indicate the upper and lower quartiles.

4.4. Discussion
4.4.1. Overview

To examine the interaction of Pd with COPT2 or the GP, the Pd response of yeast mutants expressing *COPT2y* and Arabidopsis *copt2* mutant and transgenic lines (three independently transformed *35S-COPT2, 35S*-GP*, 35S*-GP*C* lines) were investigated in a series of experiments, previously utilised in chapter three to establish an interaction of Au with COPT2 and the GP.

4.4.2. Yeast spot dilution assay suggested an interaction between *COPT2y* and Pd

In the yeast spot dilution assay, all yeast strains expressing *COPT2y* demonstrated a significant growth reduction in subsequent serial dilutions of culture in the presence of Pd, compared to the same strains not expressing *COPT2y* (+ gal vs. + glu, respectively). The growth inhibition response demonstrated by the *COPT2y* expressing strains in the presence of Pd suggested that there was an interaction between *COPT2*y and Pd, which resulted in a reduced tolerance of the yeast strains to Pd, potentially as a result of an internal metal ion concentration above non-toxic level.

4.4.3. Arabidopsis *copt2* mutant lines demonstrated reduced root growth compared to the WT

Following on from the yeast studies, which suggested an interaction between COPT2 and Pd, the phenotypic responses of the three previously characterised Arabidopsis *copt2* mutant lines were then investigated on Pd, in comparison to the WT phenotypic response. The *copt2* mutant lines had significantly shorter roots than the WT in the presence of Pd, an unexpected result. The concentrations of Pd chosen in these studies were selected as the previous work with Au suggested that a more nuanced approach, with lower metal concentrations, might be more informative of an interaction between the Arabidopsis lines and the metal being tested. Reduced expression of a potential Pd-uptake transporter (*COPT2*) would be expected to result in increased fitness as the concentration of metal ions within the tissue would be lower in the *copt2* mutant line.

It was hypothesised that exposure to the low concentration of Pd in the ½ MS(A) media resulted in an increase in the fitness of the WT, but not the *copt2* mutant lines due to reduced Pd content in these lines. Analysis of the Pd concentration by ICP-OES showed that the concentration of Pd was lower in the *copt2* lines than the WT, although this difference was not significant, and the growth conditions of the plants used in the root characterisation experiments and the element analysis are not comparable. Regardless, it is interesting to note that it has been reported that low concentrations of non-essential metals can result in increased growth. A study performed by Jayakumar et al., in 2013, investigated the changes that occurred in the nutrients of *Lycopersicon esculantum* (tomato) under different concentrations of cobalt (206). Though there is some contest, cobalt is not considered to be essential to plant growth (207). Despite the normal level of cobalt chloride concentrations in plants is stated to be as low as 0.1 – 10 g/g dry weight, the levels of macro and micro nutrients increased in response to 50 mg / kg cobalt, the lowest concentration tested, but declined when plants were growth on higher concentrations (100 – 200 mg / kg) (206). Cadmium is highly toxic to both

prokaryotic and eukaryotic organisms; in plants, it is easily taken up by the plant roots and can be loaded into the xylem to be translocated to the above ground biomass (208–210), and has been found to cause growth inhibition and plant death (211). It is toxic to the crop plants at concentrations above 5 µg / Cd / g leaf dry weight (104). In a study performed by Singh Gill et al., (2012), the response of *Lepidium sativum* (garden cress) to several Cd concentrations (0, 25, 50, 100 mg / kg Cd in soil) was investigated (212). At the lower Cd level tested (25 mg / kg Cd) the growth and photosynthesis of *L. sativum* plants was not affected by Cd, potentially due to the upregulation of S assimilation and the antioxidant machinery (212). A low concentration of Pd in the WT may have had a similar effect and resulted in an increase in WT growth due to the higher presence of these factors minimising Pd stress, and other stressors linked to the experimental set up.

4.4.4. Arabidopsis *copt2* mutant lines demonstrated reduced root growth compared to the WT

The response of the three independent, homozygous Arabidopsis *COPT2* overexpression lines (*35S-COPT2)* to Pd was investigated. The *35S-COPT2* lines had shorter roots than the WT in response to Au, and it was hypothesised that this was because of a toxic concentration of the metal ion in the *35S-COPT2* lines, but not in the WT, providing further evidence towards the interaction of *COPT2* and Pd. The interaction of Arabidopsis GP lines to Pd were then investigated, and there were no consistent significant differences between the three independently transformed lines and WT. To determine whether this may have been a result of the low concentration of Pd in the GP lines, the double transgenic response (*35S*-GP*C*) to Pd was then investigated. The *35S*-GP*C* lines demonstrated reduced root length when grown in the presence of Pd compared to the WT, though the root architecture was more complex. To determine the concentration of Pd in the copt2 mutant and transgenic lines, ICP-OES analysis was performed on the dry root and shoot biomass. There were no consistent significant differences across the Pd concentration of the three independent *copt2* or transgenic lines in response to Pd compared to the WT, but the mean Pd concentration of the WT was higher than the mean Pd concentration in *copt2* mutant and transgenic lines. Whilst there may be an interaction between COPT2 and Pd, evidenced by the response of the yeast spot dilution assay and the growth response and Pd concentration of *copt2* mutant lines, the interaction appears more complex than that with Au, and the response of Arabidopsis to Pd requires further investigation.

5. Investigating the Arabidopsis transcriptome response to Pd

5.1. Introduction
5.1.1. Overview

In previous chapters, the physiological response of Arabidopsis to Au and Pd was studied to clarify the role that COPT2 played in the uptake of these metals. The knowledge gained in these experiments suggested that though it played a part, the COPT2 transporter was not the only route for Pd uptake in Arabidopsis, and that there may be other pathways by which this metal enters the plant tissue. The response of the Arabidopsis transcriptome to Pd is examined in the following chapter, to help elucidate genes involved in mitigating metal ion, uptake, induced stress and Pd detoxification in plants. Gaining an insight into these genes, and their roles, is of paramount importance to face the challenge of genetically engineering plants to phytomine this precious resource. As demonstrated previously, increased uptake of Cu, Au and Pd by plants can negatively impact their growth and survival and gaining further knowledge about how plants avoid the potentially toxic effects of metal ion stress is vital.

5.1.2. Metal detoxification

Plants require specific metal ions, predominantly as cofactors, to enable the normal functions of enzymes and proteins. However, their accumulation, beyond physiologically required levels, can be highly toxic, interfering with proper protein function, photosynthesis, and water and nutrient uptake (213–217). Additionally, the presence of non-essential metals in the environment can also exert toxicity. Due to these conflicting issues, plants have evolved mechanisms to regulate levels of metal ions and mitigate their induced toxicity. Detoxification mechanisms include: i) chelation and ii) intracellular compartmentalisation of ions, iii) increased efflux from the plant cells, and iv) reduction of the metal ions to their zero-valent state (218). For Ag, Au and Pd, reduction of metal ions can result in the formation of NPs, which can be harvested from the plant as a source of these valuable metals, as discussed in chapters three and four.

5.1.3. Pd uptake and NP formation in bacteria

Precious little information exists about the genes involved in Pd uptake and NP formation in plants. The NPs are thought to form through the interaction of the cationic metal ions with anionic cellular components, leading to the formation of NPs via reduction, chelation or hydrolysis (219). The genetic basis behind these mechanisms has been explored to some extent in bacteria. Bacteria and fungi offer additional routes for the remediation of metal contamination in the environment, and as such are a focus of genetic research. Initially, the ability of bacteria to grow on toxic heavy metals was thought to rely primarily on their ability to efflux (220). However in 1999, Klaus et al reported that *Pseudomonas stutzeri* mediated the toxicity of Ag ions through its ability to form and accumulate NPs, depositing these in vacuole-like granules between the plasma- and outer membranes (221).

Several microorganisms have been identified with the ability to retain metal ions *in situ* and convert them to their metallic form. Broad mechanisms of NP synthesis have been identified in bacteria, including enzymatic action by reductases, interaction with peptides, and through efflux pump systems which sequester metal ions to compartments (222). The bacterial cell wall, for instance, forms NPs through electrostatic interactions; the negatively charged cell wall attracts the positively charged metal ions (222). The biosynthesis approach to reducing the toxicity of metal ions is likely part of a larger stress response (223).

The favoured route to NP formation intracellularly is enzymatic reduction and capping through redox reactions. Redox enzymes act as nucleation sites, providing electrons for the reduction of the metal ion (224). In fungi, NADH-dependent nitrate reductases are often reported as involved in this process (225) and have been implicated in the formation of Ag (225), selenium (226) and Au NPs (227). In the bacterium *Desulfovibrio fructosivorans,* hydrogenases have been found to be capable of reducing the ionic form of Pd to the metallic form (228). Fungal hydrogenases have also been implicated in the reduction of other metals, including selenium and Au (229). Following formation intracellularly, NPs tend to accumulate in the cytoplasmic membrane, cell wall or periplasmic space.

Samples from North American Pd (Canada) and gossans, intensely oxidised, weathered or decomposed rock formed from part of an ore deposit or mineral vein, from Australia were studied to assess if these PGM-rich samples could be used as substrates for phytomining. The highest available concentration of Pd was assessed at 5.38 ppm (230). In soil, a small portion of metals is available to plants as most is bound to different minerals that are more difficult to be incorporated by plants. The bioavailability of metals can change gradually by chemical weathering and biological processes. Anderson et al. (2005) stated that 2 mg / kg is the minimum concentration of precious metals in a substrate needed to yield significant concentration in a plant during phytomining, though this may be lessened as a result of the increased price of the metal in 2022 (231).

5.1.4. Identifying genes involved in Pd uptake and detoxification

To utilise plants in the remediation of polluted soils and in phytomining, we need a comprehensive understanding of the genes involved in metal uptake into plant tissue and the mechanisms plants use to manage the toxicity of these ions. To do this, there are a number of gene expression platforms including microarrays, and sequencing technologies. These platforms measure expression of mRNA. The mRNA comprises only a fraction of the total RNA (3 – 7 %), and the remaining components include the very abundant ribosomal RNA (rRNA) (80 – 90 %), transfer RNA (tRNA) and non-coding RNA (ncRNA) (3 – 17 %) (232). Using the Illumina platform RNA-sequencing (RNA-seq), it is possible to gain an insight into the quantity and sequences of mRNA present in a sample (233). This information can be used to analyse differential gene expression and identify which genes are turned on or off under certain conditions. Thus, the results can give an indication of genes involved in metal uptake and metal stress alleviation pathways.

The Illumina sequencing process, used in this work, can be divided into four stages, shown in Figure 5.1.
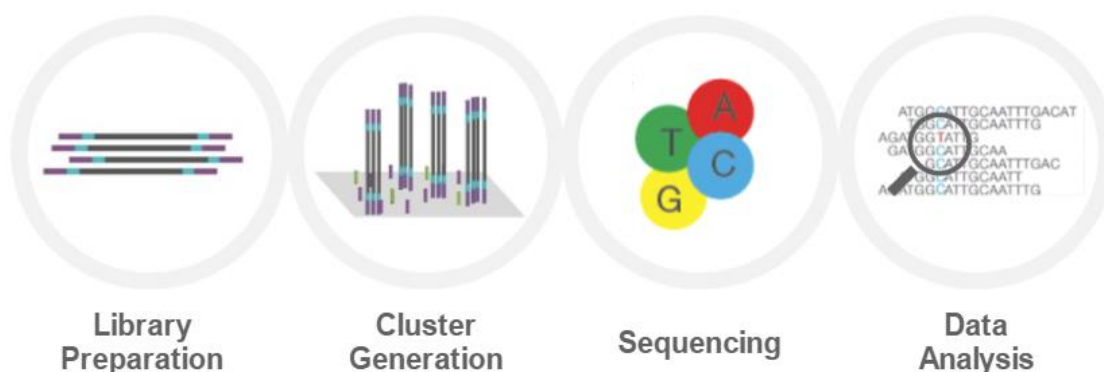
Figure 5.1. The four stages involved in the Illumina RNA-sequencing workflow, which was utilised in this work. The four stages include library preparation, cluster generation, sequencing and data analysis. Library preparation was performed in collaboration with the Genomics & Bioinformatics Facility at the University of York, cluster generation and sequencing was performed by Novagene, and data analysis was performed in collaboration with the Genomics & Bioinformatics Facility at the University of York. Figure reproduced from the 'Sequencing: Illumina Technology' course, Illumina. com (234)

The RNA samples are first prepared through extraction from cells, and the quality of the RNA checked, using a spectrophotometer-based system, or an electrophoresis-based system. The spectrophotometer-based system can be used to make wavelength comparisons (e.g., 260, 280nm) to determine integrity and total RNA concentration. An electrophoresis-based system uses a microfluidic chip to separate the RNA, which is first stained using an intercalating, florescent dye. Using quantified standards, integrity and concentration levels can be determined (235). There are several methods which can be used to remove the very abundant (80 - 90%) rRNAs, including selective enrichment of mRNA by polyA selection (present on most mRNA molecules), which was used in this work (236).

The mRNA enrichment is followed by preparation of the library for sequencing. Firstly, the mRNA is fragmented into short, uniform sizes (200 – 500 base pairs), then transcribed into cDNA using reverse transcriptase. Finally, a 3' adenylation step, ligation of adapter molecules to nascent cDNAs, and PCR amplification are performed, as shown in Figure 5.2.
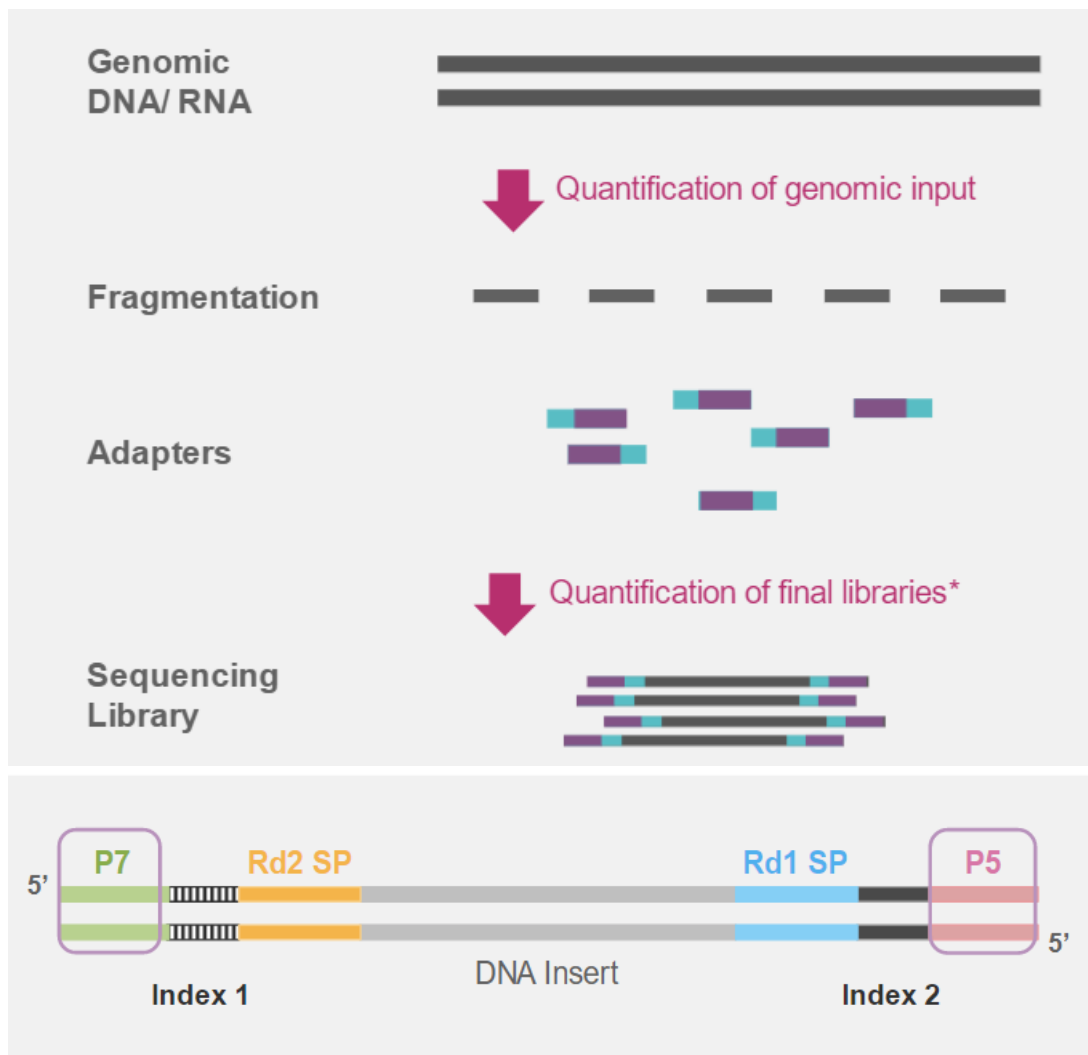
Figure 5.2. The library preparation process involved in the Illumina RNA-sequencing workflow. By the end of the library preparation process, adapters are attached on both ends of the fragments. The fragment contains P7 and P5 binding regions, which interact with oligos on the surface of the flow cell. The indexes refer to a unique sequence to maintain clarity when sequencing multiple samples. Rd2 SP and Rd1 SP refer to binding regions for sequencing primers to enable Read 1 and Read 2. Figure reproduced from the 'Sequencing: Illumina Technology' course, Illumina. com (234)

The next step in the process is cluster generation, which occurs onboard the flow cell. A flow cell is a glass slide containing fluidic lanes or channels for defined volume and spacing (234). In cluster generation, the fragments present in the cDNA library are cloned thousands of times, as demonstrated in Figure 5.3.
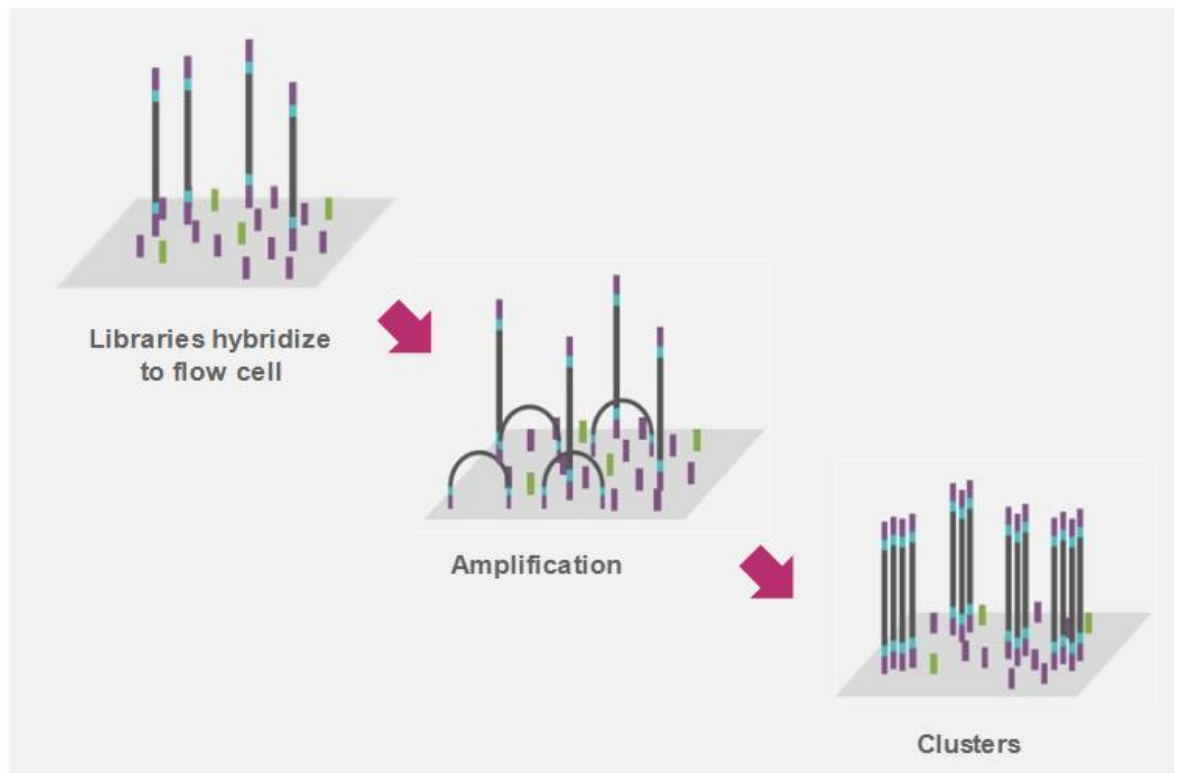
Figure 5.3. Overview of the cluster generation step as part of the Illumina RNA-sequencing process. In the first part, the adapters added to the cDNA fragments hybridise one of the two types of oligos present on the surface of the flow cell. In the amplification process, single stranded molecules flip over and hybridise to adjacent primers to form a bridge. A polymerase then synthesises the reverse strand, and the process is repeated. In the final step, the strands are linearised to prepare the strands for sequencing. Figure reproduced from the 'Sequencing: Illumina Technology' course, Illumina. com (234)

The third step, sequencing by synthesis (SBS) occurs when sequencing reagents, including fluorescently labelled nucleotides, are added to the clusters. Each of the nascently-added bases emits a unique wavelength and these are captured by sequential imaging, as shown in Figure 5.4.
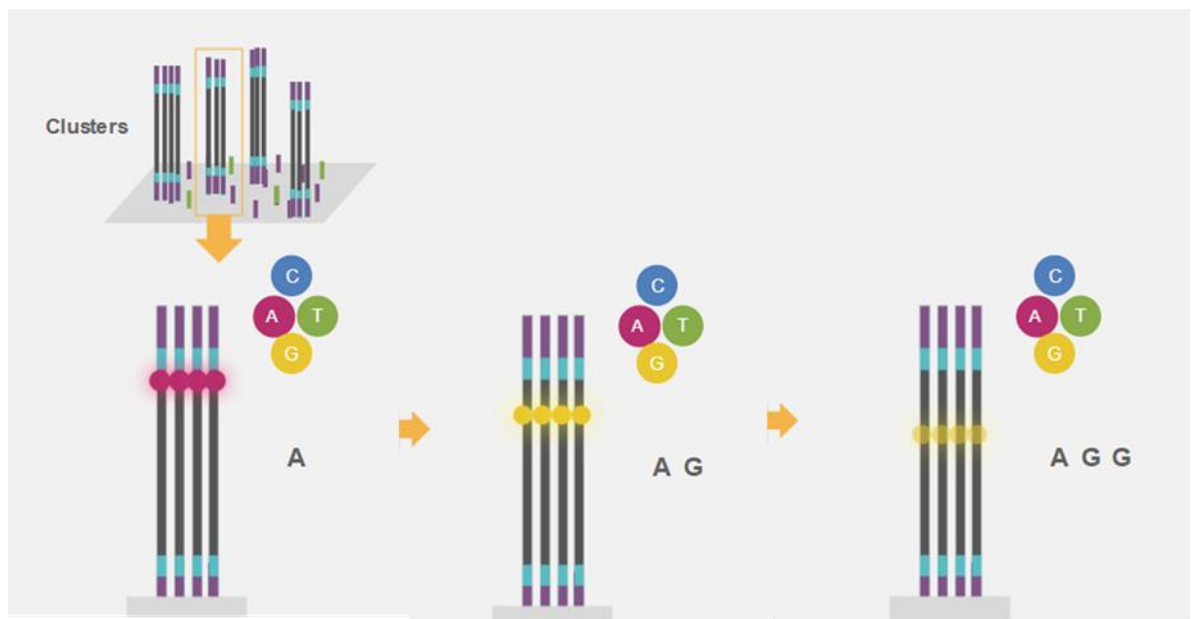
Figure 5.4. The Sequencing by Synthesis (SBS) process as part of Illumina RNA-sequencing. During this process, fluorescently labelled nucleotides are added and bind to the cDNA strand. Following each addition, the flow cell is imaged, and each of the bases emits a unique wavelength that permits identification. The process is repeated to identify the sequence of the fragment. Figure reproduced from the 'Sequencing: Illumina Technology' course, Illumina. com (234)

The sequence reads obtained from the images can then be mapped to a reference genome. If no reference genome exists, data from the RNA-seq experiment can be used to create sequence assemblies. The counts for each sequence read are quantified; either as absolute read counts or as normalised values (reads per kilobase million (RPKM), fragments per kilobase million (FPKM) or transcripts per kilobase million (TPKM)). Each of these methods attempts to normalise for sequencing depth (the number of times that a given nucleotide in the genome has been read in an analysis) and gene length (longer genes will have higher mapped reads than a shorter gene of the same expression level). The RPKM requires dividing the total read count by one million to obtain the 'per million' scaling factor, and then dividing the read counts by this scaling factor, allowing for normalisation according to the sequencing depth. To normalise for biases in gene length, these values are then divided by the length of the gene in kilobases to generate the RPKM. The FPKM is a similar technique, but specifically for paired-end RNA-seq, in which case two reads can correspond to a single fragment. The difference between RPKM and FPKM is that the FPKM considers that two reads can map to a single fragment, and so it doesn't count this fragment twice. The only difference between RPKM and TPKM lies in the order of the process: to generate the TPKM, the read count is divided by the length of each gene in kilobases first (the RPK value), then the number of RPK values per sample is divided by one million to get the 'per million' scaling factor, and finally the RPK values are divided by the 'per million' scaling factor.

RNA-seq is currently one of the most commonly used technologies for gene expression analysis for numerous reasons, as shown in Figure 5.5:

- RNA-seq data is quantifiable
- RNA-seq is more sensitive than earlier, microarray-based techniques
- The cDNA sequences used in RNA-seq can be mapped to targeted regions on the genome
- RNA-seq does not have issues with cross- or sub-standard- hybridisation, unlike the microarray technique
- RNA-seq permits the identification of new transcripts, without needing to rely on existing sequence data (237)
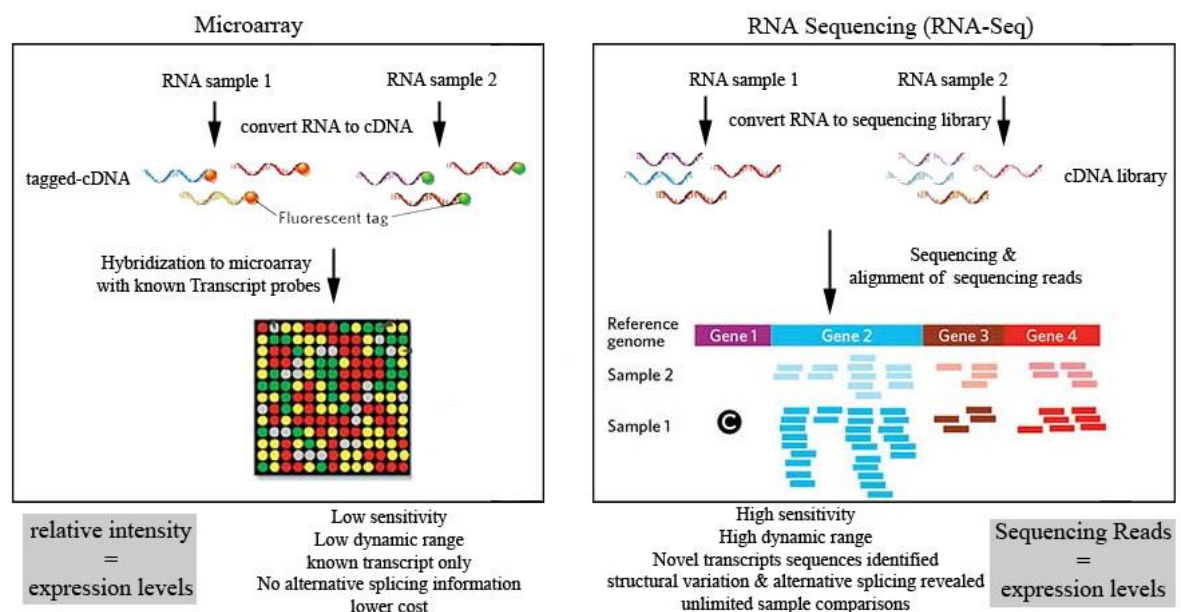
Figure 5.5. A comparison between the Microarray and RNA-sequencing techniques. The left panel shows a simplified schematic of the use of a Microarray, how expression level is defined, and features of the microarray technique. The right panel shows a simplified schematic of the RNA-sequencing technique, how expression levels are calculated, and the features of the technique. The RNA-sequencing technique is considered as a more advanced and more powerful technique due to its several advantages over microarrays. Figure reproduced from Otogenetics.com (238)

Despite the benefits of RNA-sequencing, there are drawbacks to the technique. Polyadenylated (polyA) enrichment excludes the abundant rRNAs, which would otherwise obscure the detection of less abundant transcripts; however, it also eliminates regulatory noncoding RNAs and partially degraded mRNAs (239). An alternate method, rRNA depletion, uses hybridisation capture of rRNAs followed by magnetic bead separation to separate the rRNAs from the total RNA. Zhao et al (2018) performed a comparison of the two main rRNA removal methods for RNA-seq, polyA selection and rRNA depletion (239). The researchers found that there was little difference in the number of reads mapped to the genome between approaches, but a distinct difference in the read count falling in exonic and intronic regions. A high proportion of the rRNA depletion reads mapped to intronic regions, which did not occur in the polyA selected libraries. The researchers recommended that most

studies use polyA selection over rRNA depletion (239). In this study the polyA enrichment technique was used.

5.1.5. Use of RNA-seq for differential gene expression in plants

The technology of RNA-seq has been used to elucidate gene expression in many abiotic (240–242) and biotic stresses (243,244) in plants. Due to the ability of this technique to analyse differential gene expression, it is especially useful to identify genes that are up- or down-regulated in response to stressors. The technique has been used to identify genes responsive to Cd and arsenic stress in *Oryza sativa* (rice) (245,246), Cd stress in Italian ryegrass (*Lolium multiflorum*) (247), chromium, lead and Cd in radish (*Raphanus sativus*) (248) and Pb in Arabidopsis (244).

5.1.6. Genes involved in the metal induced stress response in Arabidopsis

Stress-related mechanisms are common across treatments with different metals and metalloids, and though there are genes commonly expressed in response to different metal stressors, there are some pathways that appear unique to different metals. As part of the lead stress response in Arabidopsis, unique genes were identified relating to sulfur assimilation, GSH metabolism, jasmonic acid (JA) biosynthesis and some specific transcription factor families. Separately, genes have also been identified that are thought to reduce the toxic effects of this metal by extraction, chelation and compartmentalisation (214).

Weber et al (2006), compared the transcriptome response upon Cd and Cu exposure in the roots of Arabidopsis and the Cd -hyper tolerant metallophyte *Arabidopsis halleri.* There were three gene categories identified by this comparison: common responses, metallophyte-specific responses, and responses specific to Cd exposure. It was noted that the mechanism for resistance in *Arabidopsis halleri* lies in its metal exclusion ability as well as its more efficient sequestration of Cd in root cells (249).

Whilst not a study performed in plants, shotgun proteomic analysis of the NP synthesising *Desulfovibrio alaskenesis* (*D. alaskenesis)* in response to Pt and Pd, identified that proteins found in both datasets were predominantly related to cellular death, cell integrity and maintenance, membrane biogenesis and integrity, and amino acid synthesis. Thirteen proteins were identified with a central role in both Pd and Pt transport and reduction to NPs, as shown in Figure 5.6.
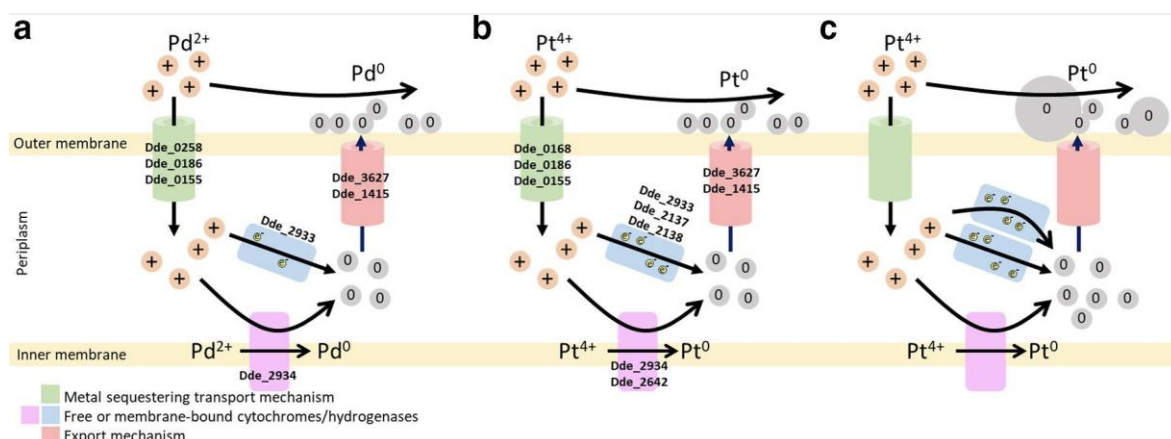
Figure 5.6. The proposed mechanism of Pd and Pt nanoparticle synthesis in *Desulfovibrio alaskensis* (*D. alaskensis*) G20 by Capeness et al (2019). Figure is based on the proteomic data presented in the Capeness et al (2019) paper for Pd (a) and Pt (b). (c) Predicted production of increased size platinum nanoparticles due to increased levels of Dde_2137. Figure reproduced from Capeness et al (2019) (250)

As the less toxic of the two metal ions, for Pd, no redox candidate proteins were identified as unique to treatment with Pd, and it was hypothesised that the detoxification mechanisms used in this condition were also utilised when the bacteria were treated with Pt. In the Pt treatment, a small subunit of the NiFe hydrogenase had an increased presence compared to the control; and artificially increasing the expression of this hydrogenase resulted in an increase in PtNP sizes from 117nm to 324nm, shown in Figure 5.7 (250).
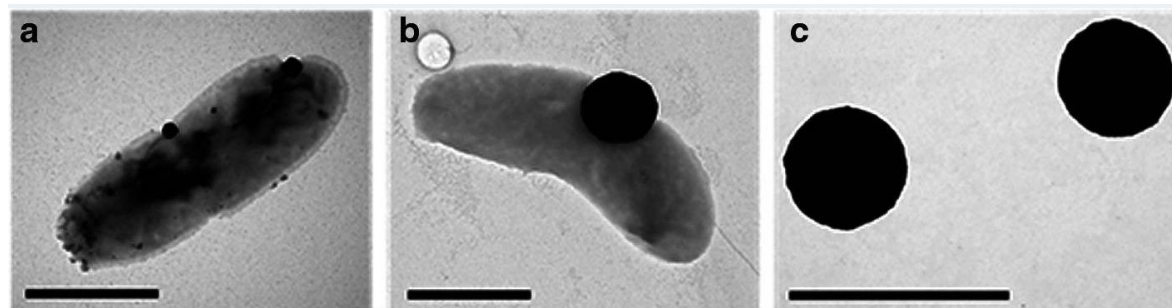
Figure 5.7. Electron micrographs of *D. alaskensis* incubated with 2 mM PtCl4 for 120 min. (a). Control containing the empty pMO9075 plasmid. (b). Containing the pMO-2137 plasmid, which results in expression of the small subunit of the NiFe hydrogenase. (c). The nanoparticles from (b) free in the media. Scale bar, 1 μm. Figure reproduced from Capeness et al, (2019) (250).

5.2. Methods

5.2.1.   Experimental set up

Hydroponically grown, five-week-old Arabidopsis Col-0 plants were exposed to Pd and harvested after 24 hours. The conditions used in this experiment were: (A) undosed Arabidopsis WT plants, harvested 24 hours after ½ MS added, and (B) 1 mM Pd exposed plants, harvested 24 hours after Pd-containing ½ MS media was added (Figure 5.8). The experiment was repeated twice, and five biological replicates were used per condition. For each sample, shoots and roots were separated and washed three times with sterile distilled water. The roots were treated with 'metal desorption' solution (2 mM $CaSO_4$ and 10 mM ethylenediaminetetracetic acid) for 10 minutes prior to a second wash. Following the wash step, tissue was patted dry and the tissue from five biological replicates pooled together. Pooled samples were snap-frozen in liquid N and stored at -80 °C in preparation for RNA extraction. Samples were homogenised by grinding in liquid N with a mortar and pestle, and RNA extracted using the *EasyPure®* Plant RNA Kit as per the manufacturer's instructions. Contaminating gDNA was removed using the DNase Max. A Nanodrop™ 2000 Spectrophotometer was used to quantify the initial concentration and quality of the samples, followed by analysis on a Qubit 4 Fluorometer for more detailed quality control.
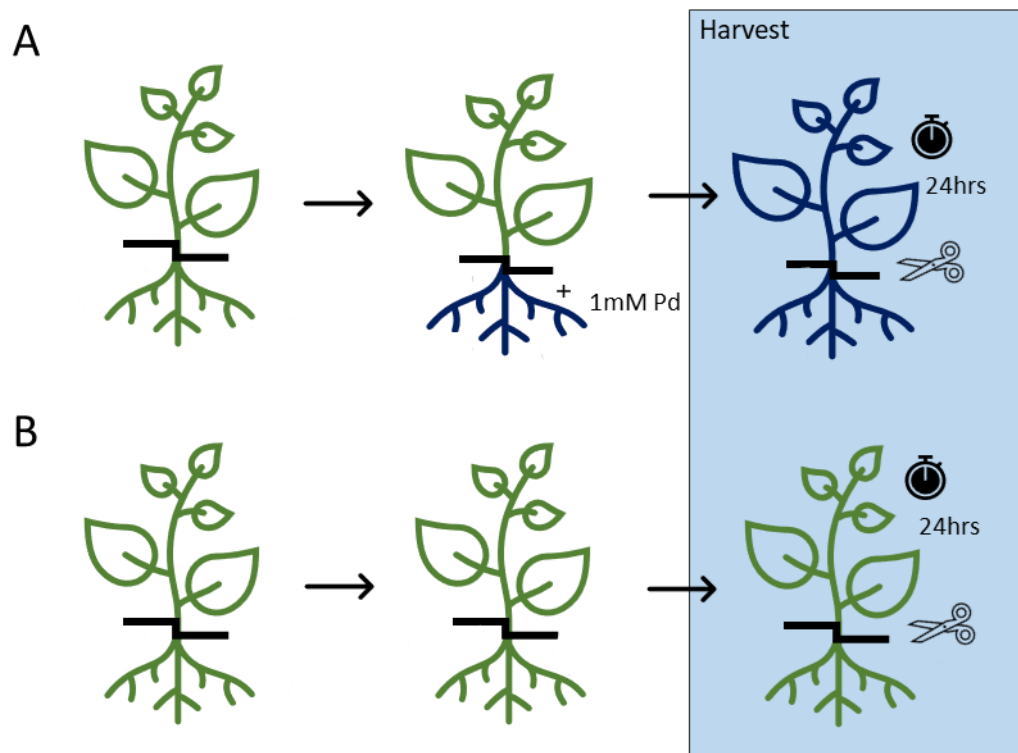
Figure 5.8. Hydroponic experiment set up for the analysis of Arabidopsis WT (Col0) transcriptome in the presence vs. absence of 1 mM Pd. Plants were grown to five-weeks-old in a hydroponic system, whereby roots were submerged in a liquid ½ MS media. At five-weeks old, the ½ MS media was swapped for (A) an undosed control (½ MS) or (B) ½ MS containing 1 mM Pd. Twenty-four hours following the swapping of the ½ MS media, plants were harvested; this involved splitting the shoot from the root tissue and snap freezing in liquid nitrogen before RNA extraction and further processing. The experiment was performed twice and the data from both experiments analysed in the transcriptome analysis.

5.2.2. Synthesis of cDNA

The population of RNA to be sequenced was transcribed to cDNA fragments, and a cDNA library generated by the Genomics & Bioinformatics Facility at the University of York. In this process, the mRNA was selectively enriched by polyA capture prior to cDNA synthesis, and adapters added to each end of the fragments to permit sequencing. Amplification of the cDNA was performed by a reverse transcriptase mediated first strand synthesis followed by a DNA polymerase-mediated second strand synthesis. The cDNA library was analysed by next-generation sequencing (mRNA-Seq, Novogene, Cambridge UK), using the Illumina HiSeq platform. The workflow process for RNA-sequencing is shown in Figure 5.9.
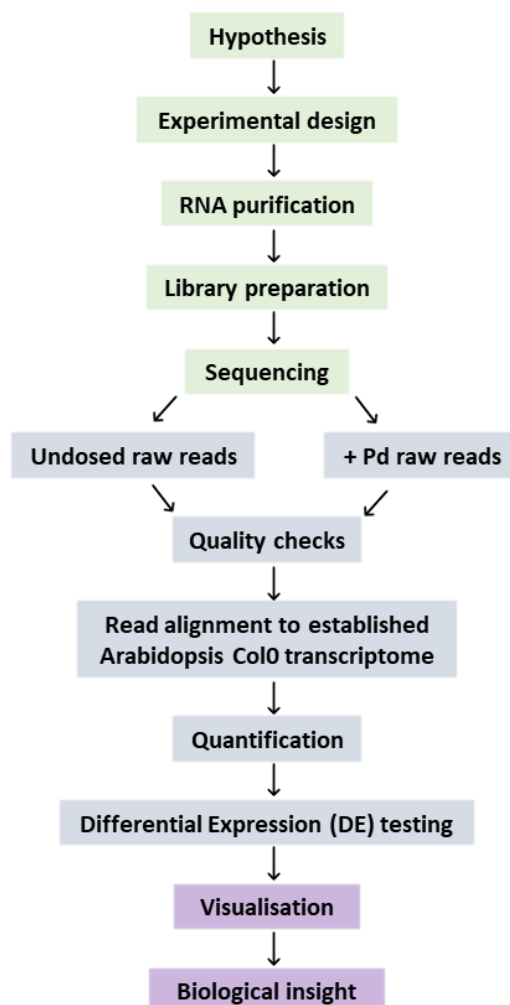
Figure 5.9. Workflow of RNA-seq used in this work. The null hypothesis to be tested was that there would be no difference between hydroponically grown, five-week old Arabidopsis WT (Col0) plants that had or had not been exposed to 1 mM Pd for 24 hours. The shoot and root tissue was separately analysed. The sequencing was performed by Novagene using the Illumina NovaSeq 6000 sequencing system, and the library type was ampified cDNA. Alignment of the reads to the established Arabidopsis genome was performed by the Genomics & Bioinformatics Facility at the University of York. Differential expression analysis was done using RStudio (accessed 2021) using RTools 3.3.0, and the DEseq2 package.

Mapping of transcripts to the Arabidopsis genome was performed by the Genomics & Bioinformatics Laboratory at the University of York. Paired-end reads were trimmed to remove adapter sequences, using CutAdapt version 2.3. Reads were mapped and quantified using the Salmon pseudo-aligner (version 1.1.0) against the Arabidopsis TAIR10.51 transcriptome with the selective alignment option ("validateMappings"), the "seqBias" and "gcBias" options, and 100 bootstraps. Differential expression analysis was conducted using Wasabi (version 1.0.1) and Sleuth (version 0.30.0), with the "read_bootstrap_tpm" option to take Salmon's bootstrapping into consideration. Sleuth's likelihood ratio test (LRT) was used to calculate differential expression values and statistical significance.

5.3. Results

Upon receipt of the transcriptomics data from Novagene, the Technology Facility at the University of York prepared the data for differential expression analysis as above. The following quality-check analyses were conducted: principal component analysis (PCA), number of reads per sample, analysis of the spread of distributions per sample and the distribution of the differentially expressed (DE) genes (DEGs) between root and shoot tissue. The PCA visualises the relationships between samples to highlight the most influential variables and determine that the data groups in an expected manner. The distribution of samples is shown in Figure 5.10A and shows that there was a clear split between the root and the shoot samples, demonstrating that the tissue type acted as the leading influence of the transcriptome response. There was a split between the undosed and Pd condition, but this was less influential than the tissue type; the data are spread along principal component 1 (tissue type), which has 85 % variance, whereas principal component 2 (condition) has only 8 % variance. The data are grouped more tightly within the root dataset, demonstrating that the undosed and Pd-treated root samples had a more similar transcriptome compared to the shoot data. As the main source of variation in the dataset is from the tissue type, the dataset was split, and the shoot and root transcriptome responses analysed separately. Figure 5.10B shows the number of reads per sample. Only two samples were below the recommended minimum 5 million paired-end sample reads line, but these were included in the dataset as they had normal distributions and did not digress from patterns established in the PCA (Figure 5.10A, C). There were 13,956 DEGs between undosed and Pd treated shoot tissue, and 3545 DEGs for the root tissue. Figure 5.10D is a Venn diagram illustrating the number of DEGs exclusive to the shoot or root tissue (11,247 and 836 genes respectively), and the genes that were common to both tissue types (2,709 genes). There were 5,995 genes that were not DE.
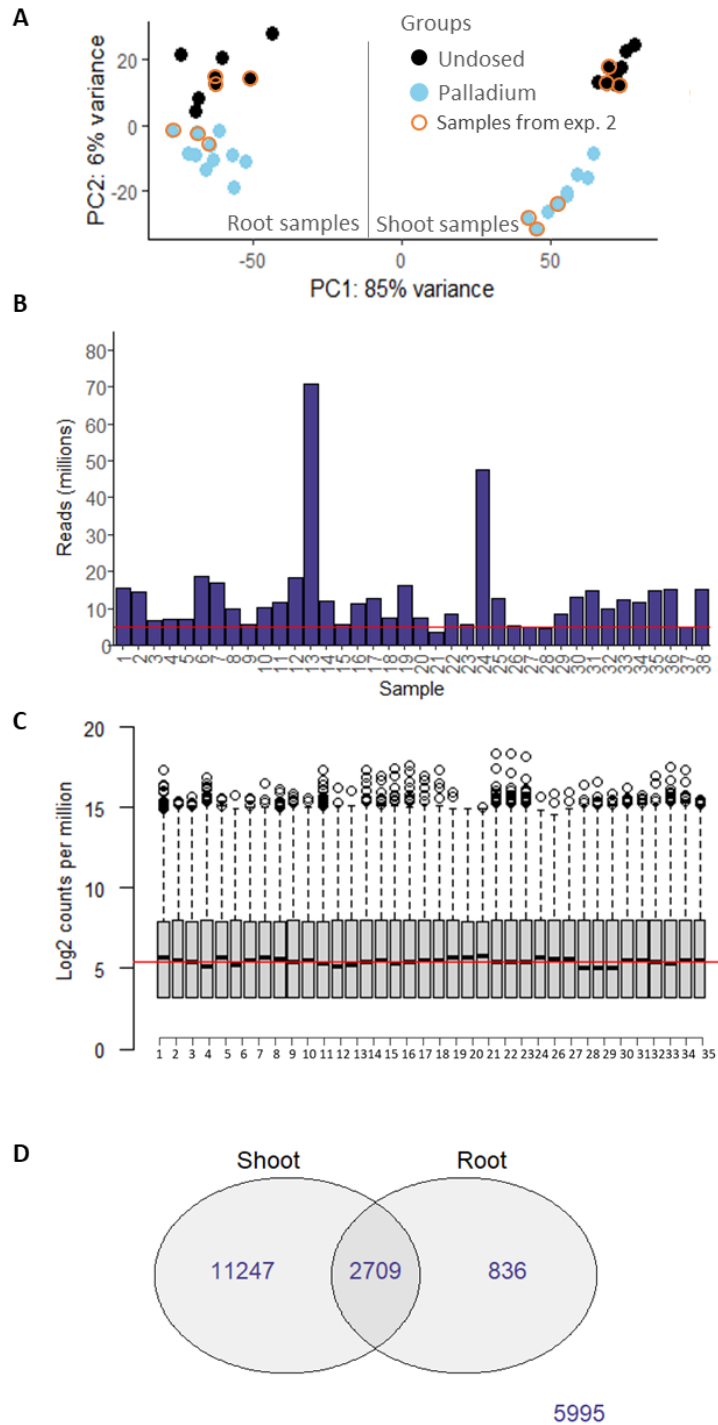
Figure 5.10. Quality checks of the samples used in the RNA-seq analysis of DEGs between Arabidopsis shoot or root tissue after root tissue had been submerged in undosed ½ MS media or ½ MS media containing 1 mM Pd. A: Principal component analysis; samples from experiment 2 are defined by an orange outline, those without an orange outline are from experiment 1; B: Read counts per sample (millions), red line at 5 million reads; C: Distribution of reads within samples, red line shows the data median; D: The number of DEGs present in shoot or root tissue, the number common to both tissue types, and those that were not DE.
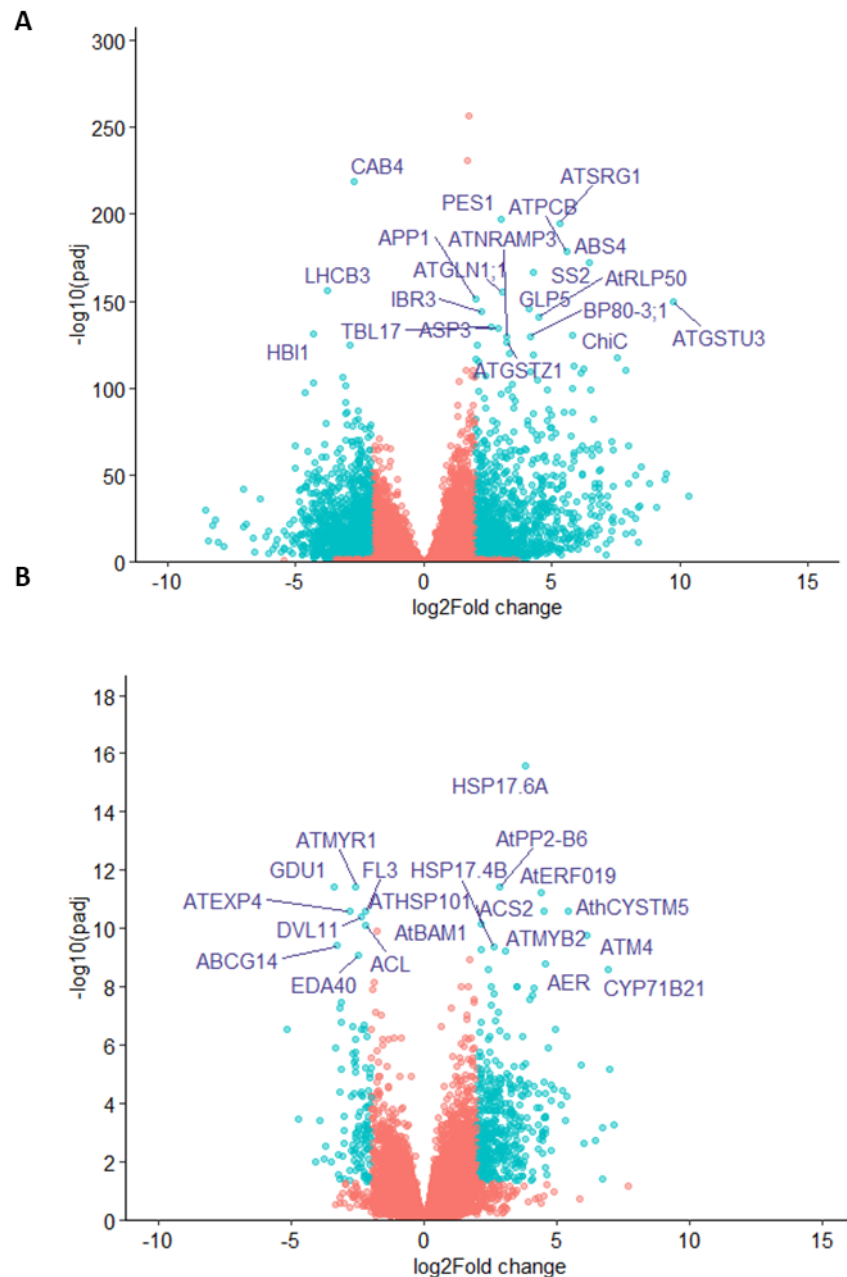
Figure 5.11. Volcano plots which show the distribution of genes following DE-analysis between undosed and Pd treated shoot (A) or root tissue (B). The points are coloured by the statistical significance (y-axis) and the magnitude of difference (x-axis): blue - statistical significance of $p < 0.05$ and log2Fold change of ± 2; red - statistical significance of $p > 0.02$ and log2Fold change within ± 2. Gene names are the top twenty most significantly DEGs in each dataset, ordered by the smallest adjusted p-value.

The results from the DE analysis are shown in Figure 5.11, which displays the distribution of genes following DE-analysis between undosed and Pd treated conditions, in the shoot or root tissue (Figure 5.11). There were a higher number of DEGs in the shoot tissue, and as can be seen in Figure 5.11, the p values of the most significantly expressed genes in shoot tissue were much lower than the DEGs in the root tissue. In both conditions, there were more upregulated DEGs than downregulated. The 20 most significantly DEGs and their roles are shown in Table 5.1.

Table 5.1. Top 20 most significantly DEGs in shoot or root tissue in response to Pd treatment in Arabidopsis

Tissue type	Gene name	log2Fold change	p-value (adj)	Role
shoot	CAB4	-2.721	0.000	Encodes a chlorophyll a/b-binding protein that is more similar to the PSI Cab proteins than the PSII cab proteins.
shoot	PES1	2.993	0.000	Involved in cellular response to N starvation.
shoot	ATSRG1	5.316	0.000	Encodes a novel member of the Fe(II)/ascorbate oxidase gene family; senescence-related gene.
shoot	ATPCB	5.579	0.000	Class III peroxidase Perx34; involved in cell elongation, light-activated expression, may play a role in generating H2O2 during defense response.
shoot	ABS4	6.471	0.000	Enables xenobiotic transmembrane transporter activity, MATE transporter
shoot	SS2	4.283	0.000	Encodes AtSS-2 strictosidine synthase. Upregulated by the plant stress hormone, Jasmonate.
shoot	LHCB3	-3.767	0.000	A component of the main light harvesting chlorophyll a/b-protein complex of Photosystem II (LHC II).
shoot	ATGLN1;1	3.043	0.000	Encodes a cytosolic glutamine synthetase, the enzyme has high affinity with substrate ammonium
shoot	APP1	2.012	0.000	Arabidopsis aminopeptidase P1. Involved in ROS homeostasis.
shoot	ATGSTU3	9.747	0.000	Encodes GST belonging to the tau class of GSTs, acts upstream of or within toxin catabolic process. Involved in the GSH mediated detoxification pathway, and the Jasmonate pathway.
shoot	GLP5	4.093	0.000	Germin-like protein, active in the plasmodesma. Involved in altering root architecture in response to Fe deficiency.
shoot	IBR3	2.265	0.000	Encodes a protein with similarity to acyl-CoA dehydrogenases. Involved in the pathogen defense response.
shoot	AtRLP50	4.482	0.000	Receptor-like protein, located in extracellular region.
shoot	TBL17	2.641	0.000	Located in golgi trans cisterna, encodes leaf-senescence-related protein. A member of the TBL (TRICHOME BIREFRINGENCE-LIKE) gene family.
shoot	ASP3	2.877	0.000	Encodes the chloroplastic isozyme of aspartate aminotransferase. Involved in aspartate biosynthesis and N metabolism. mRNA is expressed in senescing leaves.
shoot	HBI1	-4.294	0.000	Acts upstream of or within negative regulation of innate immune response. ABA related protein.
shoot	ChiC	5.789	0.000	Enables chitinase, hydrolase activity. Upregulated in response to ABA, JA, salt, and osmotic stress.
shoot	BP80-3;1	4.140	0.000	An endosome located protein.

shoot	ATNRAMP3	3.254	0.000	Encodes a member of the NRAMP metal transporter family; like its homolog Atnramp4, localized in vacuolar membrane. Involved in exporting Fe from the vacuole.
shoot	ATGSTZ1	3.213	0.000	Encodes GST belonging to the zeta class of GSTs. Involved in the GSH mediated detoxification pathway.
root	HSP17.6A	2.293	0.021	Acts within the cellular response to hypoxia. Encodes a cytosolic heat shock protein with chaperone activity, induced by heat and osmotic stress.
root	GDU1	-2.263	0.000	Glutamine dumper 1. A putative transmembrane transporter, involved in glutamine secretion. Senescence related protein.
root	ATMYR1	-2.577	0.000	Transcription factor
root	AtPP2-B6	2.824	0.000	Acts upstream or within defense response to another organism
root	AtERF019	4.420	0.000	Encodes a member of the DREB subfamily A-5 of ERF/AP2 transcription factor family. Putative transcriptional activator related to the regulation of gene expression by stress.
root	ACS2	4.509	0.000	A member of the 1-aminocyclopropane-1-carboxylate (ACC) synthase (S-adenosyl-L-methionine methylthioadenosine-lyase, EC 4.4.1.14) gene family. Upregulated in response to water deprivation and salt stress, involved in ethylene biosynthesis.
root	AthCYSTM5	5.434	0.000	Non-secreted cysteine rich peptide, upregulated in the stress response
root	ATEXP4	-2.827	0.000	Putative expansin, involved in the formation of nematode-induced syncytia in roots of Arabidopsis. Acts in root elongation
root	FL3	-2.188	0.000	Acts upstream of or within monocarboxylic acid metabolic process.
root	DVL11	-2.351	0.000	Plasma membrane located protein, interacts with the transcription factor ASIL1 to reduce cell proliferation
root	ATHSP101	2.147	0.000	Encodes ClpB1, which belongs to the Casein lytic proteinase/heat shock protein 100 (Clp/Hsp100) family. Involved in refolding of proteins which form aggregates under heat stress.
root	ACL	-2.217	0.000	Encodes a protein shown to have carboxylesterase activity, methyl salicylate esterase activity, methyl jasmonate esterase activity, and methyl IAA esterase activity in vitro.
root	ATM4	6.136	0.000	Encodes a MYB transcription factor involved in wounding and osmotic stress response. Member of the R2R3 factor gene family.
root	ABCG14	-3.269	0.000	Plasma membrane located protein, essential for root to shoot cytokinin translocation
root	HSP17.4B	2.609	0.000	Acts upstream of or within cellular response to hypoxia
root	AtBAM1	2.131	0.000	Encodes a chloroplast beta-amylase. Is necessary for leaf starch breakdown in the absence of BAM3.

root	ATMYB2	3.085	0.000	Encodes a MYB transcription factor that possesses an R2R3 MYB DNA binding domain and is known to regulate the expression of salt- and dehydration-responsive genes. Has been shown to bind calmodulin.
root	EDA40	-2.450	0.000	Nucleus located protein, putative E3 ubiquitin protein ligase, involved in gametophyte development.
root	AER	4.544	0.000	Encodes a 2-alkenal reductase (EC 1.3.1.74), plays a key role in the detoxification of reactive carbonyls. Involved in the mitigation of oxidative stress relating to Cd ion stress.
root	CYP71B21	6.936	0.000	Putative CYP with oxidoreductase activity

As shown in the simplified schematic of metal transport in a eukaryotic cell in Figure 5.12, metal transporters are a key element in the interaction of metals with cellular components for uptake and detoxification. Metal transporters move metals into the cell (Figure 5.12, i, ii or iii) and out of the cell (Figure 5.12, iv) across the plasma membrane.
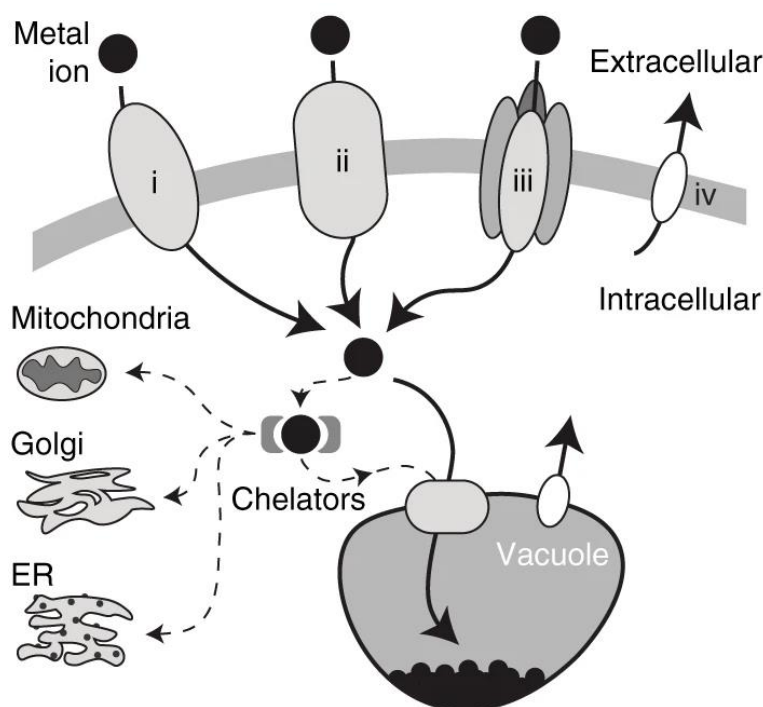
Figure 5.12. A simplified schematic of metal transport in a eukaryotic cell. Membrane transporters can be divalent cation metal transporters (i), permeases (ii), metal transporters that are modified or found to have auxiliary metal transport function (iii), or exporters which are used to remove excess metals out of the cell (iv). These transporters function in the plasma membrane as well as the membranes of cellular compartments such as the vacuole, mitochondria, golgi and endoplasmic reticulum. Alongside transporters, chelators play a large role in metal detoxification via binding to prevent the ROS generating activity of free ions, or to traffic metal ions to compartments where they will cause less damage. Figure reproduced from Sun et al. (2019) (251)

Once metals are in the cytosol, they can move to cellular compartments either with or without metal chelators. At the membranes of cellular compartments (vacuoles, golgi, mitochondria, endoplasmic reticulum), transporters act to regulate metal influx and efflux. To help elucidate the mechanism of Pd uptake and detoxification, the DEGs encoding for proteins with transporter activity in shoot or root tissue are shown in Figure 5.13 and described in Table 5.2. In shoot tissue, a total of 72 transporter encoding genes were DE, 35 of these were significantly upregulated, and 37 were significantly downregulated. There were a total of 26 significantly DEGs in root tissue, with 18 significantly upregulated, and 8 that were significantly downregulated (Figure 5.13), and these are listed in Table 5.3.
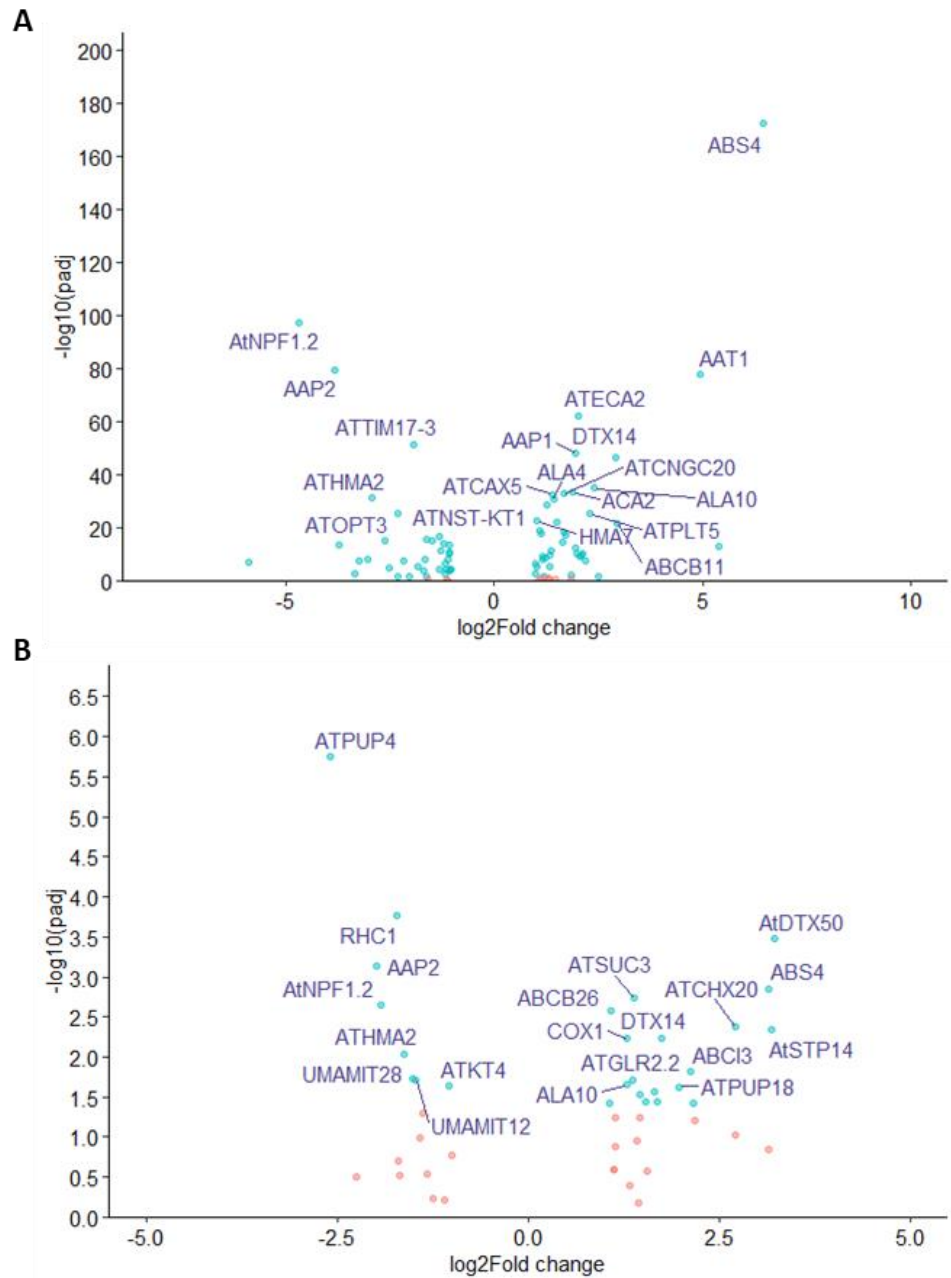
Figure 5.13. Volcano plots which show the distribution of DEGs encoding proteins with transporter activity following DE-analysis between undosed and Pd treated shoot (A) or root tissue (B). The points are coloured by the statistical significance (y-axis) and the magnitude of difference (x-axis): blue - statistical significance of $p < 0.05$ and log2Fold change of $\pm$ 1; red - statistical significance of $p > 0.05$ and log2Fold change within $\pm$ 1. Gene names are the top twenty most significantly DEGs in each dataset, ordered by the smallest adjusted p-value.
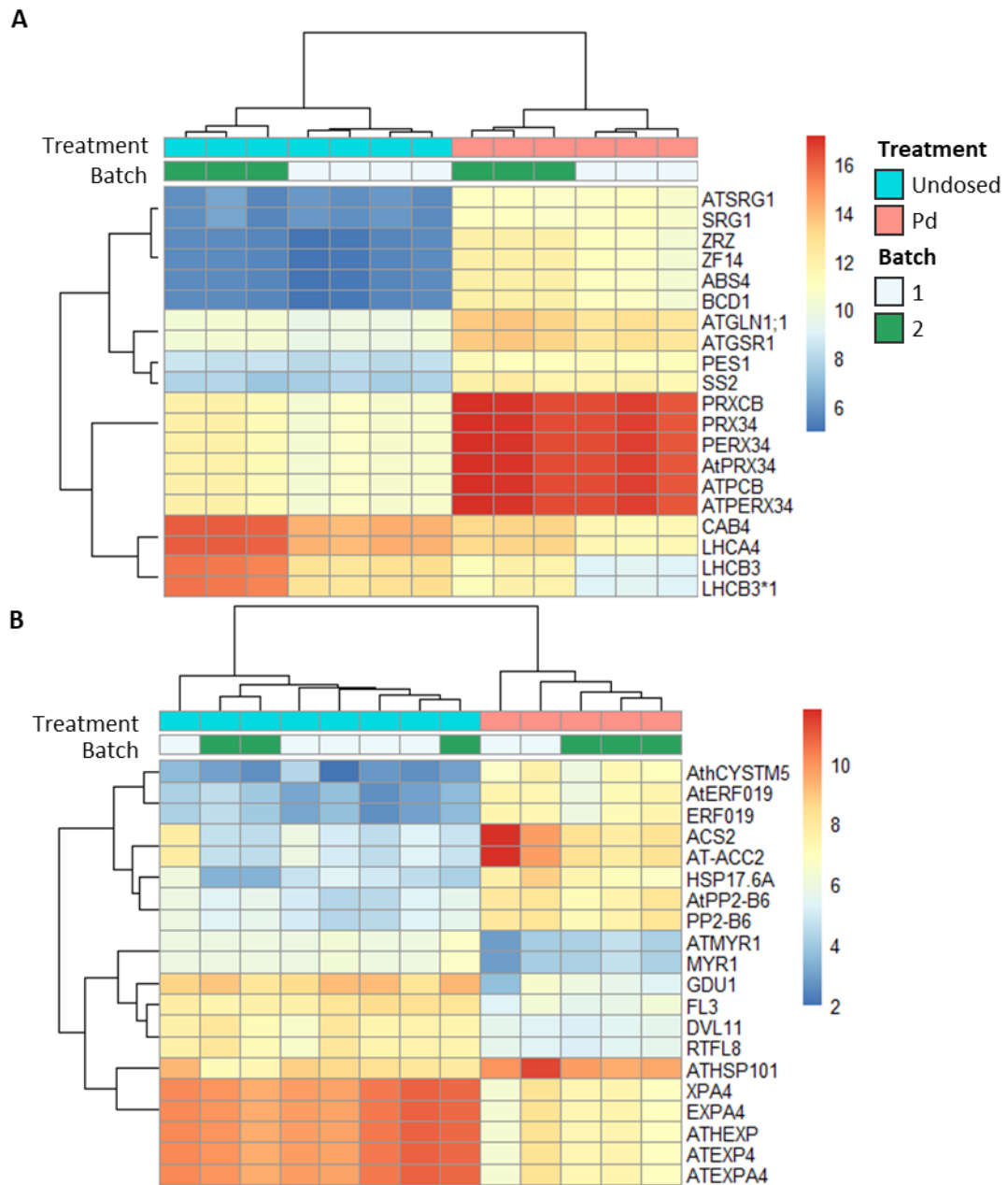
Figure 5.14. Heatmap showing the twenty most DE transporter genes in shoot (A) and root (B) tissue between undosed and Pd treated Arabidopsis five-week-old, hydroponically grown plants. Each column in the heat map represents a single sample and is coloured according to the log2Fold change of expression between undosed and Pd treated samples. Data is made up of two experiments (batch 1 & 2).

Of the DE transporter genes, there were 14 that were common between shoot and root tissue (Table 5.3). A heatmap of the top twenty significantly DE transporter genes for shoot and root tissue are shown in Figure 5.14. The heatmap shows how the samples split; with the predominant split between undosed and Pd conditions, followed by batch. As mentioned earlier, this analysis was performed on the samples from two independent experiments (batch 1 and batch 2, Figure 5.14), In shoot tissue, the samples within each experiment were most similar to one another; in root tissue there were fewer differences between the experiment batches (Figure 5.14). The two 'multidrug and toxic compound extrusion' (MATE) transporters (ABS4, DTX14) were significantly upregulated in both shoot and root tissue (Table 5.1). The Heavy Metal ATPase, AtHMA2, known to be involved in Zn homeostasis was downregulated in shoot and root tissue (Table 5.1), as was AtNPF1.2, a low affinity nitrate transmembrane transporter, present in the leaf vein phloem (Table 5.1). A plasma membrane localised MATE type transporter, RHC1, was also downregulated in shoot and root tissue (Table 5.1). Though not included in these tables as DE values were below the cut off, *COPT2* was significantly downregulated in shoot tissue in response to Pd (log2 fold change in shoots -0.787) but was not significantly changed in root tissue.

Table 5.2. The significantly DEGs encoding proteins with transporter activity in the shoot tissue in response to Pd in Arabidopsis. Genes highlighted in yellow are also present in the list of DEGs in root tissue. Though not included in these tables as DE values were below the cut off, *COPT2* was significantly downregulated in shoot tissue in response to Pd (log2 fold change in shoots -0.787) but was not significantly changed in root tissue.

Gene name	log2 fold change	p-value (adj)	Role
AAP1	1.972	0.000	Amino acid permease 1, member of AAAP family
AAP2	-3.804	0.000	Amino acid permease 1, member of AAAP family
AAT1	4.954	0.000	Encodes a member of the cationic amino acid transporter (CAT) subfamily of amino acid polyamine choline transporters. Mediates efficient uptake of Lys, Arg and Glu in a yeast system.
ABCB11	2.970	0.000	Encodes an ABC transporter. Also known as Multi-Drug Resistance 8 (MDR8)
ABCB12	-1.610	0.016	ATPase-coupled transmembrane transporter
ABCB2	-1.299	0.000	ATPase-coupled transmembrane transporter
ABCC11	1.714	0.000	Member of MRP subfamily, ABC-type xenobiotic transporter activity, multidrug resistance-associated protein 12
ABCC3	2.008	0.000	Encodes an ATP-dependent MRP-like ABC transporter able to transport GSH-conjugates as well as chlorophyll catabolites. The expression of this gene is upregulated by herbicide safeners such as benoxacor and fenclorim.
ABCG16	2.500	0.017	Jasmonate transporter. Belongs to a clade of five Arabidopsis ABCG half-transporters that are required for synthesis of an effective suberin barrier in roots and seed coats (ABCG2, ABCG6, and ABCG20) and for synthesis of an intact pollen wall (ABCG1 and ABCG16).
ABCG32	-1.152	0.001	ATPase-coupled transmembrane transporter, Encodes a member of the PLEIOTROPIC DRUG RESISTANCE family of ATP binding cassette transporters. Required for the formation of a functional cuticle.
ABCG33	-2.628	0.000	Encodes an ABC transporter. Known as Pleiotropic Drug Resistance 5
ABCG5	-2.168	0.000	ATPase-coupled transmembrane transporter, ABC-2 type transporter family protein
ABCG8	-3.698	0.000	ATPase-coupled transmembrane transporter, ABC-2 type transporter family protein
ABCI11	-1.620	0.000	Member of NAP subfamily, transmembrane transporter, ABC-transporter involved in metal homeostasis

Gene	Value	p	Description
ABS4	6.471	0.000	Encodes a plant MATE transporter that is localized to the golgi complex and small organelles and participates in determining the rate of organ initiation. It is also involved in Fe homeostasis when plants are under osmotic stress.
ACA2	1.898	0.000	ATPase-coupled cation transmembrane transporter. Encodes a calmodulin-regulated Ca(2+)-pump located in the endoplasmic reticulum. Belongs to plant 2B ATPase's with an N-terminal autoinhibitor
ACA4	-1.045	0.000	Encodes a calmodulin-regulated Ca(2+)-ATPase that improves salt tolerance in yeast. Localized to the vacuole.
AHA9	1.859	0.007	P-type proton-exporting transporter
ALA10	2.400	0.000	Encodes aminophospholipid ATPase10 (ALA10), a P4-type ATPase flippase that internalizes exogenous phospholipids across the plasma membrane.
ALA4	1.430	0.000	ATPase E1-E2 type family protein / haloacid dehalogenase-like hydrolase family protein, enables ATPase-coupled intramembrane lipid transporter activity. Involved in Mg ion binding
AMT1;2	-1.822	0.000	Encodes an ammonium transporter protein believed to function as a high affinity transporter. It is expressed in the root, primarily in endodermal and cortical cells, and contributes to ammonium uptake in the root.
ATCAT6	-1.633	0.000	Encodes a member of the cationic amino acid transporter (CAT) subfamily of amino acid polyamine choline transporters.
ATCAX1	-1.080	0.000	Encodes a high affinity vacuolar calcium antiporter. Involved in cellular manganese, Zn ion, phosphate ion homeostasis, and salt stress.
ATCAX5	1.411	0.000	Low affinity calcium antiporter CAX2 family
ATCNGC2	-1.105	0.000	A mutated cyclic nucleotide-gated cation channel, activated by cAMP, conducts K+ and other monovalent cations but excludes Na+, could be the key step mediating bulk Ca2+ influx into leaf cells after unloading from the vasculature
ATCNGC20	1.668	0.000	Cyclic nucleotide-binding transporter 1, member of a family of cyclic nucleotide gated channels.
ATDTX1	1.218	0.029	A detoxifying efflux carrier for plant-derived antibiotics and other toxic compounds, including Cd2+. Expression in rosette leaves is activated by high concentration of boron.
ATECA2	2.027	0.000	Type IIA (SERCA-type) Ca2+ ATPase, catalyzes the efflux of calcium from the cytoplasm.
ATHMA2	-2.924	0.000	Heavy metal ATPase 2, encodes a protein similar to Zn-ATPase, involved in Zn homeostasis
ATKT4	-1.257	0.000	Potassium transporter KUP3p (KUP3)
ATMTP11	-1.205	0.000	Encodes a golgi-localized manganese transporter that participates in Mn tolerance. When expressed into yeast cells, this gene confers Mn2+ tolerance.
ATMTP3	2.195	0.000	Metal tolerance protein 3. Member of Zn transporter (ZAT) family. Contributes to basic cellular Zn tolerance and controls Zn partitioning, particularly under conditions of high rates of Zn influx into the root symplast. Localizes to the vacuolar membrane.
ATNAT12	-1.031	0.000	Encodes a plasma-membrane localized nucleobase transporter capable of transporting adenine, guanine, uracil, and hypoxanthine. Likely to be a proton-nucleobase symporter.

AtNiaP	1.109	0.000	Encodes a plant nicotinate transporter that can also transport trigonelline (N-methylnicotinate).
AT-NLM1	-2.036	0.043	An aquaporin whose expression level is reduced by ABA, NaCl, dark, and desiccation. Involved in arsenite transport and tolerance, hydrogen peroxide transmembrane transport.
AtNPF1.2	-4.664	0.000	Encodes a low affinity nitrate transporter that is expressed in the plasma membrane and found in the phloem of the major veins of leaves. It is responsible for nitrate redistribution to young leaves.
ATNST-KT1	1.277	0.000	Encodes a golgi localized nucleotide sugar transporter.
ATOPT1	2.106	0.000	oligopeptide transporter
ATOPT3	-2.298	0.000	Encodes an oligopeptide transporter
ATPLT5	2.305	0.000	A plasma membrane-localized polyol/cyclitol/monosaccharide-H+-symporter, belongs to a monosaccharide transporter-like (MST-like) superfamily.
ATPROT2	1.226	0.000	Encodes a proline transporter with affinity for gly betaine, proline, and GABA. Protein is expressed most highly in the roots.
ATPUP12	1.334	0.000	Member of a family of proteins related to PUP1, a purine transporter. May be involved in the transport of purine and purine derivatives such as cytokinins, across the plasma membrane.
ATPUP13	-1.075	0.000	Member of a family of proteins related to PUP1, a purine transporter. May be involved in the transport of purine and purine derivatives such as cytokinins, across the plasma membrane.
ATPUP2	-2.517	0.000	Member of a family of proteins related to PUP1, a purine transporter. May be involved in the transport of purine and purine derivatives such as cytokinins, across the plasma membrane.
ATPUP4	-3.028	0.000	Member of a family of proteins related to PUP1, a purine transporter. May be involved in the transport of purine and purine derivatives such as cytokinins, across the plasma membrane.
ATSUC3	1.002	0.000	Encodes a sucrose transporter in sieve elements and a number of sink tissues and cell types. Gene expression is induced by wounding.
ATTIM17-1	2.134	0.000	Mitochondrial inner membrane translocase
ATTIM17-3	-1.933	0.000	Mitochondrial inner membrane translocase
ATTIP2;3	-2.306	0.017	Tonoplast intrinsic protein, transports ammonium (NH3) and methylammonium across the tonoplast membrane, gene expression shows diurnal regulation and is upregulated by ammonium (NH3).
ATUTR3	1.005	0.003	UDP-galactose transporter 3
AtVTL5	-3.221	0.000	The gene encodes nodulin-like21 whose transcript abundance was repressed under conditions of Fe-deficient growth.
ATYSL3	1.173	0.000	Yellow-stripe-like 3 proteins involved in developmental process, response to Fe ion
ATZIP9	5.405	0.000	Member of Fe(II) transporter isologue family, also acts in response to Zn ion

BASS6	1.666	0.000	Sodium Bile acid symporter family
CAT9	1.118	0.000	Encodes a member of the cationic amino acid transporter (CAT) subfamily of amino acid polyamine choline transporters.
DiT2.2	-1.068	0.000	Dicarboxylate transporter 2.2
DTX14	2.922	0.000	Xenobiotic transmembrane transporter, ATPase-coupled transmembrane transporter. MATE transporter that can export the antibiotic norfloxacin
GORK	-1.060	0.000	Encodes a guard cell outward potassium channel. Expression is suppressed during *Agrobacterium*-induced tumor formation and increased in response to water deprivation and cold.
HMA7	1.047	0.000	Heavy metal associated protein; ATP dependent Cu transporter vital for ethylene response pathway
KUP11	1.354	0.000	Potassium ion uptake transporter
MSL4	2.051	0.000	Mechanosensitive channel of small conductance-like 4, involved in response to water deprivation
NPF5.11	-1.469	0.000	Tonoplast localised, pH dependent, low affinity N transporter in shoots, expressed in leaf veins and mesophyll
PIP2;6	-1.299	0.000	Plasma membrane intrinsic protein 2;6. Involved in cell wall biogenesis, response to water deprivation
PML5	1.025	0.000	Photosynthesis affected mutant 71 like 5, member of the UPF0016 family of membrane proteins, belongs to the conserved group of Mn/Ca transporters. Might act to fine tune Mn allocation into the endoplasmic reticulum of specific cell types.
PUT1	1.362	0.000	Polyamine uptake transporter 1, an amino acid permease family protein
RHC1	-1.161	0.000	Resistant to high CO2. Encodes a plasma membrane localized MATE type transporter that participates in CO2 signaling during stomatal aperture regulation.
RTP1	-5.889	0.000	Encodes an endoplasmic reticulum (ER)-localized nodulin MtN21-like transporter family protein that negatively regulates resistance against biotrophic pathogens
STP12	-1.150	0.000	Putative sugar transporter. Expressed in nematode-induced root syncytia.
SULTR3;2	-1.681	0.000	Sulfate transporter 3, integral component of the plasma membrane
TMT3	-3.344	0.003	Tonoplast monosaccharide transporter 3
UMAMIT20	1.950	0.000	Nodulin MtN21-like transporter family protein, Usually Multiple Acids Move In and Out Transporter 20
UMAMIT28	1.164	0.000	Encodes a plasma membrane localised amino acid transporter involved in amino acid export in the developing seed. UMAMIT 28.

Table 5.3. The significantly DEGs encoding proteins with transporter activity in the root tissue in response to Pd treatment in Arabidopsis. Genes highlighted in yellow are also present in the list of DEGs in root tissue.

Gene name	log2 Fold change	p-value (adj)	Role
ATPUP4	-2.599	0.000	Member of a family of proteins related to PUP1, a purine transporter. May be involved in the transport of purine and purine derivatives such as cytokinins, across the plasma membrane. Putative water/calcium channel.
AAP2	-1.996	0.001	Amino acid permease 2, member of AAAP family
AtNPF1.2	-1.930	0.002	Low-affinity nitrate transmembrane transporter, found in the phloem of the veins of leaves
RHC1	-1.734	0.000	Resistant to high CO2. Encodes a plasma membrane localized MATE type transporter that engages in CO2 signaling during stomatal aperture regulation.
ATHMA2	-1.637	0.009	Heavy metal ATPase 2, encodes a protein similar to Zn-ATPase, involved in Zn homeostasis
UMAMIT28	-1.512	0.019	Encodes a plasma membrane-localised amino acid transporter involved in amino acid export in the developing seed
UMAMIT12	-1.475	0.019	ATPase-coupled transmembrane transporter, nodulin MtN21-like transporter family protein, Usually Multiple Acids Move In And Out Transporter 12
ATKT4	-1.043	0.023	Potassium ion transmembrane uptake transporter
ATCNGC20	1.066	0.038	Cyclic nucleotide-binding transporter 1, member of a family of cyclic nucleotide gated channels.
ABCB26	1.075	0.003	ATPase-coupled transmembrane transporter, member of TAP subfamily
ALA10	1.283	0.022	Encodes aminophospholipid ATPase10 (ALA10), a P4-type ATPase flippase that internalizes exogenous phospholipids across the plasma membrane.
COX1	1.289	0.006	Cytochrome c oxidase subunit 1, involved in the respiratory electron transport chain
ATGLR2.2	1.369	0.019	Intracellular ligand-gated ion channel, glutamate receptor
ATSUC3	1.389	0.002	Encodes a sucrose transporter in sieve elements and several sink tissues and cell types. Gene expression is induced by wounding.
PIP2;6	1.460	0.029	Plasma membrane intrinsic protein 2;6. Involved in cell wall biogenesis, response to water deprivation
AAT1	1.535	0.037	Encodes a member of the cationic amino acid transporter (CAT) subfamily of amino acid polyamine choline transporters. Mediates efficient uptake of Lys, Arg and Glu in a yeast system.

ATPUP8	1.640	0.027	Member of a family of proteins related to PUP1, a purine transporter. May be involved in the transport of purine and purine derivatives such as cytokinins, across the plasma membrane.
ATGLR2.4	1.693	0.036	Member of Putative ligand-gated ion channel subunit family, glutamate receptor 2.4
DTX14	1.738	0.006	Xenobiotic transmembrane transporter, ATPase-coupled transmembrane transporter. MATE transporter that can export the antibiotic norfloxacin
ATPUP18	1.970	0.023	Member of a family of proteins related to PUP1, a purine transporter.
ABCI3	2.122	0.015	Heme transporter, Cytochrome-C biogenesis
ATCNGC19	2.167	0.038	Member of Cyclic nucleotide gated channel family
ATCHX20	2.712	0.004	Member of Putative Na+/H+ antiporter family. Involved in the osmoregulation through K(+) fluxes and pH modulation of an active endomembrane system in guard cells. Solute:proton antiporter activity.
ABS4	3.143	0.001	Xenobiotic transmembrane transporter. Encodes a plant MATE transporter. Involved in Fe homeostasis under osmotic stress.
AtSTP14	3.183	0.000	Galactose transmembrane transporter
AtDTX50	3.217	0.000	Detoxification Efflux Carrier 50, MATE efflux family protein

5.3.1. Pathways and downstream analysis

Identification of pathways common to the DEGs was performed using clusterProfiler4.0 in RStudio, Identification of pathways common to the DE-genes was performed using clusterProfiler4.0 in RStudio, using the *enrichGO* function. An over-representation analysis (ORA) was performed to identify the significant biological processes associated with the significantly DE-genes. The ORA uses gene ontology (GO) annotations to group the DEGs by their biological pathways, to determine which are enriched in response to Pd-treatment. Gene ontology annotation was taken from the Arabidopsis TAIR annotation OrgDb package provided by the Bioconductor project (252,253) and the DE-genes were identified by a log2 fold change of > 2. The top 15 results are represented for shoot and root tissue in Figure 5.15. As shown in Figure 5.15A, a high proportion of the DE-genes in the shoot tissue were related to cellular processes:

- Vesicle-mediated transport
- Generation of precursor metabolites and energy
- Plastid organisation
- Cytoskeletal organisation
- Photosynthesis

There were also a high number of genes involved in biological processes relating to the response of the plant to metal ions, with the genes specific to Cd ions playing a dominant role. The enriched biological processes in root tissue resulting from Pd treatment are shown in Figure 5.15B. There was a much stronger prevalence of genes relating to osmotic processes; five out of the fifteen most enriched biological processes relate to oxygen stress (response to decreased oxygen levels, response to oxygen levels, response to hypoxia, cellular response to decreased oxygen levels, cellular response to oxygen levels, cellular response to hypoxia). There was also a significant enrichment of biological processes relating to the general stress, defence and immune response (regulation of response to stress, regulation of defense response, immune system processes, response to JA).
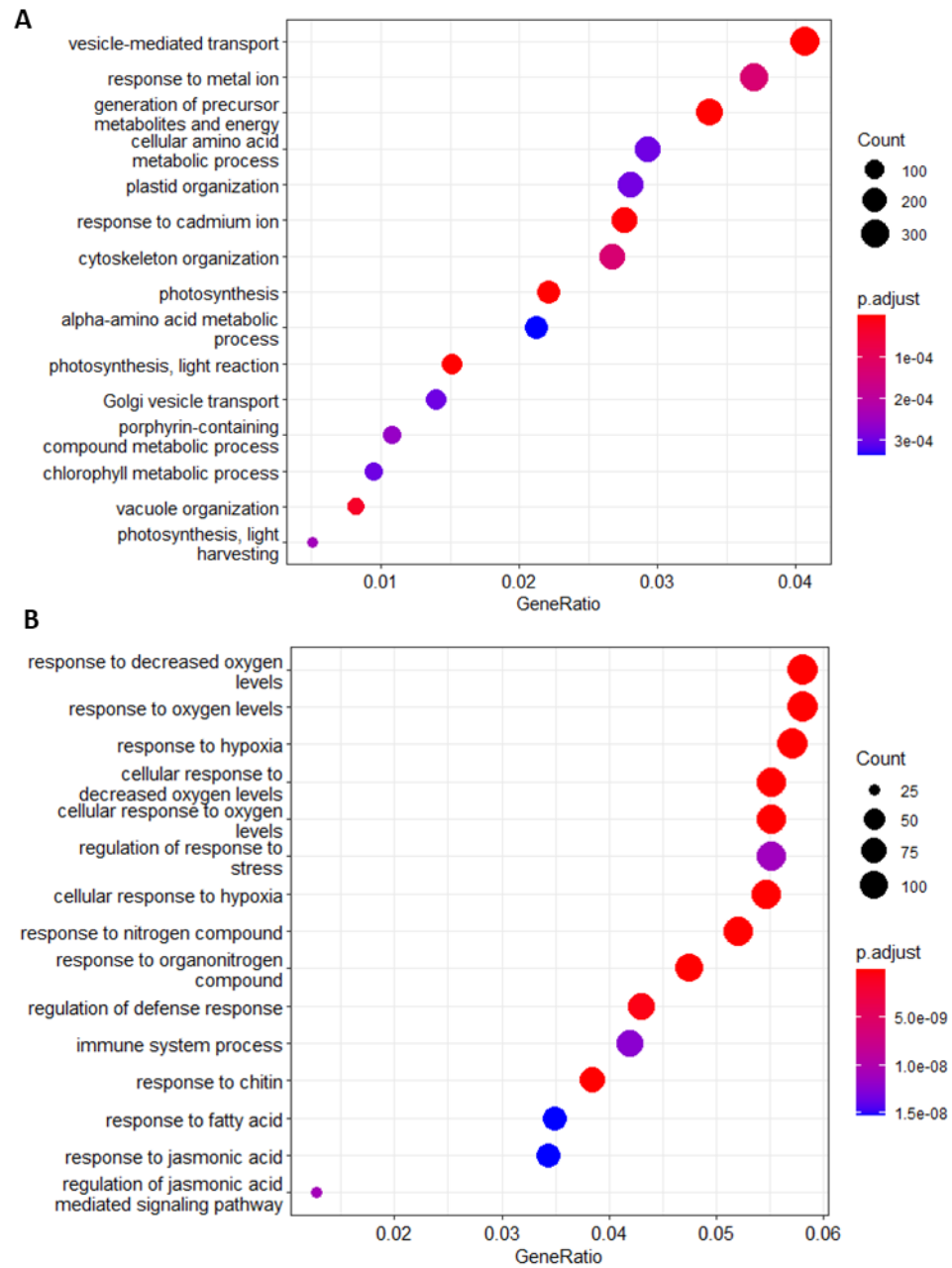
Figure 5.15. Dotplot demonstrating the results of a gene ontology (GO) enrichment analysis on the DEGs in shoot (A) and root (B) tissue between undosed and Pd treated samples (log 2 fold change > 2; adjp < 0.05).

5.4. Discussion
5.4.1.   Overview

The RNA-seq analysis of the Arabidopsis transcriptome in response to Pd demonstrated that this response is complex, involving transcription factors, transporters, aquaporins, oxidases, peroxidases, chaperones, and genes relating to cellular processes. There was a more prevalent stress and cellular death response in the root tissue, which demonstrated a downregulation of genes relating to metabolism and growth, and an upregulation of genes relating to osmotic and salt stress. The shoot tissue also demonstrated an enrichment of biological processes relating to stress and metabolism with a downregulation of photosynthesis related genes. Both tissue types showed an upregulation of senescence-related genes. The most enriched biological processes were dominated by general stress and hypoxia responses in the roots, likely a result of the low oxygen levels in the experimental system used, with a more specific metal ion response in the shoots.

Universally, genes relating to the plant stress were DE in response to Pd. These are composed of various plant stress responses: genes relating to JA, abscisic acid, ethylene synthesis, osmotic and salt stress, response to ROS and pathogen related defense genes.

5.4.2.   Metal ion transport and Cd detoxification

There was an enrichment of biological pathways relating to metal ion responses, especially in relation to Cd ions. The prevalence of Cd-specific pathways is skewed by the relatively high number of studies in the literature for this metal. However, enrichment of other genetic metal ion response pathways does suggest that the Arabidopsis response towards Pd is specific to Pd, and the Pd-DE gene set may encode increased resistance to other metal ions. Non-essential to plants, Cd is a widely spread pollutant, ubiquitous in the environment because of both anthropogenic activities, and natural geological deposits. Cadmium is readily taken up by plants likely due to its similarity to the essential plant element Zn, a necessary plant element, for which it shares multiple transporters, for instance, the ZIP family of transporters (254). In plant tissue, Cd reduces the uptake and translocation of water and nutrients (Ca, Fe, K, Mg, manganese, phosphorus, S, Zn), disrupts metabolism and increases the production of ROS, all of which inhibit plant growth and physiology (215,255,256). For instance, peroxidase induction is significantly, positively correlated to the level of Zn, Cd and Cu in the tissue of various plant species (257). Zinc, Cd and Pd can exist as divalent cations, and share some chemical properties, demonstrated by their proximity to one another in the periodic table (atomic number 30, 48 and 46 respectively). As shown in Table 5.4, the effective ionic radii of the elements are also similar, with Zn^{2+} at 74 pm, Cd^{2+} at 95 pm, and Pd^{2+} at 86 pm, which may account for the cross-over in the expression profiles of these elements.

Table 5.4. Properties of the main elements discussed in this chapter. Electronegativity is defined as a chemical property that describes the tendency of an atom or a functional group to attract electrons towards itself. It is affected by the atomic number and the distance that its valence electrons (located in the outermost shell of an atom and can be shared or transferred to another atom) reside from the charged nuclei. The higher the value of electronegativity, the more strongly that element attracts the shared electrons. On the Pauling scale, fluorine is assigned an electronegativity of 3.98 and the other elements are scaled relative to that value. A major review of crystallographic data led to the publication of revised ionic radii by Shannon (258). Shannon gives different radii for different coordination numbers, and for high [*hs*] and low [*ls*] spin states of the ions, termed 'effective ionic radii'. Shannon also gives data according to the 'crystal ionic radii', which correspond more closely to the physical size of ions in a solid. The ions are in a 6-coordinate configuration unless otherwise stated in [ ] e.g. [2]

Element	Atomic number	Atomic mass (g/mol)	Electro-negativity (Pauling scale)	van der Waals radius (nm)	Common oxidation states	Effective ionic radii, according to Shannon (pm)	Crystal ionic radii, according to Shannon (pm)
Ag	47	107.79	1.9	0.245	+1, +2	115 (+1), 94 (+2), 75 (+3)	129 (+1); 108 (+2), 89 (+3)
Au	79	196.97	2.4	0.245	+1, +3	137 (+1), 85 (+3), 57 (+5)	151 (+1); 99 (+3); 71 (+5)
Cd	48	112.4	1.7	0.249	+2	95 (+2)	109 (+2)
Cu	29	63.546	1.9	0.238	+1, +2	77 (+1), 73 (+2), 54 [*ls*] (+3)	91 (+1); 87 (+2); 68 [*ls*] (+3)
Fe	26	55.847	1.83	N/A	+2, +3, +4, +6	61 [*ls*] or 78 [*hs*] (+2), 55 [*ls*] or 64.5 [*hs*] (+3), 58.5 (+4), 25 [4] (+6),	75 [*ls*] or 92 [*hs*] (+2), 69 [*ls*] or 78.5 [*hs*] (+3), 72.5 (+4), 39 [4] (+6),
Pd	46	106.42	2.2	0.215	+2, +4	59 [2] (+1), 86 (+2), 76 (+3), 61.5 (+4)	73 [2] (+1); 100 (+2); 90 (+3); 75.5 (+4)
Zn	30	65.37	1.6	0.239	+2	74 (+2)	88 (+2)

The DE genes relating to metal ion stress in this work include xenobiotic transporters, heavy metal ATPases (HMAs), and detoxification-related genes. The response of the transcriptome also demonstrates that Pd elicits a significant interaction of genes relating to Fe starvation. The effective ionic radii of Fe^{2+} is 61 [*ls*] or 78 [*hs*], similar to the effective ionic radii of Pd^{2+} which is 86, potentially allowing for Pd^{2+} to enter via Fe^{2+} transport mechanisms. Fe deficiency responses have shown to result in an increased uptake of Cd^{2+} (259), and as Pd treatment has resulted in the differential expression of multiple Cd related genes, it is possible that Pd^{2+} is also transported into and around plants via Fe mechanisms.

5.4.3. The heavy metal ATPases (HMAs)

The heavy metal ATPase (HMA) family exists across plant species, as shown in Figure 5.16. There are eight members of the HMA family in Arabidopsis, and these metal transporters are varied in their distribution in tissues, subcellular localization, and metal specificity, and are split into two subgroups based on their specificity.
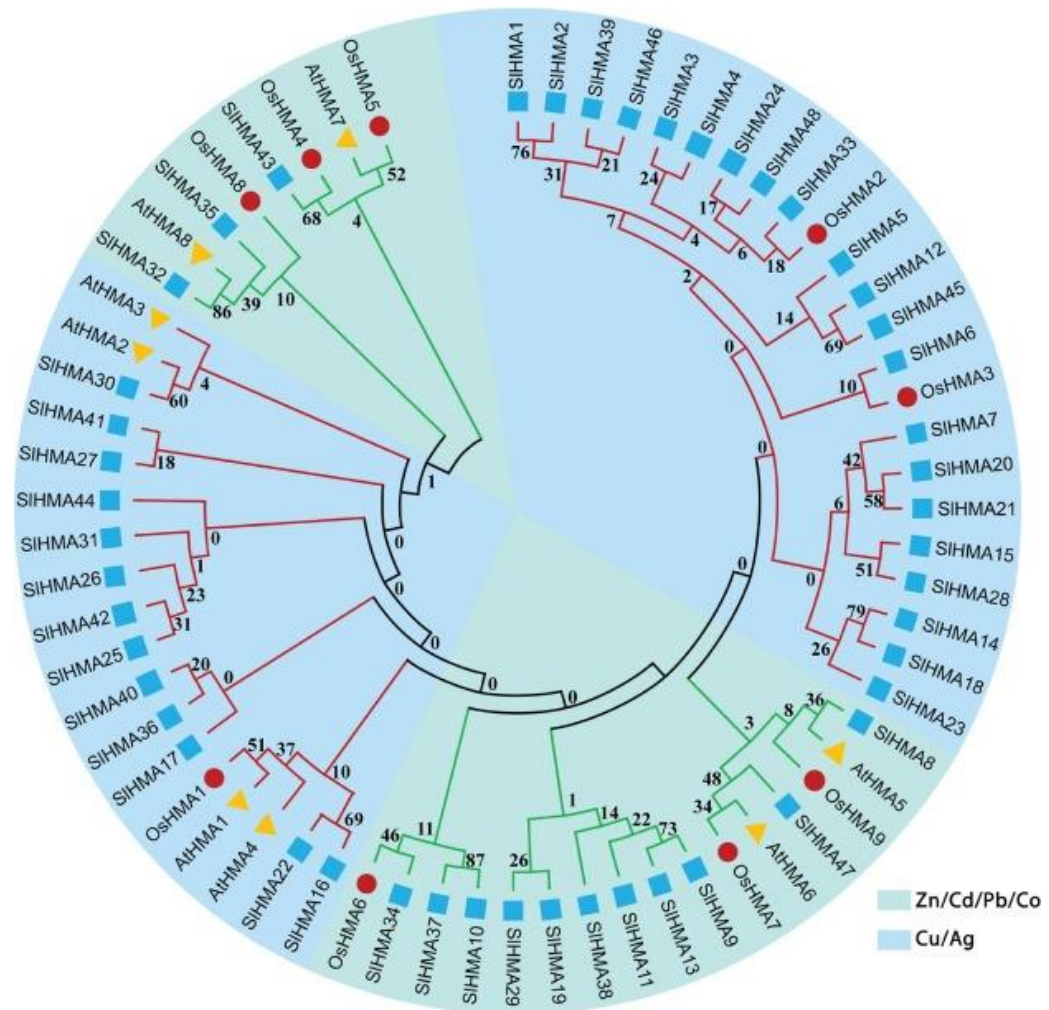
Figure 5.16. Evolutionary analysis of HMA members. The phylogenetic tree depicts the relationship between *Solanum lycopersicum* (tomato, Sl), Arabidopsis (At), and *Oryza sativa* (rice, Os) HMA proteins. Different background colors indicate the subgroups (bluish mint area represents the Zn/Cd/Co/Pb subgroup; light blue area represents the Cu/Ag subgroup). The blue solid squares, yellow solid triangles, and red solid circles represent the tomato, Arabidopsis, and rice HMA proteins, respectively. Each subgroup has two clades based on the presence or absence of the E1-E2 domain with the HMA domain. Figure reproduced from Hasan et al. (2022) with permission from Elsevier (260)

Arabidopsis *HMA2* (Zn/Cd specific) is expressed in tissues surrounding the vasculature, localised to the plasma membrane, and functions in Zn and Cd efflux from cells to maintain the root-to-shoot translocation of Zn/Cd in Arabidopsis (261). The Zn/Cd hyperaccumulating species *A.halleri* demonstrated a major QTL locus conferring Cd tolerance for *HMA4*, which has been shown to function in conjunction with *HMA2* (261). However, in this study, *HMA2* was downregulated in both

shoot and root tissue. A previous study demonstrated that the root accumulation of Zn may be preferable to plants to aerial tissue accumulation to minimise damage to photosynthetic tissues and importantly, seed production (262). Thus, the downregulation of *HMA2* is likely to result in reduced Pd^{2+} root-to-shoot translocation. This finding agrees with the results of the element analysis performed in the previous chapter, which demonstrated significantly lower Pd shoot concentration compared to the root (3.3.2.15).

There is a crosstalk between auxins and other phytohormones in response to heavy metal stress, including abscisic acid (ABA), ethylene and salicylic acid (SA) name a few (263). The phytohormone ethylene mediates a variety of signaling processes in response to abiotic stress in plants, with metal-stress resulting in an increase in ethylene production. The HMA7 protein is integral in Cu trafficking from the cytosol into the golgi apparatus, where Cu is deposited as a reserve for later use as a cofactor in enzymes involved in post-translational protein modification. The Cu is transported by HMA7 to the Ethylene Response 1 (ETR1) receptor, localised initially in the golgi apparatus and then the plasma membrane (Binder et al. 2010). The ETR1 requires Cu^{2+} for its activation and the binding of ethylene (Binder et al 2010). In yeast, *HMA7* expression rescued the Cu^{2+} dependent phenotype in a strain lacking a *HMA7 orthologue, ccc2*. (Yuan et al 1997). In the bladder campion plant (*Silene vulgaris*)*, HMA7* is upregulated following Cu treatment, as it is in this study in response to Pd (264).

5.4.4.   The Zn-regulated, Fe-regulated transporter-like protein family (ZIP)

The Zn-regulated, Fe-regulated transporter-like protein family (ZIP) are also involved in metal ion transportation in plants. As shown in Figure 5.17, there are over 100 members of the ZIP family in plants, and these have been shown to be involved in Mn, Fe, Cd, Co, Cu and Ni transport (265).
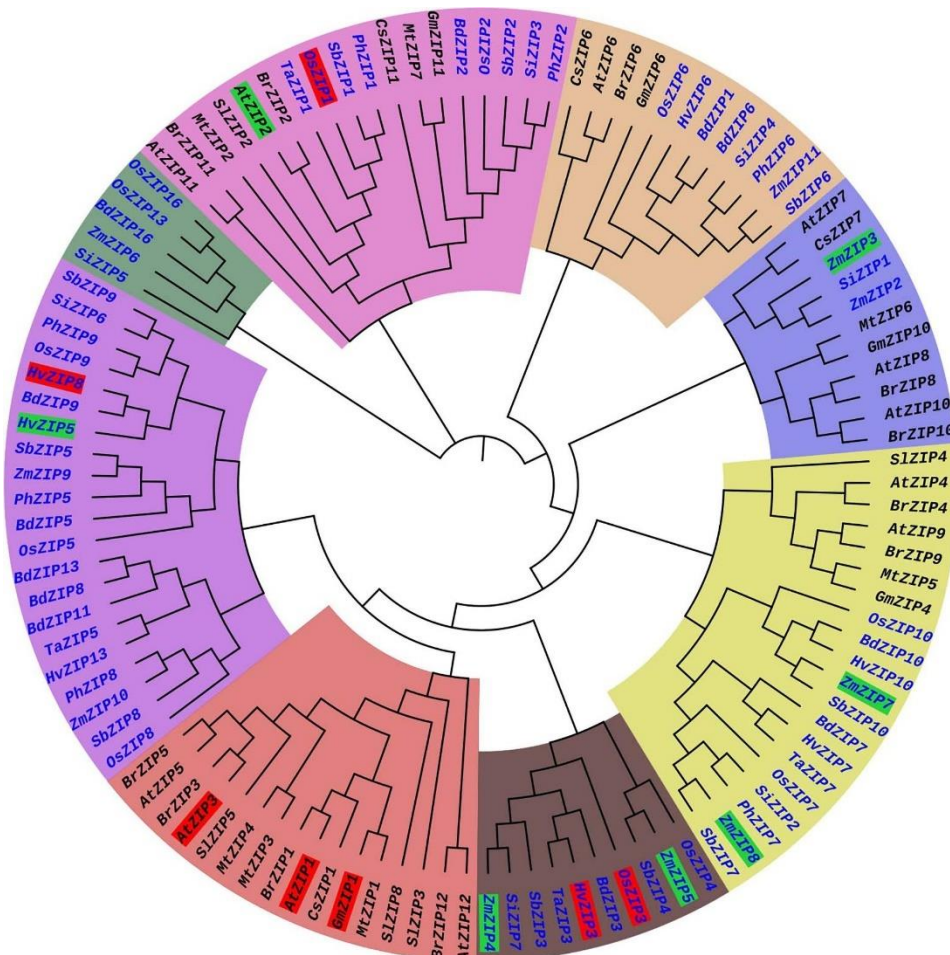
Figure 5.17. Phylogenetic tree of ZIP transporter family proteins of plants. The ZIP phylogenetic tree was constructed from 113 ZIP transporter protein sequences collected from 14 plant species. These included 8 monocot (Blue) and 6 dicot plants (Black). Each major cluster (MC1-MC8) is highlighted with different color. The low-affinity and high-affinity ZIP transporters are highlighted in red and green, respectively. The protein sequences of ZIP transporter family members were collected from Phytozome (www.phytozome.net) website. The phylogenetic tree was constructed by MEGA version 6 software with the maximum likelihood method based on the Jones-Taylor-Thornton matrix-based model. The bootstrap values are from 1000 replicates. The phylogeny tree was visualized by iTOL. Figure reproduced from Krishna et al. (2020) (254)

In the results shown above, the ZIP9 is highly upregulated in shoot tissue in response to Pd treatment, and is upregulated by Zn deficiency in Arabidopsis (266). Perhaps at the relatively high concentrations used in the hydroponic system, Pd bound, albeit weakly, in place of Zn to sufficient numbers of Zn-containing enzymes, to disrupt necessary metabolic pathways that the plants required for survival. Such disruption could result in a perceived Zn-deficiency , thereby increasing the Zn-deficiency response.

5.4.5. The multidrug and toxic compound extrusion (MATE) family of transporters

The multidrug and toxic compound extrusion (MATE) transporter family take up secondary metabolites, xenobiotics, organic molecules, hormones and are involved in Fe homeostasis, senescence, regulation of cell and organ size and disease resistance (267–270). The MATE proteins are capable of disposing of and detoxifying exogenous and endogenous toxins by extrusion using Na^+ or H^+ electrochemical gradients, in response to various stressors (271). The MATE proteins have been identified in archaea, bacteria, fungi, plants and mammals, with plant genomes encoding a far higher number of MATE proteins than other genomes (269).
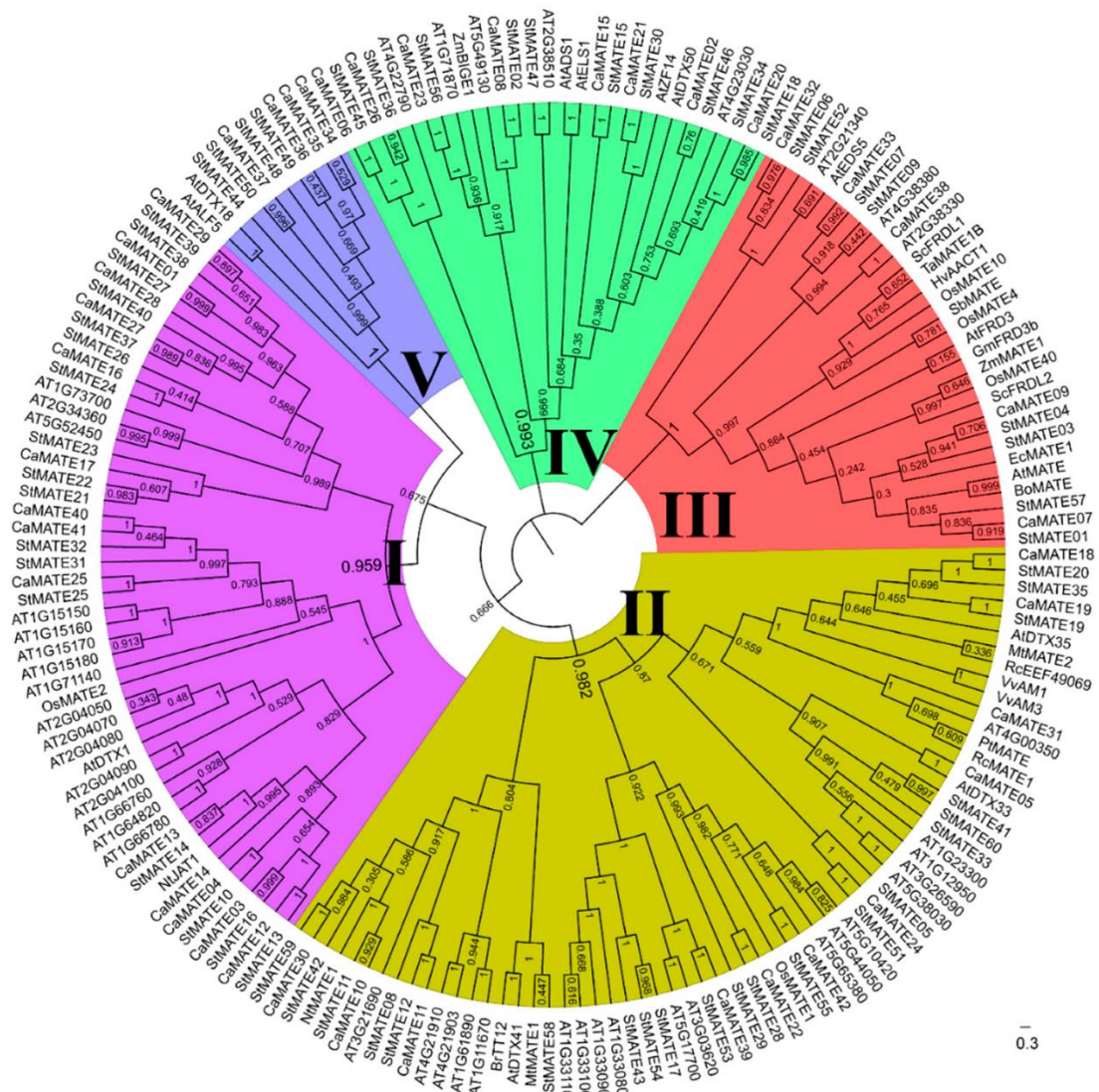
Figure 5.18. The phylogenetic relationship of 42 CaMATE (from *Capsicum annuum*), 60 StMATE (from *Solanum tuberosum*), and 56 AtMATE (from Arabidopsis) proteins alongside 25 other functional published MATE proteins. The phylogenetic tree was constructed using MEGA X with the Maximum Likelihood method and visualised with FigTree software. MATE proteins were classified into five distinct groups, as indicated by the different colours. Taken from Chen et al (2020) (272).

The structure of a MATE protein is typically 450 – 550 aa long with a conserved PF01554 domain which consists of 12 alpha-helical TMDs (273). The MATE protein family were highly represented in the DE genes in response to Pd. The MATE family of transporters are present in all forms of life, with 58 different members of the family in Arabidopsis (also known as DTX proteins), a far higher number than are present in bacteria, yeast and animals (218). These transporters are involved in diverse functions relating to abiotic and biotic stress resistance, demonstrating their non-specific action.

The MATE family member *DTX14*, upregulated in shoot and root tissue in response to Pd is located on the plasma membrane where it has been shown to export norfloxacin, a fluoroquinolone antibiotic. The *AtDTX14* transporter has 50% similarity to *AtDTX1*, which is localised on the plasma membrane of cells and is capable of detoxifying a variety of compounds including Cd ions (139). It functions from its site of synthesis after being transported by ABA-specific transporters, one of which is DTX50, which localised to the plasma membrane of vascular tissues and guard cells, regulating the efflux of ABA in response to drought, and whose transcription is upregulated in root tissue in response to Pd (274).

5.4.6.   The ATP binding cassette (ABC) transporters

The ATP binding cassette (ABC) transporters are involved in the transport of molecules across intra- and extra-cellular membranes (275). As shown in Figure 5.19, the ABC transporters are defined by the presence of an ATP-binding cassette. The ABC transporters have several conserved motifs including the Walker A and B sequences, the ABC signature motif, the H loop, the Q loop, and TMDs comprised of several hydrophobic α-helices (276). The core domains include two ATP-binding cassettes, which bind and hydrolyse ATP, and two TMDs which are involved in substrate recognition and translocation across the lipid bilayer (276).
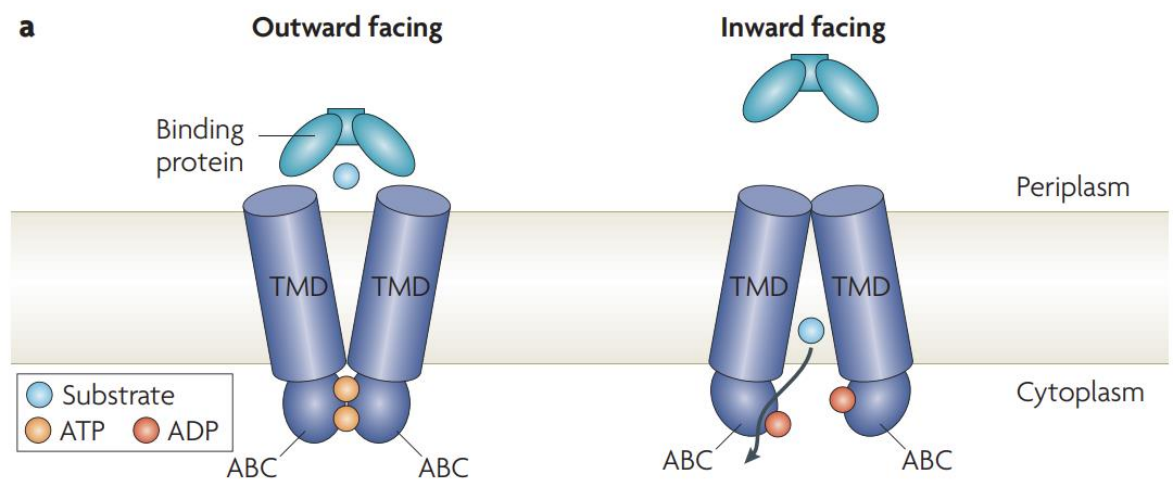
Figure 5.19. The ABC transporters. TMD refers to transmembrane domain, ABC to the ATP-binding cassette subunit, N refers to the N-terminal end of the protein sequence, C refers to the C-terminal end of the protein sequence (a) Cartoon of the modular organization of ABC transporters, which are composed of two transmembrane domains (TMDs) and two ABC domains (or nucleotide-binding domains). Two conformational states of the ABC transporter — outward facing (left) and inward facing (right), with the substrate-binding site orientated towards the periplasmic (extracellular) and cytoplasmic (intracellular) regions, respectively, are depicted to show the alternating access mechanism of transport. Reprinted by permission from Springer Nature: Nature Reviews Molecular Cell Biology, Rees et al. (2009) (277)

Plants have a high number of ABC transporters compared to other organisms, with 120 ABC transporters in Arabidopsis. There has historically been some confusion over the naming of ABC proteins, some of which continues today. Verrier et al (2008) published a 'unified nomenclature and updated inventory' of the ABC proteins, including a comprehensive collection of the previous and new name for Arabidopsis ABC proteins (278). The current classification system for ABC transporters in plants is based on the protein solubility, presence of TMDs, their function and amino acid sequence. Using phylogenetic analyses groups most eukaryotic ABC proteins into eight major subfamilies (A – H); due to the large number and diversity of the ABC proteins in plants, there is an extra subfamily present to incorporate the 'prokaryotic'-type ABC proteins that are not present in most animal genomes (I) (279).

Figure 5.20. Phylogenetic analysis of Arabidopsis ABC protein sequences. Protein sequences were aligned using ClustalX (6) and subjected to phylogenetic analysis by the distance with neighbour-joining method (7) using PAUP4.04a (8). The reliabilities of each branch point, as assessed by the analysis of 1000 computer-generated trees (bootstrap replicates), were, for the most part, 90% except for those discussed in the text. Figure reproduced from Sanchez-Fernandez et al (2001) (280)

A high degree of sequence similarity between ABC proteins doesn't necessarily indicate shared function, for example, the AtABCC7 is not orthologous or functionally equivalent to OsABCC7 or HsABCC7 (166). The ABC gene names are structured as follows: i) a species identifier based on the Latin binomial, ii) the HUGO ABC subfamily abbreviation (e.g., ABCA, ABCB), iii) a number for each gene family member. The following subgroups are part of the ABC protein superfamily: Multidrug resistance / Transporter associated with antigen processing (MDR/TAP), Multidrug resistance associated proteins (MRP), adrenoleukodystrophy protein related (ALD), organic anion binding protein (OABP), the GCN20s and the White subfamily .The roles of the ABC transporters include the transport of hormones, lipids metals, secondary metabolites and xenobiotics, as well as being involved in plant-pathogen interactions and the modulation of ion channels (166).

The multidrug resistance associated proteins (MRP, ABCC) subfamily of ABC transporters were originally thought to be involved in the vacuolar sequestration of toxic metabolites, but have more recently been shown to also be involved in plant transpiration through the stomata (281). Phylogenetic analysis of the Arabidopsis ABCC/MRPs divided them into two subclades: clade I (ABCC/AtMRP1, 2, 11 and 12) and clade II (containing the ten other members). In this work, ABCC11 was upregulated in the shoot tissue in response to Pd. Previous work suggested that ABCC1 and 2, which demonstrate similarity to ABC11, localise to the tonoplast and exhibit GSH-transferase (GST) transport activity (282). The GSTs quench reactive molecules and catalyse the conjugation of GSH to, among many substrates, heavy metals, thus protecting cells from oxidative burst (283). Other ABC proteins are discussed in more detail in this chapter, according to their role in metal uptake and stress tolerance.

5.4.7.   Phytochelatins

Phytochelatins (PCs) are gamma-glucose-cysteine (γ-Glu-Cys)-based peptides (Figure 5.21), and are made up of five families, based on the C-terminal amino acid (96). The PCs are synthesised from GSH by PC synthase in response to metal ion stress, and these complex with metals to reduce metal toxicity.
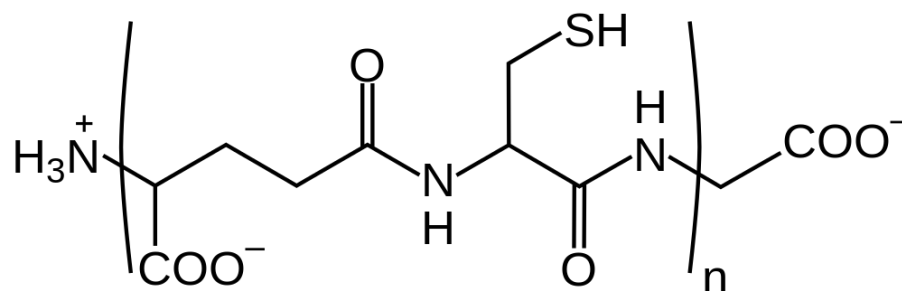
Figure 5.21. The chemical structure of phytochelatin, n = 2-11

Following Cd exposure, PCs were induced in a range of vascular and nonvascular plant, mosses, and algae (123,124,279). Yeasts have also been shown to produce PCs in response to Cd (125,284,285). Various metal treatment of plant cells has been shown to induce the expression of these peptides, including Cd, Zn, Pb, Ag, Arsenate, Hg, Cu, Ni, selenate, gallium, Pd, indium, and Sb (122,126). The PCs sequester the PC-complexed metal ions to root vacuoles by transporters such as ABCC1 or 2 (see section 5.4.6 for information on the ABC transporters)(213). Detoxification of PCs has also been demonstrated to act on Cd in plants, by integrating PCs with cytoplasmic Cd^{2+} to make a Cd-Pd complex which is then transferred into the vacuole (286). The other two members of the clade, ABCC11 (MRP8) and ABCC12 (MRP9) are also presumed to act as vacuolar transporters (287), functioning in the uptake of PCs at a lower level (288). The ABCC3, or MRP3, protein transports GSH-conjugated Cd and expression increased following Cd treatment (289,290). Whilst not directly comparable, the results of the Bovet et al. and Zientara et al. studies agree with the results demonstrated in this work; the *MRP3* expression increased followed metal (Cd / Pd) exposure.

5.4.8. The aquaporins

Aquaporins were originally discovered as water channels (Figure 5.22), explaining their name, but the knowledge of their roles has since expanded to the transport of small neutral solutes, gasses and metal ions (217). There are a high number of aquaporin isoforms in plants, with 35 and 33 homologs in Arabidopsis and rice, respectively (291). Using sequence homology, aquaporins can be divided into four subgroups: the plasma membrane intrinsic proteins (PIP), the tonoplast intrinsic proteins (TIP), the nodulin-26-like intrinsic proteins (NIPs), and the small basic intrinsic proteins (SIPs) (291).
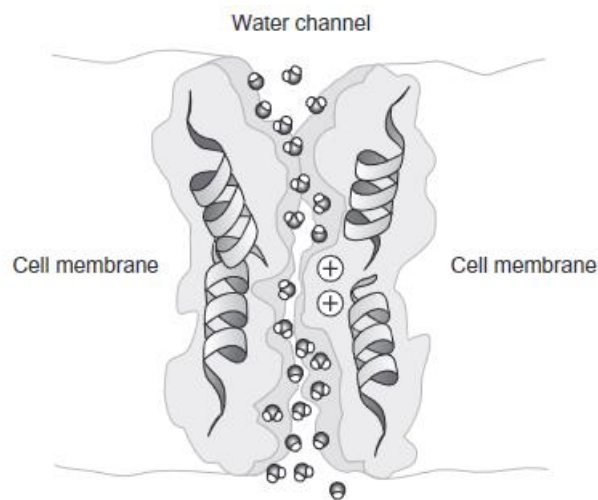
Figure 5.22. Aquaporin; water molecules pass through the aquaporin channel in single file. Figure reproduced from William Stillwell, in An Introduction to Biological Membranes (Second Edition) (292)

The Nodulin-26 like Intrinsic Protein (NIP) subfamily can transport water, glycerol, ammonia, silicic acid, and other solutes. The NIPs have the lowest water transport ability compared to other aquaporin subfamilies, but higher permeability to small organic molecules, mineral nutrients, and metal molecules (293). In the work presented here, the aquaporin *NLM1* was downregulated in the shoot tissue in response to Pd treatment . The NLM1 protein also functions in arsenite transport and tolerance, thus reducing ROS production. Disruption in NLM1 confers arsenite tolerance, and is involved in arsenite uptake when heterologously expressed in frog (*Xenopus laevis*) oocytes (294).

5.4.9. The glutathione transferases (GSTs)

In plants undergoing metal stress, there is an increased generation of ROS such as $O_2^{\bullet-}$, H_2O_2 and the $^{\bullet}OH$. The antioxidant defense mechanisms present in cells such as SOD1, catalase, peroxidases, peroxiredoxins and are complemented by metabolites such as ascorbate and GSH (295). Members of the glutathione transferase (GST) family are induced by a range of biotic and abiotic factors and are key in protecting plants against oxidative damage. The GSTs are mainly found in the cytosol, and their roles include: catalysing the conjugation of electrophilic substrates to GSH, peroxidase and isomerase activities, and binding non-catalytically to a wide range of endogenous and exogeneous ligands.

In the study presented here, there were three differentially expressed GSTs in the shoot tissue, all upregulated: *GSTU3*, *GSTZ1* and *GLN1;1*.The Arabidopsis *GSTU3* encodes a GST belonging to the tau class of GSTs and acts upstream of or within toxin catabolic process. It is involved in the GSH-mediated detoxification pathway, and the JA pathway. A known stress response gene, *GSTZ1*, was highly upregulated in response to Pd in Arabidopsis, and has been shown to be markedly induced in response to pathogen infection (296). Glutamine is a key N source in plants, and necessary to provide C-N assembly for plant growth. The glutamine synthetases help ensure that there is sufficient glutamine for plant development. The glutamine synthase 1;1 (*GLN1;1*) was upregulated in response to Pd and encodes a cytosolic glutamine synthase with a high affinity for ammonium (297).

5.4.10. Lipid metabolism

Excess metal ions alter membrane lipids indirectly as a result of the metal-catalysed generation of ROS, which causes peroxidation of membrane lipids; and through the disruption of enzymes in lipid biosynthetic pathways (216). In plants, sterols are important components of the cell membrane and lipid rafts, and are crucial for the response of plants to abiotic stress (298). Expression of the *ABCG5* orthologue was downregulated in Pd-treated shoot tissues , and seedlings of the ABC5 orthologue, *abcg5*, exhibited severe developmental problems when grown in waterlogged conditions; the shoot apical meristem was small, and the seedling failed to develop true leaves. The seedlings had high water content and reduced buoyancy in water, suggesting they were unable to retain air spaces inside the plant. The *abcg5* seedlings had more permeable cotyledons, reduced cuticular wax components, and a less dense cuticle layer than the WT (299). The downregulation of *ABCG5* in Pd-treated shoot tissue, suggests that the undosed plants exhibited higher waterlogging than the Pd treated plants. In submerged conditions, oxygen deprivation is a major problem for plant survival. Plants have evolved mechanisms to mitigate oxygen deprivation symptoms, and this is evident in the transcriptome response to Pd. While both the control condition and Pd condition were grown in identical hydroponic systems, the Pd treated plants were more responsive to hypoxia than the control plants; potentially as heavy metals have been shown to disrupt water flow by a reduction in stomatal conductance and by reducing the flow of solutes (262)

Flippases such as aminophospholipid ATPases (ALAs) transporter lipids from the exoplasmic side of the plasma membrane to the cytosolic face. (300), and ALA4 has been implicated in maintaining

the homeostasis of glyercolipids and sphingolipids (301). The ALA10 flippase was upregulated in both the shoot and the root tissue in response to Pd treatment, A P4-type ATPase flippase that internalizes exogenous phospholipids across the plasma membrane, upregulation is a plausible response to Pd-induced lipid membrane damage (223).

5.4.11. Auxin transporters

Auxin is one of the most important plant hormones controlling differentiation and response to abiotic signals. Previously shown to elicit protection from oxidative stress, auxins can increase the production of antioxidative enzymes (263). Multiple genes related to auxin signaling were differentially expressed in response to Pd; *ABCB26*, *ABCB11*, *ABCB12*, *PGP4* and *PGP2*.
ABCB26, or *TAP1*, also upregulated in shoot tissue, is localised to the chloroplast membrane, and expression is increased in response to Ca^{2+} and Al^{3+} exposure and mechanical wounding, repressed in response to high Mg^{2+} and high auxin stress treatment (302). The Arabidopsis *ABCB11*, otherwise known as encoding multidrug resistance 8 (MDR8) and P-glycoprotein 11 (PGP11), is expressed in the vascular tissue of the primary stem and located in the plasma membrane (303). The ABCB11 transporter is thought to act as an auxin importer, contributing to auxin distribution and auxin-mediated development (303), and ABCB12, also known as P-glycoprotein 12 (PGP12) has sequence similarity with PGP11, 3, 4 and 5 (clade II), and may function in a similar manner. Similarly, PGP4 has been shown to function in root development within auxin transport; PGP2, or ABCB2, (clade I), and is also related to auxin transport. (304).

5.4.12. The usually multiple acids move in and out (UNAMIT) transporters

The usually multiple acids move in and out transporters (UNAMITs) are amino acid transporters, and the increased expression of these genes is strongly related to induction of stress phenotypes and pathogen resistance, likely through a SA dependent pathway (305). The DE members of this family, *UMAMIT20* and *UMAMIT28* in shoots, were upregulated and *UMAMIT12* and *UMAMIT28* downregulated in root tissue. These expression changes may reflect increased stress responses present in the root tissue compared to the shoot tissue. Heavy metal stress induces the accumulation of specific amino acids which chelate metals in cells or in the xylem sap. Arabidopsis (306) and *Vigna radiata* (mung bean) (307) accumulate cysteine or proline respectively, in response to Cd exposure, whereas the thistle-like Ni HA *Berkheya coddii* accumulates histidine(308).

5.4.13. The jasmonic acid transporters (JAT)

Previous work has suggested there is cross-talk between the action of heavy metals and plants and JA (309). The Arabidopsis *ABCG16*, or *JAT1* which was upregulated in shoot tissue in response to Pd exposure, belongs to a clade of five half-transporters required for the synthesis of an intact pollen wall. Jasmonates (JAs) take part in various physiological process and are related to multiple plants stressors including salinity, drought and temperature (310). These molecules interact with signaling pathways generated by SA, ABA, ethylene and other molecules (310). The plant hormone jasmonyl-

isoleucine (JA-Ile) is a regulator of plant growth and an important component of multiple abiotic and biotic stress factors. Upon accumulation of JA-Ile in response to plant stresses, JAT1 facilitates JA-Ile transport into the nucleus, resulting in the loss of repression of promoters otherwise repressed by JA zim-domain proteins, leading to the activation of target genes (310).

5.4.14. The reactive oxygen species transporters (ROT)

Gamma-aminobutyric acid (GABA) rapidly accumulates in plant tissues in response to biotic and abiotic stress (311). Under oxygen deprivation, the primary stress factor in flooded soils, GABA accumulates rapidly, as do cellular levels of Ca^{2+} (311). The GABA (and glycine, betaine, and proline) transporter encoded by *PROT2* is upregulated in shoot tissue in response to Pd treatment.

5.4.15. Hypoxia related genes

Numerous genes related to hypoxia were DE in response to Pd, and are likely to be a product of the hydroponic system used to study the response of Arabidopsis to Pd. To ensure contact of root tissue with available Pd, roots were submerged in ½ MS media containing Pd as K_2PdCl_4. An advantage of this system is that the Pd is in an ionic form, and thus more readily available; in soil-based systems Pd exists in biologically unavailable forms, such as zero-valent metal, and required concentrations for toxicity studies would be prohibitively expensive. In future experiments, introducing oxygen to the growth media, via 'bubble stones' attached to air pumps might reduce the incidence of hypoxia-related genes in the Pd-treated transcriptome, and allow a definition between the response of the plant to Pd and to oxygen-deprivation.

Resistant to High CO_2 (RHC1), was downregulated in both shoot and root tissue in response to Pd and is involved in the regulation of CO_2-induced stomatal closure mediated by slow anion channels. The *rhc1* mutant has been shown to be defective in the stomatal response to CO_2, and may be related to the hypoxia genes that were differentially expressed in response to Pd in Arabidopsis (312).

5.4.16. Summary

In summary, the transcriptomic response of Arabidopsis to Pd reflects the result of genes encoding enzymatic pathways intended to act on other, essential (Zn, Cu and Fe) or more prevalent toxic (such as Cd) metal ions. As mentioned previously, Zn and Cd transport is overrepresented in the literature, which may give the impression that Pd is taken up into plant tissue via Fe or Zn transporters, as many of these have previously been shown to also transport Cd. It is known that there is a significant crossover between metal transporters or detoxification mechanisms, and I propose the same is true for Pd. Further characterisation of Zn, Fe or Cd specific transporters would answer this.
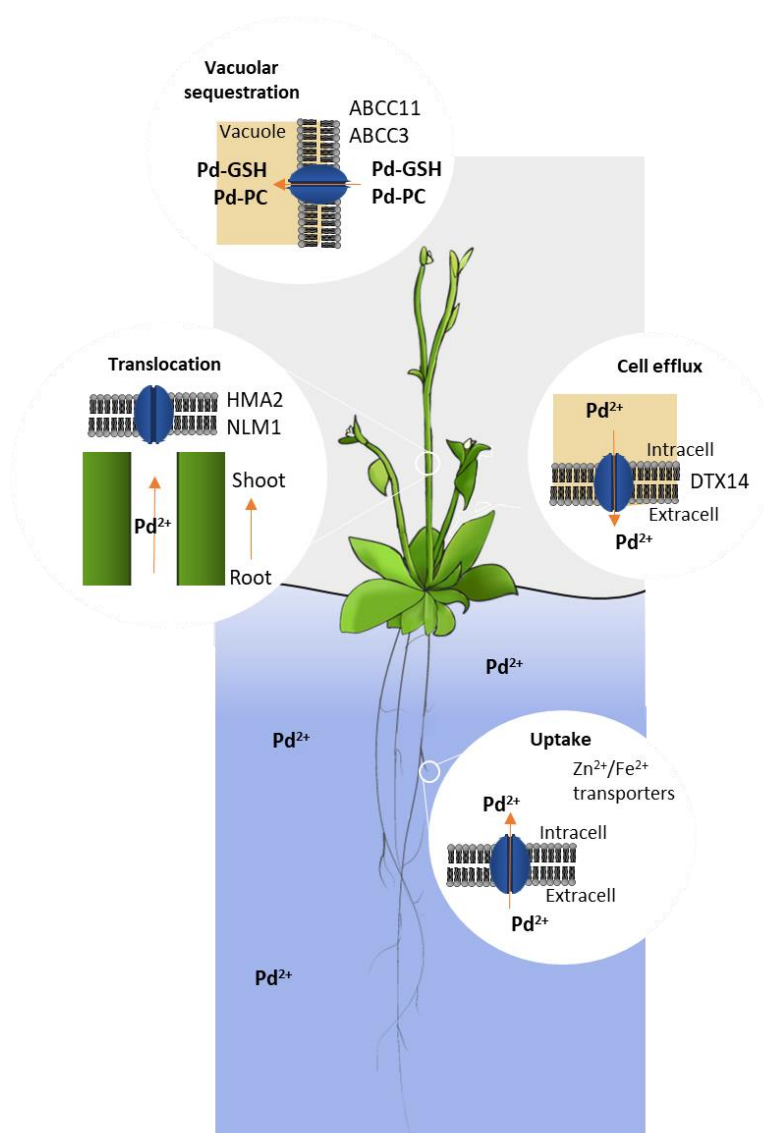
Figure 5.23. Proposed mechanism of Pd uptake, translocation and detoxification generated from the results of the transcriptome analysis of Arabidopsis plants grown in the presence of Pd in a hydroponic system. The figure does not represent more general stress responses including other signalling pathways and ROS mitigation.

For instance, reduced expression of the Cd-linked *HMA2* or aquaporin *NLM1* could result in a decrease in the root-to-shoot translocation of Pd; an increase in efflux by DTX14, GSH-mediated detoxification by ABCC11 (increase sequestration to the vacuole) and ABCC3 (Figure 5.23).

The presence of Pd in the plant tissue also elicits expression of multiple signaling pathways known to be involved in the response of plants to abiotic stresses: auxin, JA, GABA, SA, and ethylene signaling. These pathways help mitigate the effect of metal-induced generation of ROS, which would otherwise have a detrimental effect on lipid membrane and protein function. An important caveat to emphasise here is that the work presented here only establishes the level of gene expression and does not necessarily translate to protein abundance or activity. Confirmation of interesting genes should include characterisation at the protein level.

6. Final discussion

The necessary shift from a linear to a circular economy necessitates the recovery of materials for reuse; and phytomining presents a viable option towards this, following the generation or identification of appropriate phytomining species. Phytomining may offer a potentially cost-effective and environmentally friendly approach.

In chapter three, plant lines were generated with increased Au uptake and tolerance by NP formation. The interaction between Au and *COPT2* was investigated using *yeast,* Arabidopsis *COPT2,* and Arabidopsis *35S-COPT2* lines, and the potential NP-forming ability and resultant detoxification of Au ions was investigated in GP expressing plant lines. The increased expression of the *COPT2* transporter, combined with the expression of GP resulted in increased Au uptake into shoot tissue, a key feature of species necessary for phytomining.

Constitutive promoters may present problems relating to expression silencing and reduced growth, but targeted expression of *COPT2* and GP could help to overcome these issues. Table 6.1 shows several tissue specific promoters. Root specific promoters could be used in the generation of plant lines that express *COPT2* at an elevated level solely in root tissue irrespective of the Cu concentration. For example, a synthetic root-specific module (SynR2) was designed using characterised *cis*-acting element and fused with the PortUbi882 promoter to investigate the expression of GUS in transgenic tobacco plants. The root-specific action of the module was evident through qPCR analysis; there was a 2.1 fold higher root-specific expression compared to the CaMV35S promoter, though there was some, much lower, expression in the stem (313). It has been suggested that Au is translocated into the shoot tissue as an ion (81). The use of a 'green-tissue' specific promoter, such as that constructed by Wang et al (2015) (314) could be used to spatially separate the increased uptake of Au by *COPT2* and NP formation by GP to accumulate AuNPs in the harvestable tissue. Ideally, an Au-specific promoter would be identified, and the root or shoot specific expression of these genes would be induced only in the presence of Au. The CueR transcriptional activator of *E. coli* is activated by Cu, Au and Ag (315). Slight modification of CueR may be able to tune the specificity towards Au and away from Cu and Ag but would first require the mechanism of recognition to be identified. There would also need to be the addition of a 'kill switch' if these plants were to be approved for use (316). These would prevent the release of the genetically modified plant from the site of interest. Suggestions towards this include a reliance on a particular man-made 'fertilizer', without with the plant could not grow or produce seed (317). There still then would exist the problem that the DNA of the organism may persist in the environment following the death. The CRISPR technology could be used to create a kill switch that erases the DNA from the genetically modified plant (318).

Table 6.1. Demonstrations of different types of tissue specific synthetic promoters and their characteristics (319)

Name/ID	Source	Expression	Species tested	Reference
P_{RSGA}, P_{2RSGA}, P_{2RSPA}, P_{RSGPA}, P_{2RSGPA}, P_{R5SGPA}, $P_{2R5SGPA}$	P_{zmBD1}, RY repeats (R), GCN4 (G), Prolamin box (P), Skn-1 (S), ACGT and AACA motifs	Seed specific bidirectional promoters	*Zea mays*	Liu et al., 2018
BiGSSP2, BiGSSP3, BiGSSP6, and BiGSSP7	$P_{Osrbcs-550}$, $P_{Osrbcs-62}$ OsActin (*OsAct1*) OsTubulin6 (*OsTub6I*) already reported sequences	Bidirectional expression efficiencies specifically in green tissues	*Oryza sativa*	Bai et al., 2019
SynR2 SynR1	a. Synthetic module at the 5′ end of the CaMV35S (SynR1), b. module was present in both 5′ and 3′ ends (SynR2)	Root specific	*Nicotiana tabacum*	Mohan et al., 2017
GSSP1, GSSP3, GSSP5, GSSP6, GSSP7	The first intron of rice Act1, G box and GT, Different regulatory sequences from rice, tobacco and Arabidopsis ($P_{D540-544}$, $P_{Osrbcs-550}$, $P_{Osrbcs-62}$, EnP3-110)	Green tissue specific	*Oryza sativa*	Wang et al., 2015
p35S-PCHS -Ω, p35S-LCHS -Ω, pOCSPCHS-Ω, pOCS-LCHS-Ω	Petunia CHSA core promoter, Lily CHS core promoter, Ω element, CaMV 35S or OCS enhancer region	Transgenic enhancement of floral traits (Flower specific)	*Torenia fournieri*	Du et al., 2014
pCL	Created by combining two DNA cassettes: Potato patatin promoter region including a tuber specific sequence TSSR and *Arabidopsis* cor15a promoter region	Express specifically and regulate the activity of acid vacuolar invertase in potato tubers at low temperature	*Solanum tuberosum*	Li et al., 2013
EFCFS-HS-1, EFCFS-HS-2, EFCFSHS-3	EFCFS motif (AAAG),FUAS of F20 along with core promoter of FS3	Tissue specific (Expression of EFCFSHS-3 in Vascular tissues)	*Nicotiana tabacum*	Ranjan and Dey 2012
AtMYB60 promoter::GUS reporters	CaMV35S and AtMYB60 promoters	Tissue specific Expression ells)	*Arabidopsis*	Cominelli et al., 2011
A27znGlb1	Combined the elements of 27zn and Glb1promoters	Tissues specific expressions of the chimeric promoter	*Zea mays*	Shepherd and Scott 2009

This approach could be utilised by researchers in plants that are more suited to phytomining; high biomass, fast growing species, or species that grow in the environment already. High biomass plants which have already been shown to function in phytoextraction include *Helianthus annus, Cannabis sativa, Nicotiana tabacum* and *Zea mays* (272)*.* According to TAIR, the Arabidopsis *COPT2* has two orthologs in *H. annus*, four in *N. tabacum*, and one in *Zea mays* (320)*.* The targeted expression approach could be utilised using the sequences present in these species to improve Au uptake in high biomass species.

The approach utilised in chapter three was applied in chapter four to investigate the interaction of *COPT2* and GP with Pd, to attempt to generate plant lines that could accumulate increased levels of Pd with enriched 10 nm NPs. Despite promising studies in yeast and Arabidopsis *COPT2*, the double transgenic lines did not contain an increased Pd concentration, suggesting that other transporters may play a more prominent role in Pd uptake in Arabidopsis. The response on the Arabidopsis transcriptome to Pd was subsequently explored in chapter 5, and the profile of genes involved in uptake and detoxification appears similar to Cd exposure. The transcriptomic response is complex, involving changes in the expression of transcription factors, transporters, PCs, aquaporins, oxidases, peroxidases, chaperones, and genes relating to cellular processes. The most enriched biological processes were dominated by general stress and hypoxia responses in the roots, with a more specific metal ion response in the shoot tissue. The following genes could be investigated to elucidate their interaction with Pd: *NLM1/NIP1;1, HMA2, DTX14, ABCC11* and *ABCC3*. The subcellular localisation of these genes in response to Pd treatment may help to inform their usefulness; a region (~ 2 kb) upstream of the coding sequence could be fused in frame with the GFP sequence, and transformed into Arabidopsis e.g., by floral dip, as described in this work. Subsequent homozygous T3 plants could then be used for GFP fluorescence observation by confocal laser scanning microscope, as in Chang-Hong Yang et al (2021) (321). As performed in this work, the coding sequence of these genes could be cloned into the pYES2 and grown in the presence of Pd. Spot dilution assays, as performed in this work, could be used as well as element analysis by ICP-OES, as in Tiwari et al (2017) (4). The level of expression in separate tissues and with or without Pd exposure could be investigated using qPCR to confirm the results of the transcriptome analysis performed here. Further work could be performed to investigate the phenotypic response of Arabidopsis mutants in response to Pd exposure, and in the hydroponic experiments used here to determine the elemental concentration in different tissues.

7. References

1. González RC, González-Chávez MCA. Metal accumulation in wild plants surrounding mining wastes. Environ Pollut. 2006 Nov;144(1):84–92.

2. Martínez-Alcalá I, Clemente R. Phytoremediation of Metalloid-contaminated Soil. Metalloids in Plants: Advances. 2020 Apr 14;27–46.

3. Oberdorfer B. Reformation und politisch-gesellschaftliche Emanzipation. Evang Theol. 2014 Apr 1;74(2):118–26.

4. Tiwari M, Venkatachalam P, Penarrubia L, Sahi SV. COPT2, a plasma membrane located copper transporter, is involved in the uptake of Au in Arabidopsis. Sci Rep. 2017 Sep 12;7(1):11430.

5. Harumain S, Azizi Z. Phytomining of precious metals from mine wastes [phd]. University of York; 2016.

6. Anderson, Stewart, Moreno. Gold phytomining. Novel developments in a plant-based mining system. Proc Estonian Acad Sci Biol Ecol. 2003;

7. van der Ent A, Baker AJM, Reeves RD, Pollard AJ, Schat H. Hyperaccumulators of metal and metalloid trace elements: Facts and fiction. Plant Soil. 2013 Jan 1;362(1):319–34.

8. Khan AG. Role of soil microbes in the rhizospheres of plants growing on trace metal contaminated soils in phytoremediation. J Trace Elem Med Biol. 2005;18(4):355–64.

9. Padmavathiamma PK, Li LY. Phytoremediation Technology: Hyper-accumulation Metals in Plants. Water Air Soil Pollut. 2007 Sep 1;184(1):105–26.

10. Li, Ji, Luo. Visualizing hotspots and future trends in phytomining research through scientometrics. Sustain Sci Pract Policy. 2020;

11. Certain data included herein are derived from Clarivate Web of Science. © Copyright Clarivate 2022. All rights reserved [Internet]. [cited 2022 Nov 14]. Available from: https://www.webofscience.com/wos/woscc/basic-search

12. Dinh T, Dobo Z, Kovacs H. Phytomining of noble metals - A review. Chemosphere. 2022 Jan;286(Pt 3):131805.

13. Suman J, Uhlik O, Viktorova J, Macek T. Phytoextraction of Heavy Metals: A Promising Tool for Clean-Up of Polluted Environment? Front Plant Sci. 2018 Oct 16;9:1476.

14. Singh J, Kalamdhad AS. Concentration and speciation of heavy metals during water hyacinth composting. Bioresour Technol. 2012 Nov;124:169–79.

15. Parker HL, Rylott EL, Hunt AJ, Dodson JR, Taylor AF, Bruce NC, et al. Supported Palladium Nanoparticles Synthesized by Living Plants as a Catalyst for Suzuki-Miyaura Reactions. Marr AC, editor. PLoS ONE. 2014 Jan 29;9(1):e87192.

16. Yu G, Lei H, Bai T, Li Z, Yu Q, Song X. In-situ stabilisation followed by ex-situ composting for treatment and disposal of heavy metals polluted sediments. J Environ Sci. 2009;21(7):877–83.

17. Wilburn DR, Bleiwas DI. Platinum-group metals - world supply and demand [Internet]. [cited 2022 Aug 30]. Available from: https://corpora.tika.apache.org/base/docs/govdocs1/713/713764.pdf

18. Cotton S. Chemistry of Precious Metals. Springer Science & Business Media; 1997. 376 p.

19. Book. Compendium of chemical terminology. International Union of Pure and Applied Chemistry. 2014;

20. Palladium. In: Encyclopedia Britannica. 2022.

21. Haynes WM. CRC Handbook of Chemistry and Physics: A Ready-reference Book of Chemical and Physical Data. 97th ed. Haynes WM, editor. CRC Press; 2016. 2652 p.

22. Saha N, Mollah MZI, Alam MF, Safiur Rahman M. Seasonal investigation of heavy metals in marine fishes captured from the Bay of Bengal and the implications for human health risk assessment. Food Control. 2016 Dec 1;70:110–8.

23. Hossain Md Anawar, Md Zabed Hossain, I. Santa-Regina, Vladimir Strezov, Farjana Akter. Phytomining of valuable metals/metalloids from mining wastes, tailings and contaminated soils. In: Anawar HM, Strezov V, Abhilash, editors. Sustainable and Economic Waste Management. CRC Press; 2019.

24. Novo LAB, Castro PML, Alvarenga P, da Silva EF. Phytomining of Rare and Valuable Metals. In: Ansari AA, Gill SS, Gill R, R. Lanza G, Newman L, editors. Phytoremediation: Management of Environmental Contaminants, Volume 5. Cham: Springer International Publishing; 2017. p. 469–86.

25. Minguzzi C. Il contenuto di nichel nelle ceneri di Alyssum bertolonii Desv. Mem Soc Tosc Sci Nat Ser A. 1948;55:49–74.

26. Jaffre T, Brooks RR, Trow JM. Hyperaccumulation of nickel by Geissois species. Plant Soil. 1979 Feb 1;51(1):157–61.

27. Osmani, Bani, Hoxha. The phytomining of nickel from industrial polluted site of Elbasan-Albania. Eur Acad Res. 2018;Vol. V(10).

28. Rosenkranz T, Hipfinger C, Ridard C, Puschenreiter M. A nickel phytomining field trial using Odontarrhena chalcidica and Noccaea goesingensis on an Austrian serpentine soil. J Environ Manage. 2019 Jul 15;242:522–8.

29. Hipfinger C, Rosenkranz T, Thüringer J, Puschenreiter M. Fertilization regimes affecting nickel phytomining efficiency on a serpentine soil in the temperate climate zone. Int J Phytoremediation. 2021;23(4):407–14.

30. Cerdeira-Pérez A, Monterroso C, Rodríguez-Garrido B, Machinet G, Echevarria G, Prieto-Fernández Á, et al. Implementing nickel phytomining in a serpentine quarry in NW Spain. J Geochem Explor. 2019 Feb 1;197:1–13.

31. Mega ER. The Price of Gold. Sci Am. 2017 Dec 19;318(1):18.

32. PGM management [Internet]. matthey.com. [cited 2022 Jul 19]. Available from: https://matthey.com/products-and-markets/pgms-and-circularity/pgm-management/

33. Ding Y, Zhang S, Liu B, Zheng H, Chang C-C, Ekberg C. Recovery of precious metals from electronic waste and spent catalysts: A review. Resour Conserv Recycl. 2019 Feb 1;141:284–98.

34. Sinha R, Singh AK, Bauddh K, Sharma TR, Sharma P. Phytorestoration of Abandoned Mining and Oil Drilling Sites. In: Bauddh K, Korstad J, Sharma P, editors. Phytomining: a sustainable approach for recovery and extraction of valuable metals. Elsevier; 2021. p. 487–506.

35. Anderson C, Moreno F, Meech J. A field demonstration of gold phytoextraction technology. Miner Eng. 2005 Apr 1;18(4):385–92.

36. Gold prices - 100 year historical chart [Internet]. [cited 2022 Aug 30]. Available from: https://www.macrotrends.net/1333/historical-gold-prices-100-year-chart

37. Palladium prices - interactive historical chart [Internet]. [cited 2022 Aug 30]. Available from: https://www.macrotrends.net/2542/palladium-prices-historical-chart-data

38. McGrath SP, Zhao F-J. Phytoextraction of metals and metalloids from contaminated soils. Curr Opin Biotechnol. 2003 Jun;14(3):277–82.

39. Wa F 08 9457 9668. Multi Mix Systems / Technical Bulletin [Internet]. [cited 2022 Aug 25]. Available from: https://web.archive.org/web/20091023235047if_/http://www.multimix.com.au/DOCUMENTS/Technical%20Bulletin1.PDF

40. Anderson CWN, Brooks RR, Stewart RB, Simcock R. Harvesting a crop of gold in plants. Nature. 1998 Oct;395(6702):553–4.

41. Piccinin RCR, Ebbs SD, Reichman SM, Kolev SD, Woodrow IE, Baker AJM. A screen of some native Australian flora and exotic agricultural species for their potential application in cyanide-induced phytoextraction of gold. Miner Eng. 2007 Nov 1;20(14):1327–30.

42. Wilson-Corral V, Anderson C, Rodriguez-Lopez M, Arenas-Vargas M, Lopez-Perez J. Phytoextraction of gold and copper from mine tailings with Helianthus annuus L. and Kalanchoe serrata L. Miner Eng. 2011 Oct 1;24(13):1488–94.

43. National Research Council, Division on Earth and Life Studies, Water Science and Technology Board, Committee on Bioavailability of Contaminants in Soils and Sediments. Bioavailability of Contaminants in Soils and Sediments: Processes, Tools, and Applications. National Academies Press; 2003. 432 p.

44. Gold Nanoparticles: Properties and Applications [Internet]. Sigma Aldrich, Merck. [cited 2022 Aug 7]. Available from: https://www.sigmaaldrich.com/GB/en/technical-documents/technical-article/materials-science-and-engineering/biosensors-and-imaging/gold-nanoparticles

45. Auffan M, Rose J, Bottero J-Y, Lowry GV, Jolivet J-P, Wiesner MR. Towards a definition of inorganic nanoparticles from an environmental, health and safety perspective. Nat Nanotechnol. 2009 Oct;4(10):634–41.

46. Gold's contribution to society [Internet]. World Gold Council. [cited 2022 Aug 30]. Available from: https://www.gold.org/esg/golds-contribution-to-society

47. Santhosh PB, Genova J, Chamati H. Green Synthesis of Gold Nanoparticles: An Eco-Friendly Approach. Chemistry. 2022 Apr 25;4(2):345–69.

48. García-Negrete CA, Blasco J, Volland M, Rojas TC, Hampel M, Lapresta-Fernández A, et al. Behaviour of Au-citrate nanoparticles in seawater and accumulation in bivalves at environmentally relevant concentrations. Environ Pollut. 2013 Mar;174:134–41.

49. Khosravi-Katuli K, Prato E, Lofrano G, Guida M, Vale G, Libralato G. Effects of nanoparticles in species of aquacultural interest. Environ Sci Pollut Res Int. 2017 Jul;24(21):17326–46.

50. Wu M. What gives gold nanoparticles their color? [Internet]. Sustainable Nano. 2019 [cited 2022 Aug 2]. Available from: https://sustainable-nano.com/2019/11/12/gold-nanoparticles-color/

51. Siddiqi KS, Husen A. Green Synthesis, Characterization and Uses of Palladium/Platinum Nanoparticles. Nanoscale Res Lett. 2016 Dec;11(1):482.

52. Rodriguez E, Parsons JG, Peralta-Videa JR, Cruz-Jimenez G, Romero-Gonzalez J, Sanchez-Salcido BE, et al. Potential of Chilopsis linearis for gold phytomining: using XAS to determine gold reduction and nanoparticle formation within plant tissues. Int J Phytoremediation. 2007 Mar;9(2):133–47.

53. Taylor A. Gold uptake and tolerance in Arabidopsis [phd]. University of York; 2011.

54. Beattie IR, Haverkamp RG. Silver and gold nanoparticles in plants: sites for the reduction to metal. Metallomics. 2011 Jun;3(6):628–32.

55. Gardea-Torresdey JL, Parsons JG, Gomez E, Peralta-Videa J, Troiani HE, Santiago P, et al. Formation and Growth of Au Nanoparticles inside Live Alfalfa Plants. Nano Lett. 2002 Apr 1;2(4):397–401.

56. Shukla D, Vankar PS. Synthesis of Plant Parts Mediated Gold Nanoparticles. Int J Green Nanotech. 2012 Jul 1;4(3):277–88.

57. Joglekar S, Kodam K, Dhaygude M, Hudlikar M. Novel route for rapid biosynthesis of lead nanoparticles using aqueous extract of Jatropha curcas L. latex. Mater Lett. 2011 Oct 1;65(19):3170–2.

58. Johnston CW, Wyatt MA, Li X, Ibrahim A, Shuster J, Southam G, et al. Gold biomineralization by a metallophore from a gold-associated microbe. Nat Chem Biol. 2013 Apr;9(4):241–3.

59. Tan YN, Lee JY, Wang DIC. Uncovering the design rules for peptide synthesis of metal nanoparticles. J Am Chem Soc. 2010 Apr 28;132(16):5677–86.

60. Sharma D, Kanchi S, Bisetty K. Biogenic synthesis of nanoparticles: A review. Arabian Journal of Chemistry. 2019 Dec 1;12(8):3576–600.

61. Brown S, Sarikaya M, Johnson E. A genetic analysis of crystal growth. J Mol Biol. 2000 Jun 9;299(3):725–35.

62. Yeo AR, Flowers TJ. Plant Solute Transport. John Wiley & Sons; 2008. 424 p.

63. Harmsen J. Measuring bioavailability: from a scientific approach to standard methods. J Environ Qual. 2007 Sep;36(5):1420–8.

64. ISO 17402:2008; Soil quality — Requirements and guidance for the selection and application of methods for the assessment of bioavailability of contaminants in soil and soil materials [Internet]. ISO. 2022 [cited 2022 Jul 20]. Available from: https://www.iso.org/standard/38349.html

65. Kim R-Y, Yoon J-K, Kim T-S, Yang JE, Owens G, Kim K-R. Bioavailability of heavy metals in soils: definitions and practical implementation--a critical review. Environ Geochem Health. 2015 Dec;37(6):1041–61.

66. del Pozo T, Cambiazo V, González M. Gene expression profiling analysis of copper homeostasis in Arabidopsis thaliana. Biochem Biophys Res Commun. 2010 Mar 5;393(2):248–52.

67. Chen G, Liu Y, Wang R, Zhang J, Owens G. Cadmium adsorption by willow root: the role of cell walls and their subfractions. Environ Sci Pollut Res Int. 2013 Aug;20(8):5665–72.

68. DalCorso G, Fasani E, Manara A, Visioli G, Furini A. Heavy Metal Pollutions: State of the Art and Innovation in Phytoremediation. Int J Mol Sci [Internet]. 2019 Jul 11;20(14). Available from: http://dx.doi.org/10.3390/ijms20143412

69. Hassett R, Kosman DJ. Evidence for Cu(II) reduction as a component of copper uptake by Saccharomyces cerevisiae. J Biol Chem. 1995 Jan 6;270(1):128–34.

70. Bernal M, Casero D, Singh V, Wilson GT, Grande A, Yang H, et al. Transcriptome sequencing identifies SPL7-regulated copper acquisition genes FRO4/FRO5 and the copper dependence of iron homeostasis in Arabidopsis. Plant Cell. 2012 Feb;24(2):738–61.

71. Pilon M, Abdel-Ghany SE, Cohu CM, Gogolin KA, Ye H. Copper cofactor delivery in plant cells. Curr Opin Plant Biol. 2006 Jun;9(3):256–63.

72. Puig S, Andrés-Colás N, García-Molina A, Peñarrubia L. Copper and iron homeostasis in Arabidopsis: responses to metal deficiencies, interactions and biotechnological applications. Plant Cell Environ. 2007 Mar;30(3):271–90.

73. Puig S, Lee J, Lau M, Thiele DJ. Biochemical and genetic analyses of yeast and human high affinity copper transporters suggest a conserved mechanism for copper uptake. J Biol Chem. 2002 Jul 19;277(29):26021–30.

74. Peñarrubia L, Andrés-Colás N, Moreno J, Puig S. Regulation of copper transport in Arabidopsis thaliana: a biochemical oscillator? J Biol Inorg Chem. 2010 Jan;15(1):29–36.

75. Ren F, Logeman BL, Zhang X, Liu Y, Thiele DJ, Yuan P. X-ray structures of the high-affinity copper transporter Ctr1. Nat Commun. 2019 Mar 27;10(1):1–9.

76. Sancenón V, Puig S, Mira H, Thiele DJ, Peñarrubia L. Identification of a copper transporter family in Arabidopsis thaliana. Plant Mol Biol. 2003 Mar;51(4):577–87.

77. Garcia-Molina A, Andrés-Colás N, Perea-García A, Del Valle-Tascón S, Peñarrubia L, Puig S. The intracellular Arabidopsis COPT5 transport protein is required for photosynthetic electron transport under severe copper deficiency. Plant J. 2011 Mar;65(6):848–60.

78. Klaumann S, Nickolaus SD, Fürst SH, Starck S, Schneider S, Ekkehard Neuhaus H, et al. The tonoplast copper transporter COPT5 acts as an exporter and is required for interorgan allocation of copper in Arabidopsis thaliana. New Phytol. 2011 Oct;192(2):393–404.

79. Andrés-Colás N, Carrió-Seguí A, Abdel-Ghany SE, Pilon M, Peñarrubia L. Expression of the Intracellular COPT3-Mediated Cu Transport Is Temporally Regulated by the TCP16 Transcription Factor. Front Plant Sci. 2018 Jul 3;9:910.

80. Puig S. Function and Regulation of the Plant COPT Family of High-Affinity Copper Transport Proteins. Advances in Botany [Internet]. 2014 Jul 21 [cited 2022 Aug 30];2014. Available from: http://dx.doi.org/10.1155/2014/476917

81. Taylor AF, Rylott EL, Anderson CWN, Bruce NC. Investigating the Toxicity, Uptake, Nanoparticle Formation and Genetic Response of Plants to Gold. PLoS One. 2014 Apr 15;9(4):e93793.

82. Sanz A, Pike S, Khan MA, Carrió-Seguí À, Mendoza-Cózatl DG, Peñarrubia L, et al. Copper uptake mechanism of Arabidopsis thaliana high-affinity COPT transporters. Protoplasma. 2019 Jan;256(1):161–70.

83. Ali H, Khan E, Sajad MA. Phytoremediation of heavy metals--concepts and applications. Chemosphere. 2013 May;91(7):869–81.

84. Thakur S, Singh L, Wahid ZA, Siddiqui MF, Atnaw SM, Din MFM. Plant-driven removal of heavy metals from soil: uptake, translocation, tolerance mechanism, challenges, and future perspectives. Environ Monit Assess. 2016 Apr;188(4):206.

85. Tong YP, Kneer R, Zhu YG. Vacuolar compartmentalization: a second-generation approach to engineering plants for phytoremediation. Trends Plant Sci. 2004 Jan;9(1):7–9.

86. Tripathy BC, Oelmüller R. Reactive oxygen species generation and signaling in plants. Plant Signal Behav. 2012 Dec;7(12):1621–33.

87. Halliwell B, Gutteridge JM. Oxygen toxicity, oxygen radicals, transition metals and disease. Biochem J. 1984 Apr 1;219(1):1–14.

88. Apel KH. REACTIVE OXYGEN SPECIES: Metabolism, Oxidative Stress, and Signaling Transduction. Annual Review of Plant Biology; Palo Alto. 2004;55:373–99.

89. Edge, McGarvey, Truscott. The carotenoids as anti-oxidants—a review. J Photochem Photobiol A Chem. 1997;

90. Kramarenko GG, Hummel SG, Martin SM, Buettner GR. Ascorbate reacts with singlet oxygen to produce hydrogen peroxide. Photochem Photobiol. 2006 Nov;82(6):1634–7.

91. Bilski P, Li MY, Ehrenshaft M, Daub ME, Chignell CF. Vitamin B6 (pyridoxine) and its derivatives are efficient singlet oxygen quenchers and potential fungal antioxidants. Photochem Photobiol. 2000 Feb;71(2):129–34.

92. Affek HP, Yakir D. Protection by isoprene against singlet oxygen in leaves. Plant Physiol. 2002 May;129(1):269–77.

93. Schmidt K, Fufezan C, Krieger-Liszkay A, Satoh H, Paulsen H. Recombinant water-soluble chlorophyll protein from Brassica oleracea var. Botrys binds various chlorophyll derivatives. Biochemistry. 2003 Jun 24;42(24):7427–33.

94. Dalvi, Bhalerao. Response of plants towards heavy metal toxicity: an overview of avoidance, tolerance and uptake mechanism. Ann Plant Sci. 2013;

95. Ernst WHO, Verkleij JAC, Schat H. Metal tolerance in plants. Acta Bot Neerl. 1992 Sep;41(3):229–48.

96. Pal R, Rai JPN. Phytochelatins: peptides involved in heavy metal detoxification. Appl Biochem Biotechnol. 2010 Mar;160(3):945–63.

97. Hall JL. Cellular mechanisms for heavy metal detoxification and tolerance. J Exp Bot. 2002 Jan;53(366):1–11.

98. Sun R-L, Zhou Q-X, Jin C-X. Cadmium accumulation in relation to organic acids in leaves of Solanum nigrum L. as a newly found cadmium hyperaccumulator. Plant Soil. 2006 Jul 1;285(1):125–34.

99.   Thurman DA, Rankin JL. The role of organic acids in zinc tolerance in Deschampsia caespitosa. New Phytol. 1982 Aug;91(4):629–35.

100.   Godbold DL, Horst WJ, Collins JC, Thurman DA, Marschner H. Accumulation of zinc and Organic Acids in Roots of Zinc Tolerant and Non-tolerant Ecotypes of Deschampsia caespitosa. J Plant Physiol. 1984 Aug;116(1):59–69.

101.   Wang J, Evangelou BP, Nielsen MT, Wagner GJ. Computer, Simulated Evaluation of Possible Mechanisms for Sequestering Metal Ion Activity in Plant Vacuoles: II. Zinc. Plant Physiol. 1992 Jun;99(2):621–6.

102.   Krotz RM, Evangelou BP, Wagner GJ. Relationships between Cadmium, Zinc, Cd-Peptide, and Organic Acid in Tobacco Suspension Cells. Plant Physiol. 1989 Oct;91(2):780–7.

103.   Kersten WJ, Brooks RR, Reeves RD, Jaffré A. Nature of nickel complexes in Psychotria douarrei and other nickel-accumulating plants. Phytochemistry. 1980 Jan 1;19(9):1963–5.

104.   Wagner GJ. Accumulation of Cadmium in Crop Plants and Its Consequences to Human Health. In: Sparks DL, editor. Advances in Agronomy. Academic Press; 1993. p. 173–212. (Advances in agronomy; vol. 51).

105.   Krämer U, Cotter-Howells JD, Charnock JM, Baker AJM, Smith JAC. Free histidine as a metal chelator in plants that accumulate nickel. Nature. 1996 Feb;379(6566):635–8.

106.   Khr K. Evolution, structure and chemical activity of class I metallothioneins : An overview. Metallothionein. 1993;29–56.

107.   Rauser WE. Structure and function of metal chelators produced by plants: the case for organic acids, amino acids, phytin, and metallothioneins. Cell Biochem Biophys. 1999;31(1):19–48.

108.   Lane B, Kajioka R, Kennedy T. The wheat-germ Ec protein is a zinc-containing metallothionein. Biochem Cell Biol. 1987 Nov 1;65(11):1001–5.

109.   Kawashima I, Kennedy TD, Chino M, Lane BG. Wheat Ec metallothionein genes. Eur J Biochem. 1992 Nov 1;209(3):971–6.

110.   Buchanan-Wollaston V, Ainsworth C. Leaf senescence in Brassica napus: cloning of senescence related genes by subtractive hybridisation. Plant Mol Biol. 1997 Mar;33(5):821–34.

111.   Whitelaw CA, Le Huquet JA, Thurman DA, Tomsett AB. The isolation and characterization of type II metallothionein-like genes from tomato (Lycopersicon esculentum L.). Plant Mol Biol. 1997 Feb;33(3):503–11.

112.   Zhou J, Goldsbrough PB. Structure, organization and expression of the metallothionein gene family in Arabidopsis. Mol Gen Genet. 1995 Aug 21;248(3):318–28.

113.   Kusaba M, Takahashi Y, Nagata T. A multiple-stimuli-responsive as-1-related element of parA gene confers responsiveness to cadmium but not to copper. Plant Physiol. 1996 Aug;111(4):1161–7.

114.   Foley RC, Liang ZM, Singh KB. Analysis of type 1 metallothionein cDNAs in Vicia faba. Plant Mol Biol. 1997 Mar;33(4):583–91.

115.   Evans KM, Gatehouse JA, Lindsay WP, Shi J, Tommey AM, Robinson NJ. Expression of the pea metallothionein-like gene PsMTA in Escherichia coli and Arabidopsis thaliana and analysis of trace metal ion accumulation: implications for PsMTA function. Plant Mol Biol. 1992 Dec;20(6):1019–28.

116.   Zhou J, Goldsbrough PB. Functional homologs of fungal metallothionein genes from Arabidopsis. Plant Cell. 1994 Jun;6(6):875–84.

117.   Robinson NJ, Wilson JR, Turner JS. Expression of the type 2 metallothionein-like gene MT2 from Arabidopsis thaliana in Zn(2+)-metallothionein-deficient Synechococcus PCC 7942: putative role for MT2 in Zn2+ metabolism. Plant Mol Biol. 1996 Mar;30(6):1169–79.

118.   Tommey AM, Shi J, Lindsay WP, Urwin PE, Robinson NJ. Expression of the pea gene PSMTA in E. coli. Metal-binding properties of the expressed protein. FEBS Lett. 1991 Nov 4;292(1–2):48–52.

119.   Murphy A, Taiz L. Comparison of metallothionein gene expression and nonprotein thiols in ten Arabidopsis ecotypes. Correlation with copper tolerance. Plant Physiol. 1995 Nov;109(3):945–54.

120.   Pufahl RA, Singer CP, Peariso KL, Lin SJ, Schmidt PJ, Fahrni CJ, et al. Metal ion chaperone function of the soluble Cu(I) receptor Atx1. Science. 1997 Oct 31;278(5339):853–6.

121.   Glerum DM, Shtanko A, Tzagoloff A. Characterization of COX17, a yeast gene involved in copper metabolism and assembly of cytochrome oxidase. J Biol Chem. 1996 Jun 14;271(24):14504–9.

122.   Grill E, Winnacker EL, Zenk MH. Phytochelatins, a class of heavy-metal-binding peptides from plants, are functionally analogous to metallothioneins. Proc Natl Acad Sci U S A. 1987 Jan;84(2):439–43.

123.   Gekeler W, Grill E, Winnacker E-L, Zenk MH. Algae sequester heavy metals via synthesis of phytochelatin complexes. Arch Microbiol. 1988 Jun 1;150(2):197–202.

124.   Gekeler W, Grill E, Winnacker E-L, Zenk MH. Survey of the Plant Kingdom for the Ability to Bind Heavy Metals through Phytochelatins. Zeitschrift für Naturforschung C. 1989 Jun 1;44(5–6):361–9.

125.   Grill E, Winnacker E-L, Zenk MH. Synthesis of seven different homologous phytochelatins in metal-exposedSchizosaccharomyces pombecells. FEBS Lett. 1986 Mar 3;197(1–2):115–20.

126.   Maitani T, Kubota H, Sato K, Yamada T. The Composition of Metals Bound to Class III Metallothionein (Phytochelatin and Its Desglycyl Peptide) Induced by Various Metals in Root Cultures of Rubia tinctorum. Plant Physiol. 1996 Apr;110(4):1145–50.

127.   Loeffler S, Hochberger A, Grill E, Winnacker E-L, Zenk MH. Termination of the phytochelatin synthase reaction through sequestration of heavy metals by the reaction product. FEBS Lett. 1989 Nov 20;258(1):42–6.

128.   Chen J, Zhou J, Goldsbrough PB. Characterization of phytochelatin synthase from tomato. Physiol Plant. 1997 Sep;101(1):165–72.

129.   Klapheck S, Schlunz S, Bergmann L. Synthesis of Phytochelatins and Homo-Phytochelatins in Pisum sativum L. Plant Physiol. 1995 Feb;107(2):515–21.

130. Ju GC, Li X-Z, Rauser WE, Oaks A. Influence of cadmium on the production of gamma-glutamylcysteine peptides and enzymes of nitrogen assimilation in Zea mays seedlings. Physiol Plant. 1997 Dec;101(4):793–9.

131. Chen J, Goldsbrough PB. Increased Activity of [gamma]-Glutamylcysteine Synthetase in Tomato Cells Selected for Cadmium Tolerance. Plant Physiol. 1994 Sep;106(1):233–9.

132. Schäfer HJ, Greiner S, Rausch T, Haag-Kerwer A. In seedlings of the heavy metal accumulator Brassica juncea Cu2+ differentially affects transcript amounts for gamma-glutamylcysteine synthetase (gamma-ECS) and metallothionein (MT2). FEBS Lett. 1997 Mar 10;404(2–3):216–20.

133. Grill E, Winnacker E-L, Zenk MH. Occurrence of heavy metal binding phytochelatins in plants growing in a mining refuse area. Experientia. 1988 Jun 1;44(6):539–40.

134. Kneer R, Zenk MH. Phytochelatins protect plant enzymes from heavy metal poisoning. Phytochemistry. 1992 Aug 1;31(8):2663–7.

135. Salt DE, Rauser WE. MgATP-Dependent Transport of Phytochelatins Across the Tonoplast of Oat Roots. Plant Physiol. 1995 Apr;107(4):1293–301.

136. Kramer, Pickering, Prince, Raskin. Subcellular Localization and Speciation of Nickel in Hyperaccumulator and Non-Accumulator Thlaspi Species. Plant. 2000;

137. Crouzet J, Trombik T, Fraysse AS, Boutry M. Organization and function of the plant pleiotropic drug resistance ABC transporter family. FEBS Lett. 2006 Feb 13;580(4):1123–30.

138. Paumi CM, Chuk M, Snider J, Stagljar I, Michaelis S. ABC transporters in Saccharomyces cerevisiae and their interactors: new technology advances the biology of the ABCC (MRP) subfamily. Microbiol Mol Biol Rev. 2009 Dec;73(4):577–93.

139. Li L, He Z, Pandey GK, Tsuchiya T, Luan S. Functional cloning and characterization of a plant efflux carrier for multidrug and heavy metal detoxification. J Biol Chem. 2002 Feb 15;277(7):5360–8.

140. Li Y-M, Chaney R, Brewer E, Roseberg R, Angle JS, Baker A, et al. Development of a technology for commercial phytoextraction of nickel: economic and technical considerations. Plant Soil. 2003 Feb 1;249(1):107–15.

141. pYES2 Yeast Expression Vector [Internet]. [cited 2022 Nov 20]. Available from: https://www.thermofisher.com/order/catalog/product/V82520

142. Murashige T, Skoog F. A revised medium for rapid growth and bio assays with tobacco tissue cultures. Physiol Plant. 1962 Jul;15(3):473–97.

143. Perea-García A, Garcia-Molina A, Andrés-Colás N, Vera-Sirera F, Pérez-Amador MA, Puig S, et al. Arabidopsis copper transport protein COPT2 participates in the cross talk between iron deficiency responses and low-phosphate signaling. Plant Physiol © 2013 American Society of Plant Biologists All Rights Reserved. 2013 May;162(1):180–94.

144. Madden T. The BLAST Sequence Analysis Tool. In: The NCBI Handbook. National Center for Biotechnology Information (US); 2003.

145. Untergasser A, Cutcutache I, Koressaar T, Ye J, Faircloth BC, Remm M, et al. Primer3--new capabilities and interfaces. Nucleic Acids Res. 2012 Aug;40(15):e115.

146.   Koressaar T, Remm M. Enhancements and modifications of primer design program Primer3. Bioinformatics. 2007 May 15;23(10):1289–91.

147.   Pfaffl MW. A new mathematical model for relative quantification in real-time RT-PCR. Nucleic Acids Res. 2001 May 1;29(9):e45.

148.   Schneider CA, Rasband WS, Eliceiri KW. NIH Image to ImageJ: 25 years of image analysis. Nat Methods. 2012 Jul;9(7):671–5.

149.   Kawano T. Roles of the reactive oxygen species-generating peroxidase reactions in plant defense and growth induction. Plant Cell Rep. 2003 Jun;21(9):829–37.

150.   Gleave AP. A versatile binary vector system with a T-DNA organisational structure conducive to efficient integration of cloned DNA into the plant genome. Plant Mol Biol. 1992 Dec;20(6):1203–7.

151.   Gold demand by sectors [Internet]. World Gold Council. [cited 2022 Aug 30]. Available from: https://www.gold.org/about-gold/gold-demand/by-sector

152.   King HM. Uses of gold in industry, medicine, computers, electronics, jewelry [Internet]. [cited 2022 Aug 30]. Available from: https://geology.com/minerals/gold/uses-of-gold.shtml

153.   McClements J, Bar L, Singla P, Canfarotta F, Thomson A, Czulak J, et al. Molecularly Imprinted Polymer Nanoparticles Enable Rapid, Reliable, and Robust Point-of-Care Thermal Detection of SARS-CoV-2. ACS Sens. 2022 Apr 22;7(4):1122–31.

154.   Dong K, Xie F, Wang W, Chang Y, Lu D, Gu X, et al. The detoxification and utilization of cyanide tailings: A critical review. J Clean Prod. 2021 Jun 15;302:126946.

155.   Acar S. Process development metallurgical studies for gold cyanidation process. Miner Metall Process. 2016 Nov 1;33(4):161–71.

156.   Predki PF, Sarkar B. Effect of replacement of "zinc finger" zinc on estrogen receptor DNA interactions. J Biol Chem. 1992 Mar 25;267(9):5842–6.

157.   Georgatsou E, Mavrogiannis LA, Fragiadakis GS, Alexandraki D. The yeast Fre1p/Fre2p cupric reductases facilitate copper uptake and are regulated by the copper-modulated Mac1p activator. J Biol Chem. 1997 May 23;272(21):13786–92.

158.   Knight SA, Labbé S, Kwon LF, Kosman DJ, Thiele DJ. A widespread transposable element masks expression of a yeast copper transport gene. Genes Dev. 1996 Aug 1;10(15):1917–29.

159.   Dancis A, Yuan DS, Haile D, Askwith C, Eide D, Moehle C, et al. Molecular characterization of a copper transport protein in S. cerevisiae: an unexpected role for copper in iron transport. Cell. 1994 Jan 28;76(2):393–402.

160.   Lin SJ, Pufahl RA, Dancis A, O'Halloran TV, Culotta VC. A role for the Saccharomyces cerevisiae ATX1 gene in copper trafficking and iron transport. J Biol Chem. 1997 Apr 4;272(14):9215–20.

161.   Kosman DJ. Molecular mechanisms of iron uptake in fungi. Mol Microbiol. 2003 Mar;47(5):1185–97.

162.   Fürst P, Hu S, Hackett R, Hamer D. Copper activates metallothionein gene transcription by altering the conformation of a specific DNA binding protein. Cell. 1988 Nov 18;55(4):705–17.

163.   Thiele DJ. ACE1 regulates expression of the Saccharomyces cerevisiae metallothionein gene. Mol Cell Biol. 1988 Jul;8(7):2745–52.

164.   Karin M, Najarian R, Haslinger A, Valenzuela P, Welch J, Fogel S. Primary structure and transcription of an amplified genetic locus: the CUP1 locus of yeast. Proc Natl Acad Sci U S A. 1984 Jan;81(2):337–41.

165.   Welch J, Fogel S, Buchman C, Karin M. The CUP2 gene product regulates the expression of the CUP1 gene, coding for yeast metallothionein. EMBO J. 1989 Jan;8(1):255–60.

166.   Rea PA. Plant ATP-binding cassette transporters. Annu Rev Plant Biol. 2007;58:347–75.

167.   O'Malley RC, Ecker JR. Linking genotype to phenotype using the Arabidopsis unimutant collection. Plant J. 2010 Mar;61(6):928–40.

168.   Clough SJ, Bent AF. Floral dip: a simplified method for Agrobacterium-mediated transformation of Arabidopsis thaliana. Plant J. 1998 Dec;16(6):735–43.

169.   Flowers T. Solutes: what are they, where are they and what do they do. In: Anthony R. Yeo TJF, editor. Plant solute transport. Blackwell Publishing; 2008. p. 15–28.

170.   Thermo Scientific iCAP 7000 series ICP-OES [Internet]. GeneCraft Labs. PT GeneCraft Labs; 2019 [cited 2022 Aug 30]. Available from: https://genecraftlabs.com/en/product/thermo-scientific-icap-7000-series-icp-oes/

171.   Aqua Regia [Internet]. Available from: http://web.mit.edu/piuska/Public/Ekaterinburg%20more/Ekaterinburg%20research/Aqua%20Regia%20JCE.pdf

172.   H2DCFDA (H2-DCF, DCF) [Internet]. [cited 2022 Aug 22]. Available from: https://www.thermofisher.com/order/catalog/product/D399

173.   Nova Z, Skovierova H, Strnadel J, Halasova E, Calkovska A. Short-Term versus Long-Term Culture of A549 Cells for Evaluating the Effects of Lipopolysaccharide on Oxidative Stress, Surfactant Proteins and Cathelicidin LL-37. Int J Mol Sci [Internet]. 2020 Feb 9;21(3). Available from: http://dx.doi.org/10.3390/ijms21031148

174.   GoldBio. A quick overview of Agrobacterium for plant transformation [Internet]. Goldbio.com. [cited 2022 Aug 30]. Available from: https://www.goldbio.com/articles/article/a-quick-overview-of-agrobacterium-for-plant-transformation

175.   A Guide to T-DNA Binary Vectors in Plant Transformation [Internet]. [cited 2022 Nov 19]. Available from: https://goldbio.com/articles/article/a-guide-to-agrobacterium-t-dna-binary-vectors

176.   Odell JT, Nagy F, Chua NH. Identification of DNA sequences required for activity of the cauliflower mosaic virus 35S promoter. Nature. 1985;313(6005):810–2.

177.   Berardini TZ, Reiser L, Li D, Mezheritsky Y, Muller R, Strait E, et al. The Arabidopsis information resource: Making and mining the 'gold standard' annotated reference plant genome. Genesis. 2015 Aug;53(8):474–85.

178.   Cunningham F, Allen JE, Allen J, Alvarez-Jarreta J, Amode MR, Armean IM, et al. Ensembl 2022. Nucleic Acids Res. 2022 Jan 7;50(D1):D988–95.

179.   Tiwari M, Krishnamurthy S, Shukla D, Kiiskila J, Jain A, Datta R, et al. Comparative transcriptome and proteome analysis to reveal the biosynthesis of gold nanoparticles in Arabidopsis. Sci Rep. 2016 Feb 23;6:21733.

180.   Wang YH. How effective is T-DNA insertional mutagenesis in Arabidopsis? J Biochem Technol. 2008;1(1):11–20.

181.   Fu D, Beeler TJ, Dunn TM. Sequence, mapping and disruption of CCC2, a gene that cross-complements the Ca(2+)-sensitive phenotype of csg1 mutants and encodes a P-type ATPase belonging to the Cu(2+)-ATPase subfamily. Yeast. 1995 Mar;11(3):283–92.

182.   Dameron CT, George GN, Arnold P, Santhanagopalan V, Winge DR. Distinct metal binding configurations in ACE1. Biochemistry. 1993 Jul 20;32(28):7294–301.

183.   Szczypka MS, Thiele DJ. A cysteine-rich nuclear protein activates yeast metallothionein gene transcription. Mol Cell Biol. 1989 Feb;9(2):421–9.

184.   Li J, Wang W, Yuan J, Xu J, He L, Zhang X, et al. Ubiquitin-independent proteasome system is required for degradation of Arabidopsis COPPER TRANSPORTER 2. Plant Sci. 2021 Mar;304:110825.

185.   Gayomba SR, Jung H-I, Yan J, Danku J, Rutzke MA, Bernal M, et al. The CTR/COPT-dependent copper uptake and SPL7-dependent copper deficiency responses are required for basal cadmium tolerance in A. thaliana. Metallomics. 2013 Sep;5(9):1262–75.

186.   Liu T-Y, Huang T-K, Tseng C-Y, Lai Y-S, Lin S-I, Lin W-Y, et al. PHO2-dependent degradation of PHO1 modulates phosphate homeostasis in Arabidopsis. Plant Cell. 2012 May;24(5):2168–83.

187.   Connolly EL, Fett JP, Guerinot ML. Expression of the IRT1 metal transporter is controlled by metals at the levels of transcript and protein accumulation. Plant Cell. 2002 Jun;14(6):1347–57.

188.   Paez Valencia J, Goodman K, Otegui MS. Endocytosis and Endosomal Trafficking in Plants. Annu Rev Plant Biol. 2016 Apr 29;67:309–35.

189.   Tian M, Xie Q. Non-26S proteasome proteolytic role of ubiquitin in plant endocytosis and endosomal trafficking(F). J Integr Plant Biol. 2013 Jan;55(1):54–63.

190.   Keunen E, Remans T, Bohler S, Vangronsveld J, Cuypers A. Metal-induced oxidative stress and plant mitochondria. Int J Mol Sci. 2011 Oct 18;12(10):6894–918.

191.   Niemietz CM, Tyerman SD. New potent inhibitors of aquaporins: silver and gold compounds inhibit aquaporins of plant and human origin. FEBS Lett. 2002 Nov 20;531(3):443–7.

192.   Preston GM, Jung JS, Guggino WB, Agre P. The mercury-sensitive residue at cysteine 189 in the CHIP28 water channel. J Biol Chem. 1993 Jan 5;268(1):17–20.

193.   Zientek ML, Loferski PJ. Platinum-group elements: so many excellent properties [Internet]. US Geological Survey; 2014. Available from: http://dx.doi.org/10.3133/fs20143064

194.   U.S. Geological Survey, Department of the Interior. 2022 Final List of Critical Minerals [Internet]. [cited 2022 Jul 27]. Available from: https://www.federalregister.gov/documents/2022/02/24/2022-04027/2022-final-list-of-critical-minerals

195.   Aarzoo, Nidhi, Samim M. Palladium nanoparticles as emerging pollutants from motor vehicles: An in-depth review on distribution, uptake and toxicological effects in occupational and living environment. Sci Total Environ. 2022 Jun 1;823:153787.

196.   Jackson MT, Sampson J, Prichard HM. Platinum and palladium variations through the urban environment: evidence from 11 sample types from Sheffield, UK. Sci Total Environ. 2007 Oct 15;385(1–3):117–31.

197.   Fujimori E, Minamoto K, Haraguchi H. Comparative Study on the Distributions of Precious Metals (Ru, Rh, Pd, Ir, Pt, and Au) in Industrial Waste Incineration Ashes as Determined by Tellurium Coprecipitation and ICP-MS. BCSJ. 2005 Nov 1;78(11):1963–9.

198.   Astruc D, Lu F, Aranzaes JR. Nanoparticles as recyclable catalysts: the frontier between homogeneous and heterogeneous catalysis. Angew Chem Int Ed Engl. 2005 Dec 9;44(48):7852–72.

199.   Iravani S. Green synthesis of metal nanoparticles using plants. Green Chem. 2011 Jan 10;13(10):2638–50.

200.   Singaravelu G, Arockiamary JS, Kumar VG, Govindaraju K. A novel extracellular synthesis of monodisperse gold nanoparticles using marine alga, Sargassum wightii Greville. Colloids Surf B Biointerfaces. 2007 May 15;57(1):97–101.

201.   De Corte S, Hennebel T, De Gusseme B, Verstraete W, Boon N. Bio-palladium: from metal recovery to catalytic applications. Microb Biotechnol. 2012 Jan;5(1):5–17.

202.   Anderson CWN, Bhatti SM, Gardea-Torresdey J, Parsons J. In vivo effect of copper and silver on synthesis of gold nanoparticles inside living plants. ACS Sustainable Chemistry and Engineering. 2013;1(6):640–8.

203.   Losfeld G, Escande V, Vidal de La Blache P, L'Huillier L, Grison C. Design and performance of supported Lewis acid catalysts derived from metal contaminated biomass for Friedel–Crafts alkylation and acylation. Catal Today. 2012 Jul 30;189(1):111–6.

204.   Torborg C, Beller M. Recent applications of palladium-catalyzed coupling reactions in the pharmaceutical, agrochemical, and fine chemical industries. Adv Synth Catal. 2009 Dec;351(18):3027–43.

205.   Gralla EB, Thiele DJ, Silar P, Valentine JS. ACE1, a copper-dependent transcription factor, activates expression of the yeast copper, zinc superoxide dismutase gene. Proc Natl Acad Sci U S A. 1991 Oct 1;88(19):8558–62.

206.   Jayakumar K, Rajesh M, Baskaran L, Vijayarengan P. Changes in nutritional metabolism of tomato (Lycopersicon esculantum Mill.) plants exposed to increasing concentration of cobalt chloride. Int J Food Nutr Saf. 2013;4(2):62–9.

207.   Hu X, Wei X, Ling J, Chen J. Cobalt: An Essential Micronutrient for Plant Growth? Front Plant Sci. 2021 Nov 16;12:768523.

208.   DalCorso G, Farinati S, Furini A. Regulatory networks of cadmium stress in plants. Plant Signal Behav. 2010 Jun;5(6):663–7.

209.   Mendoza-Cózatl DG, Butko E, Springer F, Torpey JW, Komives EA, Kehr J, et al. Identification of high levels of phytochelatins, glutathione and cadmium in the phloem sap of Brassica napus. A role for thiol-peptides in the long-distance transport of cadmium and the effect of cadmium on iron translocation. Plant J. 2008 Apr;54(2):249–59.

210.   Lux A, Martinka M, Vaculík M, White PJ. Root responses to cadmium in the rhizosphere: a review. J Exp Bot. 2011 Jan;62(1):21–37.

211.   Sanità di Toppi L, Gabbrielli R. Response to cadmium in higher plants. Environ Exp Bot. 1999 Apr 1;41(2):105–30.

212.   Gill SS, Khan NA, Tuteja N. Cadmium at high dose perturbs growth, photosynthesis and nitrogen metabolism while at low dose it up regulates sulfur assimilation and antioxidant machinery in garden cress (Lepidium sativum L.). Plant Sci. 2012 Jan;182:112–20.

213.   Jozefczak M, Remans T, Vangronsveld J, Cuypers A. Glutathione is a key player in metal-induced oxidative stress defenses. Int J Mol Sci. 2012 Mar 7;13(3):3145–75.

214.   Liu T, Liu S, Guan H, Ma L, Chen Z, Gu H, et al. Transcriptional profiling of Arabidopsis seedlings in response to heavy metal lead (Pb). Environmental and Experimental Botany. 2009 Dec 1;67(2):377–86.

215.   Haider FU, Liqun C, Coulter JA, Cheema SA, Wu J, Zhang R, et al. Cadmium toxicity in plants: Impacts and remediation strategies. Ecotoxicol Environ Saf. 2021 Mar 15;211:111887.

216.   Devi SR, Prasad MNV. Membrane Lipid Alterations in Heavy Metal Exposed Plants. In: Prasad MNV, Hagemeyer J, editors. Heavy Metal Stress in Plants: From Molecules to Ecosystems. Berlin, Heidelberg: Springer Berlin Heidelberg; 1999. p. 99–116.

217.   Afzal Z, Howton TC, Sun Y, Mukhtar MS. The Roles of Aquaporins in Plant Stress Responses. J Dev Biol [Internet]. 2016 Feb 4;4(1). Available from: https://www.ncbi.nlm.nih.gov/pubmed/29615577

218.   Omote H, Hiasa M, Matsumoto T, Otsuka M, Moriyama Y. The MATE proteins as fundamental transporters of metabolic and xenobiotic organic cations. Trends Pharmacol Sci. 2006 Nov;27(11):587–93.

219.   Bansal V, Rautaray D, Bharde A, Ahire K, Sanyal A, Ahmad A, et al. Fungus-mediated biosynthesis of silica and titania particles. J Mater Chem. 2005 Jun 23;15(26):2583–9.

220.   Silver S, Phung LT. Bacterial heavy metal resistance: new surprises. Annu Rev Microbiol. 1996;50:753–89.

221.   Klaus T, Joerger R, Olsson E, Granqvist C-G. Silver-based crystalline nanoparticles, microbially fabricated. Proceedings of the National Academy of Sciences. 1999 Nov 23;96(24):13611–4.

222.   Hulkoti NI, Taranath TC. Biosynthesis of nanoparticles using microbes- a review. Colloids Surf B Biointerfaces. 2014 Sep 1;121:474–83.

223.   Ghosh S, Ahmad R, Banerjee K, AlAjmi MF, Rahman S. Mechanistic Aspects of Microbe-Mediated Nanoparticle Synthesis. Front Microbiol. 2021;12:638068.

224.   Gomez-Bolivar J, Mikheenko IP, Orozco RL, Sharma S, Banerjee D, Walker M, et al. Synthesis of Pd/Ru Bimetallic Nanoparticles by Escherichia coli and Potential as a Catalyst for Upgrading 5-Hydroxymethyl Furfural Into Liquid Fuel Precursors. Front Microbiol. 2019 Jun 20;10:1276.

225.   Ovais M, Khalil AT, Ayaz M, Ahmad I, Nethi SK, Mukherjee S. Biosynthesis of Metal Nanoparticles via Microbial Enzymes: A Mechanistic Approach. International Journal of Molecular Sciences. 2018 Dec;19(12):4100.

226.   Dwivedi S, AlKhedhairy AA, Ahamed M, Musarrat J. Biomimetic Synthesis of Selenium Nanospheres by Bacterial Strain JS-11 and Its Role as a Biosensor for Nanotoxicity Assessment: A Novel Se-Bioassay. PLOS ONE. 2013 Mar 4;8(3):e57404.

227.   He S, Guo Z, Zhang Y, Zhang S, Wang J, Gu N. Biosynthesis of gold nanoparticles using the bacteria Rhodopseudomonas capsulata. Materials Letters. 2007 Jul 1;61(18):3984–7.

228.   Mikheenko IP, Rousset M, Dementin S, Macaskie LE. Bioaccumulation of Palladium by Desulfovibrio fructosivorans Wild-Type and Hydrogenase-Deficient Strains. Applied and Environmental Microbiology. 2008 Oct 1;74(19):6144–6.

229.   Bacteria in Nanoparticle Synthesis: Current Status and Future Prospects [Internet]. [cited 2021 Jul 27]. Available from: https://www.hindawi.com/journals/isrn/2014/359316/

230.   Shi P, Veiga M, Anderson C. Geochemical assessment of platinum group metals for phytomining. Revista Escola de Minas. 2020;73(1):85–91.

231.   Anderson C, Moreno F, Geurts F, Wreesmann C, Ghomshei M, Meech J. A comparative analysis of gold-rich plant material using various analytical methods. Microchem J. 2005 Aug 1;81(1):81–5.

232.   A basic guide to RNA-sequencing [Internet]. Novogene. 2021 [cited 2022 Aug 3]. Available from: https://en.novogene.com/resources/blog/a-basic-guide-to-rna-sequencing/

233.   Schuster SC. Next-generation sequencing transforms today's biology. Nat Methods. 2008 Jan;5(1):16–8.

234.   Sequencing: Illumina technology [Internet]. [cited 2022 Aug 30]. Available from: https://support.illumina.com/content/dam/illumina-support/courses/Sequencing_Illumina_Technology/story_html5.html?iframe

235.   Methods to check RNA integrity [Internet]. Thermo Fisher. [cited 2022 Aug 30]. Available from: https://www.thermofisher.com/uk/en/home/references/ambion-tech-support/rna-isolation/tech-notes/is-your-rna-intact.html#:~:text=The%20most%20common%20method%20used,can%20be%20difficult%20to%20interpret.

236.   Wilhelm BT, Landry J-R. RNA-Seq-quantitative measurement of expression through massively parallel RNA-sequencing. Methods. 2009 Jul;48(3):249–57.

237.   Whitley SK, Horne WT, Kolls JK. Research Techniques Made Simple: Methodology and Clinical Applications of RNA Sequencing. Journal of Investigative Dermatology. 2016 Aug 1;136(8):e77–82.

238.   RNA Sequencing VS microarray [Internet]. Otogenetics. Otogenetics Corporation; 2017 [cited 2022 Aug 30]. Available from: https://www.otogenetics.com/rna-sequencing-vs-microarray/

239.   Zhao S, Zhang Y, Gamini R, Zhang B, von Schack D. Evaluation of two main RNA-seq approaches for gene quantification in clinical RNA sequencing: polyA+ selection versus rRNA depletion. Sci Rep. 2018 Mar 19;8(1):4781.

240.   Kang W-H, Sim YM, Koo N, Nam J-Y, Lee J, Kim N, et al. Transcriptome profiling of abiotic responses to heat, cold, salt, and osmotic stress of Capsicum annuum L. Sci Data. 2020 Jan 13;7(1):17.

241. Shen X, Wang Z, Song X, Xu J, Jiang C, Zhao Y, et al. Transcriptomic profiling revealed an important role of cell wall remodeling and ethylene signaling pathway during salt acclimation in Arabidopsis. Plant Mol Biol. 2014 Oct;86(3):303–17.

242. Li P, Cao W, Fang H, Xu S, Yin S, Zhang Y, et al. Transcriptomic Profiling of the Maize (Zea mays L.) Leaf Response to Abiotic Stresses at the Seedling Stage. Front Plant Sci [Internet]. 2017 [cited 2021 Jul 27];0. Available from: https://internal-journal.frontiersin.org/articles/10.3389/fpls.2017.00290/full

243. Wang Y-N, Tang L, Hou Y, Wang P, Yang H, Wei C-L. Differential transcriptome analysis of leaves of tea plant (Camellia sinensis) provides comprehensive insights into the defense responses to Ectropis oblique attack using RNA-Seq. Funct Integr Genomics. 2016 Jul 1;16(4):383–98.

244. Zhu Q-H, Stephen S, Kazan K, Jin G, Fan L, Taylor J, et al. Characterization of the defense transcriptome responsive to Fusarium oxysporum-infection in Arabidopsis using RNA-seq. Gene. 2013 Jan 10;512(2):259–66.

245. Huang Y, Chen H, Reinfelder JR, Liang X, Sun C, Liu C, et al. A transcriptomic (RNA-seq) analysis of genes responsive to both cadmium and arsenic stress in rice root. Science of The Total Environment. 2019 May 20;666:445–60.

246. Cao ZZ, Lin XY, Yang YJ, Guan MY, Xu P, Chen MX. Gene identification and transcriptome analysis of low cadmium accumulation rice mutant (lcd1) in response to cadmium stress using MutMap and RNA-seq. BMC Plant Biol. 2019 Jun 11;19(1):250.

247. Hu Z, Zhang Y, He Y, Cao Q, Zhang T, Lou L, et al. Full-Length Transcriptome Assembly of Italian Ryegrass Root Integrated with RNA-Seq to Identify Genes in Response to Plant Cadmium Stress. International Journal of Molecular Sciences. 2020 Jan;21(3):1067.

248. Peng H, Gao J, Song X. Identification of heavy metal-responsive genes in radish (Raphanus sativus L.) through RNA-Seq meta-analysis. Scientia Horticulturae. 2021 Oct 15;288:110402.

249. Weber M, Trampczynska A, Clemens S. Comparative transcriptome analysis of toxic metal responses in Arabidopsis thaliana and the Cd2+-hypertolerant facultative metallophyte Arabidopsis halleri. Plant, Cell & Environment. 2006;29(5):950–63.

250. Capeness MJ, Imrie L, Mühlbauer LF, Le Bihan T, Horsfall LEYR 2019. Shotgun proteomic analysis of nanoparticle-synthesizing Desulfovibrio alaskensis in response to platinum and palladium. Microbiology. 165(12):1282–94.

251. Sun GL, Reynolds EE, Belcher AM. Designing yeast as plant-like hyperaccumulators for heavy metals. Nat Commun. 2019 Nov 8;10(1):5080.

252. Wu T, Hu E, Xu S, Chen M, Guo P, Dai Z, et al. clusterProfiler 4.0: A universal enrichment tool for interpreting omics data. Innovation (Camb). 2021 Aug 28;2(3):100141.

253. Buetow KH. Bioinformatics. In: Mendelsohn J, Howley PM, Israel MA, Gray JW, Thompson CB, editors. The Molecular Basis of Cancer (Third Edition). Philadelphia: W.B. Saunders; 2008. p. 325–33.

254. Ajeesh Krishna TP, Maharajan T, Victor Roch G, Ignacimuthu S, Antony Ceasar S. Structure, Function, Regulation and Phylogenetic Relationship of ZIP Family Transporters of Plants. Front Plant Sci. 2020 May 27;11:662.

255.   Tran TA, Popova LP. Functions and toxicity of cadmium in plants: recent advances and future prospects. Turk J Botany. 2013;37(1):1–13.

256.   Chang Y-C, Zouari M, Gogorcena Y, Lucena JJ, Abadía J. Effects of cadmium and lead on ferric chelate reductase activities in sugar beet roots. Plant Physiol Biochem. 2003 Nov 1;41(11):999–1005.

257.   Chaoui A, Jarrar B, El Ferjani E. Effects of cadmium and copper on peroxidase, NADH oxidase and IAA oxidase activities in cell wall, soluble and microsomal membrane fractions of pea roots. J Plant Physiol. 2004 Nov;161(11):1225–34.

258.   Shannon RD. Revised effective ionic radii and systematic studies of interatomic distances in halides and chalcogenides. Acta Crystallogr A. 1976 Sep 1;32(5):751–67.

259.   Cohen CK, Fox TC, Garvin DF, Kochian LV. The role of iron-deficiency stress responses in stimulating heavy-metal transport in plants. Plant Physiol. 1998 Mar;116(3):1063–72.

260.   Nazmul Hasan M, Islam S, Bhuiyan FH, Arefin S, Hoque H, Azad Jewel N, et al. Genome wide analysis of the heavy-metal-associated (HMA) gene family in tomato and expression profiles under different stresses. Gene. 2022 Aug 15;835:146664.

261.   Wong CKE, Cobbett CS. HMA P-type ATPases are the major mechanism for root-to-shoot Cd translocation in Arabidopsis thaliana. New Phytol. 2009;181(1):71–8.

262.   Fatemi H, Zaghdoud C, Nortes PA, Carvajal M, Martínez-Ballesta M del C. Differential Aquaporin Response to Distinct Effects of Two Zn Concentrations after Foliar Application in Pak Choi (Brassica rapa L.) Plants. Agronomy. 2020 Mar 24;10(3):450.

263.   Mathur P, Tripathi DK, Baluška F, Mukherjee S. Auxin-mediated molecular mechanisms of heavy metal and metalloid stress regulation in plants. Environ Exp Bot. 2022 Apr 1;196:104796.

264.   Baloun J, Nevrtalova E, Kovacova V, Hudzieczek V, Cegan R, Vyskot B, et al. Characterization of the HMA7 gene and transcriptomic analysis of candidate genes for copper tolerance in two Silene vulgaris ecotypes. J Plant Physiol. 2014 Aug 15;171(13):1188–96.

265.   Pedas P, Husted S. Zinc transport mediated by barley ZIP proteins are induced by low pH. Plant Signal Behav. 2009 Sep;4(9):842–5.

266.   Martini DF. Functional analysis of AtZIP4, AtZIP6 and AtZIP9 metal transporters of Arabidopsis thaliana and Expression of Saccharomyces cerevisiae ZRC1 in different plant species [phd]. Furini A, editor. Graduate School for Health and Life Sciences; 2018.

267.   Nawrath C, Heck S, Parinthawong N, Métraux J-P. EDS5, an essential component of salicylic acid-dependent signaling for disease resistance in Arabidopsis, is a member of the MATE transporter family. Plant Cell. 2002 Jan;14(1):275–86.

268.   Green LS, Rogers EE. FRD3 controls iron localization in Arabidopsis. Plant Physiol. 2004 Sep;136(1):2523–31.

269.   Santos ALD, Chaves-Silva S, Yang L, Maia LGS, Chalfun-Júnior A, Sinharoy S, et al. Global analysis of the MATE gene family of metabolite transporters in tomato. BMC Plant Biol. 2017 Oct 30;17(1):185.

270.   Wang J, Hou Q, Li P, Yang L, Sun X, Benedito VA, et al. Diverse functions of multidrug and toxin extrusion (MATE) transporters in citric acid efflux and metal homeostasis in Medicago truncatula. Plant J. 2017 Apr;90(1):79–95.

271.   Higgins CF. Multiple molecular mechanisms for multidrug resistance transporters. Nature. 2007 Apr 12;446(7137):749–57.

272.   Yan A, Wang Y, Tan SN, Mohd Yusof ML, Ghosh S, Chen Z. Phytoremediation: A Promising Approach for Revegetation of Heavy Metal-Polluted Land. Front Plant Sci. 2020 Apr 30;11:359.

273.   Miyauchi H, Moriyama S, Kusakizako T, Kumazaki K, Nakane T, Yamashita K, et al. Structural basis for xenobiotic extrusion by eukaryotic MATE transporter. Nat Commun. 2017 Nov 21;8(1):1633.

274.   Zhang H, Zhu H, Pan Y, Yu Y, Luan S, Li L. A DTX/MATE-type transporter facilitates abscisic acid efflux and modulates ABA sensitivity and drought tolerance in Arabidopsis. Mol Plant. 2014 Oct;7(10):1522–32.

275.   Henikoff S, Greene EA, Pietrokovski S, Bork P, Attwood TK, Hood L. Gene families: the taxonomy of protein paralogs and chimeras. Science. 1997 Oct 24;278(5338):609–14.

276.   Higgins CF, Linton KJ. The ATP switch model for ABC transporters. Nat Struct Mol Biol. 2004 Oct;11(10):918–26.

277.   Rees DC, Johnson E, Lewinson O. ABC transporters: the power to change. Nat Rev Mol Cell Biol. 2009 Mar;10(3):218–27.

278.   Verrier PJ, Bird D, Burla B, Dassa E, Forestier C, Geisler M, et al. Plant ABC proteins--a unified nomenclature and updated inventory. Trends Plant Sci. 2008 Apr;13(4):151–9.

279.   Ji Y. The role of cytosolic glutamine synthetases in abiotic stress and development in Arabidopsis thaliana [phd]. University of Saskatchewan; 2011.

280.   Sánchez-Fernández R, Davies TG, Coleman JO, Rea PA. The Arabidopsis thaliana ABC protein superfamily, a complete inventory. J Biol Chem. 2001 Aug 10;276(32):30231–44.

281.   Klein M, Burla B, Martinoia E. The multidrug resistance-associated protein (MRP/ABCC) subfamily of ATP-binding cassette transporters in plants. FEBS Lett. 2006 Feb 13;580(4):1112–22.

282.   Frelet-Barrand A, Kolukisaoglu HU, Plaza S, Rüffer M, Azevedo L, Hörtensteiner S, et al. Comparative mutant analysis of Arabidopsis ABCC-type ABC transporters: AtMRP2 contributes to detoxification, vacuolar organic anion transport and chlorophyll degradation. Plant Cell Physiol. 2008 Apr;49(4):557–69.

283.   Khan. Induction of oxidative stress and antioxidant metabolism in Calamus tenuis leaves under chromium and zinc toxicity. Indian J Plant Physiol. 2007;12(4):353.

284.   Reese RN, Mehra RK, Tarbet EB, Winge DR. Studies on the gamma-glutamyl Cu-binding peptide from Schizosaccharomyces pombe. J Biol Chem. 1988 Mar 25;263(9):4186–92.

285.   Mehra RK, Tarbet EB, Gray WR, Winge DR. Metal-specific synthesis of two metallothioneins and gamma-glutamyl peptides in Candida glabrata. Proc Natl Acad Sci U S A. 1988 Dec;85(23):8815–9.

286.   Takahashi R, Bashir K, Ishimaru Y, Nishizawa NK, Nakanishi H. The role of heavy-metal ATPases, HMAs, in zinc and cadmium transport in rice. Plant Signal Behav. 2012 Dec;7(12):1605–7.

287. Kamimoto Y, Hamamoto M, Shitan N, Yazaki K. Unusual expression of an Arabidopsis ATP-binding cassette transporter ABCC11. Plant Biotechnol. 2009;26(2):261–5.

288. Song W-Y, Park J, Mendoza-Cózatl DG, Suter-Grotemeyer M, Shim D, Hörtensteiner S, et al. Arsenic tolerance in *Arabidopsis* is mediated by two ABCC-type phytochelatin transporters. Proc Natl Acad Sci U S A. 2010 Dec 7;107(49):21187–92.

289. Bovet L, Eggmann T, Meylan-Bettex M, Polier J, Kammer P, Marin E, et al. Transcript levels of AtMRPs after cadmium treatment: induction of AtMRP3. Plant Cell Environ. 2003 Mar;26(3):371–81.

290. Zientara K, Wawrzyńska A, Lukomska J, López-Moya JR, Liszewska F, Assunção AGL, et al. Activity of the AtMRP3 promoter in transgenic Arabidopsis thaliana and Nicotiana tabacum plants is increased by cadmium, nickel, arsenic, cobalt and lead but not by zinc and iron. J Biotechnol. 2009 Feb 5;139(3):258–63.

291. Maurel C, Verdoucq L, Luu D-T, Santoni V. Plant aquaporins: membrane channels with multiple integrated functions. Annu Rev Plant Biol. 2008;59(1):595–624.

292. Stillwell W. An Introduction to Biological Membranes: Composition, Structure and Function. Elsevier Science; 2016. 590 p.

293. Zangi R, Filella M. Transport routes of metalloids into and out of the cell: a review of the current knowledge. Chem Biol Interact. 2012 Apr 15;197(1):47–57.

294. Kamiya T, Tanaka M, Mitani N, Ma JF, Maeshima M, Fujiwara T. NIP1;1, an aquaporin homolog, determines the arsenite sensitivity of Arabidopsis thaliana. J Biol Chem. 2009 Jan 23;284(4):2114–20.

295. Mittler R, Vanderauwera S, Gollery M, Van Breusegem F. Reactive oxygen gene network of plants. Trends Plant Sci. 2004 Oct;9(10):490–8.

296. Gullner G, Komives T, Király L, Schröder P. Glutathione S-Transferase Enzymes in Plant-Pathogen Interactions. Front Plant Sci. 2018 Dec 21;9:1836.

297. Ji Y, Li Q, Liu G, Selvaraj G, Zheng Z, Zou J, et al. Roles of Cytosolic Glutamine Synthetases in Arabidopsis Development and Stress Responses. Plant Cell Physiol. 2019 Mar 1;60(3):657–71.

298. Rogowska A, Szakiel A. The role of sterols in plant response to abiotic stress. Phytochem Rev. 2020 Dec 1;19(6):1525–38.

299. Lee E-J, Kim KY, Zhang J, Yamaoka Y, Gao P, Kim H, et al. Arabidopsis seedling establishment under waterlogging requires ABCG5-mediated formation of a dense cuticle layer. New Phytol. 2021 Jan;229(1):156–72.

300. Poulsen LR, López-Marqués RL, McDowell SC, Okkeri J, Licht D, Schulz A, et al. The Arabidopsis P4-ATPase ALA3 localizes to the golgi and requires a beta-subunit to function in lipid translocation and secretory vesicle formation. Plant Cell. 2008 Mar;20(3):658–76.

301. Davis JA, Pares RB, Bernstein T, McDowell SC, Brown E, Stubrich J, et al. The Lipid Flippases ALA4 and ALA5 Play Critical Roles in Cell Expansion and Plant Growth. Plant Physiol. 2020 Apr;182(4):2111–25.

302. Hempel JJ. Molecular Characterisation of the Plastid-localised ABC Protein TAP1 in Arabidopsis thaliana. University of Stavanger; 2018.

303.   Kaneda M, Schuetz M, Lin BSP, Chanis C, Hamberger B, Western TL, et al. ABC transporters coordinately expressed during lignification of Arabidopsis stems include a set of ABCBs associated with auxin transport. J Exp Bot. 2011 Mar;62(6):2063–77.

304.   Geisler M, Murphy AS. The ABC of auxin transport: the role of p-glycoproteins in plant development. FEBS Lett. 2006 Feb 13;580(4):1094–102.

305.   Besnard J, Sonawala U, Maharjan B, Collakova E, Finlayson SA, Pilot G, et al. Increased Expression of UMAMIT Amino Acid Transporters Results in Activation of Salicylic Acid Dependent Stress Response. Front Plant Sci. 2020;11:606386.

306.   Domínguez-Solís JR, López-Martín MC, Ager FJ, Ynsa MD, Romero LC, Gotor C. Increased cysteine availability is essential for cadmium tolerance and accumulation in Arabidopsis thaliana. Plant Biotechnol J. 2004 Nov;2(6):469–76.

307.   Roy SB, Bera AK. Individual and combined effect of mercury and manganese on phenol and proline content in leaf and stem of mungbean seedlings. J Environ Biol. 2002 Oct;23(4):433–5.

308.   Harper, Baker, Balkwill, Smith. Nickel uptake, translocation and hyperaccumulation in Berkheya coddii. Third International Conference on. 1999;

309.   Maksymiec W, Krupa Z. Jasmonic acid and heavy metals in Arabidopsis plants - a similar physiological response to both stressors? J Plant Physiol. 2002 Jan 1;159(5):509–15.

310.   Chini A, Fonseca S, Fernández G, Adie B, Chico JM, Lorenzo O, et al. The JAZ family of repressors is the missing link in jasmonate signalling. Nature. 2007 Aug 9;448(7154):666–71.

311.   Kinnersley AM, Turano FJ. Gamma Aminobutyric Acid (GABA) and Plant Responses to Stress. CRC Crit Rev Plant Sci. 2000 Nov 1;19(6):479–509.

312.   Tian W, Hou C, Ren Z, Pan Y, Jia J, Zhang H, et al. A molecular pathway for CO_2 response in Arabidopsis guard cells. Nat Commun. 2015 Jan 20;6(1):6057.

313.   Mohan C, Jayanarayanan AN, Narayanan S. Construction of a novel synthetic root-specific promoter and its characterization in transgenic tobacco plants. 3 Biotech. 2017 Aug;7(4):234.

314.   Wang R, Zhu M, Ye R, Liu Z, Zhou F, Chen H, et al. Novel green tissue-specific synthetic promoters and cis-regulatory elements in rice. Sci Rep. 2015 Dec 11;5:18256.

315.   Stoyanov JV, Brown NL. The Escherichia coli copper-responsive copA promoter is activated by gold. J Biol Chem. 2003 Jan 17;278(3):1407–10.

316.   Mandell DJ, Lajoie MJ, Mee MT, Takeuchi R, Kuznetsov G, Norville JE, et al. Biocontainment of genetically modified organisms by synthetic protein design. Nature. 2015 Feb 5;518(7537):55–60.

317.   Chan CTY, Lee JW, Cameron DE, Bashor CJ, Collins JJ. 'Deadman' and 'Passcode' microbial kill switches for bacterial containment. Nat Chem Biol. 2016 Feb;12(2):82–6.

318.   Caliando BJ, Voigt CA. Targeted DNA degradation using a CRISPR device stably carried in the host genome. Nat Commun. 2015 May 19;6:6989.

319.   Ali S, Kim W-C. A Fruitful Decade Using Synthetic Promoters in the Improvement of Transgenic Plants. Front Plant Sci. 2019 Nov 1;10:1433.

320.   AT3G46900 (COPT2) [Internet]. [cited 2022 Jul 27]. Available from: https://www.arabidopsis.org/servlets/TairObject?name=AT3G46900&type=locus

321.   Yang C-H, Wang C, Singh S, Fan N, Liu S, Zhao L, et al. Golgi-localised manganese transporter PML3 regulates Arabidopsis growth through modulating Golgi glycosylation and cell wall biosynthesis. New Phytol. 2021 Sep;231(6):2200–14.